DTIC FILE COPY

Report No. CG-ONSCEN 02-89

AD-A215 916

SOUTH PACIFIC OMEGA VALIDATION ANALYSIS

Verne E. Hildebrand

SRS Technologies
380 Stevens Ave., Suite 313
Solana Beach, CA 92075

DTIC
ELECTE
DEC 21 1989
S D
B

August 1989

Final Report

Document is available to the U.S. public through the
National Technical Information Service
Springfield, Virginia 22161

Prepared for:

U.S. DEPARTMENT OF TRANSPORTATION
UNITED STATES COAST GUARD
OMEGA Navigation System Center
Alexandria, Virginia 22310-3998

89 12 21 022

NOTICE

This document is disseminated under the sponsorship of the Department of Transportation in the interest of information exchange. The United States Government assumes no liability for the contents or use thereof.

Technical Report Documentation Page

1. Report No.	2. Government Accession No.	3. Recipient's Catalog No.
CG-ONSCEN 02-89		

4. Title and Subtitle	5. Report Date
South Pacific OMEGA Validation Analysis	August 1989
	6. Performing Organization Code
7. Author(s)	8. Performing Organization Report No
Verne E. Hildebrand	SRS-SD-01-89
9. Performing Organization Name and Address SRS Technologies 380 Stevens Ave., Suite 313 Solana Beach, CA 92075	10. Work Unit No (TRAIS) 5462
	11. Contract or Grant No. N00123-86-D-0134, D.O. 041
12. Sponsoring Agency Name and Address U. S. Department of Transportation United States Coast Guard Omega Navigation System Center Alexandria, VA 22310-3998	13. Type of Report and Period Covered Final Report August 1988 to August 1989
	14. Sponsoring Agency Code

15. Supplementary Notes Under contract to: Naval Ocean Systems Center
Code 434
271 Catalina Blvd.
San Diego, CA 92152-5000

16. Abstract

This report, the sixth in the Omega Validation series assesses the Omega Very Low Frequency radio navigation system performance in the South Pacific Ocean area. Our general overview describes (1) a new emphasis for this and following validations on establishing signal quality through characterizing zones of signal-self-intereference, (2) validation planning, (3) measurements and (4) analysis undertaken. Regions of self-interference due to equatorial zone propagation are predicted, and analyzed for each Omega signal. Zones of signal interference caused by propagation the long way around the world (long-path) are predicted and assessed. Navigation accuracy and signal coverage is assessed.

For most of the validation region Omega fully meets navigation expectations. The prediction guidance in the form of Propagation Phase Corrections, zones of poor signal quality (Modal and Long-Path), and Station Coverage are largely correct. A relatively small but significant zone of predicted inadequate coverage during certain periods of the day was identified and assessed. Confirmation however, was essentially circumstantial because no data was available within or close to the predicted zone.

17. Key Words			18. Distribution Statement
Omega	Correction	Long-path	Document is available to the U.S. Public through the National Technical Information Service, Springfield, Virginia 22161
Navigation	Radio Wave	Phase	
Accuracy	Database	Signal-to-noise	
Propagation	Analysis		
Prediction	Modal		

19 Security Classif (of this report)	20. Security Classif. (of this page)	21. No of Pages	22 Price
Unclassified	Unclassified		

Form DOT F 1700.7

[THIS PAGE IS THE BACK SIDE OF THE TECHNICAL REPORT DOCUMENTATION]

ACKNOWLEDGEMENTS

The authors wish to acknowledge several individuals who have made major contributions to the investigations supporting this South Pacific Validation Analysis.

Mr. Carl Kugel of the U.S. Naval Ocean Systems Center in San Diego, California, was responsible for the major portion of data processing. His many years of experience were invaluable in ensuring that artifacts of instrumentation were removed prior to our analysis. His guidance was a great aid to understanding the many subtleties and complexities associated with data interpretation.

Mr. Eric Swanson of the U.S. Naval Ocean Systems Center in San Diego, California, provided a wealth of background information, both historical and technical. He contributed to many fruitful discussions regarding coverage assessment and interpretation of theoretical factors.

Mr. Randolph Doubt and Ms. Becky Casswell of the U. S. Coast Guard Omega Navigation System Center in Alexandria, Virginia,were instrumental in providing data from the OMEGA MASTERFILE and the shipboard collection program.

Commander R. J. Wenzel, Commanding Officer of the U. S. Coast Guard Omega Navigation System Center and Mr. Randolph Doubt provided extensive valuable guidance in establishing a new emphasis for the remaining Validation Analysis projects.

Accession For
NTIS GRA&I ☑
DTIC TAB ☐
Unannounced ☐
Justification
By
Distribution/
Availability Codes
Dist | Avail and/or Special
A-1

METRIC CONVERSION FACTORS

Approximate Conversions to Metric Measures

Symbol	When You Know	Multiply By	To Find	Symbol
LENGTH				
in	inches	*2.5	centimeters	cm
ft	feet	30	centimeters	cm
yd	yards	0.9	meters	m
mi	miles	1.6	kilometers	km
AREA				
in^2	square inches	6.5	square centimeters	cm^2
in^2	square feet	0.09	square meters	m^2
yd^2	square yards	0.8	square meters	m^2
mi^2	square miles	2.6	square kilometers	km^2
	acres	0.4	hectares	ha
MASS (weight)				
oz	ounces	28	grams	g
lb	pounds	0.45	kilograms	kg
	short tons (2000 lb)	0.9	tonnes	t
VOLUME				
tsp	teaspoons	5	milliliters	ml
Tbsp	tablespoons	16	milliliters	ml
fl oz	fluid ounces	30	milliliters	ml
c	cups	0.24	liters	l
pt	pints	0.47	liters	l
qt	quarts	0.95	liters	l
gal	gallons	3.8	liters	l
ft_3	cubic feet	0.03	cubic meters	m^3
yd_3	cubic yards	0.76	cubic meters	m^3
TEMPERATURE (exact)				
°F	Fahrenheit temperature	5/9 (after subtracting 32)	Celsius temperature	°c

* 1 in = 2.54 (exactly). For other exact conversions and more detailed tables, see NBS Misc. Publ. 286. Units of Weights and Measures. Catalog No. C13.10:286.

Approximate Conversions from Metric Measures

Symbol	When You Know	Multiply By	To Find	Symbol
LENGTH				
mm	millimeters	0.04	inches	in
cm	centimeters	0.4	inches	in
m	meters	3.3	foot	ft
m	meters	1.1	yards	yd
km	kilometers	0.6	miles	mi
AREA				
cm^2	square centimeters	0.16	square inches	in^2
m^2	square meters	1.2	square yards	yd^2
km^2	square kilometers	0.4	square miles	mi^2
ha	hectares (10,000 m^2)	2.5	acres	
MASS (weight)				
g	grams	0.035	ounces	oz
kg	kilograms	2.2	pounds	lb
t	tonnes (1000kg)	1.1	short tons	
VOLUME				
ml	milliliters	0.03	fluid ounces	fl oz
l	liters	2.1	pints	pt
l	liters	1.06	quarts	qt
l	liters	0.26	gallons	gal
m^3	cubic meters	35	cubic feet	ft^3
m^3	cubic meters	1.3	cubic yards	yd^3
TEMPERATURE (exact)				
°c	Celsius temperature	9/5 (then add 32)	Fahrenheit temperature	°F

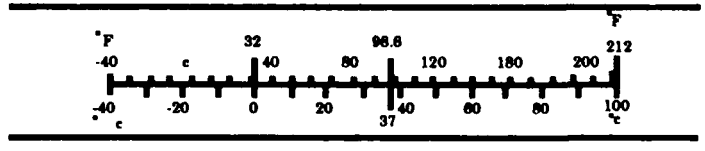

TABLE OF CONTENTS

LIST OF FIGURES

APPENDIX A

APPENDIX B

APPENDIX E

LIST OF TABLES

EXECUTIVE SUMMARY

This executive summary highlights the South Pacific Omega Navigation Validation. Material presented includes (1) a brief description of Omega, (2) the Omega validation purpose and goals, (3) the objectives, and emphasis for this validation, (4) analysis findings, and (5) conclusions.

INTRODUCTION

Omega is a Very Low Frequency (VLF) radio navigation system providing airborne, marine, and terrestrial users with a continuous, worldwide, position-fixing capability. Omega, which became operational on an interim basis in 1968 and was declared fully operational in 1982, consists of eight transmitters located in Norway, Liberia, Hawaii, North Dakota, La Reunion, Argentina, Australia, and Japan. The typical position-fix accuracy achieved with Omega is 2-4 nmi, 2-drms.

The U. S. Coast Guard Omega Navigation System Center (ONSCEN) is assessing the capability of Omega, through a validation program, consisting of seven regions. Five regions have been validated: the Western Pacific, the North Atlantic, the North Pacific, the South Atlantic, and the Indian Ocean. This South Pacific Validation, the sixth, is complete with this report. Analysis for a revisit to the Western Pacific and the seventh region, the Mediterranean Sea, will follow thereafter.

The VLF signal properties dictating the quality of Omega operation are received phase and signal-to-noise ratio (SNR); measured phase is most fundamental to position-accuracy. For navigational use or system planning, four types of predictions are used in determining OMEGA operational characteristics: (1) phase of signals, (2) signal level, (3) atmospheric noise, and (4) signal phase quality. Phase prediction is determined by the Swanson model. SNR is derived from signal level calculations using propagation models of the Naval Ocean Systems Center (NOSC) and The Analytical Sciences Corporation (TASC), and noise predictions are based upon CCIR measurement data. Signal phase quality is predicted using a recent set of propagation calculations by TASC and compared with the Overlay and Parametric models of TASC and NOSC respectively. Signal phase quality is degraded by self-interference, which results when a signal is dominated by a condition of propagation not intended for Omega use. One type of self-interference occurs under

certain conditions at night on the direct propagation path when higher-ordered modes are generated and sustained (modal). Another type of self-interference occurs when a signal propagating the long way around the world (long-path) under nighttime propagation dominates the shorter path (short-path) daytime propagation. The areas where self-interference can occur are called either modal zones or long-path zones. Validations assess conformity of predictions to the received signals.

SOUTH PACIFIC VALIDATION

This validation consisted of three parts: (1) planning, (2) measurement, and (3) analysis and reporting.

Planning included (a) predicting navigation performance in the region, (b) identifying areas of predicted signal quality problems, and (c) designing measurements to test predictions. Navigation performance was assessed using theoretical calculations to predict signal level, signal-to-noise ratio, and phase regularity for all signals. Areas having signal quality problems include zones of signal self-interference and poor SNR. Special measurements included use of aircraft to record modal interference patterns.

Measurement included collection of Omega data on aircraft, at fixed sites, and on ships. The primary data for assessing signal quality were collected by a U. S. Coast Guard C-130 aircraft, which involved about 150 flight hours over a period of 6 weeks. The fixed site data aided the calibration of the flight data and helped determine conditions during the flights. Fixed sites with atomic reference oscillators provided the most definitive data for assessing signal quality. Merchant vessels with combined Omega/Satellite receivers made several transits where Omega and Satellite fix data were recorded.

The analysis includes (a) assessing data and comparing it with predictions; (b) evaluating measured position-fix accuracy; and (c) interpreting the results. Analysis emphasis is on locating signal self-interference and then on testing for good SNR on the other signals. Navigation assessment compares measured with predicted position, using signals found to have good quality.

ANALYSIS FINDINGS

The short-path and the long-path self-interference assessments are presented separately because the different types of interference occur at different times, and because the required analysis work is quite different. Each of the Omega signals was assessed for self-interference, in order to establish zones classified by those phenomena that cause the interference. Our findings are that for the largest part of the validation region, as shown in Figures 3-4 and 3-5 on pages 38 and 39 respectively, high quality navigation is achieved.

Short-Path Interference Analysis: The short-path predicted modal zones are found to be mostly correct. The data suggest that the predicted highly extended Near Station Modal zones for Hawaii and Japan should be shortened. That part of the Hawaii modal zone boundary predicted to be along the 205° bearing needs to be moved counterclockwise, thereby making this zone larger.

Predictions show phase quality to be a problem at night for a sizable area located about 1000 nmi southeast of Hawaii as shown in Figure 3-6, page 43. The area for 13.6 kHz is larger than for 10.2 kHz. Within this sizable area, regions of two-station, (Australia [G] and Japan [H]) and three-station (Australia [G], Japan [H], and Hawaii [C]) coverage are predicted. For locations in part of the three-station area the bearings to Hawaii and Japan are within a few degrees, thus greatly limiting the navigation value of the available combinations. The predicted area of poor coverage is not confirmed because no measurements were made close enough to the area. However, collectively the findings support the prediction well enough to lend credence to the prediction.

We found that the modal problem, though largely a nighttime phenomenon, may exist for a large part of the time that a propagation path is undergoing the day/night transition. The more distant stations with longer paths are often important for navigation in this validation region because of modal effects on signals from the closer stations. Unfortunately, transition intervals for signals from the more distant stations can be long, occupying sixty to eighty

percent of the time. Modal effects are somewhat dependent on ionosphere conditions, both meteorological and seasonal. This is evidenced in the data by variability in modal occurrence. This variability strongly suggests that boundaries will move about, thus increasing the difficulty of certifying a model.

Long-Path Interference Analysis: The TASC calculations of field strength versus distance were extended beyond the station antipodes, and day/night portions were combined to reflect expected propagation conditions at times of specific interest. This extended model, while not elegant, allowed (1) estimating the maximum excursion of the long-path signal into the short-path region, and (2) estimating the time a boundary between long-path and short-path crosses a monitoring site. This model provided a coupling between the acquired data and the long-path boundary predictions, particularly those predicted by the parametric model.

Five stations were predicted and observed to exhibit long-path interference effects within the validation region. The data show requirements for boundary adjustments in all models, but do not directly support placement of the boundaries. This study supports the accumulating evidence that long-path effects are an important and not yet well established factor in navigation signal selection. While the documentation of long-path needs further refinement, the techniques we used proved useful, and demonstrated the feasibility for additional analysis.

Navigation Accuracy Analysis: Spot checks of the data confirm that navigation accuracy for the majority of fixes is within that expected. The analysis thus focuses on assessing situations flagged as possible exceptions. Examples are given which suggest possibilities for improving predicted phase correction models during the day/night transition times on propagation paths. Other examples suggest large variability about predicted phase when the propagation path is at high latitudes during local winter. These situations are best flagged for caution in signal selection for navigation.

Signal-to-Noise Analysis: The SNR coverage analysis was limited to checks near boundaries of coverage to determine if any cases exist where the mea-

sured SNR is less than predicted. The predictions were found to be generally conservative. In all areas SNR did not limit adequate station selection.

CONCLUSIONS

This validation provides significantly improved perspectives on navigation reliability in the South Pacific. For most of the validation region Omega fully meets navigation expectations. Also the prediction guidance is correct over most areas. The identification of a potential problem area of inadequate signal coverage is not so much a new discovery as it is the result of a careful study of modal zone boundary placement. The role of a validation is to report findings, and in this case, the findings heavily depend upon predications for extrapolation to locations of boundaries. We recommend that adjustments be made to prediction boundaries and that these findings, after proper review, be included as part of navigation guidance.

In summary, the analysis found that Omega works very well over the vast majority of the South Pacific validation region. In a significantly large area up to six of the eight Omega signals can simultaneously incur modal effects. The predicted modal interference and values of SNR are largely confirmed, with the exception of the large southwestward extent of the near-zone modal interference predicted for Hawaii and Japan. Long-path self-interference also occurs on five of the eight Omega signals at certain times within the validation region. These long-path effects add further complexity to the navigation solution. However, with good station selection guidance the Omega system is reliable and meets accuracy specifications.

1.0 INTRODUCTION

This section lays the foundation material to support the validation analysis and gives a synopsis of the material presented in the following sections. The background material includes a brief description of Omega, Very Low Frequency Radio Waves, the Omega Validation Program, and the Objectives of this and future validations.

1.1 BACKGROUND

1.1.1 OMEGA NAVIGATION SYSTEM

Omega is a Very Low Frequency (VLF) radio navigation system providing airborne, marine, and terrestrial users with a continuous, worldwide, position-fixing capability (See SWANSON 1983, Ref. 1, for an excellent review). The system, which became operational on an interim basis in 1968 and was declared fully operational in 1982, consists of eight transmitters located in Norway, Liberia, Hawaii, North Dakota, La Reunion, Argentina, Australia, and Japan. These transmitters are given corresponding letter designations (A) through (H). Omega uses the internationally allocated navigation band between 10 and 14 kHz. The typical position fix achieved with Omega is within 2 to 4 nmi, 2-drms. Omega is operated through international cooperation with the U. S. Coast Guard Omega Navigation System Center (ONSCEN) having management and coordination responsibility for the United States. System synchronization is the responsibility of the Japanese Maritime Safety Agency. Transmitters not on U. S. soil are operated and maintained by host nation agencies. Navigation receivers are produced by manufacturers in several countries.

1.1.2 VLF AND OMEGA

The fundamental measurement in Omega is the phase of the received VLF signal. Omega operates under the predication that measured phase can be related to location on the earth. For navigation, the phase of several received signals (two or three depending upon navigation mode) must be both measurable and of good quality. The signal-to-noise ratio

(SNR) must be sufficiently high to permit accurate phase measurement. It has been shown in all previous validations that a sufficient number of signals are receivable with adequate SNR to provide reliable navigation. Poor SNR on a received signal can be detected by the receiver, and the signal can be "deselected" so that this signal is not used for the navigation fix. For reliable navigation, received phase must closely match phase prediction for the receiver location. Unpredictable phase deviations from predictions can occur in certain instances due to signal self-interference. Self-interference results when a signal is dominated by a mode of propagation not intended for Omega use. Undesired modes occur at night on the direct propagation path because higher-ordered modes may, under certain conditions, be easily generated and sustained. Undesired modes also occur when a signal propagating the long way around the world (long-path) under nighttime propagation dominates the shorter path (short-path) under daytime propagation. These phase disruptions caused by signal self-interference are insidious, because they cannot be reliably detected by Omega receivers, and they may exist even on the strongest signals in the area.

VLF signals propagate in a waveguide formed by the earth's surface and the lower boundary of the ionosphere. Both surface conductivity and ionosphere parameters affect the signal attenuation and phase velocity of propagation. While surface conductivity effects are static, ionosphere parameters are dynamic, due to variations in the solar illumination (resulting from the earth's rotation and seasons), solar disturbances, and ionosphere wind and electric current systems. Thus, VLF signals incur both (1) static variations in phase and amplitude, due to navigation receiver location changes, and (2) time variations, due to a dynamic ionosphere. These variations must be accounted for in establishing position.

Omega navigation uses four types of predictions versus location: (1) phase of signals, (2) signal level, (3) atmospheric noise, and (4) signal phase quality. Phase prediction is based upon the Swanson model. SNR is derived from signal level calculations using propagation models of the Naval Ocean Systems Center (NOSC) and The Analytical Sciences

Corporation (TASC) and noise predictions based upon CCIR (International Radio Consultative Committee) data. Signal phase quality is predicted using a recent set of propagation calculations by TASC and compared with the Overlay and Parametric models of respectively TASC and NOSC. Each of these processes will be described as part of the analysis presentation. Validations assess conformity of predictions to the received signals.

1.1.3 OMEGA VALIDATION

The U. S. Coast Guard Omega Navigation System Center (ONSCEN) is responsible for assessing the overall worldwide capability of the Omega Navigation System. This responsibility is being addressed by a formalized regional validation program described by Scull (SCULL 1978, Ref. 2) and Doubt (DOUBT 1984, Ref 3). This program, composed of seven validation regions, is presently well along. Five regions have been validated and reported. This South Pacific Validation, the sixth, is complete with the publication of this report. For the remaining validations, the specific data collection campaigns have been completed. Previously reported validations include the Western Pacific in the fall of 1977 (KARKALIK 1978, Ref. 4 & 5), the North Atlantic in the summer of 1978 (CAMPBELL et al 1982, Ref. 6 & 7), the North Pacific in the summer and fall of 1979 (LEVINE 1980, Ref. 8 & 9), the South Atlantic in the spring of 1980 (WATT et al 1983, Ref. 10 & 11), and the Indian Ocean in the fall of 1983 (KUGEL 1984, SWANSON 1985 et al, Ref. 12,13 & 14). As described in section 2.3 DATA MEASUREMENT, there are three major data collection categories: airborne, shipboard, and fixed-site measurements. The fixed sites are usually installed before the flights and remain installed to obtain long-term measurement of temporal variation. Shipboard data is obtained when arrangements can be made with ships transiting the regions. Thus, the data collection effort for a given validation may extend up to the time of data analysis and report preparation.

Traditionally, however, the data collection period is more closely associated with the aircraft flights. These flights were completed in early 1985 for the South Pacific, as discussed herein, in the Spring of 1986 for the Western Pacific (revisited once the Australia signal became available in

1982), and in November 1987 for the Mediterranean. The Western Pacific data reduction is completed. The analysis phase, presently underway, will be completed in the Spring of 1990. The Mediterranean data reduction and analysis/report preparation for both the Western Pacific and Mediterranean will follow thereafter.

1.1.4 VALIDATION OBJECTIVE

The major objective for the validation program has always been to report the observed reliability of predictions and the accuracy obtained using the Omega Navigation System. Another objective has been to build up a database to support refinement of phase and signal-to-noise ratio predictions. The perspectives for achieving the primary objective, however, have evolved with time. This evolution is partly due to the "learning curve" associated with Omega utilization and to better insights regarding propagation. We are now greatly benefitting from (1) the lessons learned in the previous validations, (2) the significant refinement of propagation prediction models, and (3) propagation measurements collected over many years. This subsection describes some of the changes in perspectives and the resulting new emphasis placed on the validation process.

The initial validation emphasis was on signal coverage as defined by Signal-to-Noise Ratio (SNR) and on measuring obtainable navigation accuracy. The previous validations have amply demonstrated that, as predicted by computer models, there is high redundancy of signal coverage in most parts of the world. It has also been more widely appreciated that signal strength does not necessarily lead to accurate navigation. Phase perturbations, caused when a navigation signal interferes with itself, can create complications under certain conditions. These perturbations, collectively called self-interference, are described in section 2.1.1 under the subtitle *How VLF signals propagate*. Self-interference is sometimes prevalent in the strongest signals available for navigation. When self-interference can exist, navigation quality can no longer be guaranteed. It is now perceived that a key element in Omega validation must be to assess how well signal self-interference is predicted.

The objectives of this and remaining Omega validations are (1) to compare coverage predictions with measurements, with emphasis on signal self-interference, (2) to report on measured navigation accuracy, and (3) to describe observations which differ from predictions.

1.2 VALIDATION SCOPE

The results of this validation are reported in two forms: (1) this validation report for the South Pacific region, and (2) archive material containing the processed data and analysis notes generated in the validation. This validation report is prepared as ONSCEN's report to the community describing the validation findings. The archive material is less formal and is intended as a repository for the supporting documentation to the validation results. The archive material is highly technical and data intensive and of interest primarily to experts who want to check certain aspects of the validation or use the data for other investigations.

The primary focus for this analysis is the use of signals in navigation. The analysis identifies and selects areas and/or boundaries of special interest or concern first in terms of coverage from a single station and second in terms of coverage from all stations. An assessment is then made of the total signal resources available for navigation in the area or across the boundary of concern.

We note that the focus on Navigation has served well in establishing analysis guidance and in organizing the presentation material. However, in order to determine signal quality for use in navigation it has also been necessary to build a case for selecting good signals. Starting with theory we built a model for guidance and then identified signals of good/poor quality phase and amplitude. We have maintained a geographic/position orientation as much as possible. In addition, when appropriate, we have addressed the total Omega signal assets available for navigation in an integrated manner.

General: The steps in this validation consist of (1) planning, (2) acquiring data, (3) selecting and reviewing models for analysis guidance, (4) interpreting data based upon derived guidance, and (5) communicating the findings through comparison of results with previously published predictions.

Three major topics are addressed: (1) occurrence of good/poor phase quality, (2) occurrence of adequate/inadequate signals (SNR), and (3) expected/observed navigation accuracy. The phase quality factors addressed were problems of signal self-interference (modal interference, higher-ordered mode dominance, and long-path interference).

Phase Quality: This validation effort placed maximum emphasis on locating signal self-interference regions and only a minimum on assessment of SNR coverage. It is increasingly clear that self-interference can be an important factor in decreasing navigation reliability. The geographic extent of self-interference is much greater than was realized at the time Omega was developed. The short-path (modal effects) and long-path self-interference assessment is presented separately because of occurrence at different times and because the required analysis is quite different. In addition, the theoretical support available to us for modal analysis is much stronger than for long-path. We were unable to evaluate the long-path effects in nearly as much detail as the modal effects. Each of the Omega signals was assessed for zones of self-interference occurrence and classified by causing phenomenon.

The signal self-interference analysis has four major parts: (1) a description of the guidance derived for assessing modal interference and higher-ordered mode dominance, (2) a presentation and interpretation of the data with respect to modal effects, (3) a description of the guidance used to assess long-path effects on navigation, and (4) a presentation and interpretation of the data with respect to long-path interference. The guidance for parts one and three is derived from (1) the results of signal prediction calculations, (2) coverage diagrams, (3) previous experience, and (4) a preliminary overview of the data.

Signal-to-Noise Quality: What is important in the SNR analysis is to determine from the collection of signals with predicted "good" phase that a sufficient number have adequate SNR. A minimal effort was expended in investigating the signal-to-noise aspect of signal coverage. The focus was on determining whether at least three usable signals, having reliable phase and adequate signal, are available at all times (including accounting for station down times) over the South Pacific region. Since poor phase quality and poor SNR do not necessarily coincide in time, the time factor is important. As noted previously, experience has shown that signal coverage predictions of SNR are generally adequate for station selection. Furthermore, much evidence exists that atmospheric noise variability is so high that the uncertainty of validating SNR from limited measurements argues against adjustment of contours based on the limited data of validations. As emphasized by Swanson in the Indian Ocean Validation report (SWANSON 1985, Ref. 14), inadequate SNR can be sensed and compensated for in data processing by the navigation equipment.

Navigation Accuracy: Assessment of navigation accuracy is only meaningful when good quality signals are used. Thus, the process for assessing navigation accuracy is (1) to determine, for those locations where measurement data is available, what signals are predicted to be good and when, and (2) using good signals to measure the statistical accuracy of position fixes for representative propagation conditions. Good signals are determined by the phase and signal quality analysis described above. Representative propagation conditions include times of various path conditions, all daylight, all night, or in transition.

Data were selected from both fixed sites and ship transits for assessing navigation accuracy.

In addition to the above presented background material, the following subsection gives an encapsulated description of the material presented in this report.

1.3 REPORT OVERVIEW

Before proceeding with the main body of the report, we consider it helpful to give the reader an overview of the flow of information, along with some important findings. First to set the stage, it must be appreciated that Omega validation is an immense undertaking, only slightly eased by dividing the world into seven regions. The South Pacific, being by far the largest region, has vast expanses in which it is impossible to install fixed monitors. Moreover, Omega signal propagation is very complex, involving many propagation factors and variables. The ideal assessment would involve a sampling strategy, both spatial; and temporal, that far exceeds any realistic budget. As a consequence of these considerations, a validation must be conducted with extremely sparse data. Accordingly, heavy use must be made of theoretical predictions, which in essence is the topic of validation

Section 2.0, Methodology, provides a foundation for the analysis presented in section 3 EXECUTION AND FINDINGS. A reader not well versed in Omega, VLF propagation theory, and past validations may find this material particularly helpful. It is important to recognize that the validation program started over 13 years ago and that each validation experience, as well as much other research, has contributed to the knowledge base. The philosophy for conducting the validation analysis has changed significantly from previous reports: detail is provided to cover these aspects.

Material reviewed includes: (1) an examination of those guiding principles that are particularly germane to a validation analysis, (2) a description of how these principles are used to guide the preparation of a validation and analysis plan, (3) the preparation of a plan, and (4) the implementation of the plan for data collection and interpretive analysis. Emphasis is given to a description of those factors contributing to reduced navigation accuracy.

Section 3.0, Execution and Findings, provides a summary of the measurement operations, data assessment, selection of analysis guidance models, and the data analysis and interpretation effort.

This section sets the stage for evaluation and comparison of Omega coverage prediction presented in Section 4 INTERPRETATION OF VALIDATION ANALYSIS. The sequence of presentation follows the previously described philosophy that (1) navigation accuracy assessment should be conducted on good quality signals, and (2) to select good quality signals a determination must first be made on signal quality. Thus, much of the report emphasis is on signal self-interference, due to modal and long-path effects. The material is presented in sufficient detail to provide a flavor for the overall activities. More details on analytical guidance are presented in Appendices A, for modal effects; and C, for long-path effects. Amplifying details on data analysis and interpretation are presented in Appendices B, for modal effects; and D, for long-path effects.

These appendices contain a large amount of material, since the analysis must depend heavily upon models for interpretation of the data and for extending results from measurements to regions where no data was obtained. Three sources of guidance were available to us: two coverage models, the Overlay and Parametric model, and a recent set of Omega signal propagation calculations. Each source differed somewhat in placing important boundaries. We believe that the most recent propagation calculations provided important contributions to our findings. Unfortunately the calculations required extensive conversion, shown in Appendices A and C, to allow direct comparison with the other models and to be useful for geographic predictions. Our interpretation is heavily based upon the insights gained from this conversion process. Furthermore we feel that the insights have important consequences for predictions. Also, as will be noted in the presentation, we had to draw conclusions based upon very little concrete information. We felt that in order to build the strongest possible case overall, a large number of somewhat weak cases needed to be presented.

Our findings show that for the vast majority of the validation region, (shown in Figures 3-4 and 3-5 on respectively pages 41 and

42,) high quality navigation is achieved. Predictions show phase quality to be a problem at night for a sizable area located about 1000 nmi southeast of Hawaii as shown in Figure 3-6, page 43. The area for 13.6 kHz is larger than for 10.2 kHz. Poor SNR was not a problem for adequate station selection, a finding consistent with all previous validations.

Section 4.0, Interpretation of Validation Analysis, places the validation findings in perspective with expectations and the three coverage predictions, (the material of Appendices A and C, the Overlay model and the Parametric model.) We found that all models were largely in close agreement. Yet, we would contend that many of the small differences noted are important for both coverage prediction and for establishing credence of predictions where confirming measurements have not been made. Adjustments to predictions of signal self interference are recommended, which provide better guidance are recommended to determine where certain signals should not be used for navigation. The two-station area at 10.2 kHz identified in Section 3 would disappear with adjustments, but geometry factors for the Hawaii and Japan signals make the navigation problem very real. Furthermore, the system has lost robustness in this area because there is no backup for station down-time.

The comparison of multiple models is particularly important in that the system user, or at least the manufacturer of user equipment, needs a source of system coverage information. Overlay and Parametric models have been available for some time. While the model outlined in this report is at present an engineering analysis tool, it is the most current, most detailed and easiest to use for purposes of validation. The community will benefit from each model and from knowing the similarities and differences between them.

Section 5.0, Summary and Conclusions, shows that over most of the validation region Omega fully meets navigation expectations, and

that prediction guidance is correct over most areas. The identification of a potential problem area of inadequate signal coverage is not so much a new discovery as it is a result of acareful study of modal zone boundary placement. The role of a validation is to report findings. It is noted however that the findings have made extensive use of predictions to extend interpretations from locations of actual measurement to locations for expected boundries. We recommend that adjustments be made to prediction boundaries and that the findings of this analysis, after proper review, be included as part of navigation guidance.

2.0 METHODOLOGY

This section describes the principles and processes used in this validation. This material is intended to provide an amplifying foundation for the analysis presented in section 3 EXECUTION AND FINDINGS. A reader well versed in Omega, VLF propagation theory, and past validations may choose to skim this material. Since the philosophy for conducting the validation analysis has changed significantly from previous reports and since the self-interference effects may be new material for some readers, we provide more detail to cover these aspects.

2.1 VALIDATION GOALS

This subsection documents the planning processes from evaluating the validation needs to defining specific analysis tasks. The analysis criteria and the processes used for the validation are established here. The focus is on the navigation product. Thus, the order of presentation for deriving validation guidance builds from providing a navigation service (the bottom line) through the chain up to the basic knowledge making such a service feasible.

2.1.1 GUIDING PRINCIPLES

Omega was conceived and implemented to provide worldwide, low cost, moderately accurate navigation services using VLF radiowave signals. Omega's intended use is primarily for in-transit navigation with other means used for transit end points. Although the system accuracy design goal was 2 to 4 nautical miles (2 drms), accuracy of 1 to 2 nautical miles was visualized and on average is realized where the signals consist of good phase quality.

Uncertainties in propagation prediction and geophysical variabilities lead to less accuracy at certain times and locations. Part of the validation challenge is (1) to determine when and where navigation accuracy

is less than optimal, and (2) what accuracy can be achieved through deselection of signals having reduced quality.

Assessing position-fixing accuracy and its variability is greatly facilitated by understanding how relevant geophysics governs position fixing and how its dynamics contribute to position uncertainties. The following discussion builds a chain from the navigation product to each of the contributing physical elements. The chain is then examined for guidance in achieving the validation objectives.

How Omega uses VLF for position fixing. The fundamental measurement used in Omega is the phase of the VLF signal. The navigation service provides both stable signals for phase measurements and predictions of what the measured phase should be at any position and time. The prediction part of this service is being validated. Accurate phase prediction can be difficult, because received phase is dependent on propagation parameters and varies in a complex manner with position and time.

The most basic method for obtaining a position fix (using hyperbolic phase difference curves) requires that phase be measured on a combination of three signals at one frequency to provide two lines of position (LOPs). The signals must be chosen so that the derived LOPs have sufficient angular separation to allow accurate location of their intersection. Four common frequencies are transmitted from each station. When mode 1 propagation is the dominant, these frequencies have a well-defined phase relationship at the receiver. Phase is measured as a part of a cycle. Since the same phase value recurs at regular distance intervals separated by a cycle of propagation distance, a phase measurement can represent many positions. The distance interval covering a full cycle of measured phase is called a lane. Each frequency produces a different phase repetition pattern, thus different lane widths. Phase measurements are compared on up to four frequencies to establish a position for that frequency combination. This position is unique over a larger distance interval than a position determined from any single frequency. Defining position within the range of this interval is required of the user and is not a consideration of the validation.

Optimal navigation is obtained from strong signals having good geometries and predictable phases. The ideal navigation process picks the best combinations of signals for position fixing. Accuracy of a position fix generally can be improved by using additional frequencies and stations. The challenge is to correctly weight signals in a position-averaging process. Geometric relationships can be calculated in a receiver from rough position fixes and SNR can be measured; both can be applied as weighting factors. Phase quality presently cannot be determined within the navigation receiver, nor can it always be reliably predicted due to uncertain propagation factors. Thus, the best approach is to deselect signals whose phase quality may be in question.

Corresponding to the validation objectives, the validation assessment determines the accuracy of phase prediction at selected representative times, locations and Omega frequencies. Since phase predictions are made for expected conditions, validations must measure deviations from predicted phase and must determine if signal self-interference is the cause. Phase prediction amounts to propagation prediction, which in turn amounts to prediction of the parameters that govern propagation. Such parameters may be empirical.

How VLF signals propagate. VLF signal propagation can be modeled as occurring in a waveguide formed by the earth's surface and the lower boundary of the ionosphere. The waveguide height (earth to ionosphere) is high enough to allow energy to propagate via several modes. The efficiency with which modes are excited and propagate depends on the guide height in terms of signal wavelength and propagation direction relative to the earth's magnetic field. At the Omega frequencies the excitation and propagation efficiency of all modes can be quite sensitive to small changes in these parameters. Omega is designed to use the measured phase of the first-ordered mode. The presence of higher-ordered modes at significant levels causes problems.

Surface and ionosphere conductivity affect propagation, as does variability of the ionosphere. Ionosphere variability is caused by :

(1) variations in the solar illumination resulting from

(a) the earth's rotation,

(b) the earth orbiting the sun, and

(c) solar disturbances, and

(2) meteorological influences,

(a) seasonal

(b) weatherlike patterns

These ionospheric changes cause time variations in the phase and amplitude of signals at every location on the earth. Some of the ionospheric changes are systematic and thus predictable, some are systematic but governed by unmeasurable phenomena, and some are transient or random – these latter are largely unpredictable.

Predictable characteristics affecting signals include the following:

(1) VLF signal propagation attenuation due to geometric spreading. (As the distance between a transmitter and a receiver increases, the received signal level decreases);

(2) rate of attenuation due to surface conductivity, which decreases as the surface ranges from sea water through various terrains to arctic ice;

(3) predominant ionosphere changes over a 24-hour period, transitioning from midday to late night and back to midday;

(4) changes in phase at a given location, caused by changes in sun declination;

(5) mode excitation and signal attenuation due to the signal's magnetic heading and dip angle;

(6) amplitude increase due to signal convergence at the antipode.

Signal characteristics that are not as accurately predictable but capable of being modeled include the following:

(1) propagation across the day/night terminator,

(2) VLF signal modal interference,

(3) signal self-interference due to simultaneous reception of signals over both the short-path and long-path.

Presently unpredictable but boundable characteristics are:

(1) variations in ionosphere profiles thought to be caused by meteorological conditions, and

(2) variations caused by solar radiation disturbances, namely solar flares which produce Sudden Ionospheric Disturbances (SIDs), Polar Cap Disturbances (PCDs), and Geomagnetic Storms.

(3) ionosphere variations due to changes in latitude.

Fortunately, the unpredictable phenomena rarely lead to major navigation errors.

Phase perturbations that create complications can be integral to the navigation signals. Phase perturbations result from signal self-interference. There are two dominant mechanisms: (1) round-the-world, long-path propagation interfering with the short-path, and (2) modal interference created when the different modes of propagation within the bounded earth-ionosphere waveguide are of comparable amplitude.

The first type of self-interference, long-path/short-path, results mainly from the fact that the Omega signals propagate long distances with relatively low attenuation and that the propagation conditions on the two paths may be very different.

These propagation differences include the following:

(1) propagation attenuation is significantly less for eastward propagation relative to westward propagation;

(2) signal attenuation is significantly different for day versus night propagation; and

(3) signal attenuation varies with the conductivity of the earth's surface.

The second type of interference results from two mechanisms. One mechanism (near modal) occurs close to the transmitter, where the received signal is composed of many propagated modes, each having a different phase velocity and attenuation. The higher-ordered modes generally dampen rather rapidly but have sufficient strength close to the transmitter to produce an interference pattern. However, when the transmitter is at a low or low mid latitude, the interference pattern may extend to large distances under nighttime propagation. The other mechanism (mode conversion) occurs at nighttime for propagation across or near the geomagnetic equator (over approximately ±7 degrees magnetic latitude) and for propagation across very low conductivity terrain such as the Greenland icecap. Energy is imparted to the higher-ordered modes which then can achieve amplitudes comparable to the dominant first mode. For both mechanisms, one of the higher-ordered modes may become the dominant mode. Each mode (several may be of comparable amplitude) propagates at a different velocity. Thus, the phase may vary in a complex manner with distance. The interference causes the measurement of phase to deviate (lead and lag) from what is expected if propagation is only via mode 1. On occasion, the deviations are large enough to cause a cycle jump. A cycle jump implies a switch in dominant modes. This switch may occur at a fixed measurement site without a cycle jump. In this case the switch is evidenced when a large phase change and possibly an amplitude dip occurs that differs from the expected mode 1 diurnal pattern. A higher-ordered mode may become dominant over a large distance interval. Since such phase fluctuations, mode switching, or higher-ordered mode dominance are not a part of

the Omega navigation model, their occurrence results in position errors.

The modal interference, higher-ordered mode dominance and long-path effects can be particularly important in assessing Omega navigation validity. This modal interference is a nighttime propagation problem that is most pronounced for propagation at low latitudes. Higher-ordered mode dominance, once created, can extend great distances into high latitudes. Accurate predictions (upon which deselection decisions are based) regions with strong modal conversion are particularly important, because no other means presently exists for mitigating conversion effects.

Use of Prediction Models. Four types of predictions for Omega have been used in past validations. These are predictions of navigation phase, signal coverage (i.e., boundaries within which phase is considered reliable and within which SNR is predicted adequate), best selection of station pair combinations, and regions of signal self-interference. The primary prediction is average incident phase from all stations for any receiver location, time-of-day, and season. Phase predictions assume that the first order mode is sufficiently dominant that received phase will increase regularly with distance from a transmitter. Propagation parameters used in the average phase predictions are "fine tuned" using the OMEGA MASTERFILE of phase data, gathered through a network of monitoring sites. The OMEGA MASTERFILE is a database maintained by ONSCEN that contains hourly phase and phase-difference data from the worldwide network of OMEGA monitor sites. Because the OMEGA MASTERFILE database is quite large and includes measurements from widely dispersed locations around the world, average predictions should be quite accurate where the phase varies systematically with distance. Empirical adjustments, however, do not necessarily give good predictions for locations significantly removed from measurement sites. It is the role of a validation to assess, within a region, the accuracy of position fixes to the greatest extent practical. Since position fixes are based upon expected phase, the validation is an assessment of predicted phase. If assessments from a sufficient number of measurement sites all show

small variations in position, the compilation would ideally also add credence to predictions for the whole area where propagation is predicted quite similar.

The quality of average phase predictions is best validated from well surveyed fixed-site measurements of received phase with a high-quality reference oscillator. Phase-difference measurements, which are obtained by comparing phases between two received signals, are used when a highly stable local reference oscillator is not available. For navigation position determination, phase-difference data is used to determine Lines of Position (LOPs). While complicating the interpretation, phase-difference data is a satisfactory substitute. To test phase prediction, care must be taken to ensure that the measured signal is not contaminated with additional complexities such as signal self-interference or local interference.

Coverage predictions are generated using full wave calculations of signal propagation, integrated with an atmospheric noise prediction model. Predictions are average signal quality, SNR, and phase "purity." Two types of displays are produced: *Overlays* showing contours of SNR and phase quality threshold boundaries, and *Parametric Displays* showing signal navigation quality using symbology as the indicator. Both of these types of displays are presented and used in section 4.1.2 COMPARISON OF ANALYSIS WITH COVERAGE PREDICTIONS to assess the analysis findings. Composite signal coverage prediction is an extension of the basic coverage prediction that shows coverage of all stations versus location on a single diagram.

Validation requires determination of the actual existence of a predicted condition or quality. Ideally, sufficient analysis would be conducted to assess both time and position variability of the predictions. Unfortunately, the ideal case does not exist; much ingenuity is required to test the predictions from the few measuring sites, most of which are not optimally located for achieving these objectives. Some tests would have to be made to determine how far and how well extrapolations can be made from the specific measurement locations. A less desirable but

more practical alternative is to simply report agreement or disagreement between predictions and measurements.

Modal interference, mode switching, and higher-ordered mode dominance predictions are made using full-wave calculations. Achieving accurate position fixing requires knowing how the phase behaves with time and position. The presence of higher-ordered modal effects on a signal must be ruled out. If phase always changed regularly with distance (this was the basis for Omega design), prediction would be much less complex. Unfortunately, important cases occur, primarily under nighttime propagation, when received phase varies in a much more complex manner.

Much has been learned in recent years about the occurrence of higher-ordered modes. Their occurrence, called a multimode condition, is a nighttime phenomenon except for regions very close to transmitters. When multimode occurs, it can appear at various times throughout the night. The frequencies on which multimode is significant vary with position and propagation conditions. The occurrence of a cycle jump on phase recordings is a strong indicator of the presence of higher-ordered modes. Much evidence shows that the cycle jump results when the propagation conditions are undergoing significant change. Assuming that measurements are of good quality, a cycle jump is observed only if the contributing modes transit through phase opposition. Thus, a cycle jump is observed over only a small portion of the region where two or more modes are close in amplitude. Many other clues needed to assess the presence of modal effects, are available from comparison of phase data from multiple frequencies.

In the next subsection we discuss the plan for deriving the validation products.

2.2 VALIDATION PLAN

This subsection describes conversion of goals to planned practical accomplishment at an overview level, discusses what can be done and what is practical, describes use of theoretical guidance and predicted performance, describes types of measurements, reasons for use, their history value and interrelationships.,and describes problems of implementation, site selection and operational factors.

The South Pacific validation technical activity was divided into three phases: (1) planning, (2) measurement, and (3) analysis and reporting.

2.2.1 PLANNING SUMMARY

The planning phase entailed the following activities:

- Use of models to predict navigation performance in the region.
- Identification of areas where signal self-interference is predicted to be a problem and explore boundaries in the region where SNR = -20 db and -30 dB.
- Design of measurements to test for predicted signal self-interference and SNR boundaries.

For both planning and analysis, propagation and phase prediction models were relied upon to indicate the likely occurrence of modal structure. Naval Ocean Systems Center (NOSC) personnel made assessments of Omega navigation performance in the validation region using theoretical calculations of Omega signal propagation. Predictions of signal level, signal-to-noise ratio, and phase regularity were made for all Omega signals available in the South Pacific region. Tools used were the NOSC state-of-the-art propagation models (FERGUSON 1970, Ref. 15, BICKEL et al 1970, Ref. 16, PAPPERT et al 1972, Ref. 17, SNYDER 1981, Ref. 18) and The Analytical Science Corporation (TASC) waveguide model (GUPTA et al 1979, Ref. 19). These tools provided the best means for assessing the modal structure dependence upon distance, magnetic azimuth, magnetic dip angle, and ionospheric profile parameters.

Next, boundaries in the region were identified where $\Delta\emptyset$ = 20 CEC and SNR = -20 db and -30 dB. (A boundary is the dividing line at which a specific threshold level of the signal characteristic exists. For example, a threshold of signal-to-noise ratio (SNR) is the contour on a geographic display at which SNR = -20 dB.) The waveguide-mode prediction model showed the regions where potential navigation accuracy problems exist, indicating where observations of Omega signals should be made. These regions were determined as functions of geophysical conditions (i.e., solar illumination and season). The planning phase is described in detail in subsections 2.3 DATA MEASUREMENT and 2.4 A PLAN FOR VALIDATION ANALYSIS.

2.2.2 MEASUREMENT SUMMARY

The measurement phase entailed the following activities:

- Collection of Omega data to test the predictions with monitors at fixed sites, on aircraft, and on ships.
- Obtain navigation fixes both with Omega and satellite navigation for reference.

The objective of the measurement phase was to provide data for assessing position fix accuracy of both fixed and mobile recording sites and for verifying the predicted location, extent, and time evolution of both modal zones and SNR boundaries. Twenty-three aircraft flights were conducted, ten fixed sites were located within the validation region, and eleven ship transit segments recorded data. The data collection locations/transits and the data gathered are described in subsection 3.2, DATA ASSESSMENT.

2.2.3 ANALYSIS SUMMARY

The analysis phase consisted of the following activities:

- Refine predictions of signal self-interference zones and format for suitable comparison with data.

- Assess modal effects in validation region and compare with predictions.
- Evaluate Signal/Noise measurements and compare with predictions.
- For signals of good phase quality and adequate SNR, assess position fix accuracy.
- Interpret results.

The models and techniques used and the detailed results are described or referenced in the subsections entitled 3.3 SIGNAL SELF-INTERFERENCE ANALYSIS, 3.4 LONG-PATH INTERFERENCE ASSESSMENT, 3.5 SIGNAL-TO-NOISE RATIO ASSESSMENT, and 3.6 NAVIGATION ACCURACY ASSESSMENT.

2.3 DATA MEASUREMENT

The major measurement activities included the following:

- In-flight measurements on dedicated flight.
- Long-term measurement of temporal variation at fixed sites.
- Shipboard phase and position measurement from ships transiting the area.

The selected boundries for magnitude of phase fluctuation and SNR were used as one basis for selecting fixed monitor sites, aircraft flight paths, and ship transits. Availability of installation sites was another basis.

2.3.1 SITE SELECTION

The selection of sites and data to be monitored at each site for the validation required tradeoffs between the kinds of data needed and the practical aspects of obtaining the data (e.g. availability and location of equipment).

Placement of monitors was determined largely for practical support reasons. A requirement was that the selected sites provided good data for checking theoretical signal parameters and provided calibration points for the aircraft instrumentation.

To obtain the optimum set of data within the bounds of the available resources, a combination of data collection efforts was undertaken:

(1) long-term fixed-site recording, primarily utilizing those sites that were set up for obtaining data for the OMEGA MASTERFILE;

(2) short-term fixed-site recording, using much higher time resolution and calibrated (at the time of the site visit) for measurement of signal-to-noise ratio and to calibrate the aircraft collected data;

(3) a series of aircraft flights that transited the area; and

(4) placement of navigation receivers upon ships transiting this region,

2.3.2 MEASUREMENT OPERATIONS

The measurement activities were conducted in three separate operations: fixed-site monitoring, measurements aboard an aircraft flying between many of the fixed sites, and independent shipboard operations conducted as part of normal ship transits. Each of these measurement operations will be described in this subsection.

2.3.3 FIXED SITES

ONSCEN has established a global network of monitoring sites as part of the continuing evaluation of Omega signal behavior throughout the world. Normal monitoring operations were conducted by on-site personnel and collected data forwarded to ONSCEN. For selected sites, NOSC personnel conducted calibration measurements that allowed obtaining "absolute" signal field strength data. The procedure was to use special equipment to calibrate the amplitude measurements made with the fixed-site MX-1104 Omega Monitor Receivers, and then to use data from

these receivers to calibrate the aircraft data during flyovers. Equipment at the fixed sites compares received phase with either an internal oscillator or precision external standard and records the data on magnetic tape. Depending upon the quality of the reference frequency, the data are processed by ONSCEN as measured phase or LOP phase differences and included in the OMEGA MASTERFILE data bank. OMEGA MASTERFILE data were excerpted for selected sites.

The calibrated signal amplitude and phase monitoring equipment installed at the ONSCEN sites is basically the Magnavox MX-1104 receiver with a variable attenuator in the calibration line. Data from all sites consisted of SNR and phase relative to the local oscillator (a Cesium Frequency Standard at some locations) for seven stations and the calibration channel at the three frequencies of 10.2, 11-1/3 and 13.6 kHz. The selected sites for amplitude calibration had attenuated calibration signals injected at the receive antenna. (The interested reader is refered to reference 14, Indian Ocean Validation, section 3, for more information on equipment characteristics and calibration methods.) The calibration signal was adjusted to be comparable in amplitude with the received noise, thereby calibrating the observed noise variations. The calibrated noise then was used to determine signal amplitude in the signal measurement channels by noting the SNR.

2.3.4 MOBILE RECORDING

Mobile data collection activities included ship transits and aircraft flights.

U. S. Coast Guard C-130 Aircraft Flights. Technical staff from NOSC and ONSCEN flew special monitoring equipment on a series of flight radials across the validation region. Most of the flights were nearly along a radial from one of the Omega transmitters. Monitoring equipment was installed aboard a C-130 cargo aircraft operated by the U.S. Coast Guard (USCG). The aircraft flights encompassed approximately 150 flight hours and a total mission duration of 6 weeks during February and March 1985. The aircraft was equipped with two Litton 211 Omega Navigation System (ONS) receiver-processor units (RPU) and the Hewlett-

Packard 3581 Wave Analyzer/Selective Level Meter for data measurement and the Magnavox GPS T-Set for obtaining reference positions.

Shipboard Data. Merchant vessels with Magnavox MX-1105 Omega/ Satellite Navagation receivers installed on board made several transits in the validation area between August 1985 and May 1986. Ship navigation personnel collected frequent navigation-fix data with the MX1105 Receivers. The data were recorded and forwarded to ONSCEN. Data supplied consisted of taped readings of fix quality and fix error recorded at hourly intervals and at the time of each satellite pass. A Satelite (Transit) fix interpolation routine provided all data points with an associated position thus permiting a much higher density of position referenced Omega data processing.

The Magnavox MX-1105 Omega/Satellite receiver equipment configuration for shipboard installations is similar to that for the ONSCEN ground monitors, in that the basic components are the receiver and MFE-5000 cassette recorder. The MX-1105 is similar to the MX-1104 but also incorporates a receiver for satellite TRANSIT data and uses speed log and gyrocompass information to enhance position determination.

2.4 A PLAN FOR VALIDATION ANALYSIS

This subsection describes the analytical plan prepared for the validation analysis. The spirit of a plan is indicated by using the future tense. We believe the future tense helps to communicate the perspective of a planning viewpoint, that is, expectations prior to undertaking the actual analysis. The analysis experience, described later, identifies how the analysis had to deviate from the plan. This plan is intended to be both a living document, to be modified by experience, and a guide for the remaining validations. As noted previously, the validation effort concentrates on analysis of modal interference effects, and therefore this discussion centers on these procedures.

A plan for data analysis and interpretation: The first priority will be to determine, by site location, what propagation characteristics are predicted to exercise a dominant influence on the signals. Primarily, this

determination process identifies useful signals and segregates regions where higher-ordered modes have a major effect. SNR boundaries need to be checked and long-path interference bounded to establish useful signals. The existence of multimode conditions at night needs to be tested.

Analysis of flight data is to be conducted first to identify possible regions of multimode occurrence. Calculations of field strength versus distance made by TASC (GUPTA 1980) and supplied by ONSCEN is also reviewed and comparisons made with flight data.

If very little or no indication of multimode is evident on either flight data or from calculations in a region well beyond the region of interest, multimode is probably not significant. However, multimode could exist beyond regions where it is predicted or observed. If possibilities for multimode are predicted, they may occur under conditions other than those observed. Boundaries for multimode have to be predicted using calculations. If good agreement between flight data and calculations for all or most flights is observed, it is assumed that calculations provide good predictions. Calculations can then be used with high confidence to make predictions for locations where measurements were not made. Good agreement requires interpretation. Such interpretation is best supported by sensitivity tests where ionospheric parameters are varied parametrically over a range of plausible conditions. Disagreement suggests that calculation parameters should be adjusted. (Such sensitivity tests have not been made.)

Fixed-site data analysis will be grouped into two categories based upon the aircraft data analysis: data affected and data not affected by multimode. Data not affected by multimode will be reviewed for consistency with Propagation Phase Corrections (PPCs) recorded in the OMEGA MASTERFILE. Noted gross inconsistencies of measured LOPs with PPCs will be flagged (Ideally the measured station pair phase difference plus the PPC equals the LOP). Some samples of received-phase data from sites outside a multimode area will be analyzed as a control to establish that the criteria for identifying multimode are valid.

For those sites where multimode is expected, two types of analysis will be conducted. First, for sites with atomic frequency references, the received phase of individual transmissions will be scanned to detect significant deviations from the expected diurnal pattern. Deviations will be flagged and correlated between frequencies as a test for multimode. Occurrence of multimode will be noted. Second, for sites without atomic frequency references, phase-difference (LOP) data will be scanned in the same manner. The multimode assessment will be summarized and comments regarding agreement with present predictions provided.

Minimal assessment of measured SNR will be made to provide some consistency with previous validation reports. SNR predictions for local day and transition times will be tested by selectively comparing predicted and measured SNR at those sites where SNR from a station is either the lowest for the region or close to the threshold of being too low to measure.

Shipboard data will be used to augment fixed-site data, primarily to test for modal interference.

A navigation accuracy assessment will be conducted as the final phase of the validation analysis. The assessment will consist of two parts, examination of data from fixed sites and from shipboard measurements. The analysis process will depend on the type of data available. First, all data sets known to contain signal self-interference and inadequate SNR will be removed from the analysis files. For sites where an atomic frequency reference was used, measured phase will be compared with predicted phase. This phase comparison is the most desirable, since it evaluates each individual signal. For sites without an atomic frequency reference, phase-difference data will be compared with predicted phase difference for selected station-pair combinations. For shipboard data, phase-difference comparisons will be made.

Planning Comments: A more detailed description of the analysis processes used is presented in section 3.3 SIGNAL SELF-INTERFERENCE ANALYSIS and section 3.4 SIGNAL-TO-NOISE RATIO ASSESSMENT. We note that this planned process was modified significantly, especially with respect to using aircraft data as the focus for identifying modal

conditions. From the analysis of prediction calculations and from the early stages of data analysis, it became evident that much of the modal competition was not easily recognized in the flight data. Consequently much more dependence was placed upon fixed-site data.

3.0 EXECUTION AND FINDINGS

This section provides the details of the validation effort, in this sequence: measurement operations, data assessment, data analysis, and analysis interpretation.

3.1 MEASUREMENT SUMMARY

This subsection summarizes the measurement phase of the validation: what flights were conducted and when, what fixed sites were operated and what transpired, and what ship transits were made and data collected. Measurement activities are compared to the plan and expectations.

The validation regions are basically centered on large ocean areas; consequently data collection is often challenging. In the South Pacific possible monitor site locations were along (1) the western coast line of South America, (2) the islands strewn across the region, particularly in the northwestern part, and (3) the eastern coast of Australia.

In the South Pacific a major concern for modal interference was that it might occur on signals from the Omega transmitters on Hawaii (Station C) and North Dakota (Station D) because of their close proximity and good geometry. For these transmissions, modal effects were expected to be most severe in the western portion of the validation region (largely from Tahiti westward). Possibilities for other modal effects were recognized; for instance, Liberia was a strong candidate. The aircraft flights were oriented so as to obtain optimum information on the transmitters in or near the validation region. Fixed sites were either a part of the long-term monitoring program or were chosen to aid calibration of the aircraft flight data and to assist in determining if the conditions measured during overflight were typical.

To review, combinations of data collection efforts were undertaken which consisted of (1) long-term fixed-site recording, primarily utilizing sites set up for obtaining data for the Omega navigation OMEGA MASTERFILE, (2) short-term fixed-site recording, usually with much higher time resolution and calibrated measurements of signal-to-noise ratio, (3) a series of aircraft

flights which transited the area, and (4) data collected from navigation receivers aboard selected ships operating in this region.

The fixed-site recording stations for the South Pacific, designated by circled dots, are presented in Figure 3-1. The primary sites are within the hatched area indicating the validation region. Secondary sites lying outside this validation region were also used to measure signals traversing the region. The data collected at the fixed sites were obtained with MX-1104 receivers.

The primary data for assessing modal structure was collected by a U. S. Coast Guard C-130 aircraft. The flight paths for the South Pacific region are shown in Figure 3-2. The South Pacific flights were generally flown at night, when the most serious modal effects were expected to occur. As noted, obtaining all-night propagation paths for widely dispersed transmitters is not possible. Thus many or most of the signals were recorded with the terminator crossing the propagation path during at least part of the first flight.

For data collected on ships, both Omega and Transit satellite fixes were made and compared. The South Pacific ship tracks for which data were obtained are shown in Figure 3-3. The ship transits provide some additional spatial information (1) around New Zealand, (2) between Tahiti and New Zealand, (3) along the coast of Antarctica, and (4) on an important transit from Panama to Tahiti.

3.2 DATA ASSESSMENT

This subsection describes the database acquired, assesses its quality, cites archival repository for data, provides examples to illustrate type and quality, and emphasizes aircraft data and modal effects.

Three types of measurements could be made from the received signals when calibrated: (1) signal levels, (2) signal-to-noise ratio, and (3) phase. Measured phase generally was converted to phase difference to remove oscillator drift, since most of the receiving sites do not have particularly stable oscillators. At three locations (Arequipa, Tahiti and Wellington) atomic frequency references were used and the measured phase could be

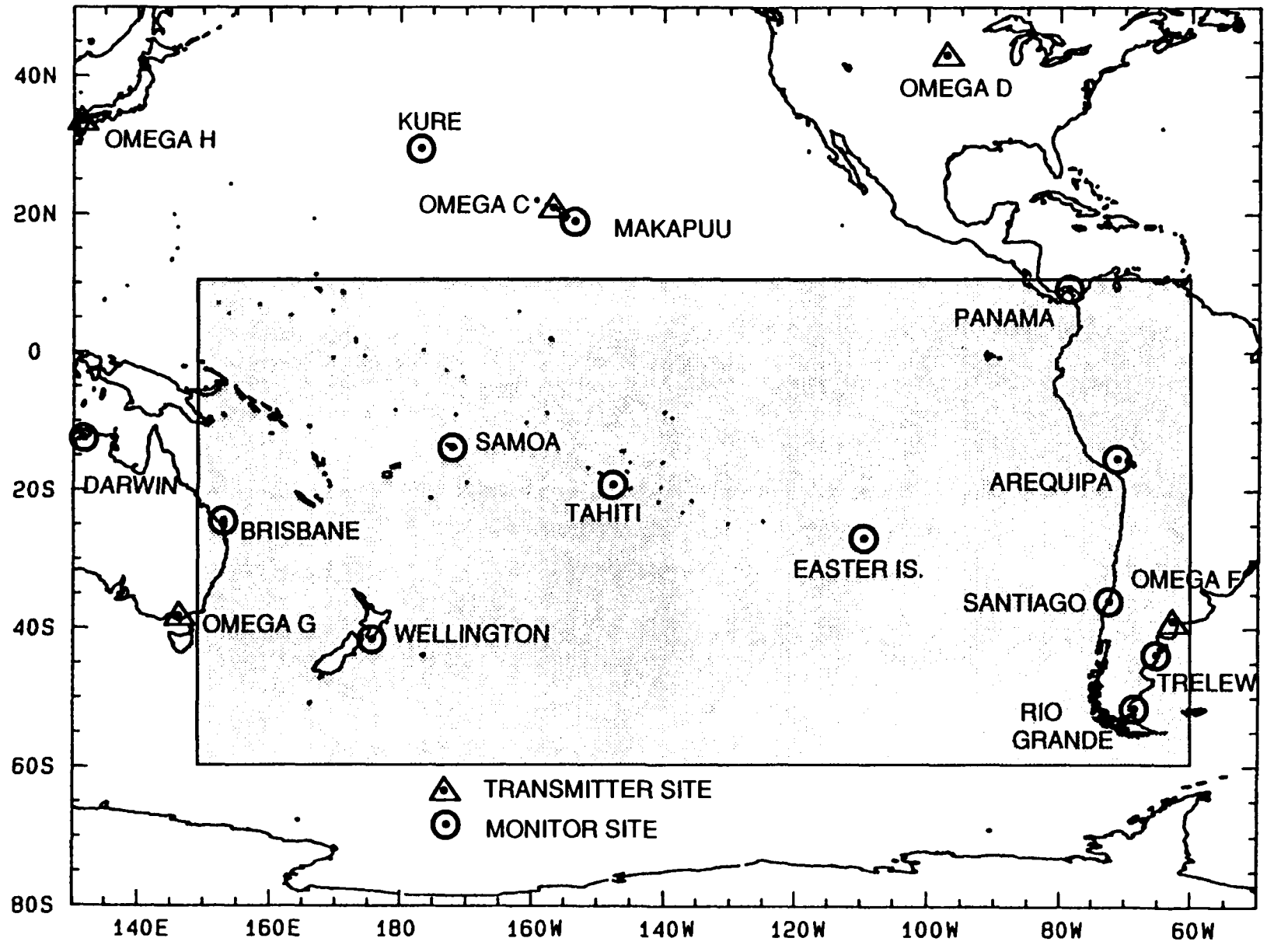

Figure 3-1. South Pacific Omega Ground Monitor Sites

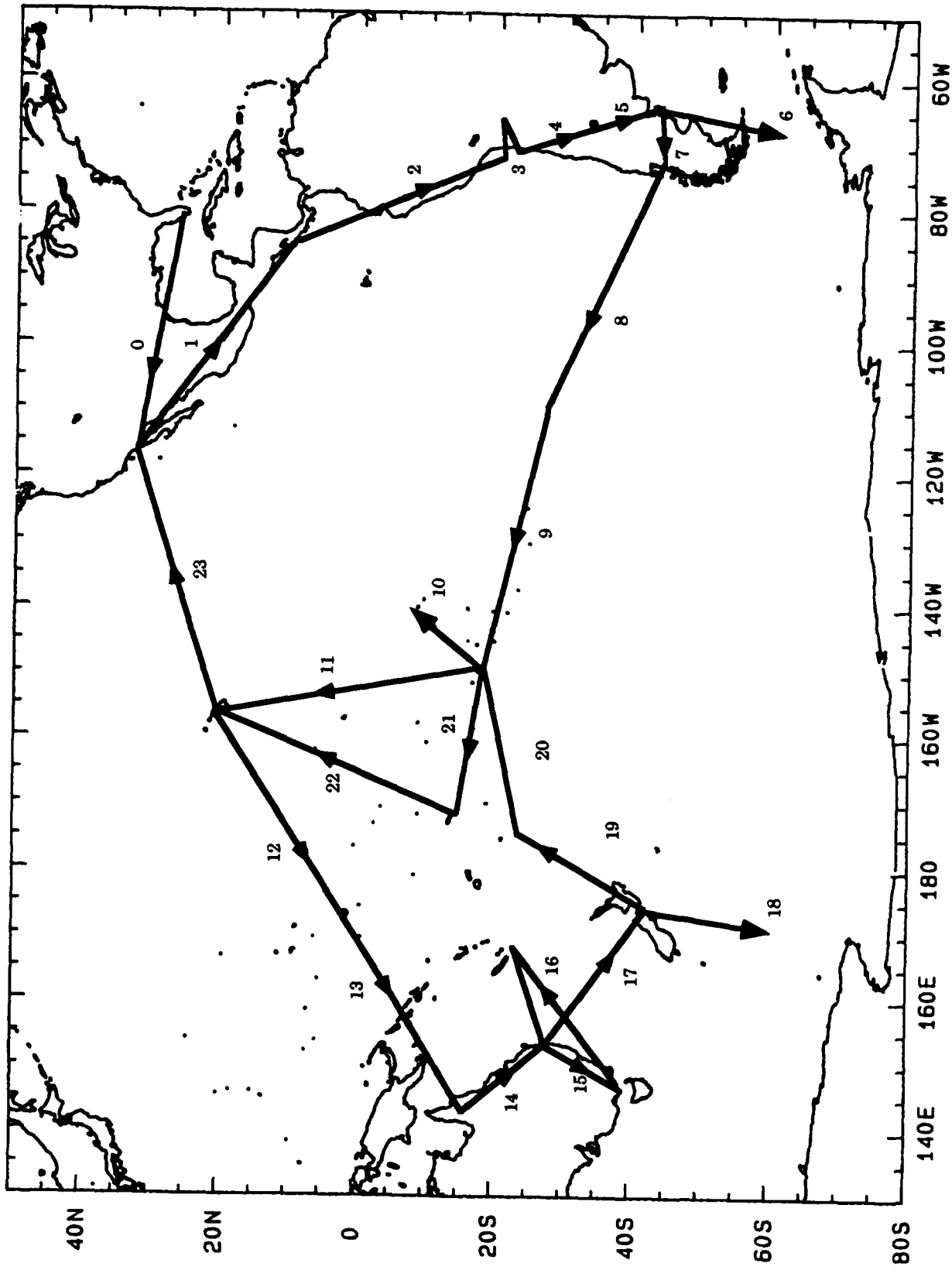

Figure 3-2 Flight Itinerary for USCG C-130 Aircraft

A/C FLT NO.	ORIGIN ID	ORIGIN TERMINAL NAME	DESTINATION ID	DESTINATION TERMINAL NAME	FLT. RANGE (N.MI.) DIR.	FLT. RANGE (N.MI.) PLAN	FLT. HOURS (@ 280 KT) DIR.	FLT. HOURS (@ 280 KT) PLAN	RADIAL HEADINGS	XMTR OVER-FLTS
00	PIE	CLEARWATER	SAN	SAN DIEGO	1802	1802	6+25	6+25	DIRECT	
01	SAN	SAN DIEGO	SJO	SAN JOSE	2275	2275	8+10	8+10	DIRECT	
02	SJO	SAN JOSE	LIM	LIMA	1388	1390	5+00	5+00	F338	
03	LIM	LIMA	AQP	AREQUIPA	420	420	1+30	1+30	DIRECT	
04	AQP	AREQUIPA	MDZ	MENDOZA	1001	1794	3+35	6+25	F338	
05	MDZ	MENDOZA	REL	TRELEW	647	724	2+20	2+35	F338	ARG
06	REL	TRELEW	RGA	RIO GRANDE	640	1424	2+15	5+05	F188	ARG
07	RGA	RIO GRANDE	PMC	PUERTO MONTT	771	1029	2+45	3+40	F188, F279	ARG
08	PMC	PUERTO MONTT	IPC	EASTER ISLAND	1975	1988	7+05	7+05	F279	
09	IPC	EASTER ISLAND	PPT	TAHITI	2292	2292	8+10	8+10	DIRECT	
10	PPT	TAHITI	PPT	TAHITI	2000	2006	7+10	7+10	D229	
11	PPT	TAHITI	HNL	HONOLULU	2383	2395	8+30	8+35	C167	HAW
12	HNL	HONOLULU	NR	NAURU	2441	2497	8+45	8+55	C238	HAW
13	INR	NAURU	KIE	BOUGAINVILLE	754	1686	2+40	6+00	C238	
14	KIE	BOUGAINVILLE	BNE	BRISBANE	1275	1860	4+35	6+40	C238	
15	BNE	BRISBANE	HBA	HOBART	964	995	3+25	3+35	G047, G174	AUS
16	HBA	HOBART	BNE	BRISBANE	964	2447	3+25	8+45	G174, C221	AUS
17	BNE	BRISBANE	WLG	WELLINGTON	1354	1354	4+50	4+50	DIRECT	
18	WLG	WELLINGTON	WLG	WELLINGTON	2000	2246	7+10	8+00	MCMURDO	
19	WLG	WELLINGTON	TBU	TONGA	1308	1336	4+40	4+45	C202	
20	TBU	TONGA	PPT	TAHITI	1460	1460	5+15	5+15	DIRECT	
21	PPT	TAHITI	PPG	PAGO PAGO	1232	1232	4+25	4+25	DIRECT	
22	PPG	PAGO PAGO	HNL	HONOLULU	2265	2320	8+05	8+15	C202	HAW
23	HNL	HONOLULU	SAN	SAN DIEGO	2267	2267	8+05	8+05	C064	HAW
24	SAN	SAN DIEGO	PIE	CLEARWATER	1802	1802	6+25	6+25	DIRECT	

Table 3-1. Flight Itinerary for USCG C-130 Aircraft.

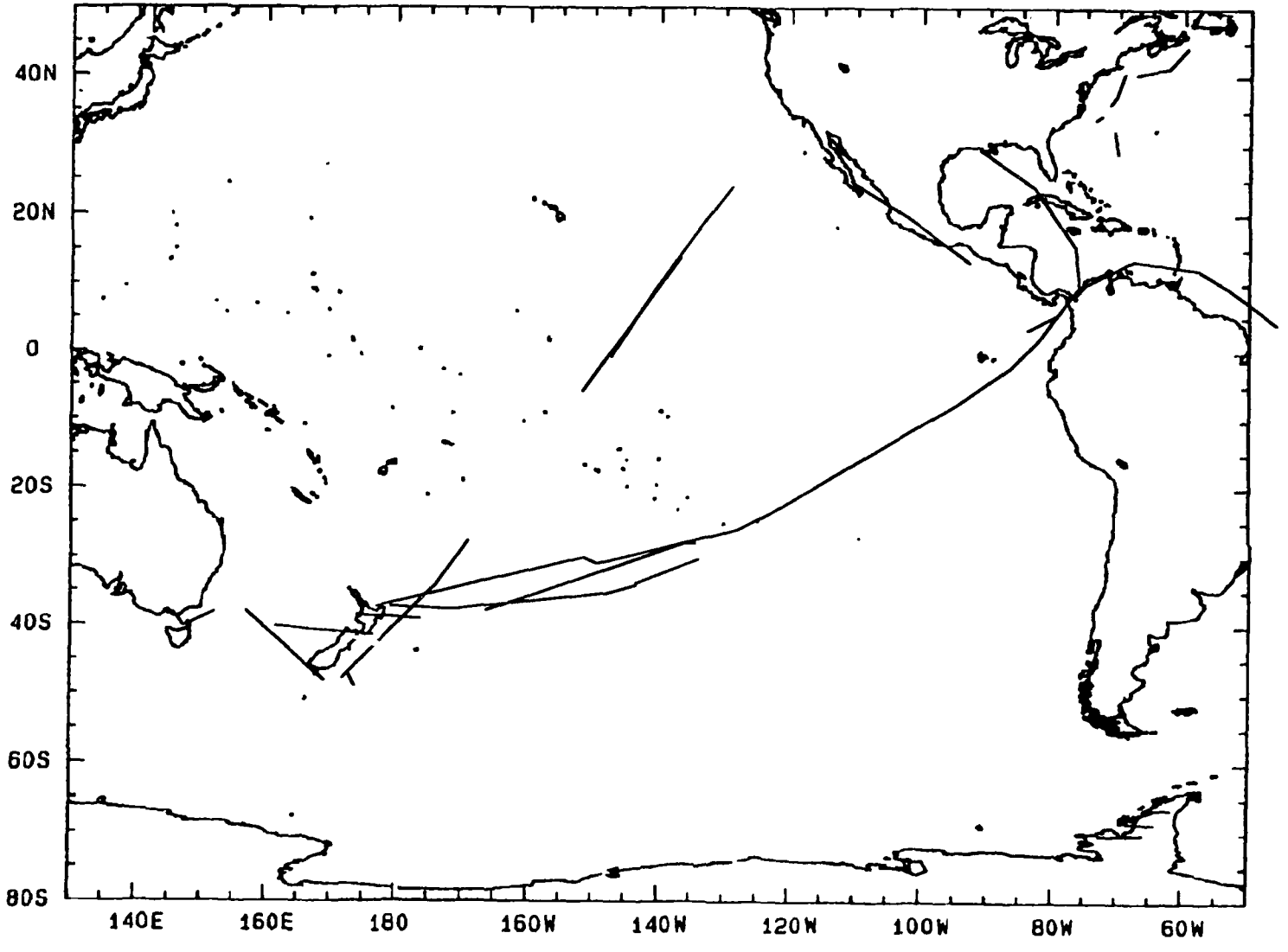

Figure 3-3. Approximate Routes for Vessels supplying MX-1105 Data

used directly. This phase data proved to be extremely valuable, both in support of the flight data interpretation and in devising effective procedures for assessing the phase-difference data.

Evidence of modal interference is readily noted in measurements of signal level versus distance. South Pacific aircraft data is plotted in the form of field strength versus distance in megameters. The criterion used for identifying severe modal interference in the data was that the signal level variation between successive relative maxima and minima exceeds 20 dB. As noted in the Modal Analysis section, it was found that modal competition from traversing modal conversion zones does not always produce fade patterns easily identifiable in flight data.

Because top priority was given to determination of modal interference caused by trans-equatorial propagation, the aircraft data were selected as the prime data for analysis. These data were augmented by the fixed-site data to obtain confirmation of observations and to determine temporal variation; primary fixed sites for the South Pacific are Tahiti, Samoa, Wellington, and Brisbane. Data from these fixed sites soon became the primary source for determining modal effects. The phase-difference data from other fixed sites was not used extensively because of time and resource limitations. Shipboard data was used, to the extent possible, to confirm the existence of modal interference in the ocean areas where fixed-site data were not available.

3.3 SIGNAL SELF-INTERFERENCE ANALYSIS

This subsection describes the analysis conducted to assess the occurrence of self-interference on the navigation signals. The overview presents a rationale for our order of presentation. This is followed by a general description of the analysis models developed to guide analysis. A detailed description of the model development is contained in appendixes A and C. The analysis is then summarized, again with amplifying details provided in appendixes B and D. This subsection sets the stage for evaluation and comparison of Omega coverage prediction presented in section 4 INTERPRETATION OF VALIDATION ANALYSIS.

3.3.1 OVERVIEW

The presentation is given as follows: (1) a discussion of the analysis guidance derived from results of signal prediction calculations, coverage diagrams, previous experience and a preliminary overview of the data, and (2) presentation and interpretation of the data sequentially by location. The primary interest is navigation, which depends upon signal availability, obtainable phase accuracy, and established confidence in predictions. Navigation is position oriented; thus we have chosen to focus on position and position accuracy as the analysis key. Our analysis presentation will identify and select subregions and/or boundaries of special interest or concern, and then assess the total signal resources available for navigation as related to the subregions and boundaries. The analysis was most effective when the data from all frequencies was compared for evidence of self-interference. Likewise, we feel that the total information content in the Omega navigation signals requires emphasis as a resource for navigation; thus the analysis of all frequencies is integrated.

A factor in conducting this and other validations is that resource constraints, time, data, and cost all imposed important limitations on establishing definitive conclusions. As described below, a less than ideal match often existed between the predictions of important regions and boundaries and the data available for assessment.

3.3.2 ANALYTICAL GUIDANCE

Several investigations have been made of Omega Signal Coverage that include consideration of signal self-interference (GUPTA 1980, SWANSON 1983, NALBANDIAN 1986 and GUPTA 1988). Each of these investigations offered significant insights for our analysis. Predictions made by Gupta and Swanson are compared with results of this analysis in section 4 *INTERPRETATION OF VALIDATION ANALYSIS.* Nalbandian and Tench produced a PC computer-based software program that displays signal coverage, the day/night terminator, and great circle propagation paths on maps. This software helped gain insight into the various geophysical factors contributing to predicted and observed signal reception. NOSC provided mode-sum calculations for selected station propagation radials that corresponded with selected flight paths. These calculations provided the most detailed samples of mode structure versus distance. The continuing

work of TASC in support of ONSCEN has produced the most detailed information. Their series of calculations was particularly useful because the strength of each contributing mode was plotted along with the mode sum.

No attempt was made to evaluate the merits of the various prediction models. Please note that all of these models are theoretical and thus cannot be expected to predict in detail the observed real world. Nevertheless, the models can provide a great deal of insight regarding what can be expected and how to interpret what is observed. Our primary goal in using predictions/calculations was to obtain guidance for the analysis interpretation. Following the analysis presentation a comparison of analysis products and various prediction methods is made.

Self-interference is defined as any condition where the navigation signal is not dominated by the mode for which the system was designed, i.e., mode 1 and short-path propagation (See section 2.1.1 *GUIDING PRINCIPLES* for discussions on propagation theory and self-interference/modal factors). Signal self-interference effects are placed into four categories for this analysis:

Near Modal: Mode competition originating close to a transmitter; this can extend to large distances when the attenuation rates of competing modes are only slightly different.

Mode Conversion: Mode competition resulting from propagation factors other than Near Modal, usually as a result of mode conversion occurring in propagation within the equatorial zone or across very low conductivity terrain. Also applied to the zone of higher-ordered mode dominance following propagation through an interacting region.

Mode Switching: Another mode achieving dominance at some distance from a transmitter; this results when an initially weaker higher-ordered mode has a lower attenuation rate than the first mode.

Long-path: Phase unpredictability caused by the first mode long-path signal's domination or interference with the first mode short-path signal.

The modal interference analysis consisted of preparing charts of zones where signal quality was suspect due to various types of modal interference. The Long-Path interference assessment was done separately, because this effect predominates when the short-path is in daylight, while the other effects occur when the short-path is mostly in darkness. Analysis guidelines rather than

formalized charts were prepared. The charts and analysis guidelines were then compared with the data collected on aircraft flights and at fixed sites.

Our most detailed guidance for determining the possibility of one of these self-interference conditions was derived from a series of calculations for Omega signal field strength versus distance for 10.2 and 13.6 kHz, produced by TASC for ONSCEN (GUPTA 1988). A sample of a calculation is shown in Appendix A Figure A-1. This series of calculations was the most complete set available. When we compared these plots with previous calculations, significant differences were found. Thus, rather than use existing geographic displays, we considered it prudent to convert the information in this series from radials to geographic plots of signal self-interference for each station. The creation of the geographic plots is described in Appendix A *Generation of Geographic Plots Showing Modal Competition.*

The first task was to examine the sets of calculations for each station in order to identify the possibility of one or more of the three modal conditions above. The three most important model features useful for analysis guidance are (1) the structure (signal fluctuation with distance) in the mode sum, (2) what modes contribute to the mode sum, and (3) what mode is dominant in the validation region. One important additional consideration is to assess how the propagation might differ for seasons other than local summer in the validation region when the data were acquired. This assessment was based largely on intuition and determination of differences in solar illumination patterns.

The results of the geographic plot preparation are described for each of the stations in the following subsections.

3.3.3 DISCUSSION OF ANALYTICAL GUIDANCE

We must emphasize that this material was prepared for analysis guidance. The material is intended to serve as a benchmark to assist in interpreting the data. These charts are not intended at this stage for navigation guidance.

The Omega navigation system is designed with redundant signal coverage. Conservatism suggests a policy of station deselection if the phase quality is in question. Thus, our analytical approach was first to determine, by geographic areas, which signals were candidates for deselection because of predicted un-

usable phase. Then, using available "good" phase signals, we determined the expected navigation capability by taking into account signal-to-noise ratio and geometry factors. We emphasized those subregions where the largest number of signals are flagged for possible unusable phase. If many signals are in question, it is much more important to determine the correctness of the prediction. On the other hand, if good signal redundancy exists, deselecting a signal is of little consequence.

Composite charts for 10.2 and 13.6 kHz were made from the charts for each station described in Appendix A. These composite charts show the locations of possible unusable phase that may occur at some time during the diurnal day. The composite charts are shown in Figures 3-4 and 3-5 for 10.2 and 13.6 kHz respectively. The shading of the zones of different coverage, shows the number of station signals that are in question. The shaded legend shown to the right of Figures 3-4 and 3-5 covers six levels. The predicted good signals are called out in each zone. For 10.2 kHz, Figure 3-4, a very small zone centered at 7°N, 137°W has six signals of possible unusable phase. The good signals are Australia and Japan. Adjacent to this zone are three zones showing five rejects and three good stations. The boundary surrounding these four zones is of the greatest interest.

For 13.6 kHz, Figure 3-5, the zone of six questionable signals is much larger, as are the three adjacent zones containing five questionable signals. The zone of six signals is centered at 6°N, 128°S. The good signals are Australia and Japan. An additional concern is that, in those zones where Hawaii (C) is predicted to be the third good signal, the bearings from Hawaii and Japan to locations within the zones are generally within a few degrees. In effect, the poor geometry relationship negates the value of one of these signals.

As shown in Figure 3-5, the 13.6 kHz signal also has three additional zones where only three signals are predicted to provide good coverage. These zones are all covered by four or more signals at 10.2 kHz. Assuming that these zone locations are valid, the concern would be during good station down times and then primarily for lane resolution.

A composite chart was made as shown in Figure 3-6, that combined the zones containing five or more signals of possible unusable phase for 10.2 and 13.6 kHz respectively and showed the aircraft flights. These areas need particular

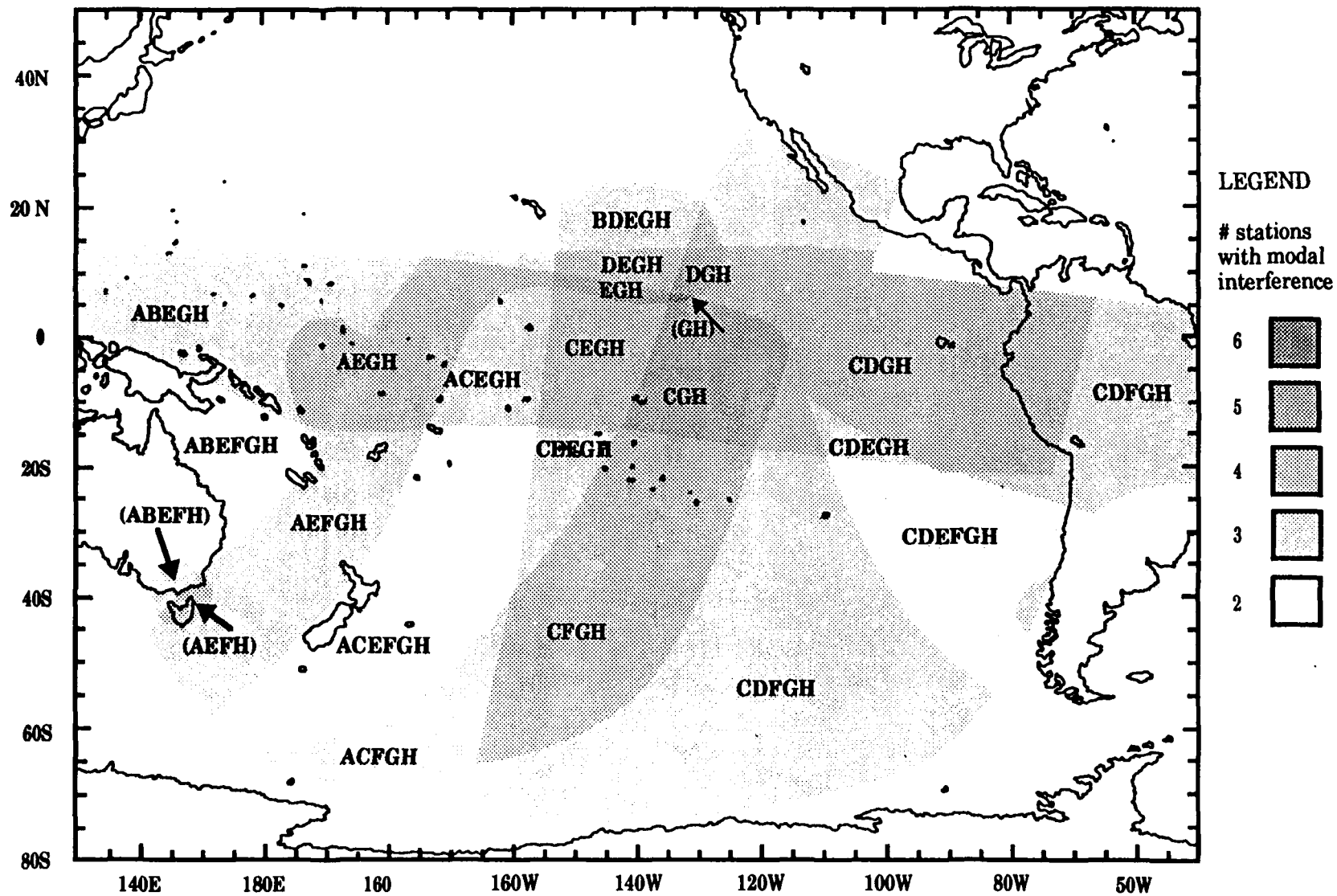

Figure 3-4. Composite Chart of Nighttime Propagation Modal Zones, 10.2 kHz

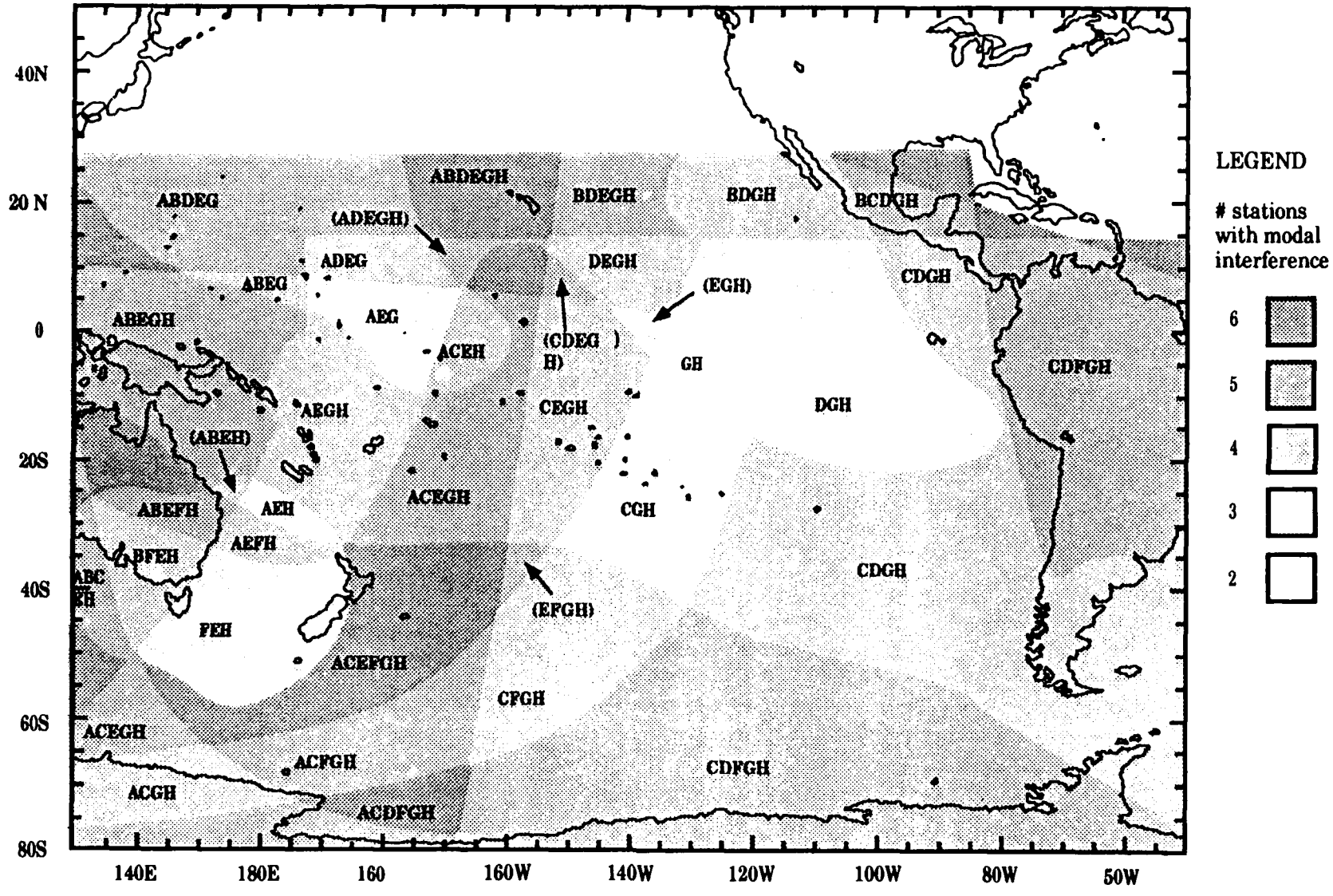

Figure 3-5. Composite Chart of Nighttime Propagation Modal Zones, 13.6 kHz

attention in the analysis. Unfortunately the zones of most concern lie primarily within the large segment not covered by aircraft or fixed-site validation measurements. Some shipboard data were collected on one transit through this area. The lack of data for the areas shown in Figure 3-6 contributes significantly to the uncertainty of analysis interpretation.

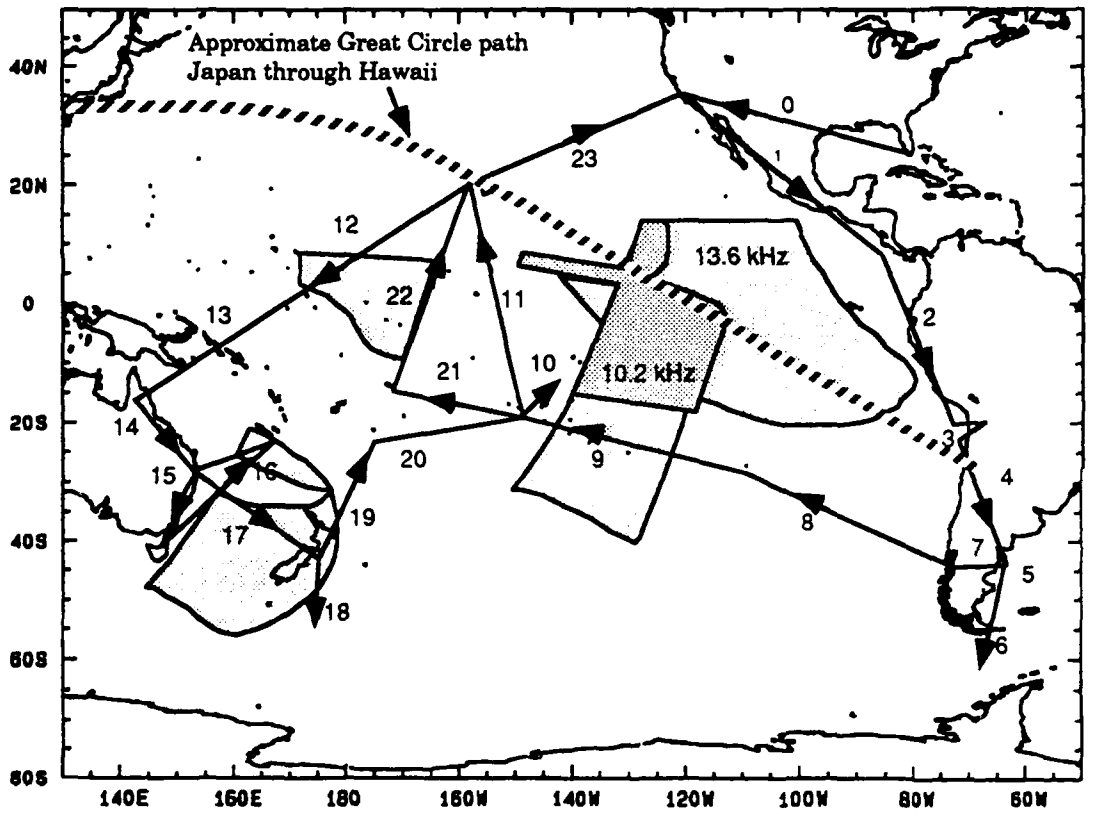

Figure 3-6. Areas Containing 5 or More Night Modal Zones, 10.2 and 13.6 kHz.

The propagation prediction calculations in this section were used as guidance for data analysis assessment and as a model for extending measurements to the total South Pacific Validation region. We emphasize that these charts are for nighttime propagation on each signal path and thus are time static: they do not take into account the diurnal variability of the zones of unusable phase. They are also seasonally static: variations in solar illumination at the poles are not integrated into the analysis. While these charts are considered a good model for validation data assessment, further interpretation is needed to derive navigation guidance.

3.3.4 DATA INTERPRETATION

OVERVIEW

The data interpretation was a complex process involving extensive preparation of the data and the comparison of many different data segments to achieve the interpretation presented here. The results of this interpretation are summarized in this subsection. A more detailed description of the interpretation process and findings is presented in Appendix B.

The procedure used in Appendix B for data interpretation was to work across the validation region following the sequence of flights. The process used for each flight was (1) to determine for each station what the calculations predicted would be the dominant mode and signal amplitude structure along the flight and at each flight terminal; (2) to compare flight amplitude data with calculations; and (3), where available, to examine fixed-site phase data for possible modal effects.

Since the flight paths usually varied in both distance and azimuth with flight time, it was necessary to construct a predicted signal from a cross section of calculated radials. When the distance from the transmitter was large, the available radials, generally calculated at ten degree intervals, produced rather sparse prediction values along the flight path. This sparseness was a problem when the computed signals changed markedly between radials. Cross sections were prepared for each station for each flight. The cross-section data were then compared with received flight amplitude data.

The fixed-site phase and phase-difference data were used for two purposes. First, a check was made to determine, as much as possible, the propagation conditions at the time of flights. Second, a check was made to determine how the data at flight time related to the total data set available at that site.

The fixed-site data were processed in several different ways depending upon the stability of the frequency reference at the measurement site. At those sites where the received phase was referenced to an atomic frequency standard, the diurnal phase for each received frequency was examined for evidence of modal influence. At sites where an atomic frequency reference was not available but the reference frequency was stable, the cumulative phase difference was measured between

successive midpath noon times on the best quality signal. This phase difference was then incrementally subtracted from all measurements. The ideal result was a nearly stable diurnal phase curve for each measured signal. In most cases, the reference oscillator frequency offset was sufficiently constant over a 24-hour period that the corrected phase plots could easily be evaluated for signal self-interference. When the reference oscillator was not sufficiently stable, phase-difference data between two received stations was examined. In using phase-difference data, an attempt was made to use a strong signal containing only a first mode as a reference for evaluating those signals suspected of having modal interference.

We note that it is easier to recognize the existence of modal competition in the presence of normal propagation variability by comparing the diurnal-phase data between multiple frequencies.

MODAL COMPETITION DATA ANALYSIS SUMMARY;

As noted in the overview for this subsection on signal analysis of self-interference (section 3.3.1 *OVERVIEW*), the primary focus for analysis is based on position. Position is what the navigator is interested in. The positions of recorded data are along aircraft flights, ship transits and at fixed recording sights. We found that the analysis was more definitive when it was possible to examine a group of data consisting of several aircraft flights and a fixed site as a hub for the flights. An example of such a group consists of the flights (9, 10, 11, 21, 20) to and from the hub Tahiti. This group, taken collectively, produces a more coherent picture. Not all flights fit into a convenient group.

The ship data were more representative of fixed sites (little change with time) and tended to be more isolated from the other measurement places. The shipboard data was most useful in conducting a qualitative check on position-fixing accuracy rather than on modal effects.

We have chosen to summarize the analysis by following the flights in approximate sequence, starting with the northeast corner of the validation region and progressing generally westward. Some exceptions are made in following the sequence of flights when it is considered beneficial to group the flights around a

hub. An example is the Hawaii hub group which includes flights 11, 23, 12 and 13, and 19 and 22.

Flight 1: (28 Jan 1985; 2240-0700) This flight data collection started near San Diego and ended just before Panama, Figure 3-6. This flight was north of the validation region, yet many signal propagation radials (either entering or exiting the validation region) cross this flight path.

Flight 1 Overall Summary: The data were neither consistent or inconsistent with calculations. Overall the data did not show the magnitude of structure or distance effects expected from the calculations. Collectively this supports an interpretation that the propagation parameters were changing throughout the flight. Some of the observed lack of predicted mode structure was on signals from northern latitudes. This may be partly seasonal. Seasonal changes in propagation are observed but have not been incorporated into VLF propagation models. Lacking more definitive information, we assume that the modal conditions shown in the calculations prevail.

Flight 2 and Arequipa: (28 Jan 1985; 0150-0800 GMT) This flight originated in Costa Rica and terminated west of Arequipa, Figure 3-6. This flight originated north of the equatorial zone and crossed most of the zone during the second half of the flight. Phase data were obtained for the Arequipa site.

Flight 2 Overall Summary: We conclude that the flight data provided a weak case for determining mode dominance or self-interference conditions. The trends identified provided some support for the calculations. Overall, the calculations showed more structure than was observed in the flight data. On the other hand, the Arequipa diurnal phase data produced clear evidence for the existence or nonexistence of either mode competition or mode switching. The findings from Arequipa are in general agreement with boundaries established for that location from calculations shown in the composite charts of Figures 3-4 and 3-5. The Argentina 10.2 kHz boundary should be moved slightly north, west, or northwest. The onset of mode switching from Argentina is expected to be very abrupt in moving northward; thus it is probably not safe to move this boundary very far. The Hawaii boundary probably does not extend as far east as shown. Based upon the lack of modal structure in the flight data and the clear single mode dominance at Arequipa, the worst case condition shown on the Hawaii chart,

Figure A-7, is not probable. We estimate that the boundary, at least for this time of year, is slightly west of the mode crossover line shown in Figure A-7. Caution should be exercised in moving boundaries, especially for other seasons, as propagation conditions may change with time and season.

Flight 3: (28 Jan 1985; 1100 to 1300 GMT) Flight 3 was a short flight from Lima to Arequipa. Since Arequipa was in early daylight, the flight did not produce data useful for modal analysis.

Flight 4: (30 Jan 1985; 2200 to 0600 GMT) This flight originated west of Arequipa and flew over the Argentina transmitter. All of the flight was well south of the equatorial mode-conversion zone. Phase data obtained at the Arequipa site was described as part of flight 2.

Flight 4 Overall Summary: The combined flight and monitor-site data support the phase dominance conditions established by predictions. A zone boundary for Norway at 10.2 kHz was predicted near the middle of the flight path. The flight data show modal, but the particular mode dominance cannot be tested. The zone boundary for La Reunion at 10.2 kHz is predicted from calculations to be approximately 1/3 along the path. The flight data show evidence of modal. Considering the strong modal effects evident at Arequipa, the zone could extend farther south than predicted.

Flights 5, 6, and 7 Argentina Near Zone Radials: (01, 02 and 04 Feb. 1985; respectively 0600 to 1130, 1630 to 2200, and 1930 to 0100) These flights were most useful for assessing the near-zone modal effects for the Argentina transmitter.

Flights 5, 6 and 7 Overall Summary: The predictions place the greatest extent of near-zone modal to the east of the Argentina transmitter. No flights covered this sector of the near zone. The predictions along flights 5 and 6 show the zone to extend slightly farther than the data indicates. When considering ionosphere variability and the need for safe predictions, the near zone boundary is considered appropriately located at night for the two radials checked.

Flight 8: (06 Feb. 1985) This flight originated west of the Argentina transmitter and followed approximately a 280° radial from the transmitter to Easter Island. The flight path does not cross any boundaries between the modal zones shown in Figures 3-4 and 3-5.

Flight 8 Overall Summary: With the exception of the Hawaii signal, the modal zones predicted from calculations are largely confirmed. All signals appear to have somewhat less modal than the calculations show. The Hawaii signal has much less modal structure than the calculations predict. Adjustment of the Hawaii modal zone boundary to smaller distances than the calculations predict is the only change that appears appropriate. As yet, how much adjustment to recommend and whether the adjustment should be by seasons is uncertain.

Flight 9: (09 Feb. 1985) This flight originated at Easter Island and terminated at Tahiti. Several modal-zone boundaries are crossed along the flight path, the most significant being for North Dakota (see Figures 3-4 and 3-5). Phase data obtained at Tahiti are described as part of the next flight group.

Flight 9 Overall Summary: The data recorded on flight 9 follow the established pattern from previous flights indicating the boundaries where modal-dominance switches are not easy to define from the flight data. This is particularly true where the switch in dominance is due to bearing from the transmitter rather than distance, and where the dominance is the result of either terrain conductivity effects or traversing the equatorial mode conversion zone. We conclude that, insofar as the data can be interpreted, the data support the zone boundaries established from calculations. Some adjustments may be possible, but an overall decision should be based on all of the analysis and is better addressed in the analysis summary.

Tahiti Phase Data and Flights 10, 11, 20, and 21: (11 & 13 Feb., 1 & 3 Mar. 1985) Tahiti is the hub for all of the flights grouped for this sub-analysis. The Tahiti phase data provide a definitive interpretation of modal conditions, especially diurnal switching of modes, and is thus strong support for interpretation of the adjacent flight data. Tahiti and all of these flights are to the east of the most critical subregions for unusable phase (see Figures 3-4 and 3-5).

Tahiti Area Overall Summary: The phase data for Tahiti confirm the calculation predictions of modal zones at Tahiti. The flight data tend to support both the predictions and the Tahiti data. As observed before, the flight data are weak indicators of the transition between modal zones. The Hawaii signal has modal structure that extends 300 km further south than predicted. Other positions of

zone boundaries could not be determined with sufficient accuracy to test predictions.

Hawaii Area and Flights 23, 22 and 12: (6 & 4 Mar & 15 Feb. 1985) Two objectives are emphasized for analysis in the Hawaii area. The first objective is to explore the extent of the near zone for Hawaii, and the second is to test those predictions for Hawaii and the associated flight paths that can confirm predictions for the South Pacific Validation region. Flights from or to Hawaii (number 23 to San Diego, number 11 from Tahiti, number 22 from Samoa, and number 12 & 13 to north east Australia), produce a good test of the Hawaii signal near-zone predictions.

Hawaii Area Overall Summary: The region around Hawaii largely fits predictions. For both the Hawaii and Japan signals on bearings to the southeast, the modal structure could, on the average, be somewhat less than predicted. Where a higher-ordered mode dominance was predicted, the flight data supported or at least did not conflict with the predictions. The 202° radial from Hawaii shows significant modal structure on the Hawaii signal. The modal-zone boundary for Hawaii should be moved counter-clockwise a few degrees, at least for February. Until further confirmation is obtained, the other calculation predictions should be considered valid.

Flight 13: (16 Feb. 1986) Flight 13 was located in the northwest end of the validation region on an extended radial from Hawaii to northern Australia. In that part of the validation region covered by flight 13, the signals of primary concern for possible self-interference are stations (B) Liberia antipode, (C) Hawaii, (D) North Dakota, and (F) Argentina.

Flight 13 Overall Summary: No disagreements were found with the predictions from calculations. The tests for modal where predicted were weak. The predictions from calculations should be used to define regions of modal problems until additional testing is undertaken.

Flights 14, 15, 16: (18, 21 & 22 Feb 1985) These flights were in the vicinity of Australia. In that part of the validation region covered by these flights, the signals of primary concern for possible self-interference are stations (C) Hawaii, (D) North Dakota, and (G) Australia. Hawaii and North Dakota are predicted to

have mode 2 dominant from traversing the equatorial zone. The predicted near-zone modal of Australia was measured in this flight set.

Flights 14, 15 & 16, Overall Summary: The near-zone modal boundary for Australia was checked at night on two radials. Both sets of measurements showed that at least for those nights and on the measured radials the boundary distance should be increased. The distance increase should be about 100% for both frequencies.

The predicted mode 2 dominant conditions for both the Hawaii and North Dakota signals was confirmed.

Long-path effects were noted on the the Argentina signal. We estimate that the long-path interaction could be significant for as much as 14 hours along the eastern edge of Australia.

Wellington, NZ site and Flights 17, 18 & 19: (24, 26 & 28 Feb. 1985) The area around New Zealand is predicted to have five signals available to the west and six to the east. New Zealand is predicted to be on the border of the modal zone for the Hawaii signal, within the modal zone for the North Dakota signal and on the border for near zone modal for the Argentina signal.

Wellington site and Flights 17, 18 & 19, Overall Summary: The major uncertainties in prediction of signal quality were for the Hawaii, North Dakota and Australian signals. Both the Hawaii and North Dakota signals are within a modal zone in the vicinity of Australia.

The modal-zone border for Hawaii, derived from calculations, needs to be moved further to the east, at least for February. Since the calculations predict a very abrupt transition from mode 1 dominance to mode 2 dominance with bearing change, it is difficult to estimate how far east the boundary should be moved.

For North Dakota, the calculations predicted that the New Zealand area is well within the mode 2 dominance zone. The confirmation from measurements adds support for the calculation model. Some evidence was produced to suggest that the 13.6 kHz boundary may actually extend farther south in the area of flight 18 than predicted. The prediction that the 13.6 kHz modal near zone would extend close to New Zealand was confirmed. A

conservative approach is to place this boundary slightly to the east of Wellington.

3.3.5 SUMMARY OF SIGNAL QUALITY ANALYSIS

This analysis has consisted of two parts: signal coverage in terms of Signal-to-Noise Ratio, and phase quality in terms of concerns for signal self-interference.

The signal-coverage analysis consisted of a quick check to determine if any cases existed where the measured SNR was less than the predictions. The procedure was to determine where and when the measured SNR fell below the threshold margins of coverage predictions, these being -20 and -30 dB SNR. Only a few cases of inadequate SNR were noted.

The phase-quality analysis consisted of preparing charts of zones where signal quality was suspect due to various types of modal self-interference. The interference conditions considered were (1) near-zone modal; (2) mode conversion zones, trans-equatorial or trans-polar; and (3) zones of higher-ordered mode dominance following mode conversion or due to less propagation attenuation of the higher-ordered modes. These charts were then compared with measurements from aircraft flights and from fixed sites. The zones predicted modal shown in the figures of Appendix A and the composite charts of modal zones, Figures 3-4 and 3-5, were found to be largely correct.

Several adjustments to the predictions of modal problem areas are suggested by the data, primarily in the zone locations for the Hawaii and Japan signals. The lobe to the east and southeast of Hawaii for the Hawaii signal can be reduced. No measurements were made close enough to the expected real boundary to allow a definitive reduction. Similarly, the lobe extending to the southeast of Japan for the Japan signal can be reduced. Again, data were insufficient to determine reliably what adjustments can be safely made. Finally, the Hawaii modal-zone boundary predicted along the 205° bearing needs to be moved counterclockwise. The predicted onset of modal competition was shown to be very sensitive to bearing. A better determination of proper placement for this boundary could be achieved by more detailed modeling over the range of angles between expected negligible and full mode competition, 195° to 210° bearing from Hawaii. A variety of possible propagation parameters should be analyzed.

Please note that the composite charts on modal zones, Figures 3-4 and 3-5, do not include time intervals for the conditions cited. Better guidance can be provided by assessing the diurnal characteristics of each signal to determine the times for which each modal zone is active. Much of the data indicate that modal effects, when present, can occur from near the beginning of sunset on the propagation path to near the end of sunrise on the path. Modal effects are observed to be somewhat ionosphere-dependent, as noted by the percentage of occurrences. These percentages are expected to change as the seasons progress. Some of the boundaries are thus expected to move; the question is how much.

Finally, it is worth restating that the modal problem is largely a nighttime propagation phenomenon. When a path is in daylight, the modal problems go away. However, these problems may exist for a large part of the day/night transition times. These transition times can be a high percentage (60 to 80%) of the 24-hour day for many of the locations examined.

3.4 LONG-PATH INTERFERENCE ASSESSMENT

3.4.1 OVERVIEW

The objective in assessing long-path interference effects is to determine within the validation region whether the coverage predictions adequately determine when and where stations need to be deselected. The determination needed is the placement of the boundary for the long-path zone. This boundary shows the long-path's maximum extent into the short-path region.

The occurrence of long-path signal interference has a quite different pattern in terms of location and time than the above described short-path signal self-interference. Long-path interference can extend in either direction from the signal antipode, depending upon which propagation direction along the great circle paths has the lowest signal loss. Typically the long-path/short-path boundary will move along each great circle path in a daily cycle from an initial location to its maximum extent on one side of the antipode, back through the antipode to the its maximum extent on the other side of the antipode and then return to its initial location. The maximum extent along any given radial of the

long-path signal into the short-path side occurs when any nighttime propagation conditions are completely on the long-path. The most extensive long-path interference is almost always to the east of the antipode of each station. However, terrain conductivity and solar illumination conditions have a strong influence on the location of the long-path/short-path boundary.

The assessment of long-path effects is challenging because identification of the effects must be inferred from the measurement data that are (1) a composite of many possible phenomena, (2) seldom acquired at optimum locations, and (3) from a few locations that are widely separated. For these reasons interpretation of the data depends heavily upon using a model to guide the interpretation. Data from both fixed sites and aircraft is used to test for long-path effects. Each group of data, fixed sites and aircraft, required a different analysis procedure.

3.4.2 ANALYTICAL GUIDANCE

The assessment of long-path effects created this dilemma: the objective of the validations is to report observations as opposed to conducting research or developing a model. Yet we found the data almost impossible to interpret without some guidance as to what to expect. Nor were we able to acquire a model for predicting long-path effects that we considered adequate to provide the needed guidance. Our requirement was to assess the prediction of boundaries and as predicted by the parametric model from data at locations generally far from the boundary. We concluded that the most useful parameter was the time dynamics of boundary movement. The parametric model which provides the best description of long-path effects does not provide the needed time and special detail. Consequently we prepared a simple model by extending the TASC Omega propagation calculations as described in Appendix C.

The technique (described in more fully in Appendix C) consisted of a simple drafting procedure to extend the field strength predictions beyond the 19 Mm distance provided by TASC. The major challenge was to account for the fact that the long-path prediction had to include a mix of day and night propagation. We expect that modeling propagation across a terminator cannot be well represented without using full-wave computational techniques. Thus our method is at best a first order approximation consisting of connecting the appropriate extended

segments of TASC's day and night propagation calculations. Nevertheless the resulting predictions proved useful in guiding our data interpretation.

Since the long path always includes at least as much daylight propagation as the extension beyond the antipode, the method for connecting the day and night portions must be carefully considered. When day is on the first part of the path, the higher-ordered modes are highly attenuated before the night portion begins. Thus, except for mode conversion such as propagation in the equatorial conversion zone, the nighttime fields, which comprise the long-path part, would be expected to have mostly mode 1 content. When night is on the first part of the path, the higher-ordered modes are highly attenuated after the day portion begins. Thus the daytime fields, extending into the long-path region, would be expected to have mostly mode 1 content. Based upon this reasoning we used only the mode 1 component of the TASC predicted signals to construct the boundary of long-path dominance. The method used is illustrated in Appendix C.

Since the data collection locations were seldom at the long-path boundary's maximum extent a means of estimating this maximum extent relative to the measurement locations to be devised. For sites within the long-path region part of the time, prediction of the time of boundary crossings provides a test of the model. Two crossings occur each day, one as the boundary moves outward from the antipode and one as it moves towards the antipode. The prediction of these crossings requires estimating how the boundary moves in relation to the terminator. This movement is related to the maximum extent of the boundary, to the relative attenuation rates of each path and to the rate of movement of the terminator along the path. For this analysis we simply used calculations of the day/night terminator positions on the earth's surface to estimate where to switch from day to night propagation or vice versa should be made. More refinements to this model are easy to devise and should be added for future analysis.

Comparison of measured crossing times relative to predicted ones provides guidance for adjusting the predictions. The adjusted predictions are then used to determine the maximum extent boundary of long-path effects. The findings of this comparison analysis is described in the next subsection.

3.4.3 DATA INTERPRETATION

A summary of findings regarding long-path effects is presented here; a more detailed description is in Appendix D. The model predicts that five of the eight Omega stations have long-path effects within the South Pacific validation region. These stations are Norway, Liberia, North Dakota, La Reunion, and Argentina. For these stations long-path effects were confirmed on at least Liberia and La Reunion. The phase records of both of these stations exhibited very strong and lasting long-path effects at Arequipa. The boundary for the Liberia long-path zone definitely lies much farther east than the prediction showed. We estimate from the data analyzed that the boundary should be placed near or east of 40° W. Longitude at 15° S. Latitude. Data from sites placed farther east should be examined to properly locate the Liberia long-path zone boundary. We estimate that the La Reunion long-path zone extends almost to the west coast of Africa as predicted by the model. This estimate is based on the observed long duration between long-path boundary crossings shown in the Arequipa data. Tests for long-path effects on the other stations were generally inconclusive, since the analyzed data were not well suited to obtaining definitive assessments of the predictions. The opportunities for further analysis exceeded our budget resources. As noted in Appendix D, both data from some sites without atomic frequency references and much of the aircraft data were not fully analyzed. The data processing requirements to place the data in interpretable form were in excess of our resources. We believe this unprocessed data, while difficult to retrieve, contains useful and much needed information.

3.4.4 DISCUSSION OF LONG-PATH EFFECTS FINDINGS.

The investiga'' ›n of long-path effects was cursory thus, we are hesitate to make definitive claims. The extension we made of calculations predicts that long-path effects cover large areas and for long time intervals. The data show that phase deviations from the predicted short-path phase can be very large, over 100 centicycles even when the long-path signal is not clearly dominant. Of course, long-path dominance produces the wrong sense of direction for platform movement. While our analysis does not provide a good test of the model used for guidance we are confident that the

predictions give a realistic indication of the long-path problem and thus of the importance of validating locations of zone boundaries.

In conclusion we feel that this described analysis technique provides a good start for assessing/validating long-path effects. The guidance obtained allowed us to make some estimates of long-path zone boundaries and the data showed that adjustments were needed for the Liberia signal boundary. The model can easily be used and further calibrated with additional measurements. The evidence clearly shows that long-path effects are an important part of validation assessment. We consider the data obtainable from any single validation region to be insufficient to conduct a definitive analysis because of measurement site locations relative to zone boundaries and because of the wide separation between sites. However, it is expected that if an analysis includes many regions and the data is used to validate and refine a model, high confidence can be achieved in using a model to place long-path zone boundaries.

3.5 SIGNAL-TO-NOISE-RATIO ASSESSMENT

This subsection describes the signal-to-noise-ratio analysis and presents the findings on how well the measurements support the predictions. SNR topics presented are SNR Data, Observed SNR performance, SNR predictions, Comparison, and Summary.

3.5.1 SNR DATA

The SNR data measured for the validation were received on Magnavox MX-1104 receivers at the fixed sites. Received SNR from all eight Omega stations was recorded at three South Pacific monitor sites: Rio Grande, Easter Island, and Tahiti. The data were provided in the form of computer-generated plots for two-week periods of the average and standard deviation of SNR for three frequencies: 13.6, 11.33, and 10.2 kHz. Figure 3-7 is an example of the SNR versus time curves. As shown in Table 3-2, the data were collected during the months of February and March 1985 at all three monitor sites. In addition, recordings were made during January and March 1985 at Rio Grande and Tahiti. Supplemental data were provided on

receipt of the Norway signal at Rio Grande for other months during 1985 and 1986.

3.5.2 OBSERVED SNR PERFORMANCE

The SNR versus time curves were examined to identify the occasions when the SNR fell below two thresholds: -20 dB and -30 dB. When either the average SNR or the upper or lower standard deviation fell below the threshold, the time was recorded. The following paragraphs discuss the SNR results by monitor site.

Rio Grande Site: Table 3-3 shows the results of observations at Rio Grande. All the SNR observations from four Omega transmitters (***Hawaii, North Dakota, Argentina,*** and ***Australia***) were greater than -20 dB at all three frequencies for all hours of the day. Also, the frequencies of 13.6 and 11.33 kHz from the ***La Reunion*** station were above the -20 dB threshold at all times. The lower standard deviation curve for the 10.2 kHz signal from La Reunion fell below the threshold for periods of two hours, from 0200-0400 GMT during January and from 1230-1430 GMT during April. Thus, the La Reunion signal was below the -20 dB threshold about 16 percent of the time during the time intervals cited.

The curve for the average SNR from the station in ***Japan*** was above the -20 dB threshold over 99% of the time. All observations at all frequencies during February and at 13.6 kHz during both January and March were above the threshold. For the remaining observations there were time periods of two to five hours between 1900-0000 GMT (daylight on most of the path) when the lower standard deviation curve (16% of the observations) fell below -20 dB.

The curve for the average SNR from the station in ***Liberia*** was above the -20 dB threshold over 98% of the time. All observations at 13.6 kHz during both February and March were above the threshold as were the 11.33 kHz observations during March and April. For the remaining observations there were time periods of two to five hours when the lower standard deviation curve and time periods of one hour when the average SNR curve

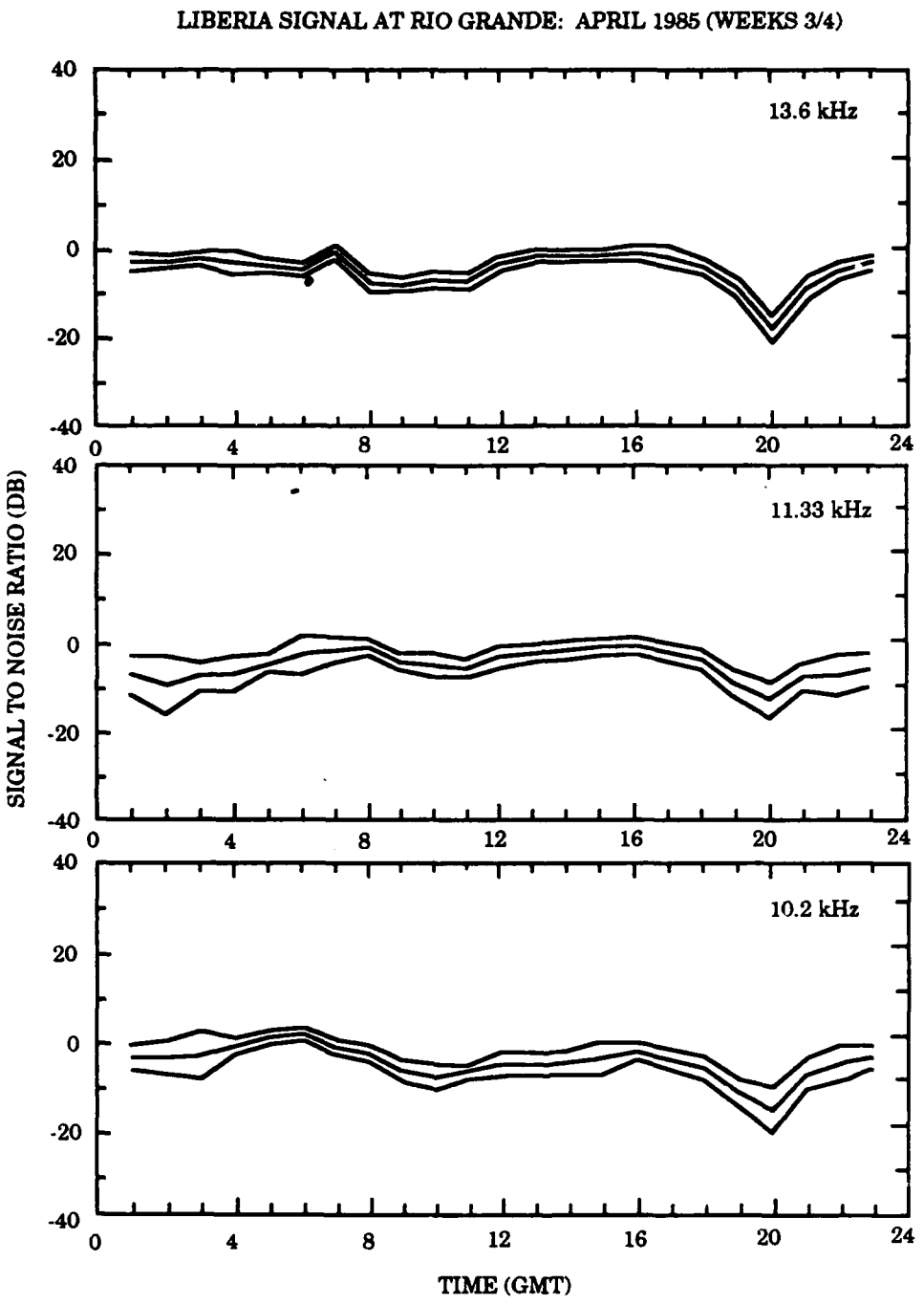

Figure 3-7. Sample Monitor Data

RECORDING SITE	A-NORWAY	B-LIBERIA	C-HAWAII	D-N.DAKOTA	E-LA REUNION	F-ARGENTINA	G-AUSTRALIA	H-JAPAN
RIO GRANDE								
JAN 85	X	X	X	X	X	X	X	X
FEB 85		X	X	X	X	X	X	X
MAR 85		X	X	X	X	X	X	X
APR 85	X	X	X	X	X	X	X	X
MAY 85	X							
JUN 85	X							
AUG 85	X							
FEB 86	X							
APR 86	X							
MAY 86	X					•		
JUN 86	X							
TAHITI								
JAN 85		X	X	X	X	X	X	X
FEB 85	X	X	X	X	X	X	X	X
MAR 85	X		X	X	X	X	X	X
APR 85	X		X	X	X	X	X	X
EASTER ISLAND								
FEB 85		X	X	X	X	X	X	X
MAR 85		X	X	X	X	X	X	X

Table 3-2. SNR Data Reviewed

		NORWAY	LIBERIA	HAWAII	N. DAKOTA	LA REUNION	ARGENTINA	AUSTRALIA	JAPAN
RIO GRANDE									
JAN 85	13.6	12*	3	0	0	0	0	0	0
	11.3	9*	5	0	0	0	0	0	5
	10.2	8*	4	0	0	2	0	0	3
FEB 85	13.6	ND	0	0	0	0	0	0	0
	11.3	ND	2	0	0	0	0	0	0
	10.2	ND	2	0	0	0	0	0	0
MAR 85	13.6	ND	0	0	0	0	0	0	0
	11.3	ND	0	0	0	0	0	0	3
	10.2	ND	1	0	0	0	0	0	5
APR 85	13.6	7*	0.3	0	0	0	0	0	2
	11.3	4*	0	0	0	0	0	0	2
	10.2	11*	3	0	0	2	0	0	3

* Data not available for full 24 hours
ND No data available

Table 3-3. Number of hours when SNR <-20 dB at Rio Grande

fell below -20 dB. For the most part, these observations of less than -20 dB SNR occurred during the time interval 1900-2100 GMT (transition from day to night at the transmitter), but there were some at 0700 in January.

There were no observations for either February or March 1985 from ***Norway***, and there were several time periods in January and April when there were no data. For January and April, there were few periods of time when the curves were consistently above -20 dB. It is estimated that about 80% of the observations at 13.6 kHz, and 60% of the observations at 11.33 and 10.2 kHz were above the -20 dB SNR threshold during January. During April, over 80% of the observations were above the threshold at all three frequencies.

Tahiti Site: Table 3-4 shows the results of observations at Tahiti. The statistics generated for two-week intervals were combined into monthly intervals except for March 1985. The March data was the only period where the statistics produced any significant differences. During the four month period, all the SNR observations from four Omega transmitters were greater than -20 dB at all three frequencies at all hours of the day. These

TAHITI			NORWAY	LIBERIA	HAWAII	N. DAKOTA	LA REUNION	ARGENTINA	AUSTRALIA	JAPAN
	JAN 85	13.6	ND	2	0	0	0	0	0	0
		11.3	ND	0	0	0.5	0	0	0	0
		10.2	ND	2	0	1	0	0	0	0
	FEB 85	13.6	17	2	0	0	0	1	0	0
		11.3	14	0	0	0	0	0.7	0	0
		10.2	2	0	0	2	0	0.5	0	0
	MAR 85	13.6	21	ND	0	0.2	0	1	0	0
		11.3	15	ND	0	0.2	0	0.5	0	0
		10.2	16	ND	0	1	0	0.5	0	0
	MAR 85	13.6	21	ND	0	0	0	1	0	0
		11.3	15	ND	0	0	0	0.5	0	0
		10.2	16	ND	0	1	0	0.5	0	0
	APR 85	13.6	24	ND	0	0	0	0	0	0
		11.3	24	ND	0	0.1	0	0	0	0
		10.2	24	ND	0	1	0	0	0	0

ND No data available

Table 3-4. Number of hours when SNR < – 20 dB at Tahiti

transmitters are ***Hawaii, La Reunion, Australia,*** and ***Japan***. Also, the frequencies at 13.6 and 11.33 kHz from the ***North Dakota*** station were above the -20 dB threshold at nearly all times; on a few occasions the lower standard deviation curve fell below the threshold for less than 1/2 hour. The lower standard deviation curve for the 10.2 kHz signal from ***North Dakota*** fell below the threshold for a period of one to two hours around 1300 to 1500 GMT (night-to-day transition on the path).

The curve for the average SNR from the station in ***Argentina*** was above the -20 dB threshold all of the time. All observations at all frequencies during January and April were above the threshold. For the remaining observations there were time periods of less than one hour when the lower standard deviation curve fell below -20 dB. These observations occurred around 1400-1500 GMT (night to day transition on the path).

There were no observations for either March or April 1985 from ***Liberia***. The curve for the average SNR from the station in Liberia was above the -20 dB threshold all of the time. Only observations at 13.6 kHz during both January and February and 10.2 kHz during January were below the threshold. These observations were for time periods of two hours occurring between 0500 and 1000 GMT (day to night transition on the path).

There were no observations for January 1985 from ***Norway***. During the other three months, the upper standard deviation curves were frequently below the -20 dB threshold, and there were very few periods of time when all curves were consistently above -20 dB. The one exception is 10.2 kHz during February when only the period 1600-1800 GMT showed low SNR values; otherwise SNR was above the -20 dB threshold. For February it is estimated that only about 80% of the observations at 13.6 kHz, 70% of the observations at 11.33 kHz and 90% of the observations at 10.2 kHz were above the -20 dB SNR threshold. During March these percentages were 60%, 73% and 70%, and in April they drop to 20%, 40%, and 40%.

Easter Island Site: Table 3-5 shows the results of observations at Easter Island. There were no observations for Easter Island in January or April 1985 or for ***Norway*** at any time. All observations for ***Hawaii,***

		NORWAY	LIBERIA	HAWAII	N. DAKOTA	LA REUNION	ARGENTINA	AUSTRALIA	JAPAN
EASTER ISLAND									
FEB 85	13.6	ND	0	0	0	12*	0	0	0
	11.3	ND	7	0	0	18*	0	0	0
	10.2	ND	9	0	0	8*	0	0	0
MAR 85	13.6	ND	3	0	0	17*	0	0	0
	11.3	ND	9	0	0	18*	0	0	0
	10.2	ND	15	0	0	11*	0	0	0

* Data not available for full 24 hours
ND No data available

Table 3-5. Number of hours when SNR < – 20 dB at Easter Island

North Dakota, Argentina, Australia, and ***Japan*** were above the -20 dB threshold for all three frequencies. For ***Liberia***, 13.6 kHz showed the best performance and 10.2 kHz the worst. The ***Liberia*** observations were less than -20 dB for periods ranging from 3 to 15 hours. The ***La Reunion*** observations were less than -20 dB for periods ranging from 8 to 18 hours.

3.5.3 SNR PREDICTIONS

Appendix C of the South Pacific Test Plan combines computations for signal amplitude versus radial distance with noise predictions that yield contour diagrams of -20 and -30 dB SNR for all stations as determined from the Coverage Model (GUPTA et al 1979). The contours shown are an expanded set constructed from the basic coverage diagrams published for ONSCEN (GUPTA et al 1980). Appendix D of the South Pacific Test Plan presents contour diagrams of -20 and -30 dB SNR for single stations. These contours are also determined from the Coverage Model. The contours shown are single month/time contours on an expanded map scale for only the validation area. The contours are for each Omega station for the month of February at 0600 and 1800 GMT and are constructed from the basic coverage diagrams documented by Gupta (GUPTA et al 1980). These prediction contours at the 0600 and 1800 GMT control times are used as a basis for comparing the observations in the next section.

3.5.4 COMPARISON

3.5.4 COMPARISON

Table 3-6 compares the SNR observations for 0600 and 1800 GMT during the month of February with the predictions discussed above. There are 48 combinations analyzed, consisting of three monitor sites, eight transmitting stations and two times of day. In four of these cases there was no data. In all the remaining 44 cases, the observed SNR was greater than or equal to that predicted. In 29 of the cases, SNR was predicted to be greater than -20 dB and the observations confirmed the predictions. In the remaining 15 cases, SNR was predicted to be less than or equal to -20 dB. In each of those cases, the observed value was greater than predicted by as little as 2 to as much as 29 dB .

			A-NORWAY	B-LIBERIA	C-HAWAII	D-N.DAKOTA	E-LA REUNION	F-ARGENTINA	G-AUSTRALIA	H-JAPAN
RIO GRANDE										
	T 06	PRED	< -30	> -20	> -20	> -20	> -20	> -20	-30	< -20
		OBS	ND	-1	7	2	-9	20	-1	-5
		DIFF	XX	OK	OK	OK	OK	OK	-29	> -15
	T 18	PRED	< -30	< -20	> -20	> -20	> -20	> -20	-20	> -20
		OBS	ND	-10	-2	-8	-8	20	-6	-8
		DIFF	XX	> -10	OK	OK	OK	OK	-14	OK
TAHITI										
	T 06	PRED	-30	< -30	> -20	< -20	< -20	> -20	> -20	> -20
		OBS	-9	-9	12	-2	-10	8	10	8
		DIFF	-21	> -21	OK	> -18	> -10	OK	OK	OK
	T 18	PRED	< -30	< -30	> -20	> -20	> -20	-20	> -20	> -20
		OBS	-22	-3	13	-5	-1	-5	8	8
		DIFF	> -8	> -27	OK	OK	OK	-15	OK	OK
EASTER ISLAND										
	T 06	PRED	< -30	< -30	> -20	> -20	< -30	> -20	> -20	> -20
		OBS	ND	-2 / -7	12 / 6	1 / -2	-25	15 / 10	7 / 4	7 / 4
		DIFF	XX	> -23	OK	OK	> -5	OK	OK	OK
	T 18	PRED	< -30	< -30	> -20	> -20	< -30	> -20	> -20	> -20
		OBS	ND	-15	7 / 7	-1 / -1	-28	6 / 6	2 / 2	2 / 3
		DIFF	XX	> -15	OK	OK	> -2	OK	OK	OK

ND No data available
OK Observed Equal to Prediction

Table 3-6. Comparison of SNR Observations with Predictions

3.5.5 SUMMARY

As predicted, redundant SNR coverage exists throughout the South Pacific validation area. This has been confirmed by analysis of SNR data from selected stations at the monitor sites. There are six Omega transmitters that provide SNR greater than -20 dB most of the times at Tahiti and Rio Grande and there are five at Easter Island.

3.6 NAVIGATION ACCURACY ASSESSMENT

3.6.1 OVERVIEW:

In undertaking the accuracy assessment phase of this validation, our perspective is that the nominal accuracy of OMEGA has been well established in past validations. We expect that the demonstrated accuracy is valid in the South Pacific and all remaining validation regions. For this reason we have chosen a new emphasis for accuracy assessment. In previous analyses, the available database was essentially processed into statistical compilations of measured LOPs and compared with predictions. In contrast, we have made spot checks using small data samples and representative locations and conditions. Our method, while confirming accuracy, is to primarily identify deviations from predicted accuracy and to focus on factors that can lead to improved utilization of OMEGA. This section, with the amplifying support of Appendix E, presents highlights of our findings.

3.6.2 DISCUSSION:

In order to conserve resources to focus on the principle objective, that of flagging deviations from predictions, we have been very selective in data processing. First, signals that have been identified as having problems from the other analysis (trans-equatorial modal, long-path interference or trans-polar) were not examined in this phase. Second, spot checks and quick scans were made to confirm close agreement with predictions. When the data did not meet our expectations a more detailed analysis was undertaken. Generally our expectations were based upon predictions and

undertaken. Generally our expectations were based upon predictions and what we considered reasonable variability due to propagation effects. Where trends are noted we use illustrative examples to describe the observed effects.

The analysis reported in Appendix E consists of three major parts:

(1) samples of tabulated two week segments of phase data which are compared with the computed PPCs (Propagation Phase Corrections) to illustrate observed trends

(2) samples of recorded phase for 24 hour intervals that are compared to the associated PPC, to illustrate observed trends or deviations considered significant

(3) samples of measured LOPs acquired during ship transits showing navigation fix accuracy and illustrating observed trends in signals.

Whenever possible, we examined phase data rather than phase difference data. This allowed us to attribute observations of the propagation to a single path. The illustrations provided, except the shipboard measurements, are phase data from fixed receiving sites having an atomic reference oscillator. This simplifies description of the observed effects.

3.6.3 SUMMARY OF ACCURACY ANALYSIS:

We found that, except for a few significant exceptions to be described, OMEGA phase accuracy is as specified. When signals are good, the median values are close to predicted and the deviation from the median is quite small; well within 10 CECs for the median, 10 CECs deviation from the median during midday on a path, and 20 CECs deviation at night. The predicted day/night phase change generally was very close to observed.

One significant exception is observed biases during the day/night transition times. Systematic deviations from predicted phase were observed in all examined cases. As shown in Appendix E with several examples, both sunset and sunrise transitions could benefit from time and slope adjustments. A pronounced characteristic of calculated PPCs is the

midday value. In the several dozen cases examined we never observed the magnitude of overshoot predicted. The mismatch is greatest when the transition is the most abrupt, i.e. short duration.

Many of the good signals in the South Pacific validation region undergo long transition times. For this reason, improving navigation accuracy for these times has added significance. The observed biases, occasionally as much as 20 CECs, appear to be reducible through improved calibration.

For a range of locations, several of the "good" signals propagate at high latitude, near Antarctica. Several measurements show, that under certain solar illumination conditions, the received phase varies greatly with propagation conditions. The possibility of large phase variability should be noted, although we do not know under what conditions, or over what area such variability will occur. The examples shown in Appendix E are for the Argentina and La Reunion signals in New Zealand. The effects on these signals noted in the Brisbane data were different than for New Zealand. The ship transit data also shows evidence that these signals do not fit predictions well.

The Japan signal at Brisbane does not fit predictions as well as expected. We suspect that some modal effects are involved, but not enough to negate navigation at Brisbane. We take this evidence as a flag to check Japan signal quality North of Brisbane. A more detailed analysis of the Brisbane data is warranted.

Overall, these findings fit the patterns established in other sections of this report and previous validations. OMEGA generally provides the navigation accuracy expected. Further improvements to the propagation predictions can and should be made. Our increasing knowledge of VLF propagation and its attended geophysics, adds to the awareness of complex factors determining the quality of navigation signals and consequently to our ability to refine navigation guidance.

4.0 INTERPRETATION OF VALIDATION ANALYSIS

This section places validation findings in perspective with expectations and other coverage predictions, and states specifically what was found to agree or disagree with those expectations and predictions.

In this section a comparison is made between the analysis findings reported in Section 3, the Analysis Model, and the two principal types of coverage prediction models used in navigation planning and analysis: the coverage overlay (GUPTA et al 1980, Ref. 21), and the parametric prediction (SWANSON 1983, Ref 22). Charts of each model prediction, showing individual station signal coverage of good quality phase, are presented as part of the comparison (for example, see Figures 4-1, 4-2, and 4-3).

4.1 PREDICTION MODELS

The foundation on which these models are built is highly complex. The reader is referred to the referenced documents for a description of model details. All three predictions are based primarily on theoretical models with feedback derived from measurements. Each theoretical model relies heavily on the fullwave propagation computational techniques developed at NOSC. In addition, in each case extensive use has been made of calculations prepared by TASC. Different sets of calculations made at various times were used by the different developers. Each model incorporates expert judgment of the developer.

For each model, only those features which address signal self-interference are considered. Again we emphasize that modal interference occurs at night on the short propagation path, while long-path interference occurs during the day on the short-path. For the coverage Overlay Model, the display used is the predicted boundary line beyond which phase deviation is predicted greater than 20 centicycles (CEC). For the Parametric Model, symbols are used to geographically present navigation signal quality. Table 4-1 defines the symbols used in the charts. The symbols of particular interest are N, Near interference; M, Modal; L, Long-Path; and, – , Disturbed.

Character	Limitation/ Meaning	Elaboration
N	Near	Within 1 Mm of station and potentialy subject to skywave-groundwave interference.
A	Antipode	Within 2 Mm of antipode and subject to antipodal interference
#	No Signal	SNR worse than -40 dB in 1oo Hz bandwidth
M	Modal	Second mode dominates or is within 1 dB of first mode
L	Long-Path	Long-path dominant or equal to short
-	Disturbed	Unwanted self-interference within 10 dB; either long-path or second mode
3	SNR in -30's	-40 < SNR >_-30 dB in 100 Hz Bandwidth; Usable in well installed good receiver
2	SNR in -20's	-30 < SNR >_-20 dB in 100 Hz Bandwidth
1	SNR in -10's	-20 < SNR >_-10 dB in 100 Hz Bandwidth
0	SNR in -20's	-10 < SNR >_-0 dB in 100 Hz Bandwidth
Blank	Loud and Clear	Signal should be well received by poorly installed mediocre receiver

Table 4 – 1. Parametric Coverage Display Code

4.2 COMPARISON OF THE VALIDATION ANALYSIS WITH COVERAGE PREDICTIONS

The analysis findings are compared with the two published models, addressing in sequence the predictions for each station. For the following discussion, the prediction models described above are called the Analysis Model (developed in Section 3), the Overlay Model (GUPTA 1980, Ref. 21), and the Parametric Model

(SWANSON 1983, Ref. 22). The process is to compare the predicted coverage for each station by showing a selected figure for each model and by discussing the findings in relation to the models.

(A) Norway:

For Norway the Analysis Model and the overlay modes show quite different boundaries of good phase. The northern boundry of the Analysis Model is created by the effects of low latitude propagation mode conversion. Given that the Tahiti data shows strong evidence of mode switching, we argue that the boundary should be north of Tahiti for both 10.2 and 13.6 kHz. For the Overlay Model at both frequencies, the position and shape of the boundries for the northwest corner on the chart are not consistant with the predicted abrupt occurence of modal onset with bearing change.

The Analysis Model shows a subregion of no modal effects at 10.2 kHz in the area around the lower part of South America extending to Antarctica. The existence of this subregion is not confirmed. Both of the other models predict an unreliable signal for this subregion. Since the propagation path

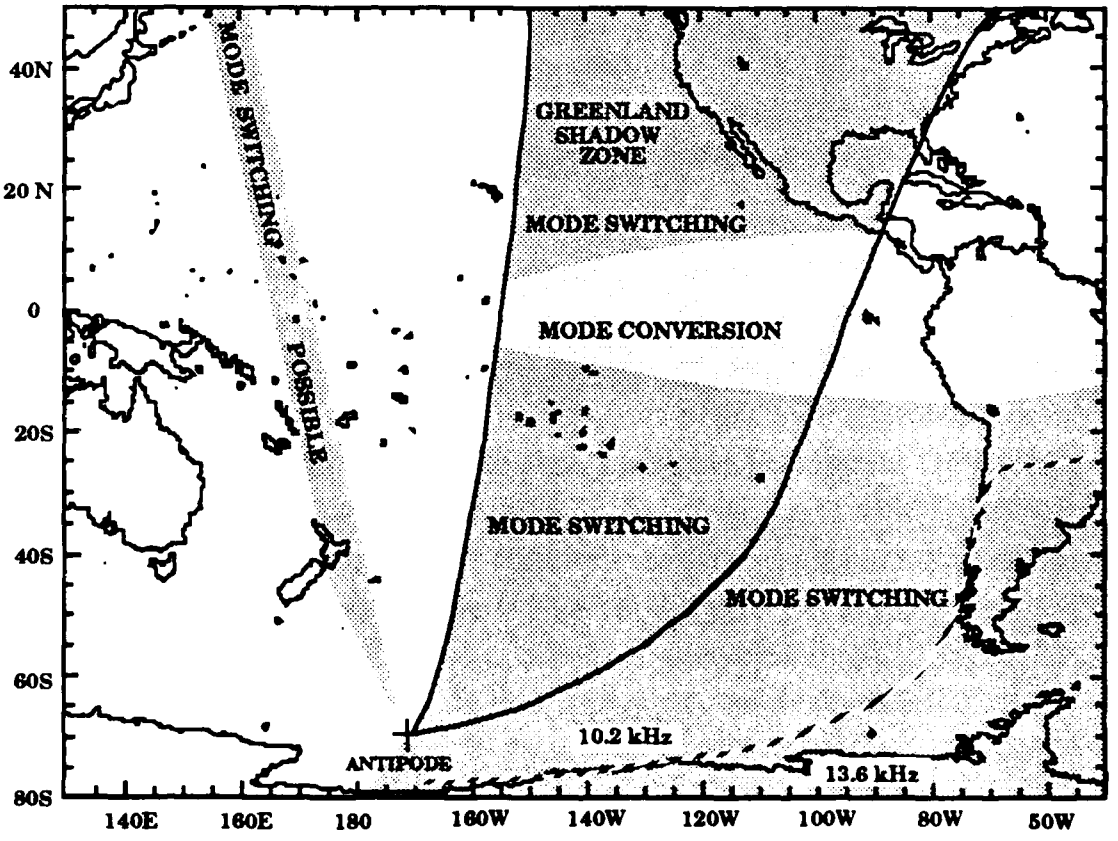

Figure 4-1. Norway Signal Self-Interference; Analysis Model

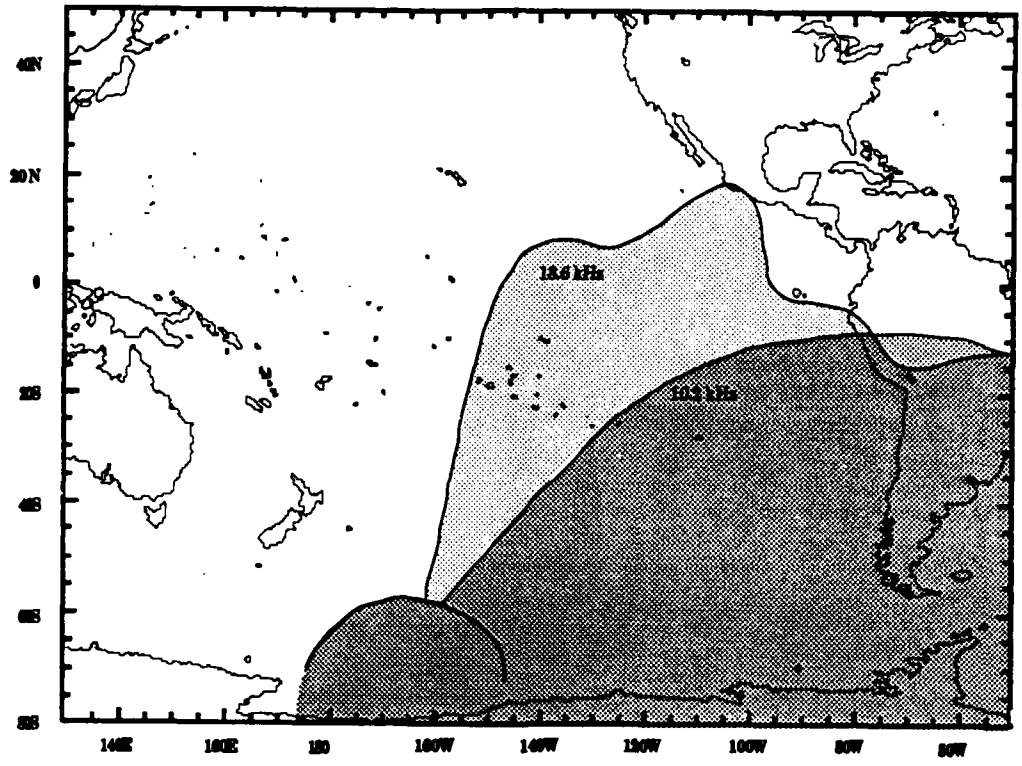

Figure 4–2. Norway Signal Self-Interference; Overlay Model

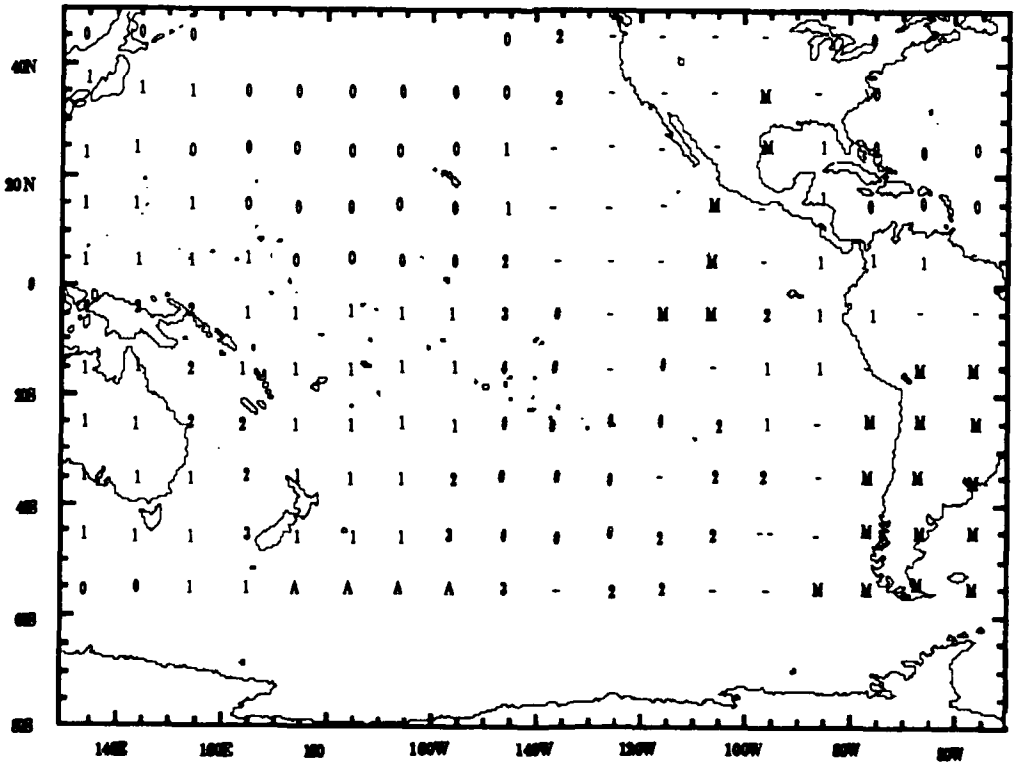

Figure 4–3. Norway Signal Self-Interference; Parametric Model

to this area is predicted to traverse a modal conversion zone, the mode 1 phase may be unreliable. Designating this area for signal deselection is considered prudent.

At 13.6 kHz the boundaries predicted by the Analysis and Overlay Models are fairly close, except the Analysis Model places the eastern part of the boundry farther north. In the Overlay model at 13.6 kHz, the extension of the boundary at 110° West Longitude north to Mexico is probably due to the influence of modal effects caused by propagation over the low conductivity Arctic terrain. The predicted shape and width of this extension is expected to be quite sensitive to the terrain model and ionosphere parameters. Although we flag the entire shadow zone of Greenland as a potential problem area for 13.6 kHz, this problem has not been confirmed by measurements.

If low latitude mode conversion is the mechanism that dictates boundaries, then the Analysis Model should be more correct for the following reasons. The calculations used for the Analysis Model show that the onset of modal conversion occurs at a near constant Geomagnetic Latitude on the transmitter side of the equator over the bearing sector where mode conversion takes place. The magnitude of modal effect is about the same over the angle range where conversion takes place. Onset with bearing change is abrupt at both the eastern and western ends of the conversion zone.

The Parametric Model predicts transequatorial-zone modal effects on the Norway signal over South America and right along the Chile coast. A disturbed zone, including some modal, extends in the Greenland shadow down below the equator and merging with a no signal condition. The zone of predicted levels 1 and 2 lying in between (above 100° West) is flagged as incorrect. The data shows that modal competition occurs at least as far west as Tahiti. Only the selection of proper boundaries and time durations is in question.

The weak signal condition predicted over much of the eastern half of the validation region appears appropriate for times when Greenland is in continuous daylight. The received signals at Tahiti were fairly strong

during February and early March, except for a brief period at sunrise. By late March and during April the SNR was much less.

The Parametric Model shows modal effects extending northward almost to the central United States. This modal zone has a shape similar to our extension of long-path during Northern Ionosphere summer months. The Analysis Model shows the potential for modal effects when signal propagation is over North-Eastern Canada. We did not confirm any of these predictions.

(B) Liberia:

All three predictions for Liberia are generally consistent at both 10.2 and 13.6 kHz. The practical result is that Liberia is not usable most of the time, except possibly on the far western end of the validation region. When the short-path is primarily night propagation, modal effects are strong. When night is primarily on the long-path, this path produces the dominant signal across the Pacific.

The Analysis Model places the modal effects, short-path dominant, further west than the Parametric Model does at 1200 GMT. For February/March the Analysis Model predicts that the long-path covers a major portion of the South Pacific Ocean; see Figure C-12. The placement of the long/short-path boundary in this area is largely academic, since the result is either modal or long-path. More reliable choices of signals are available.

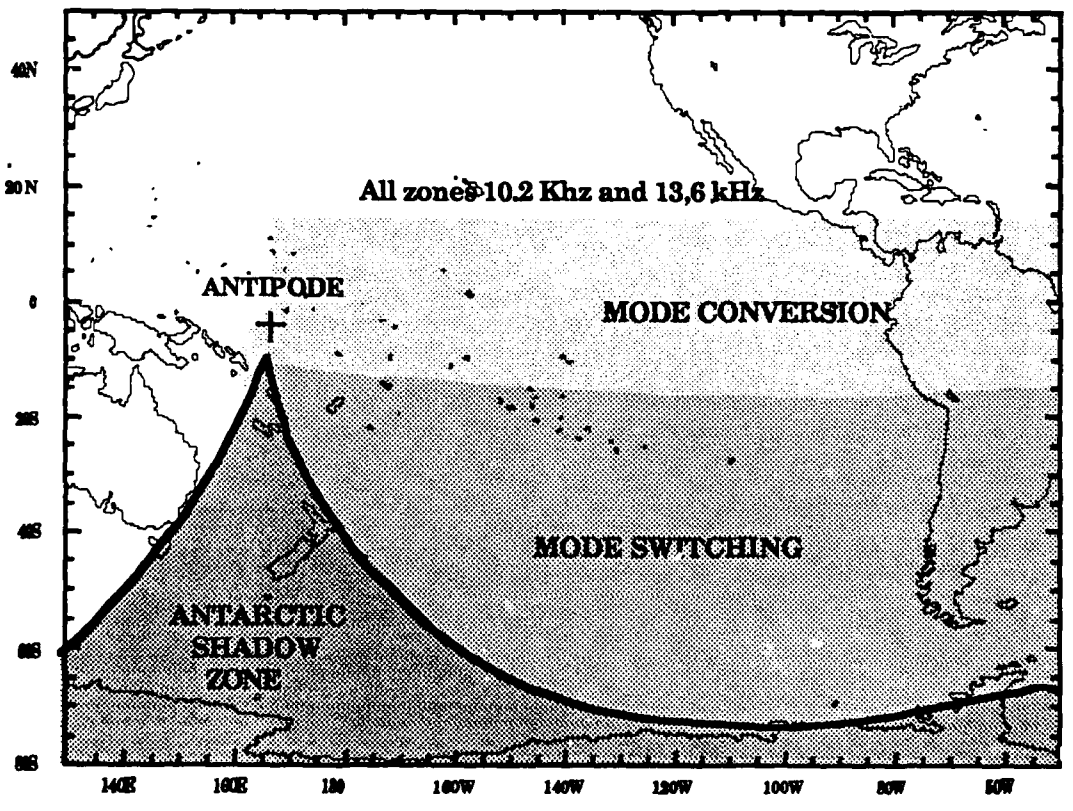

Figure 4–4. Liberia Signal Self-Interference; Analysis Model

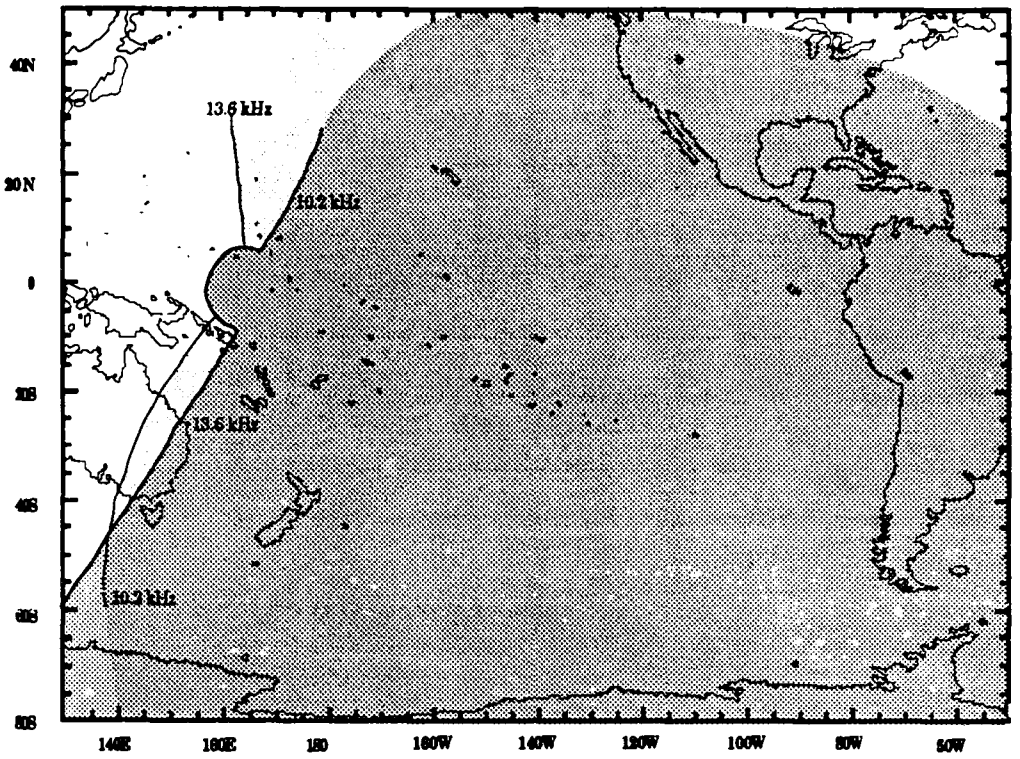

Figure 4–5. Liberia Signal Self-Interference; Overlay Model

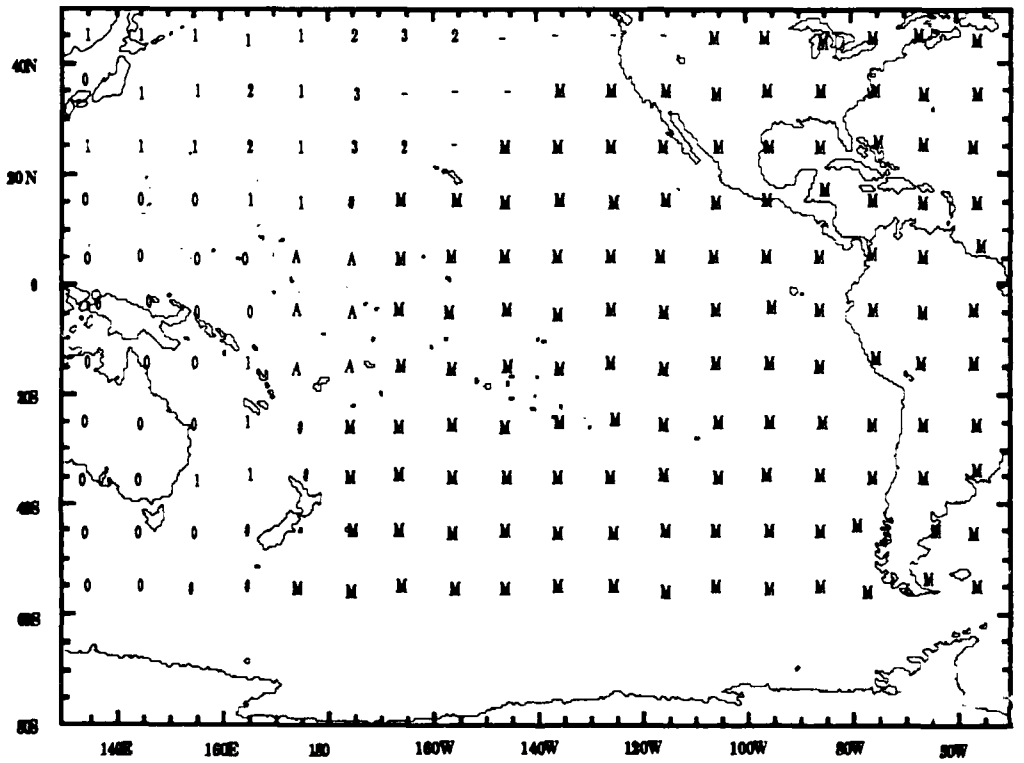

Figure 4–6. Liberia Signal Self-Interference; Parametric Model

(C) Hawaii:

For Hawaii the Analysis and Overlay model predictions are largely in agreement for placement of the modal-zone boundaries. The large extension to the southeast is very similar, as is the effect of the transequatorial zone mode conversion. The modal boundary for each frequency extending southeast is one of the key boundaries creating the areas of two and three station coverage depicted in Figure 3-6.

The Parametric Model only shows 10.2 kHz. This original model did not show the near-zone extension to the east because this extension is produced by the third ordered mode. The third ordered mode is not included in the Parametric Model. The near-zone extension was added later and is shown in Figure 4-9, using italic letters. Swanson's Parametric Model addition, which is for 10.2 kHz, more closely matches the Analysis Model curve for

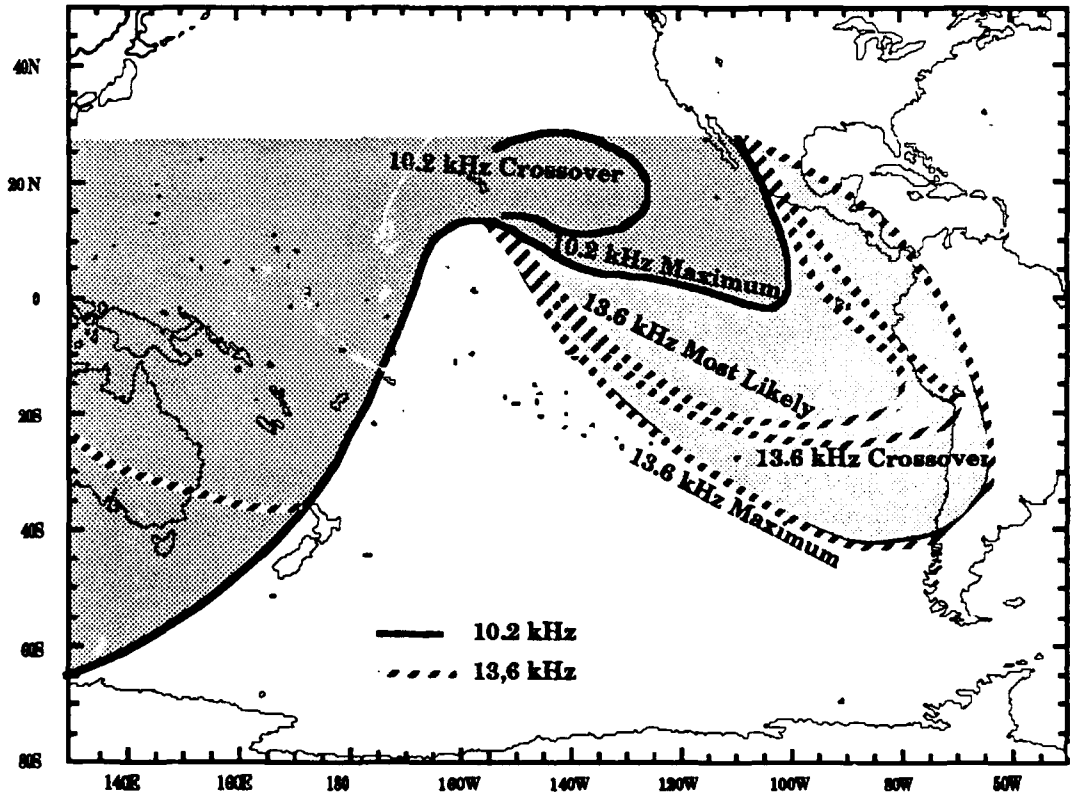

Figure 4-7. Hawaii Signal Self-Interference; Analysis Model

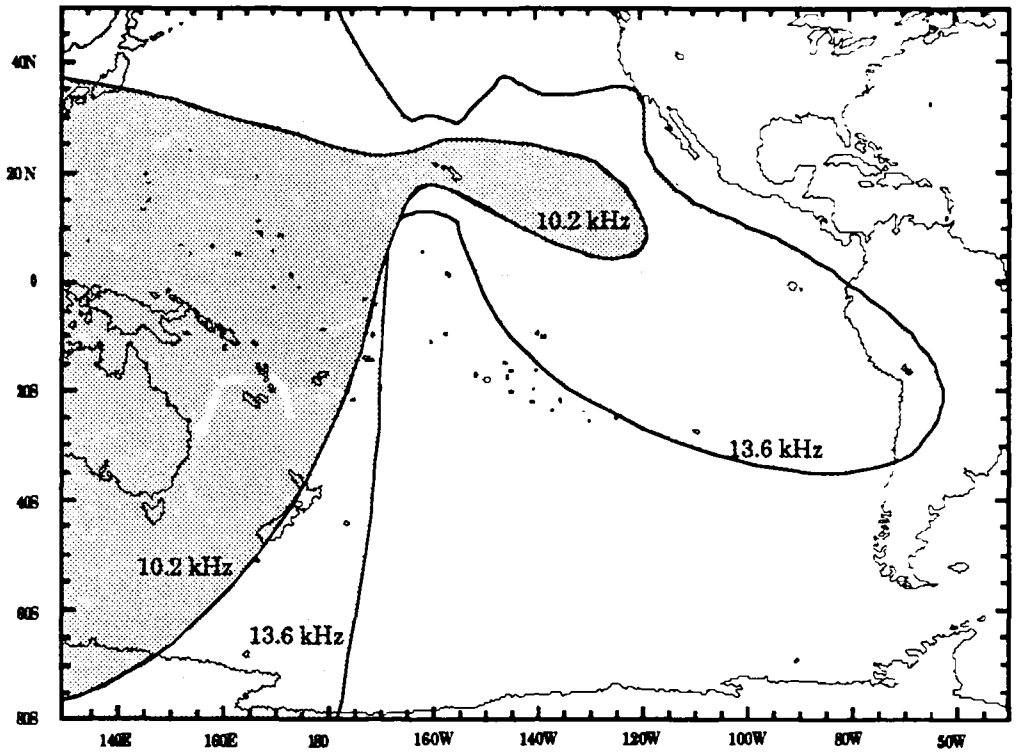

Figure 4–8. Hawaii Signal Self-Interference; Overlay Model

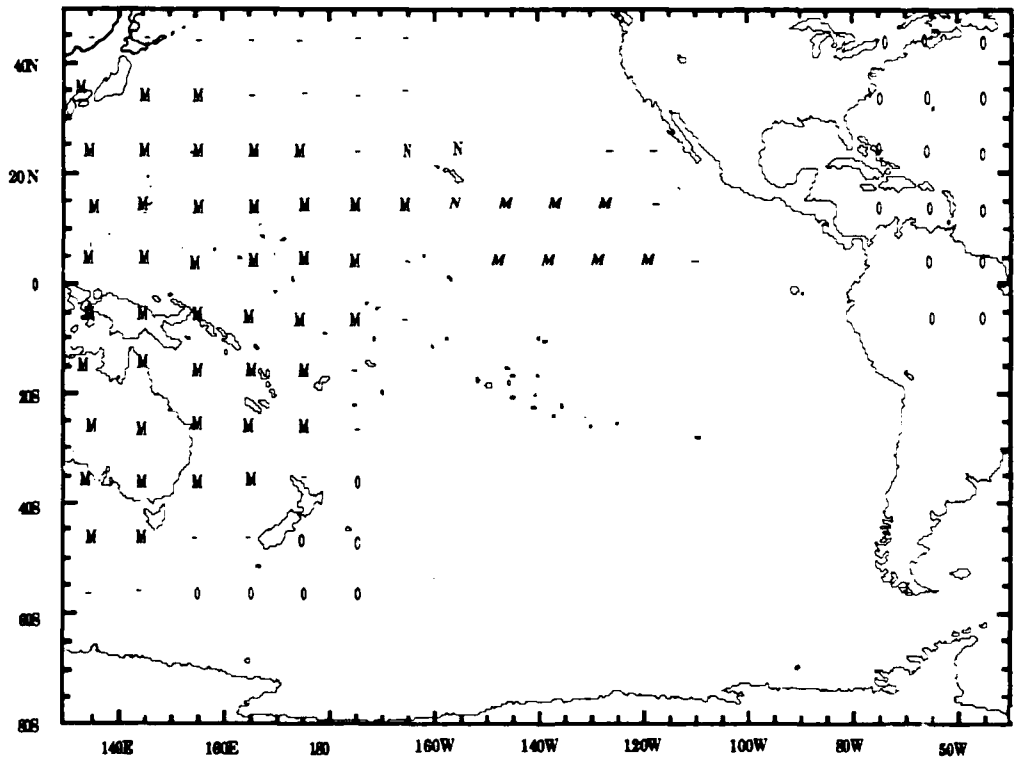

Figure 4–9. Hawaii Signal Self-Interference; Parametric Model

13.6 kHz Most Likely. The proper placement of the modal zone east of Hawaii is important because of the high traffic into Hawaii. Fortunately the radials to the U. S. west coast lie north of this region of protrusion. The great circle route to Panama is much more affected. The modal boundary shown by the Parametric Model in the vicinity of New Zealand lies to the east of New Zealand.

The measurements show a need for adjustment of both the Analytical and Overlay Models in three areas. First, the curve for13.6 kHz needs to be retracted in its southeast extension. A more probable curve, labeled "13.6 Most Likely", is shown in Figure 4-7. This curve is primarily derived from judgment based on the Arequipa phase data and the overall shape of this boundary segment. The Easter Island phase data, when analyzed, should help in estimating the placement of this boundary. Second, the boundary for 10.2 and 13.6 kHz almost directly south of Hawaii was observed to be at least 300 Km south of the boundary of the Analysis Model. The Overlay Model boundary for 10.2 kHz is placed even further north than the Analysis Model places it. Third, the Wellington phase data shows that Wellington is within the modal zone for 10.2 kHz, requiring that this boundary be moved slightly east of that in the Analysis Model. Wellington is outside the modal zone for 13.6 kHz. The NOSC calculations and flight data, Figure B-12, show that the 13.6 kHz signal has small modal structure beyond Samoa. What cannot be determined from these calculations or data is what mode emerges as dominant. Assuming that the Wellington data gives this answer, then the 13.6 kHz modal boundary over Australia should be moved further north than the Analysis Model predicted. Measurements along the south coast of Australia would help to resolve this boundary placement. A few more calculations (NOSC's Mode-Conversion Model calculations better predict the data) will provide guidance as to how far east to move the boundaries for 10.2 and 13.6 kHz in the vicinity of Samoa and New Zealand. All three of these models place the boundary too far west.

A further unresolved issue is the predictability of the mode 1 phase after having propagated through a mode-conversion zone. A brief inquiry to several colleagues did not yield any evidence that the predictability had been either determined or tested. Our Analysis Model boundary for 13.6 kHz

does not reflect the possibility that even though mode 1 may be dominant south of Australia the phase may be unpredictable. The phase may be unpredictable because in the conversion zone other modes may be converted to mode 1 such that the resultant mode 1 component will be the product of an unknown mix of signal components.

(D) North Dakota:

With respect to North Dakota signal predictions, the shape and the extent of the overall modal zone determined for the Analysis Model is quite different from the other models. The key features contributing to the derived shape for the Analysis Model are the abrupt modal onset with rotation of propagation radial bearing, the extent of modal effects along the onset radial, and the close tie of strong modal conversion to a constant magnetic latitude, about 7° north of the magnetic equator. The two other models place the modal zone further to the west and show a wide variation in magnetic latitude for the northern boundary. The Overlay Model shows the 13.6 kHz signal extending beyond 20° N. latitude around 160° E. longitude. The TASC calculations used in this analysis show this region to be mode 1 to within 10° N. latitude.

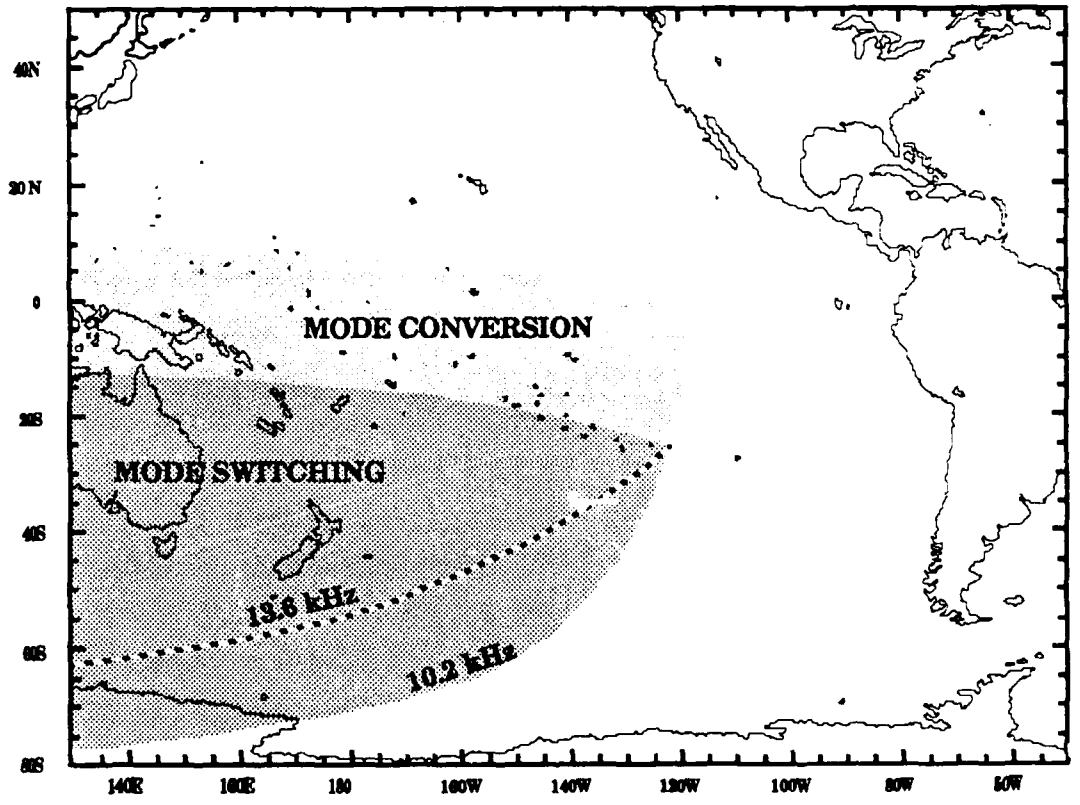

Figure 4-10. North Dakota Signal Self-Interference; Analysis Model

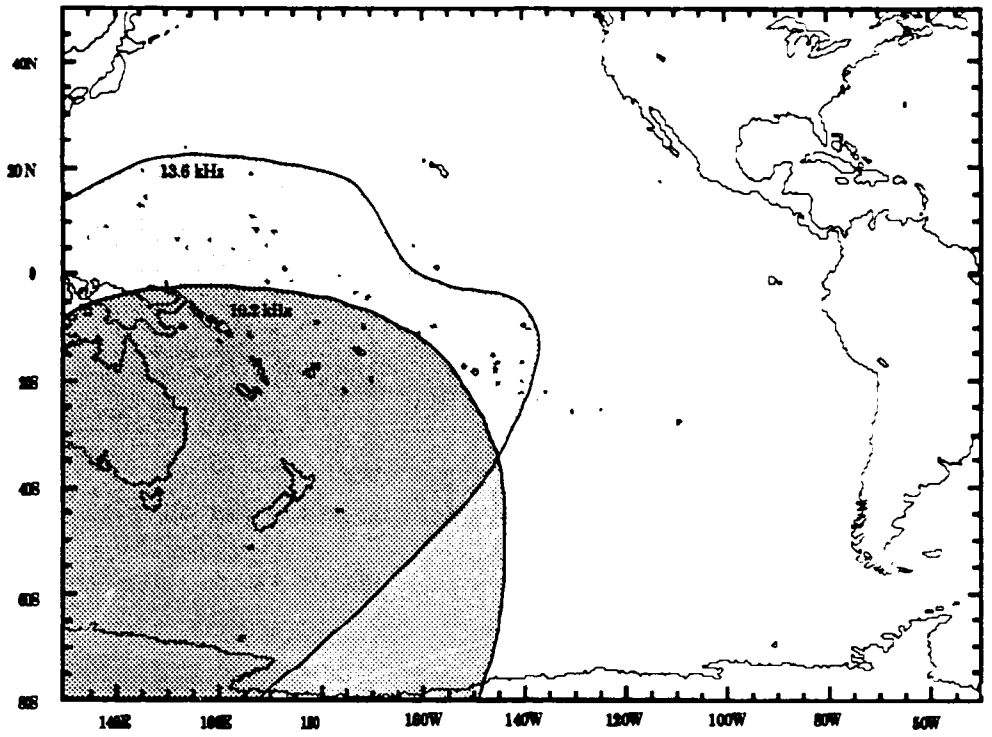

Figure 4–11. North Dakota Signal Self-Interference; Overlay Model

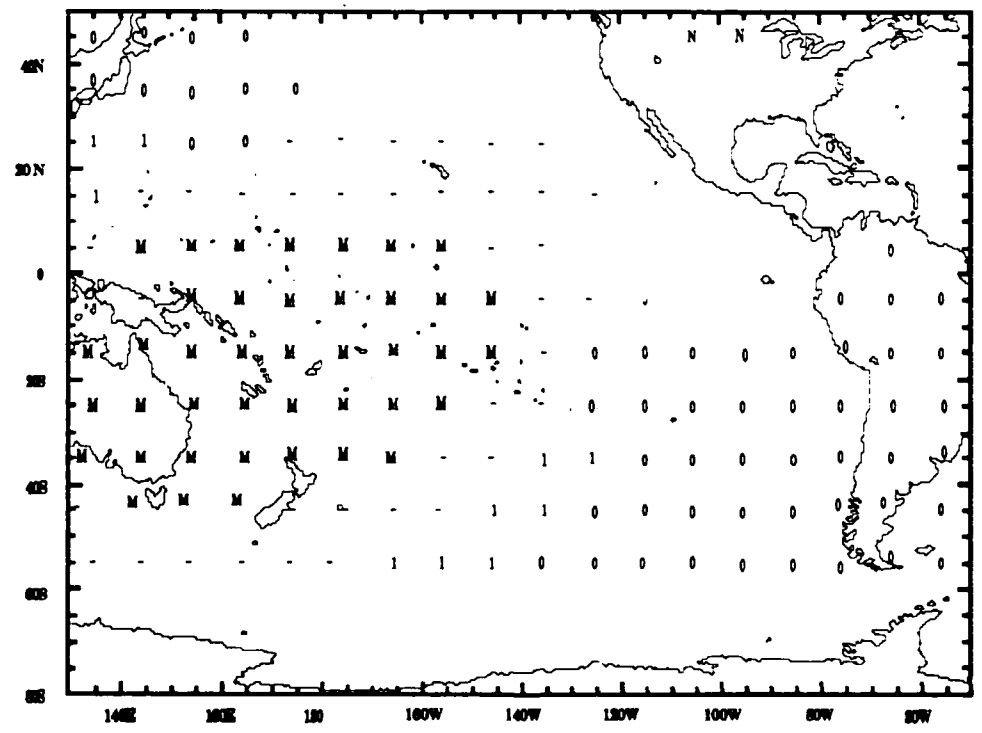

Figure 4–12. North Dakota Signal Self-Interference; Parametric Model

The Parametric Model implies a gradual buildup of self-interference to the point where modal effects become dominant. The Analysis Model derived a different interpretation, a much more abrupt onset of modal effects starting at the equatorial mode conversion zone.

The data does not provide for a resolution of the differences predicted between the models. The only fixed site located where a difference was predicted is Tahiti. This site is predicted to be outside the boundary of 10.2 kHz for the Overlay Model, inside the boundary of 10.2 kHz for the Analysis and Parametric Models, and inside the boundary of 13.6 kHz for the Parametric and Overlay Models. The data show modal effects at all frequencies, with 13.6 kHz being the weakest. Collectively, the data simply is not definitive.

The placement of the northeastern and western boundary for North Dakota is a critical part of determining the areas of two- and three-station coverage shown in Figure 3-6. Resolution of the location of this boundary, though considered very important, was not possible using the data of this validation.

Our long-path analysis shows Australia to be within the long-path of the North Dakota signal for about six hours (1800 - 2400). This prediction was not confirmed. Analysis is defered until the Western Pacific validation report.

This page blank

(E) La Reunion:

The coverage situation with La Reunion is very complex due to the long paths involved, paths' crossing the transequatorial zone, the presence of Antarctica on some paths, and a wide variation in solar illumination of the paths to determine when the La Reunion signal is reliable in the eastern part of this region. A much more detailed model is needed than was developed for this analysis. The most detailed model must include propagation path illumination effects for time and season. As will be described, the prediction factors are highly variable with location and time in this part of the region. Thus the measurement data cannot be extended very far beyond the locations of measurement. The importance of La Reunion concerns the question of its availability where few other good signals exist. These locations are within the two-station and three-station segments of Figure 3-6 (predicted not available) and as the fourth station (predicted available) above and below the westward extending arm in this

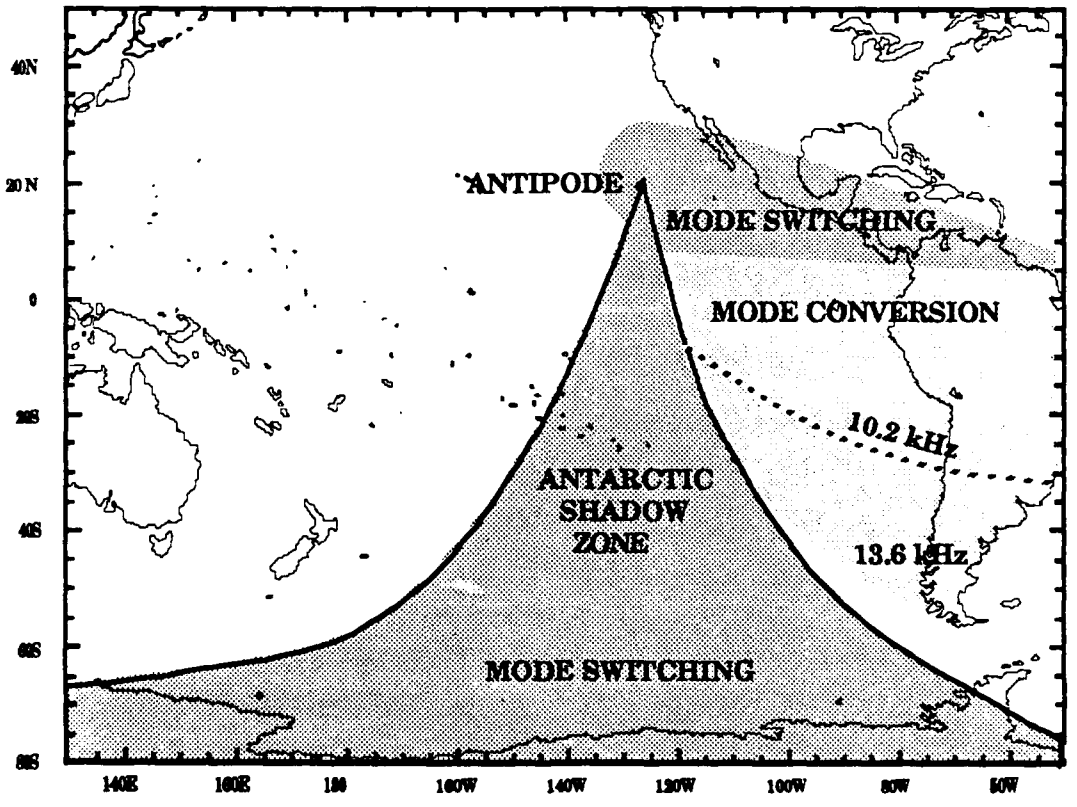

Figure 4-13. La Reunion Signal Self-Interference; Analysis Model

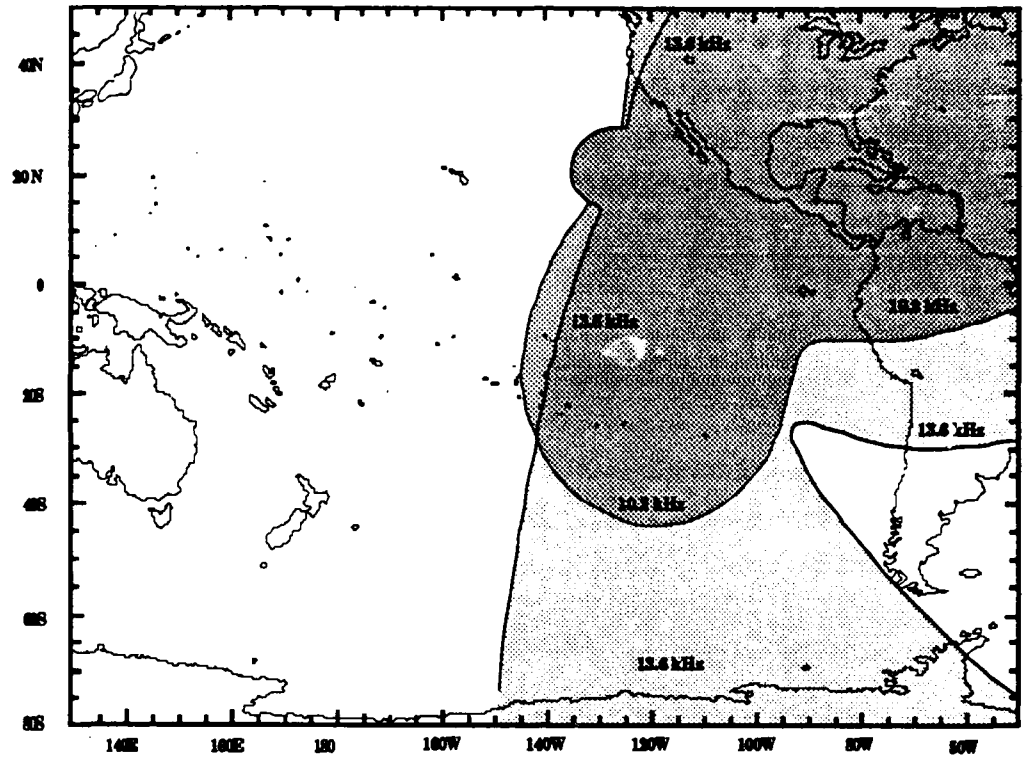

Figure 4–14. La Reunion Signal Self-Interference; Overlay Model

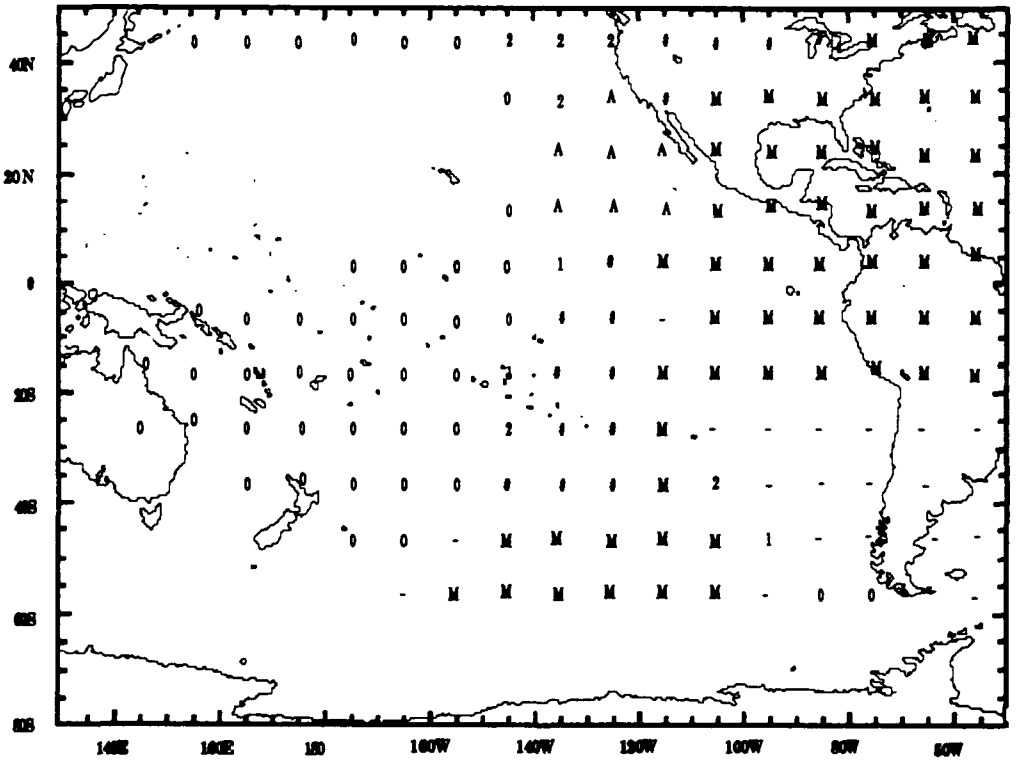

Figure 4–15. La Reunion Signal Self-Interference; Parametric Model

figure. The Hawaii signal, even with good quality, has a poor geometry relationship with Japan for accurate position fixes in the regions both below the arm and in the upper part of the outlined area. Because of this poor geometry, the more distant stations assume even greater importance than is usually the case.

Inside the area labeled "Antarctic Shadow Zone" in Figure A-11 the reliability of the La Reunion signal is highly questionable for many reasons. During February the long-path must dominate a part of this sector below the antipode most of the time, primarily because of short-path high propagation loss in traversing the daylight Antarctica. There is also a sector about 30° wide centered about the 180° radial in which an all-night path does not occur.

In the eastern segment the maximum duration of an all-night propagation path varies from three hours east of Arequipa to zero time on a great circle arc extending from 80° S latitude, 80° W longitude to the antipode.

Our long-path analysis shows that the Liberia signal east of 140° West Longitude is long-path a large part of the day. Thus, one or the other self-interference effects would dominate. We conclude that the La Reunion signal is not suitable for navigation use in this eastern zone.

To the west of the shadow zone the La Reunion signal is predicted to be good. Two factors diminish the likelihood of a high quality navigation signal. First, the path is high latitude, and second, the path is almost always in a day/night transition. During February, the all-day condition on the propagation path lasts for two hours (0230 - 0430) and the all-night condition for one hour (1430 - 1530). During July all-night lasts from zero to two hours, depending on latitude within the areas of interest. The shadow zone is predicted to be mode 2 when all-night conditions occur.

In comparing prediction models, though details differ, the conclusions cited above are valid for each model. The Analysis Model, as stated above, produces the most sharply defined boundaries believed to be more consistent with the geophysical factors.

This Page Blank

(F) Argentina:

The three prediction models all predict the Argentina signal modal zones in the South pacific validation region. Both the Analysis and Overlay Models predict the 13.6 kHz boundary to lie south of the 10.2 kHz boundary. The Overlay Model extends this zone much farther south than the Analysis Model, extending below Wellington. Tahiti, Wellington and Samoa fixed-site data can contribute to a resolution between predictions. The Tahiti data shows clear mode switching at 11.3 and 13. 6 kHz and modal contamination at 10.2 kHz. The Wellington data shows clean mode 1 signals on all frequencies at all times. The Samoa data has not yet been analyzed. These results are all considered consistent with the Analysis Model boundary placement.

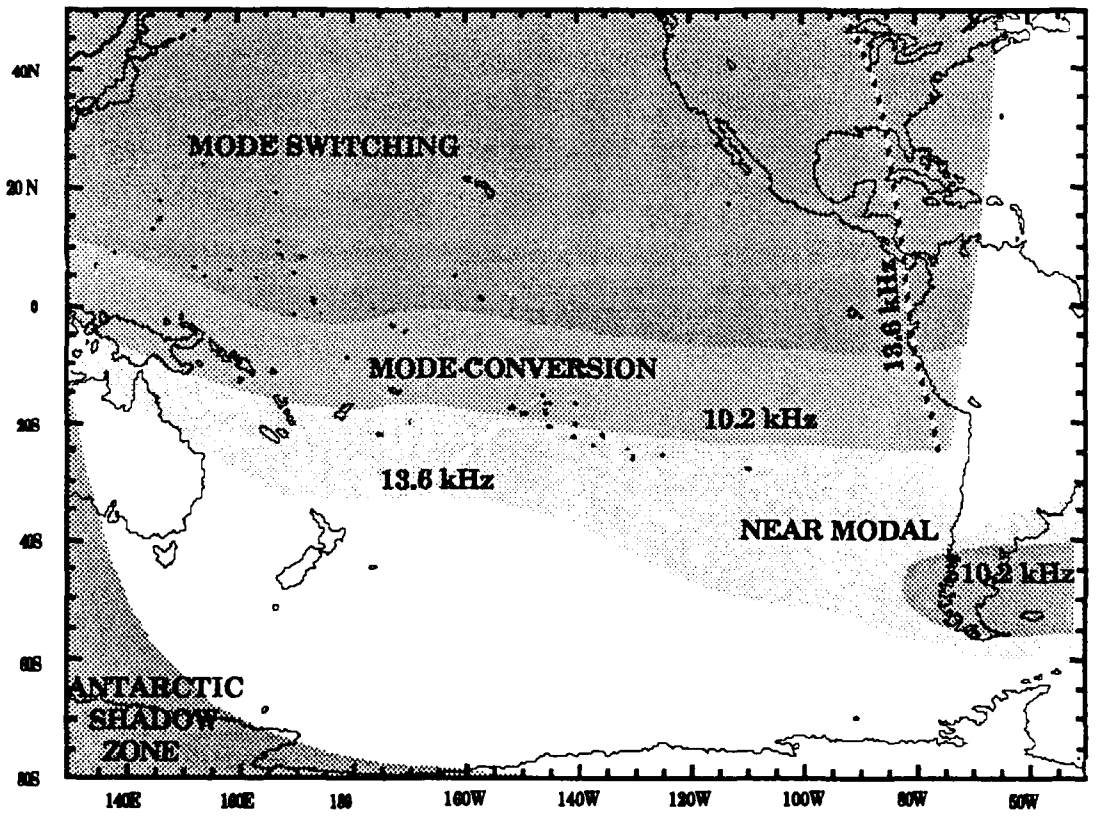

Figure 4-16. Argentina Signal Self-Interference; Analysis Model

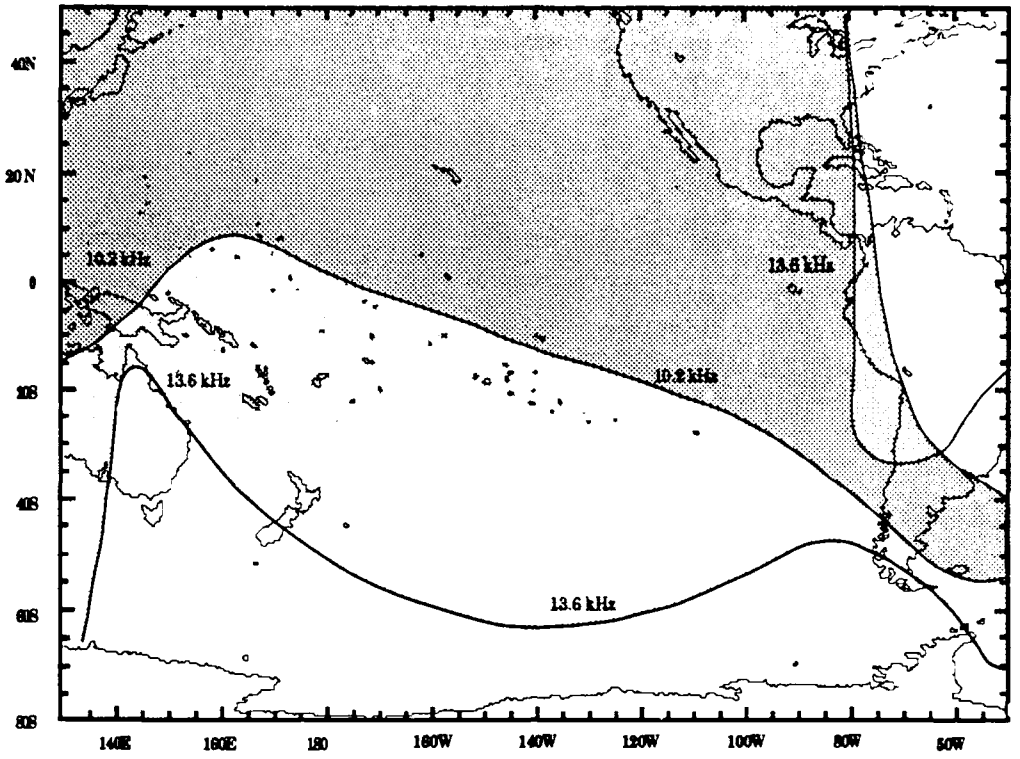

Figure 4–17. Argentina Signal Self-Interference; Overlay Model

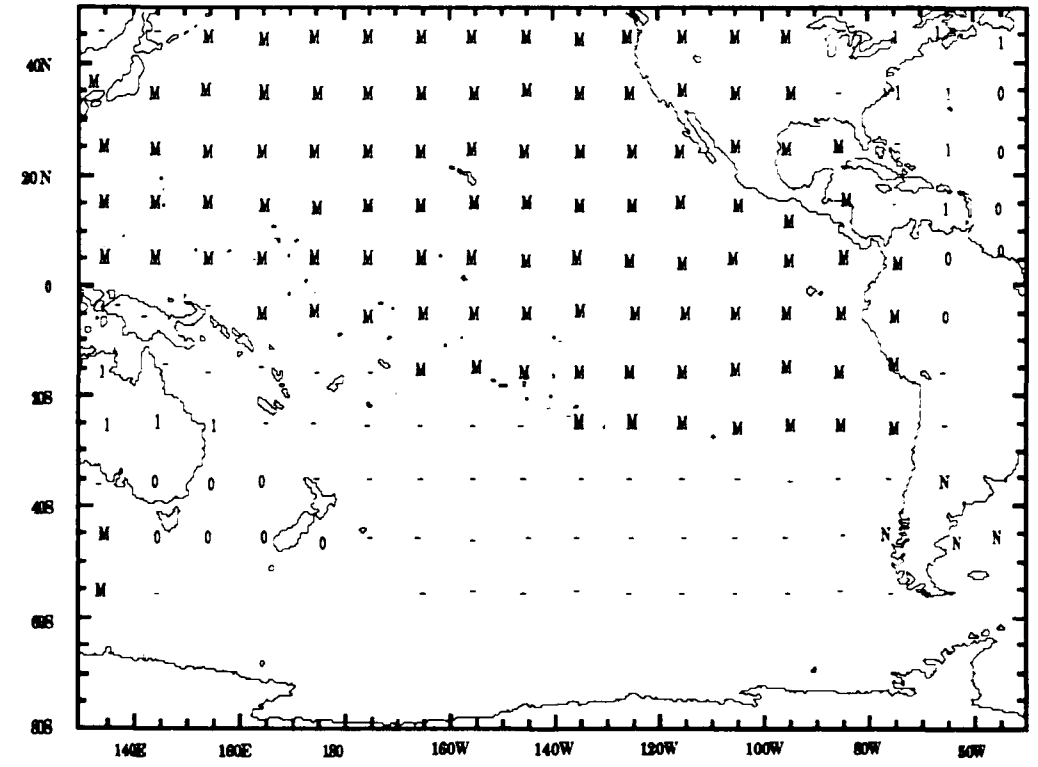

Figure 4–18. Argentina Signal Self-Interference; Parametric Model

The eastern boundary differs to some extent between the Analysis and Overlay Models. The difference is attributed to the propensity in the Overlay Model to draw wide "corners" and to our choice of a more eastern radial to signify the cutoff bearing. Lacking more detail, we felt there is good reason to place the modal cutoff along the 350° radial. The Arequipa data shows that the Analysis Model boundary for 10.2 kHz needs to be placed slightly farther north or west in the vicinity of Arequipa. This is true for the Overlay Model as well.

For the Overlay Model, the western edge of the boundary curve for both frequencies dips down, 13.6 kHz sharply. We assume that this is to account for long-path interference. We agree that at those times when long-path is of concern the boundaries are in this vicinity.

The Parametric Model, within the resolution provided, fits the 10.2 kHz boundaries of the other models. This model defines the long-path positions and times along the western edge of the validation region. The prediction of long-path is consistent with the Analysis Model.

Our analysis of long-path effects predicts that the zonal boundary extends across the Pacific from Central Mexico to about Brisbane, Australia. The placement of this boundary has not been validated.

This Page Blank

(G) Australia:

The Australia self-interference consists of two mechanisms, the near-zone and the long-path. The near-zone is covered in sufficient detail to compare only the Analysis and Overlay Models. The two models show very similar areas for both frequencies but quite different boundary shapes. The differences in shape are worth investigating both theoretically and by measurement.

The data acquired in this validation allowed approximate establishment of the boundary on only one radial, that to Wellington. On this radial the two model predictions match quite closely. The fixed-site Wellington data showed that the boundary placement was in agreement with observation on that radial.

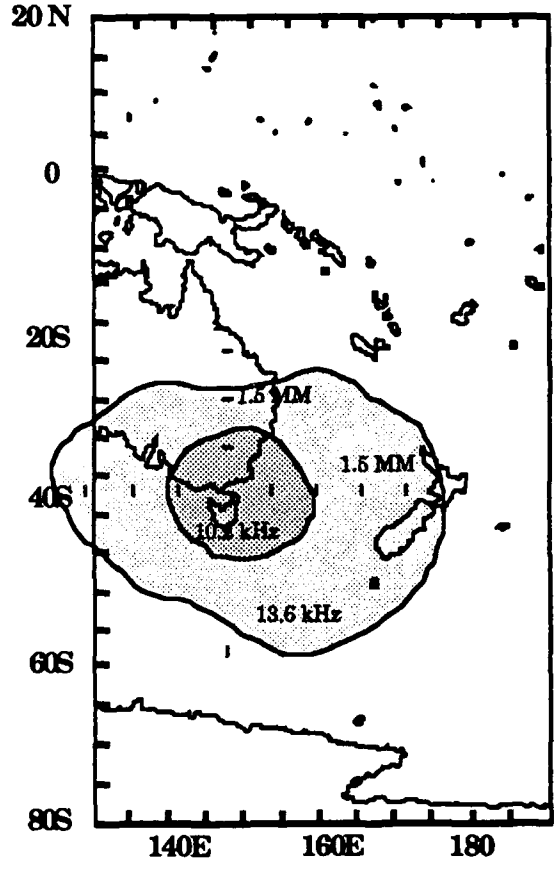

Figure 4-19. Australia Signal Self-Interference; Analysis Model

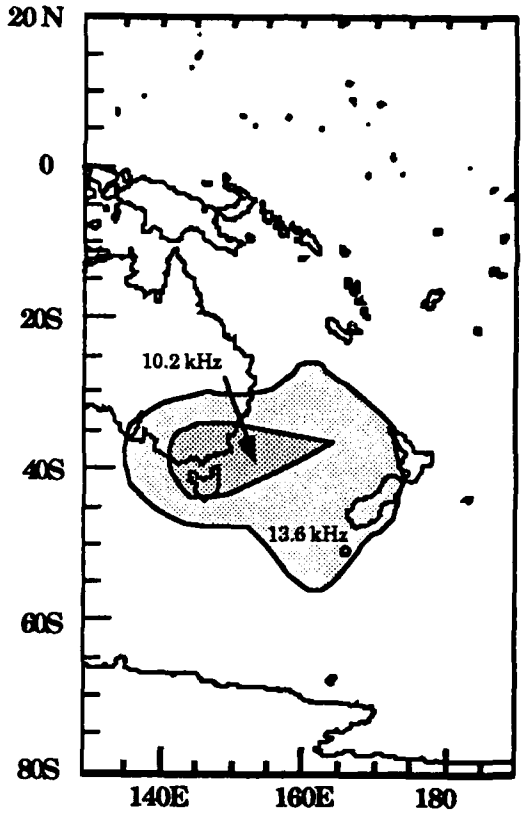

Figure 4–20. Australia Signal Self-Interference; Overlay Model

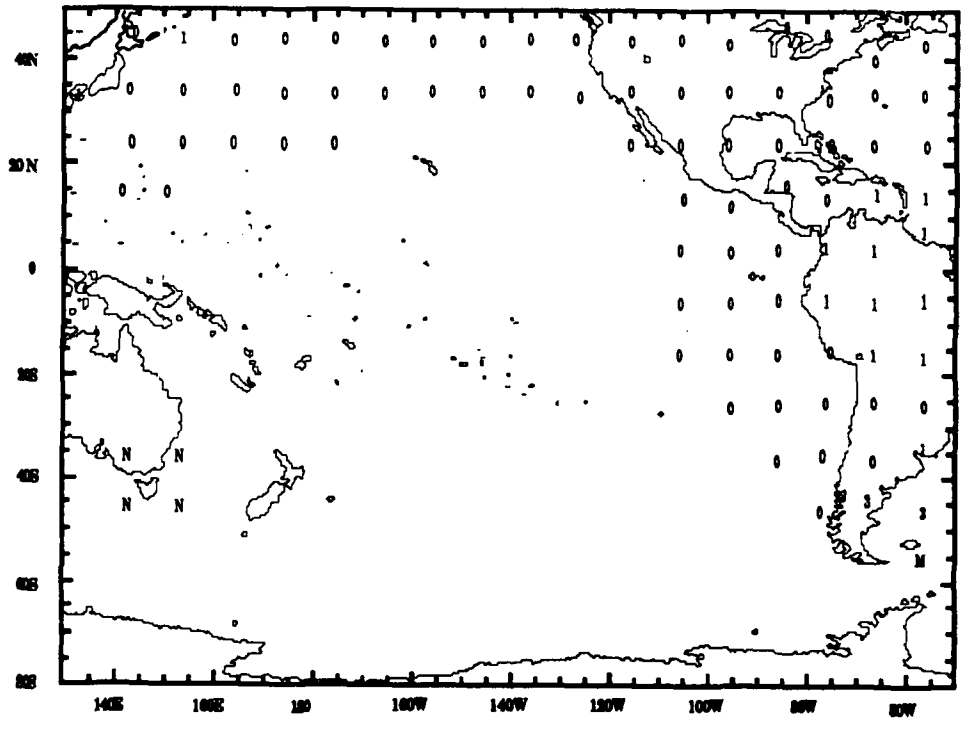

Figure 4–21. Australia Signal Self-Interference; Parametric Model

The Overlay Model predicts that at 10.2 kHz the long-path will encroach into the eastern edge of the validation zone, reaching as far west as the middle of South America. Our analysis of long-path boundaries for Australia predicts approximate concurrence with the Overlay Model. The parametric prediction shows no long-path west of the antipode. The Arequipa data shows modal effects part of the days on 10.2 kHz and at the times long-path is expected. We estimate that long-path effects extend to near Arequipa about 20% of the diurnal days. It was not possible to determine if long-path actually became dominant at Arequipa. No long-path effects at 13.6 kHz were expected or observed in the validation region.

This page Blank

(H) Japan:

The Analysis and Overlay Models predict modal zone boundaries extending into the northwest segment of the validation region that are very similar in extent and shape. The Parametric Model does not predict this modal zone, possibly because it is fairly small at 10.2 kHz.

In our data analysis we could only deal with the 13.6 kHz boundary, the 10.2 kHz boundary being north of the data collection area. The data showed that, at least for the time of measurement, the 13.6 kHz boundary did not extend as far southeast as predicted. This finding was consistent with a similar finding on the boundary extending southeast from Hawaii. We conclude that this boundary should be moved closer to the transmitter, possibly by about 1.5 Mm.

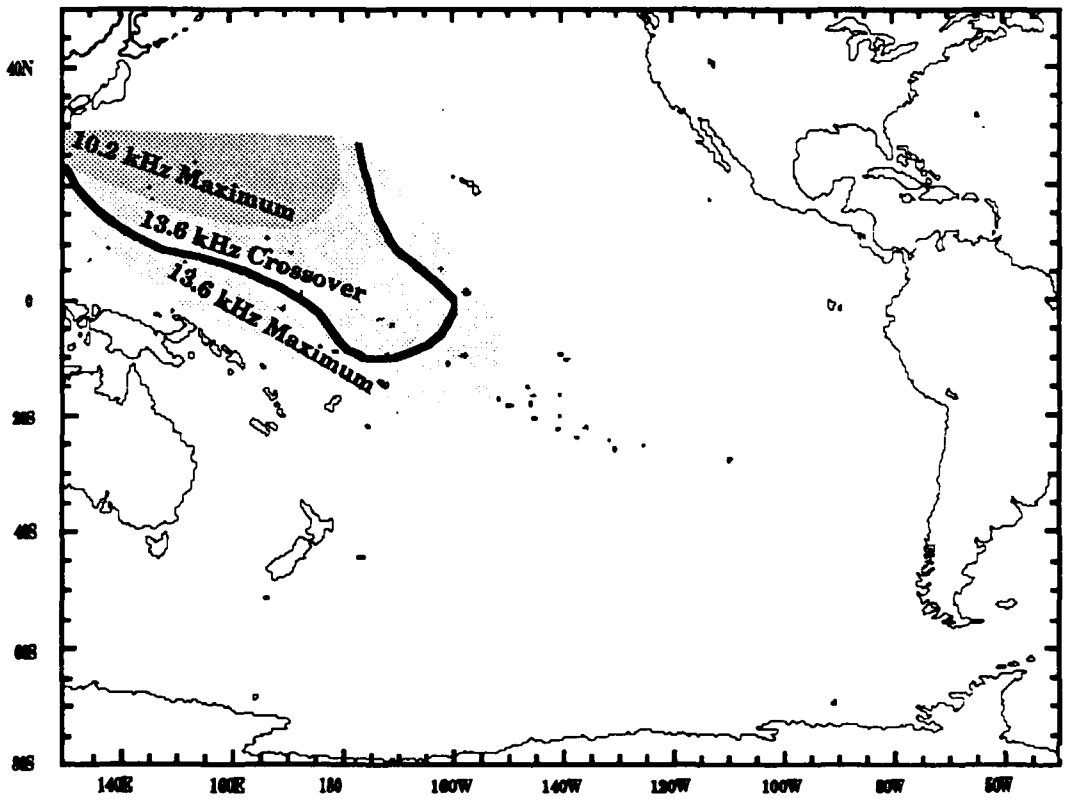

Figure 4-22. Japan Signal Self-Interference; Analysis Model

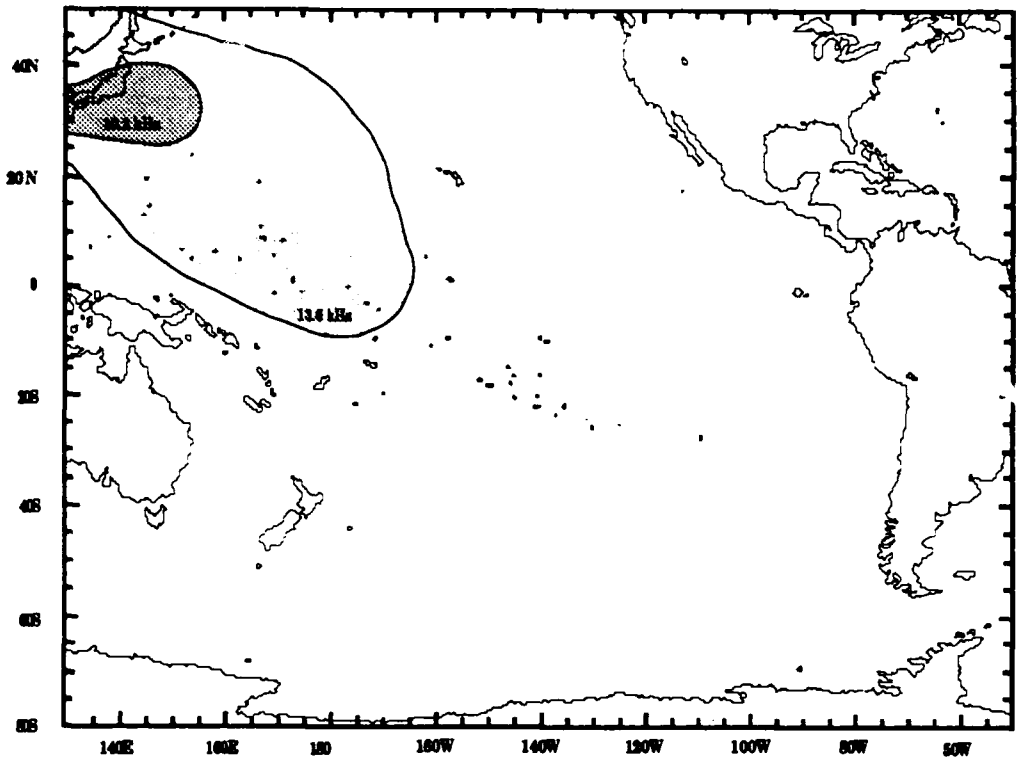

Figure 4–23. Japan Signal Self-Interference; Overlay Model

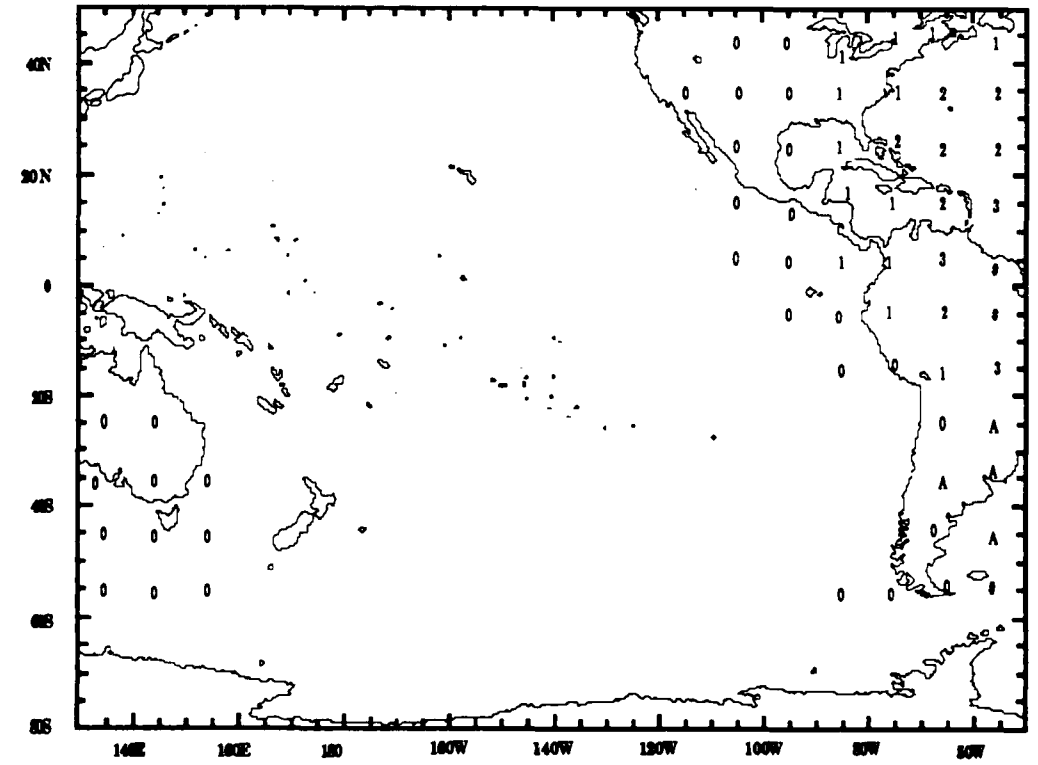

Figure 4–24. Japan Signal Self-Interference; Parametric Model

Neither the Overlay nor Parametric Models predict long-path encroachment into the eastern edge of the validation region. The Parametric Model does predict what is labeled a very weak signal over central South America. The Arequipa data at 10.2 kHz indicates modal competition on some of the days at times most consistent with long-path interference if it does occur. Further investigation is needed to determine if the observed effects result from long-path or from the receiver losing track due to a weak signal. The examination of both Australia and Japan records together should help establish a more definitive interpretation.

5.0 SUMMARY AND CONCLUSIONS

This section summarizes the overall validation project, places findings in perspective with goals and implementation plans, and states specifically what was found to agree or disagree with expectations and predictions.

In this section a brief review of the overall validation is presented with emphasis on the analysis. This is followed by a comparison of the analysis results with available coverage prediction models. Following this comparison the validation conclusions are presented. Included in the conclusions are specific recommendations both on the use of the analysis findings and in addressing unfinished business.

5.1 SUMMARY

This subsection reviews what has been presented, makes specific comparisons between expectations or predictions and analysis findings, and sets the stage for discussing conclusions by reviewing important points.

OVERVIEW

For this and the remaining validations, emphasis has been placed upon establishing zones of signal self-interference. The rationale for this emphasis is that it has been amply demonstrated that enough signal redundancy exists in most parts of the world so that SNR is not a problem. On the other hand, signal self-interference has proven to be a more significant problem than it was thought to be in the early stages of Omega development and operation. Signal self-interference exists on at least a few stations in all parts of the world. While weak signal levels can easily be measured and deselection made, self-interference cannot be easily measured. Thus either the receiver or navigator must rely on predictions.

Over the past few years much has been learned, and information has been derived that could be utilized for this validation. Some of the key knowledge and tools available were reviewed as an introduction to the validation project. As is always the case, a practical plan had to be devised for data

collection that coped with constraints on the resources of money, equipment, time and geography.

Validations are a particular challenge because large regions must be covered, usually over large ocean areas where very few measurement opportunities exist. The measurement phase was designed to capitalize on what was practical and to best utilize resources based upon the planners' perspectives at the time of implementation.

In section 3.3.2 a revised prediction model was devised to provide analysis guidance for data assessment. The prediction model, based on a large set of recent calculations by Gupta, defined zones of possible self-interference for each station. Composite charts were prepared (Fig 3-21 for 10.2 kHz and Fig 3-22 for 13.6 kHz) to identify areas where the greatest potential problems might occur and to assign priorities for data analysis and interpretation. The prediction model showed the existence of a region about 0° to 20° S Latitude, 110° to 150° W Latitude in which self-interference potentially existed for many signals. This prediction was generally confirmed from the data analysis.

5.2 CONCLUSIONS

This subsection presents in concise form the important findings of the validation, makes recommendations regarding use of the validation findings, and identifies topics for future investigation.

The analysis has led to the identification of a fairly large area within the South Pacific validation region where the potential exists for inadequate signal coverage, due to phase quality, for part of the day. The area exists for all Omega frequencies and includes subareas of both two (G & H) and three-station coverage, with the third station being (C) Hawaii. For part of the areas where Hawaii is usable, the geometry is such that the bearings to Hawaii and Japan are within a few degrees. In effect, the poor geometry

relationship negates the value of one of these signals. The identified area was well removed from measurement locations.

For those areas where only two or three stations were predicted to have good phase quality, at least the good stations also had sufficient signal-to-noise for accurate phase measurement.

The measurement analysis, because of measurement location limitations, was not able to derive definitive information either to confirm the existence of the region or to validate its boundaries. Collectively, however, the analysis findings were sufficiently supportive of the Analysis Model to lend reasonable credence to the model predictions.

We conclude that the Omega signal self-interference boundaries established by the Analysis Model as adjusted by the measurement analysis provide a significantly improved perspective on navigation reliability in the South Pacific. We recommend that the modal boundaries resulting from this validation be adopted in the Omega navigation model, giving due consideration for conservatism.

With respect to further possible analysis, the highest priority is to explore further the navigation consequences of the areas for predicted low or inadequate coverage. This could be partially accomplished by extracting more modal competition information from the fixed sites, Easter Island, Panama and Samoa. This requires extensive data processing because the sites do not have atomic frequency references. The ideal approach would be to design and conduct a special measurement campaign.

Our navigation accuracy analysis demonstrated that for the most part accuracy was found to be within predictions, especially for mid-path day and night. We feel that the phase prediction model for transition times could benefit from additional calibration. We noted several examples of large variability of phase about the median. Most cases were for propagation at high latitudes close to the day/night terminator. We flag these conditions for caution in navigation use.

The analysis conducted in this validation produced new insights into signal self-interference, both long-path and modal, that could be profitably applied to other geographic regions. Improved guidance in signal coverage conditions would be the benefit derived from applying these insights. Determining long/short-path boundaries continues to be a problem because of the lack of a good theoretical model and definitive measurements. Addressing both aspects of the problem are straightforward processes.

Finally, the data for modal interference close to transmitters is very sparse, especially the number of measured radials and the documentation of time variability. The three transmitters included in this validation, Hawaii, Argentina, and Australia, are all at boundaries to other validations; thus data could be combined to derive a more complete characterization. All of these transmitters are close to important transit paths: Hawaii is a major terminal; Argentina is close to Cape Horn; and Australia is next to Bass Strait. The increased knowledge of near field parameters could be generally applied to all other stations.

REFERENCES

1. Swanson, E.R., "OMEGA," Proceedings of the IEEE, Vol. 71, No. 10, Pages 1140-1155, October 1983.

2. Scull, D. C., "Omega Worldwide Calibration and Validation," Proc. of Conference on Navigation in Transportation, DOT-TSC-RSPA 78-22, September 1978.

3. Doubt, R.J., "OMEGA Navigation System Regional Validation Program," Navigation: Journal of The Institute of Navigation, Vol. 31, No. 3, Pages 155 - 164, Fall 1984.

4. Karkalik, F.G., "OMEGA Validation Over the Western Pacific Area," Navigation: Journal of The Institute of Navigation, Vol. 25, No. 4, Pages 395 - 404, Winter 1978-79.

5. Karkalik, F.G., Sage, G.F., and Vincent, W.R., "Western Pacific OMEGA Validation, Volume I, Technical Report," International OMEGA Navigation System, April 1978.

6. Campbell, L.W., "OMEGA Validation in the North Atlantic," in Proc. 5th Annu. Meet. of the Int. Omega Assoc. (Aug 5-7, 1980). p 24.

7. Campbell, L.W., Servaes, T.M., Dr., and Grassler, E.R., "North Atlantic OMEGA Navigation System Validation, Final Report," 21 July 1980, Analytical Systems Engineering Corp, June 1982.

8. Levine, P. and Woods, R., "North Pacific OMEGA Navigation System Validation," in Proc. 6th Annu. Meet. of the Int. Omega Assoc. (Aug 18-20, 1981). p 3.

9. Levine, P., Megatek Corporation, "North Pacific OMEGA Navigation System Validation: Draft Final Report," October 1980.

10. Watt, T., "Results of the South Atlantic OMEGA Validation," in Proc. 8th Annu. Meet. of the Int. Omega Assoc. (July 18-22, 1983). p 17.

11. Watt, T.M., Bailie, G.J. and Sutphen, M., "South Atlantic OMEGA Validation, Vol. I: Summary, Analysis, Appendices A-E," Systems Control Technology, Inc., Palo Alto, CA, January 1983.

12. Kugel, C., "Indian Ocean OMEGA Signal Validation," in Proc. 9th Annu. Meet. of the Int. Omega Assoc. (Aug 6-10, 1984). p 20.

13. Swanson, E.R., Doubt, R.J., and Kugel, C.P., "Indian Ocean Validation," in Proc. 10th Annu. Meet. of the Int. Omega Assoc. (July 22-26, 1985). pp 11-1 to 11-11.

14. Kugel, C., Swanson, E.R., and Doubt, R.J., "Indian Ocean Validation Final Report," Navel Ocean Systems Center, in publication.

15. Ferguson, J.A., "A Report on the NELC Integrated Prediction Program (PREDPROG)," NELC TN 1630, 16 February 1970.

16. Bickel, J. E., Ferguson, J.A., and Stanley, G. V., "Experimental Observation of Magnetic Field Effects at Night," Radio Science, Vol. 5, no. 1, p. 19, 1970.

17. Pappert, R.A. and Snyder, F. P., "Some Results of a Mode Conversion Program for VLF", Radio Science, Vol. 7, no. 10, p. 913, 1972.

18. Snyder, F. P., "Trans-Equatorial Propagation of Very Low Frequency Radio Waves," NOSC TD 431, 15 April 1981.

19. Gupta, R.R., B.E. Griffiths and P.M Creamer, "An Extended Omega Amplitude Prediction Model," The Analytical Sciences Corporation TR-1319-2, December 1979.

20. Gupta, R.R "Radial Profiles of 10.2 and 13.6 kHz Omega Signals," The Analytical Sciences Corporation TM-2687 (multiple volumes), July 1988.

21. Gupta, R.R., S.F. Donnelly, P.B. Morris, and R.L. Vence, Jr., "Omega system 10.2 kHz signal coverage diagrams." in *Proc. 5th Annual Meeting of the Int. Omega Assoc.* (Bergen Norway, Aug 5-7 1980), pp 22-1-22-36.

22. Swanson, E.R., "OMEGA coverage and performance predictions," paper presented at the 8th Annual Meeting of the Int. Omega Assoc., Lisbon, Portugal July 18-22 1983.

23. P. B. Morris, J. L. Shuny, and C. E. Quade, "Long-path prediction errors," in Proc. 7th Annu. Meet. of the Int. Omega Assoc., (Arlington, Va. Oct. 12 - 14, 1982), pp. 23-1 – 23-17.

24. Swanson, E.R., "OMEGA Coverage in India: A Case Study," NELC TR 1974, 15 January 1976.

Appendix A

Generation of Geographic Plots Showing Modal Competition

The set of plots described in this appendix address the nighttime propagation modal conditions, Near Modal, Mode Conversion, and Mode Switching, described in Section 3.3.3.2 of the report. The Long-Path interference will be addressed in Appendix C. A geographic plot is constructed for each station.

The analysis of modal conditions was derived from a series of calculations for Omega signal field strength versus distance for 10.2 and 13.6 kHz produced by TASC for ONSCEN (GUPTA 1988, Ref. 20). A sample calculation is shown in Figure A-1. The legend on the right identifies each of the curves. The ionosphere parameters used for calculations are shown in Table A-1. No allowance has been made for expected ionosphere variation with latitude and season. The first task was to examine the sets of calculations for each station to identify the possibility of

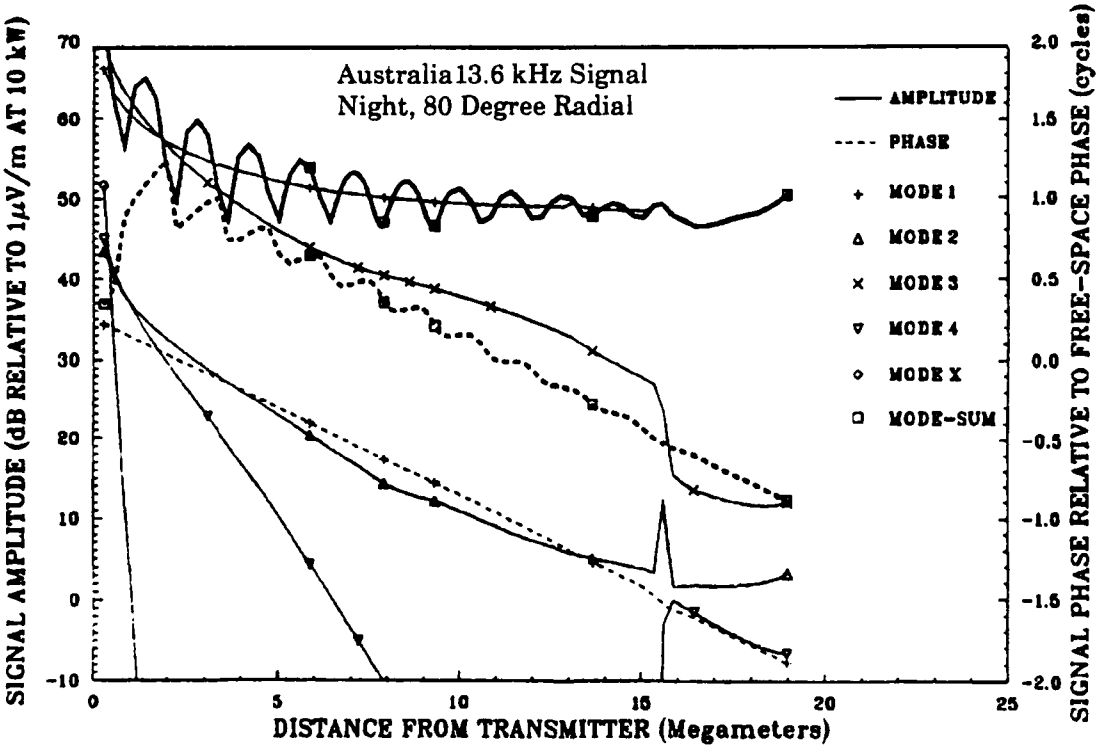

Figure A-1. Example of Omega Signal Calculation of Field Strength.

Ionosphere Illumination Condition	IONOSPHERE PARAMETERS	
	Reflection Height (km)	Conductivity Gradient (km $^{-1}$)
Day	70	0.3
Night	87	0.5

Table A-1. Day and Night Ionosphere Parameters.

self-interference conditions. The three most important model features useful for analysis guidance are (1) the structure (signal fluctuation with distance) in the mode sum, (2) the modes that contribute to the mode sum, and (3) the mode that is dominant in the validation region.

A summary of the analysis for creating each geographic plot is presented as follows:

(A) NORWAY:

The zones of possible poor phase for night propagation on Norway signals in the South Pacific are shown in Figure A-2. Two contributing factors are involved: propagation across Greenland and other low conductivity terrain, and propagation across the equatorial zone. A sample calculation for the Norway signal is shown in Figure A-3. The sections depicting the different propagation conditions are marked on this Figure. The calculations for propagation paths across low conductivity terrain show a high sensitivity in cumulative phase to path parameters at night. This sensitivity is not nearly as pronounced for the day. Apparently this phase sensitivity is closely associated with mode conversion occurring in nighttime propagation across low conductivity terrain.

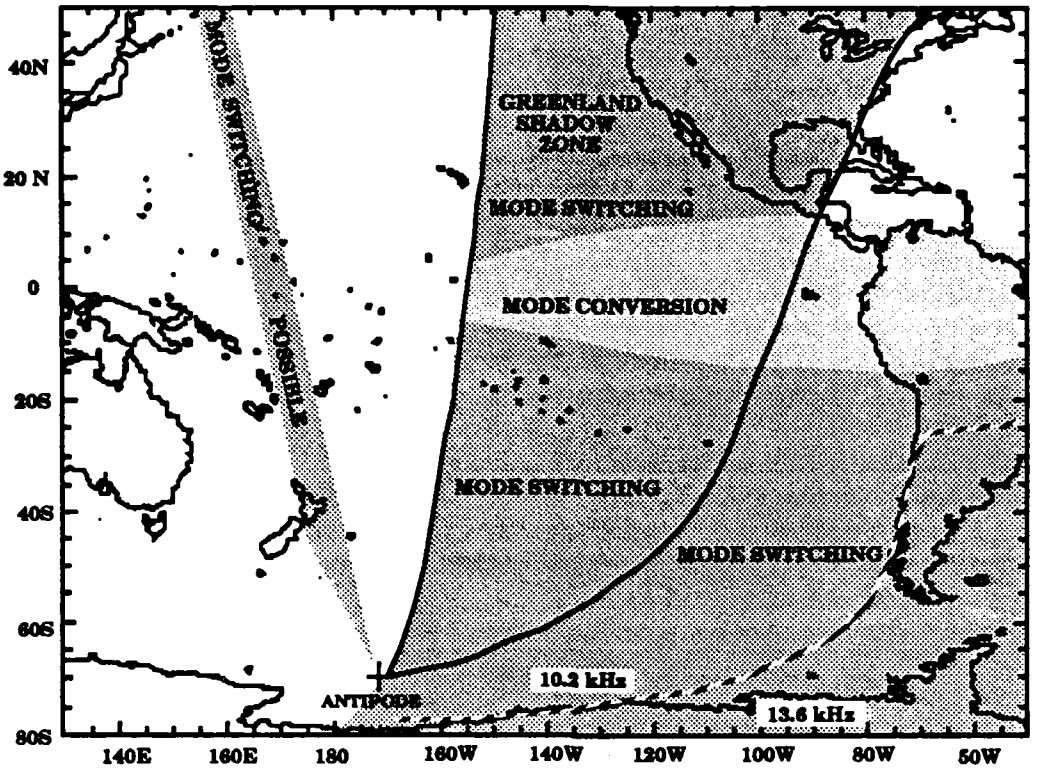

Figure A–2. Uncertain Phase Zones for the Norway Signal

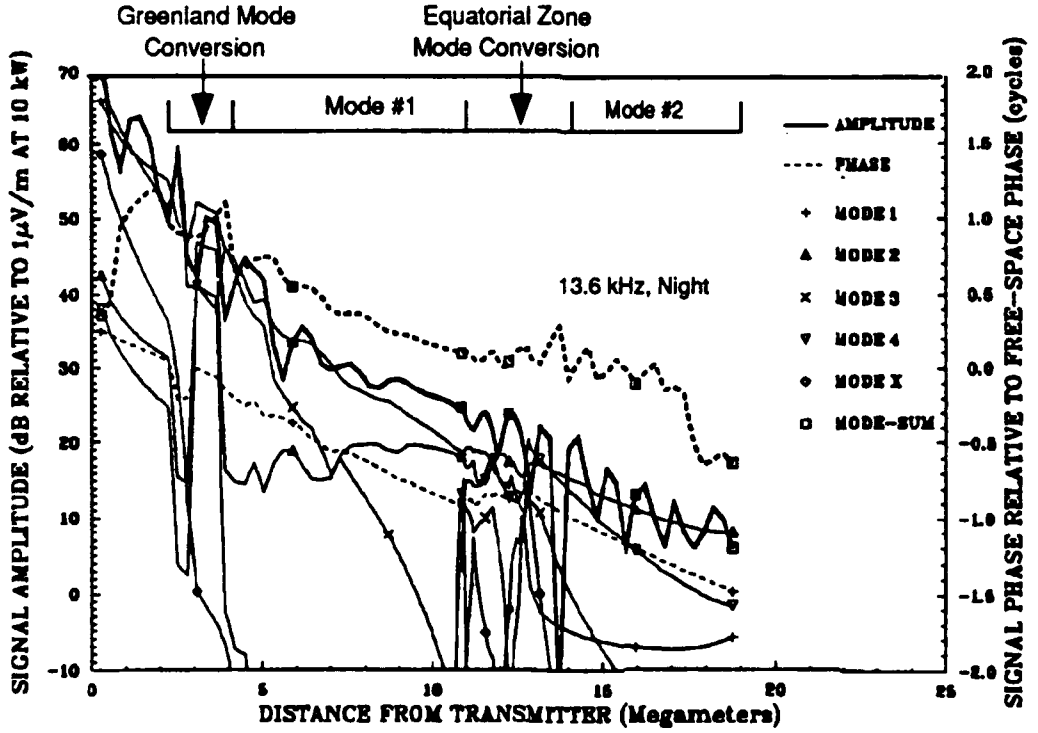

Figure A–3. Calculations of the Norway Signal Propagated Along the 290° Radial.

Within the equatorial zone (±7.5° magnetic latitude) mode competition is incurred (*Mode Conversion*) because of efficient conversion of the dominant mode to higher-ordered modes. Beyond the equatorial zone for most of the validation region, mode 2 is dominant (*Mode Switching*). Not much evidence of modal interference (large signal amplitude fluctuations with distance) is predicted where mode 2 prevails. This is because mode 2 is sufficiently strong that, when it is in phase opposition to mode 1, the signal cancellation is minimal. Figure A-2 shows another zone of striations to the west of the Greenland shadow zone. The calculations show that mode 2 can become dominant for certain radials (usually alternate radials) traversing Siberia.

The predicted dominance of mode 2 in this area appears to be highly sensitive to the terrain conductivity features used in calculations. The calculations also indicate that verification of this switching between dominance and non-dominance of mode 2 would require obtaining data at many locations across the zone.

The propagation for local winter in the validation region is expected to be quite different due to the effects of propagation over the Arctic and Antarctic. In austral winter the Arctic is in daylight and the signal incurs as much as 40 dB attenuation over low conductivity terrain, such as Greenland. Antarctica incurs night conditions with its attendant mode conversion. The resultant loss beyond Antarctica is minimal, but the phase has an uncertain history. Much of the southern part of the South Pacific region is dominated by the long-path signal traversing Antarctica. This long-path dominance extends quite a distance up into the Greenland shadow zone.

The antipode of Norway is at 66.42 S, 166.85 W just above Antarctica. During the validation data collection phase, the long-path signals of concern traversed the continuous daytime Antarctica, thereby incurring about 40 dB additional attenuation.

The area at nighttime (2330 to 1100 on the eastern edge and 0830 to 2000 on the western edge during February) over which unusable phase may be possible covers over 50 percent of the South Pacific validation region.

The negligible illumination of the polar part of the propagation path to this region during the validation data collection period appears to allow night conditions to prevail.

B) LIBERIA:

The zones for night propagation of possible poor phase on Liberia signals in the South Pacific are shown in Figure A-4. The Liberia station is at the northern edge of the equatorial zone and propagation to the northern part of the South Pacific region is within this zone. The Mode Conversion zone extends for large distances and shows highly complex modal conversion. All signals traversing this *Mode Switching* zone are predicted to be mode 2 dominant because of the transequatorial propagation. The calculations show that the relative strength of the modes leaving the equatorial zone can vary greatly with azimuth. Thus, within the *Mode*

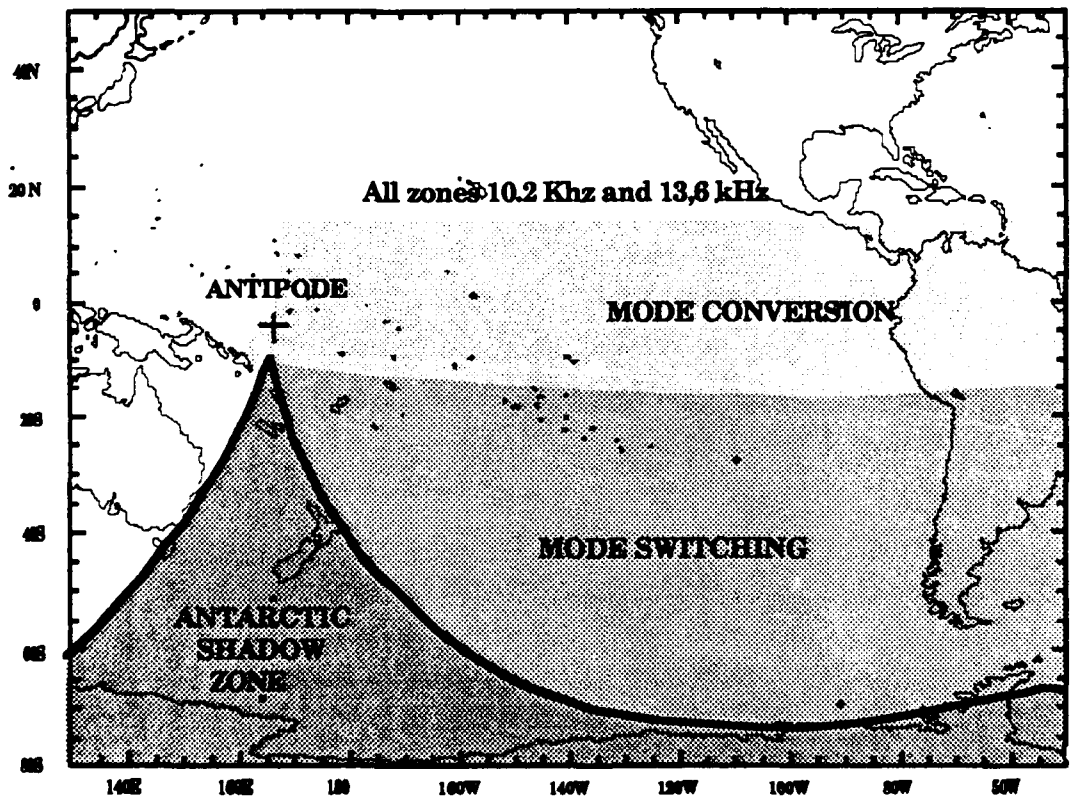

Figure A-4. Modal Competition Zones for the Liberia Signal.

Switching zone on some radials large modal structure is predicted, while on others, very little structure is predicted. Figure A-5 shows a representative calculation of the Liberia signal showing mode conversion.

The total area at nighttime over which unusable phase may be possible is over 80 percent of the South Pacific validation region. The all-night condition occurs from 2330 to 0630 on the eastern edge, but no all-night condition occurs west of Samoa.

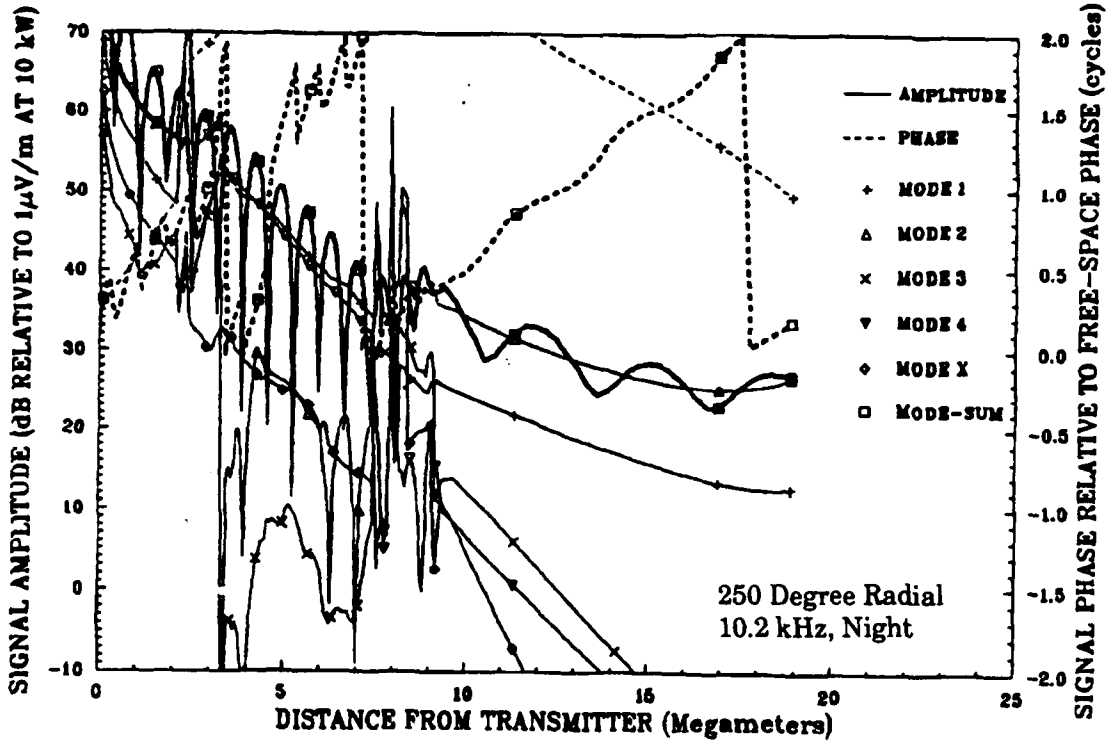

Figure A-5. Calculations of Liberia Signal Propagated to South Pacific.

(C) HAWAII:

Near Modal is predicted to be a potential problem in eastward propagation from Hawaii. To review: in the *Near Modal* condition multiple modes are radiated from a transmitter, each with a different launch efficiency, attenuation rate and phase velocity. In some cases at nighttime, multiple modes remain close in amplitude for significant distances from the transmitter. The navigation signal is considered

unreliable if a higher-ordered mode is dominant. The boundary beyond which mode 1 is dominant is quite variable, as is propagation. Generally, Near Modal would be a potential problem only from stations near or within the validation region. Hawaii is a possible exception. The extent to which this condition extends from Hawaii into the South Pacific validation zone is questionable. An example of a possible worst-case propagation situation is shown in Figure A-6. This Figure shows the Hawaii signal on a 120° radial for 10.2 and 13.6 kHz. At 10.2 kHz mode 1 is shown to be dominant beyond 2.2 Mm, but mode 3 is of sufficient amplitude to cause a significant interference pattern to about 8 Mm. Furthermore, if the relative modal excitation factors or relative attenuation rates change just slightly, mode 3 could be dominant to beyond 5 Mm. At 13.6 kHz mode 3 is shown to be dominant to 9 Mm; beyond that, mode 1 is dominant. Again, slight changes in propagation parameters could cause the mode crossover distance to move several megameters in either direction. The challenge is to establish a safe distance for each radial beyond which the higher-ordered mode is unlikely to become dominant; that is the distance at which the use of each transmission becomes reliable. Sensitivity studies conducted with a multi-frequency VLF/LF sounder showed that on the propagation path from Hawaii to San Diego ionosphere gradients of $\beta = 0.85$ were frequently required to account for the measured propagation. Such a gradient supports much stronger multi-mode propagation. We are not aware of a detailed analysis, either theoretical or experimental, conducted for Omega signals, especially for those radials showing maximum extent of modal competition.

For Hawaii, the possible extent of unreliable phase is shown in Figure A-7. The zone to the east of Hawaii is caused by *Near Modal*. The set of calculations show that the interference pattern extends to much greater distances at 13.6 kHz than at 10.2 kHz. Shown in this Figure are: (1) boundaries for the predicted crossover of mode dominance between modes 2 and 1 at 10.2 and 13.6 kHz, (2) estimates of possible maximum

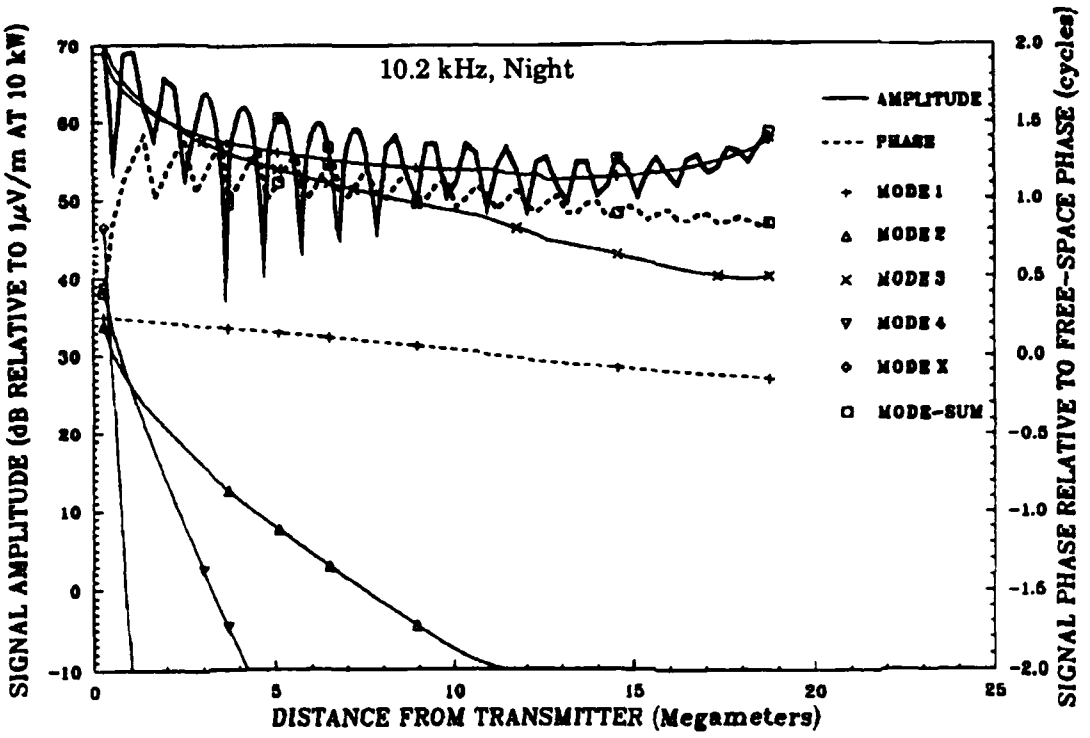

Figure A-6a. Hawaii Signal Propagation on the 120° Radial
10.2 kHz, Night

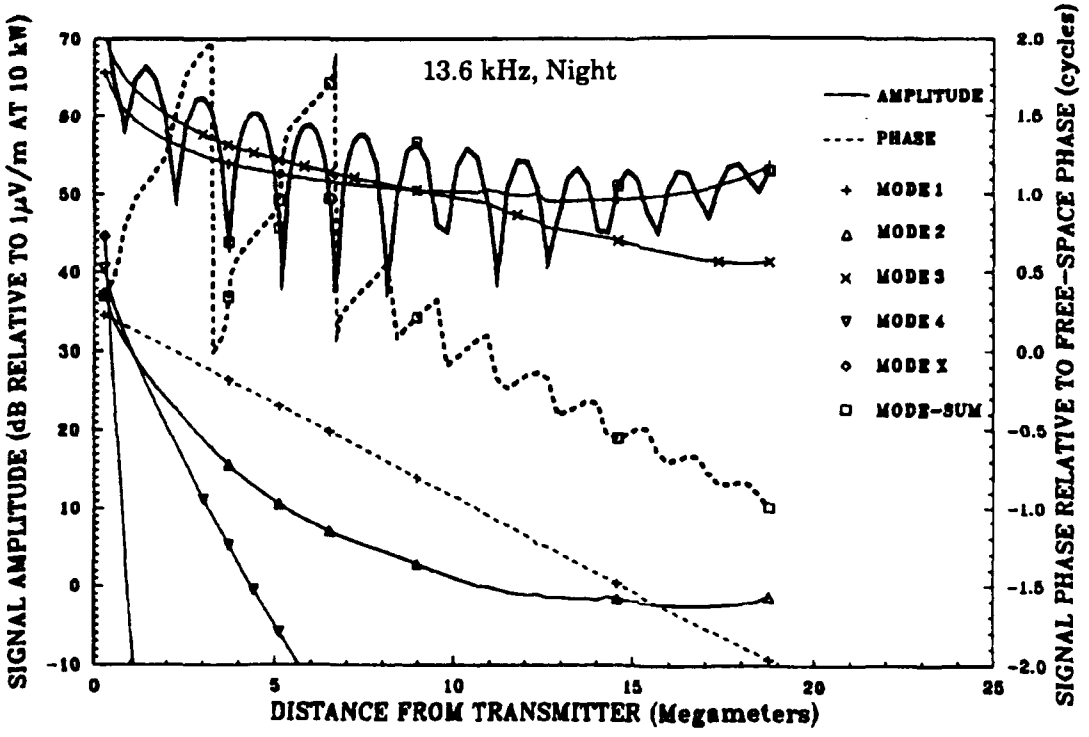

Figure A-6b. Hawaii Signal Propagation on the 120° Radial
13.6 kHz, Night

boundaries where mode 2 could possibly be dominant, and (3) a possible lesser crossover boundary for 13.6 kHz (labeled "Most Likely"). The rationale for each of these boundaries will be described in the discussion of data interpretation in section 4.0, *INTERPRETION OF VALIDATION ANALYSIS.*

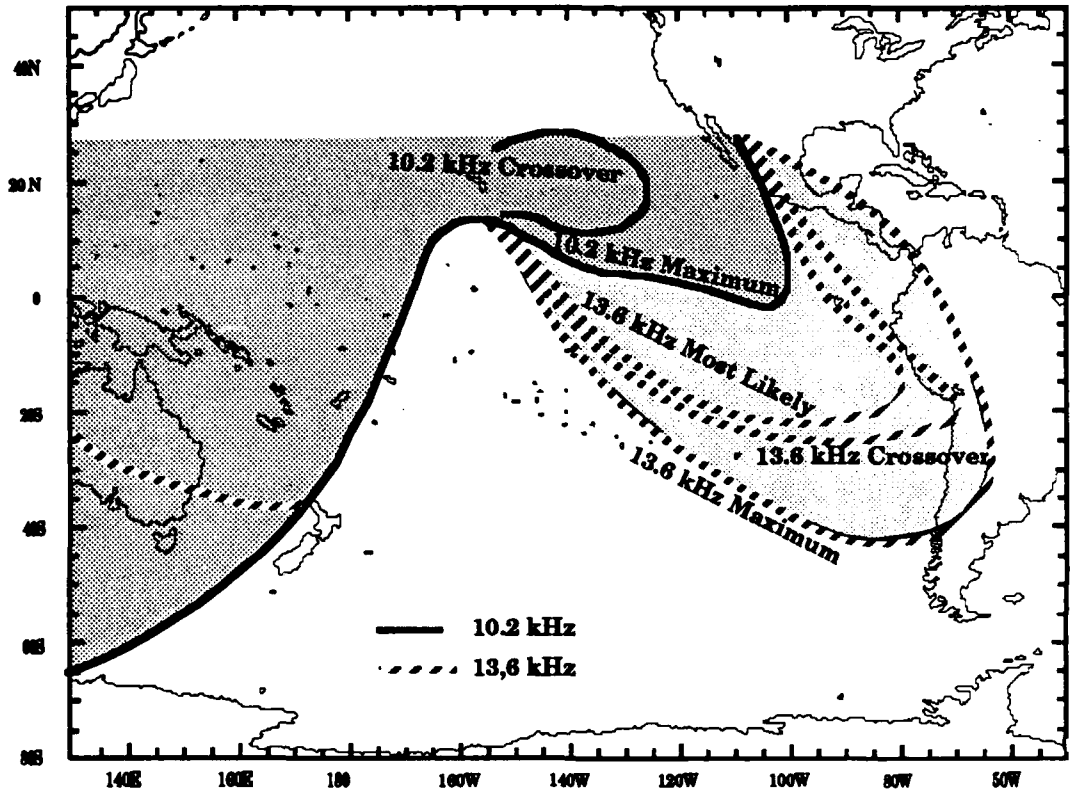

Figure A-7. Modal Competition Zones for the Hawaii Signal.

For radial bearings westward of 180°, mode conversion that occurs as the signal propagates across the equatorial zone becomes the dominant factor in determining the area of unreliable signal. The onset of mode conversion occurs within a very short heading change interval. This is illustrated in Figure A-8, which shows the calculated signals at two headings, 200° and 205° for respectively 10.2 and 13.6 kHz. The equatorial zone lies approximately between 2.5 and 3.8 Mm. A small amount of mode conversion is noted at the 200° heading by a slight increase in the level of modes 2 and 4 in the transequatorial region. At the 205° heading, mode conversion has become very strong with, at 10.2 kHz,

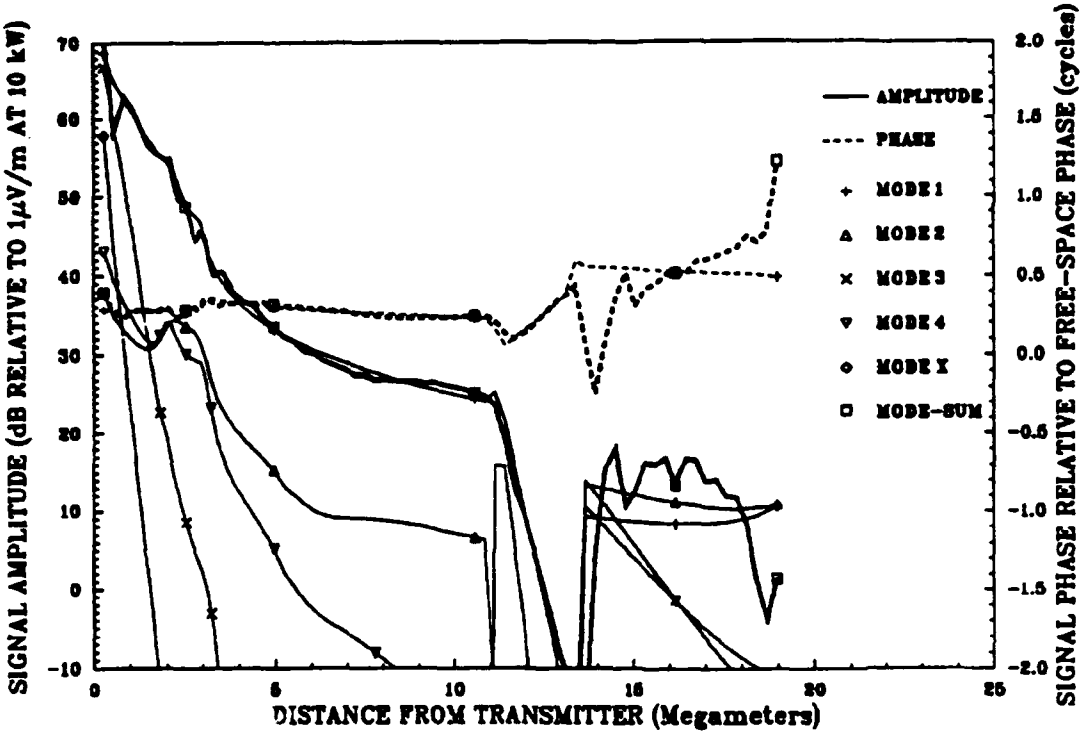

Figure A-8a. Hawaii Signal Propagation on 200° Radial, 10.2 kHz, Night.

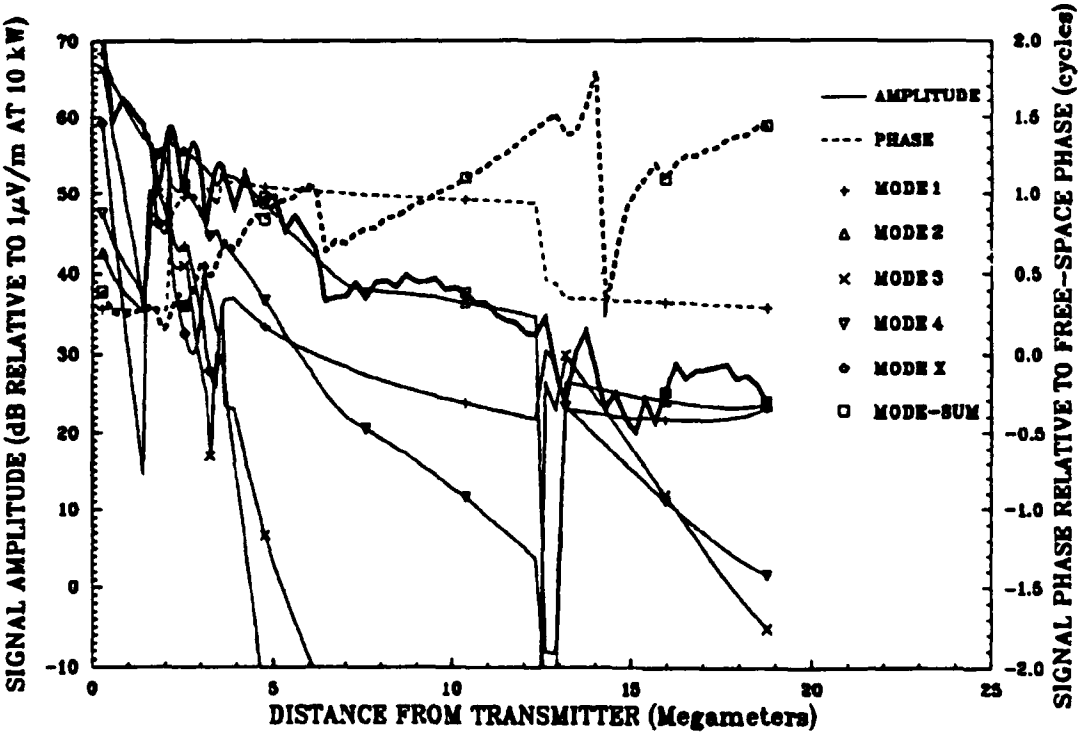

Figure A-8b. Hawaii Signal Propagation on 205° Radial, 10.2 kHz, Night.

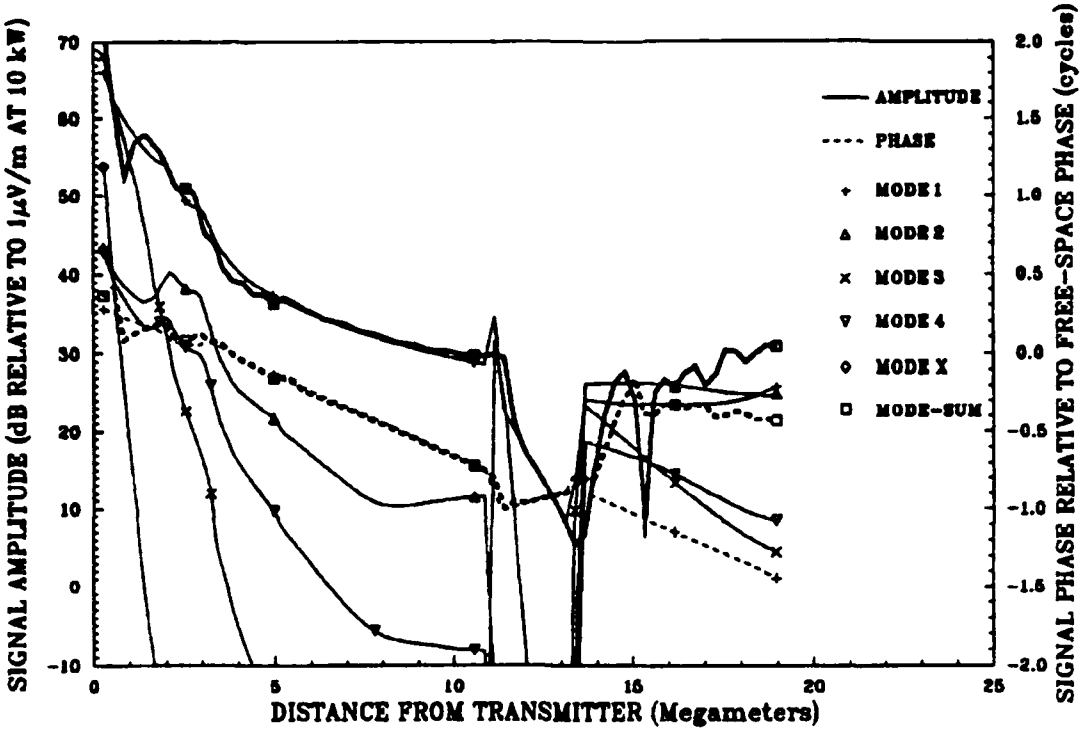

Figure A-8c. Hawaii Signal Propagation on 200° Radial, 13.6 Khz, Night.

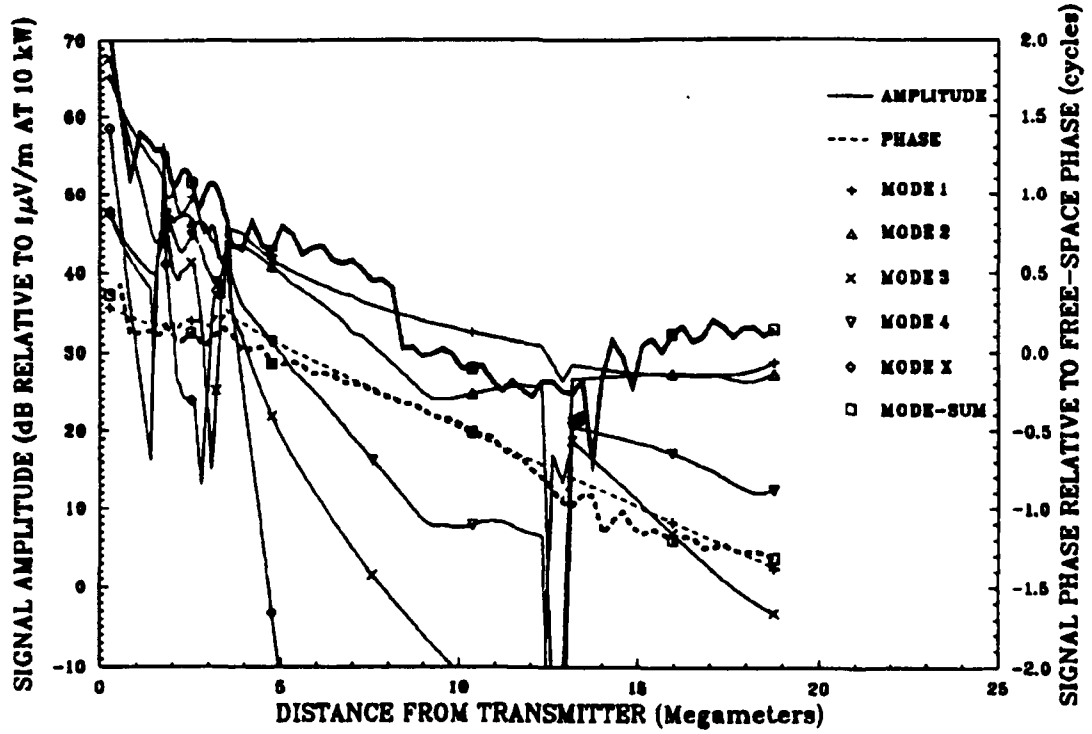

Figure A-8d. Hawaii Signal Propagation on 205° Radial, 13.6 Khz, Night.

mode 2 being the dominant mode beyond the conversion region. At 13.6 kHz, mode 1 exits the region slightly dominant. By a radial bearing of 210°, mode 2 is dominant to 7.4 Mm. Beyond the equatorial zone, mode competition may or may not exist, depending upon the relative level of the modes exiting this zone. The calculations show that the modal levels are quite sensitive to radial bearing. It is possible that the modal levels would also be quite sensitive to ionosphere parameters. The sensitivity to ionosphere parameters could lead to a seasonal effect, a possibility not investigated.

The total area at nighttime (0430 to 1130 GMT on the eastern edge and 0830 to 1700 on the western) over which unusable phase may be possible is as much as 50 percent of the South Pacific validation region. During daytime no signal self-interference problems are expected in the South Pacific validation region.

D) NORTH DAKOTA:

The zones for nighttime propagation of possible poor phase on North Dakota signals in the South Pacific are shown in Figure A-9. The signal from North Dakota incurs modal conversion in propagation in the equatorial zone at headings greater than 205°. A sample calculation showing the equatorial zone effects is shown in Figure A-10. For both 10.2 and 13.6 kHz mode 2 is dominant exiting this zone. The northern boundary moves northward with more westward propagation, as does the magnetic equator. As with Hawaii the buildup of modal conversion occurs very quickly as the signal's direction of propagation increases beyond 200°. Mode 2 for 10.2 kHz extends to Antarctica, while at 13.6 kHz it is eventually exceeded by mode 1. The modal interference structure and magnitude in the zone below the equator varies in a complex manner in relation to frequency and direction of propagation. The total area at nighttime (2330 to 1130 on the eastern edge and 0900 to 1300 on the western edge) over which unusable phase may be possible is as much as 60 percent of the South Pacific validation region. For all daytime propagation no modal signal self-interference is expected.

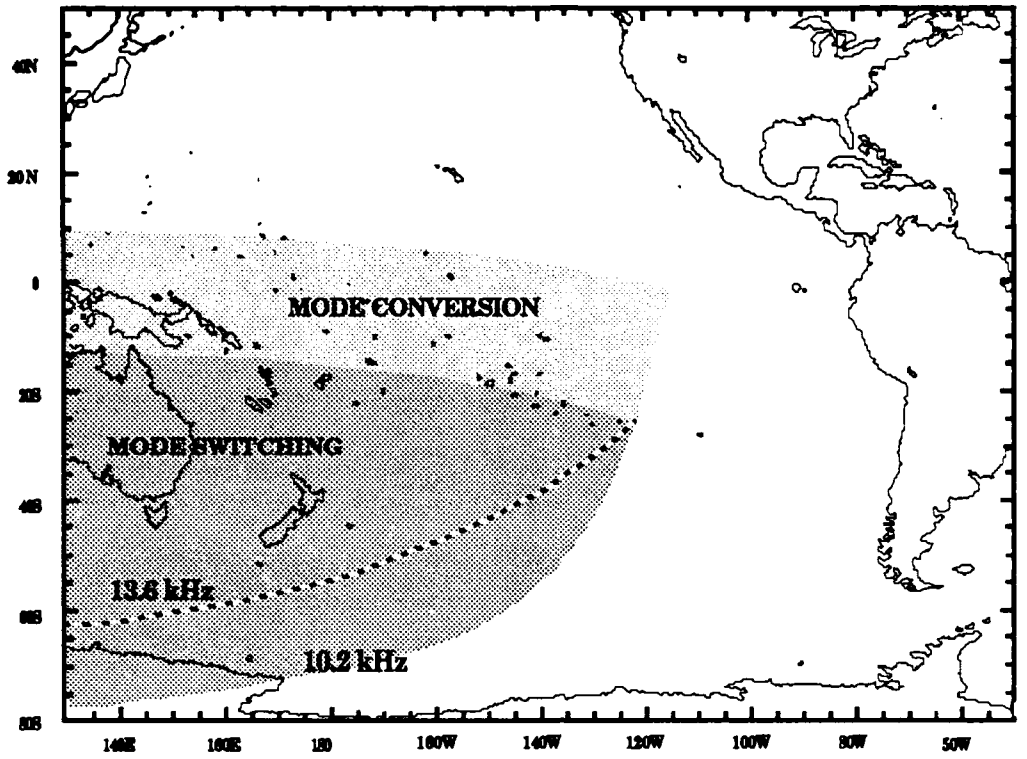

Figure A-9. Modal Competition Zones for the North Dakota Signal.

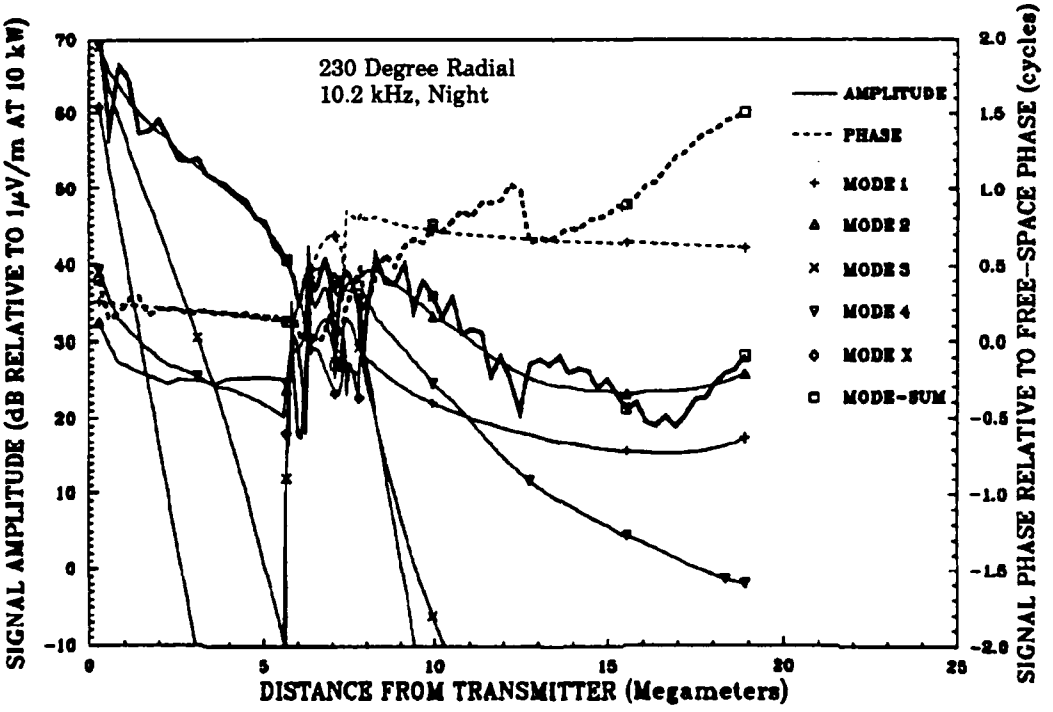

Figure A-10. North Dakota Signal Propagation to the South Pacific.

(E) LA REUNION:

The zones of possible poor phase on La Reunion signals in the South Pacific are shown in Figure A-11. A sample calculation showing the equatorial zone effects is shown in Figure A-12. During austral summer the Antarctica shadow incurs 40 dB additional attenuation; much of this zone was probably covered by long-path from the north during the data collection period. Long-path signals (on radials 335° to 20°) could be dominated by either mode 2 or 1, depending upon effects of traversal of both the equatorial zone north of the transmitter and the Arctic low conductivity areas. For the short-path propagation, the equatorial zone mode conversion starts at the 180° radial, and after exiting from the Antarctic shadow, the 200°radial causes mixed mode or mode 2 dominance extending in the equatorial zone to the eastern end of the validation region. The propagation direction is to the north and west in this eastern zone.

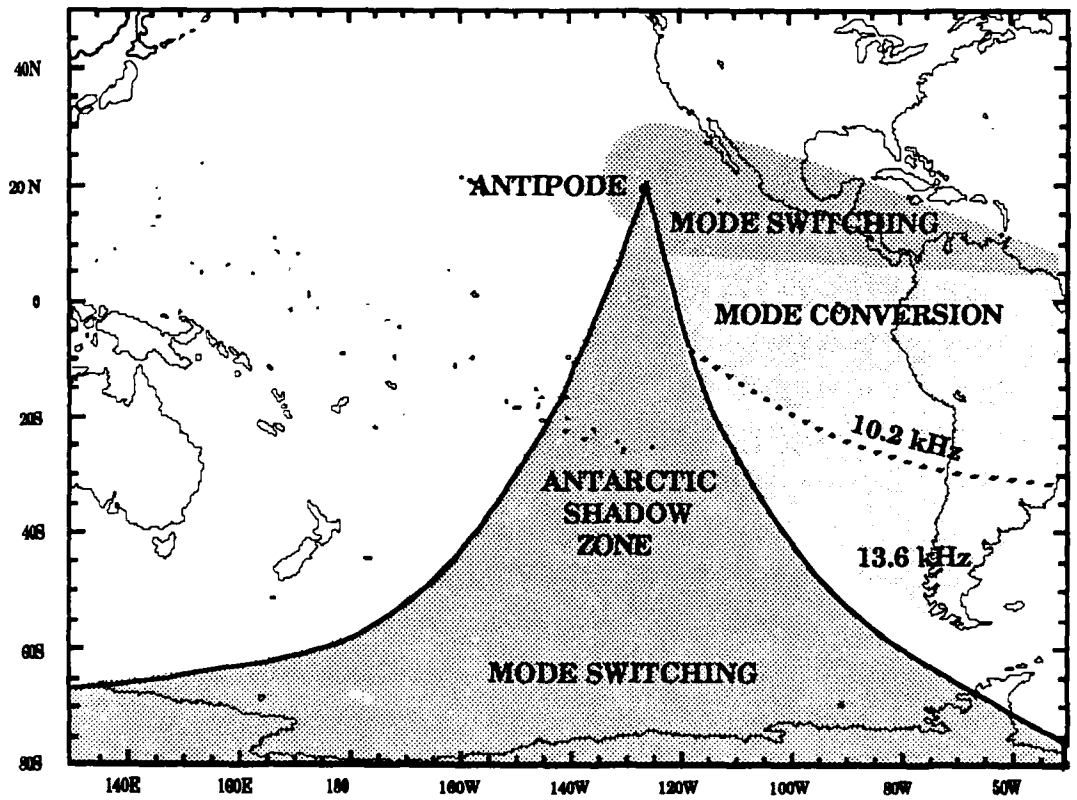

Figure A-11 Modal Competition Zones for the La Reunion Signal

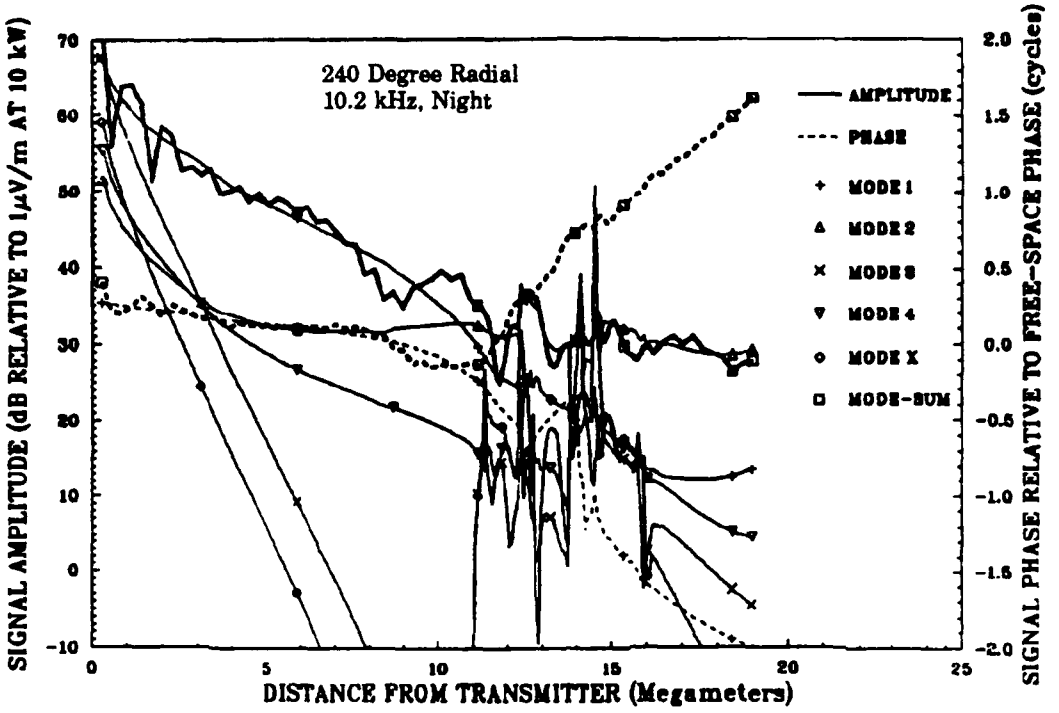

Figure A-12. La Reunion Signal Propagation to the South Pacific.

Propagation across Antarctica during austral winter (24-hour night in Antarctica) causes conversion to mode 2 dominance at both 10.2 and 13.6 kHz, producing a *Mode Switching* zone in the Antarctic shadow. Propagation across Antarctica creates the dominant effect (155° to 200° radials) even after propagation across the equatorial zone.

The total area at nighttime over which unusable phase may occur is as much as 30 percent of the South Pacific validation region. All night on the propagation path in late February starts on the eastern edge with sunset at about 1130 GMT and moves westward reaching its maximum extent at 0200 GMT. The western all-night boundary follows approximately the eastern edge of the Antarctica shadow zone. Westward of this boundary a total night propagation path is not possible in February.

The boundary where the short and long-path signals are equal varies from a maximum eastern position near the equator at 15° W Longitude (0800 to 1500 GMT) to a maximum western position about at the western boundary of the antipode zone (135° W Longitude at 0200). The eastern boundary would

be a large arc crossing South America a few degrees below the Argentina transmitter. The western boundary would be a tight semicircle around the antipode until intersection with the north/south radials. The long-path extension beyond the antipode is expected to be mode 1.

(F) ARGENTINA:

The zones of possible poor phase on Argentina signals in the South Pacific are shown in Figure A-13. Four zones are depicted. The 10.2 and 13.6 kHz signals have different envelopes of bad signals. The 10.2 kHz envelope showing the start of unusable phase is closely tied to the southern boundary of the equatorial zone (mode conversion). Mode 2 dominance occurs after exiting the equatorial mode conversion zone (mode switching). The eastern boundary reflects the decay of the equatorial effect. The 13.6 kHz southern boundary reflects a much more complex situation. Many modes are excited efficiently; mode 3 is initially dominant on most of the radials. Often mode 2 becomes dominant near 2 Mm, but at some headings mode 1 can become slightly dominant for up to 1.5 Mm. Once the equatorial zone is reached, rapid mode conversion takes place with many modes switching around. Beyond the equatorial zone, mode 2 is predicted dominant. The Near Modal zone for 13.6 kHz would probably be highly dependent upon propagation conditions and thus be quite different from time to time. A sample calculation showing the mode interaction effects is shown in Figure A-14.

The Antarctic shadow zone is mostly to the west of the validation region. This zone is far from the antipode (20.97N, 114.81 E). Due to propagation across the Antarctic during daylight, the signals are expected to be very weak during local summer. During parts of winter the signal in this zone could be either mode 1, 2 or 3, depending on the radial and distance.

The *Near Modal* zone, i.e. close-in, for 10.2 kHz shows an oval shape, extending eastward beyond the edge of Figure A-13 to a distance of 2.7 Mm. The north and south distances are around 0.6 Mm, and the western boundary extends to 1 Mm. For 13.6 kHz, the *Near Modal* zone is predicted to extend across the validation region to the northwest. To the north and

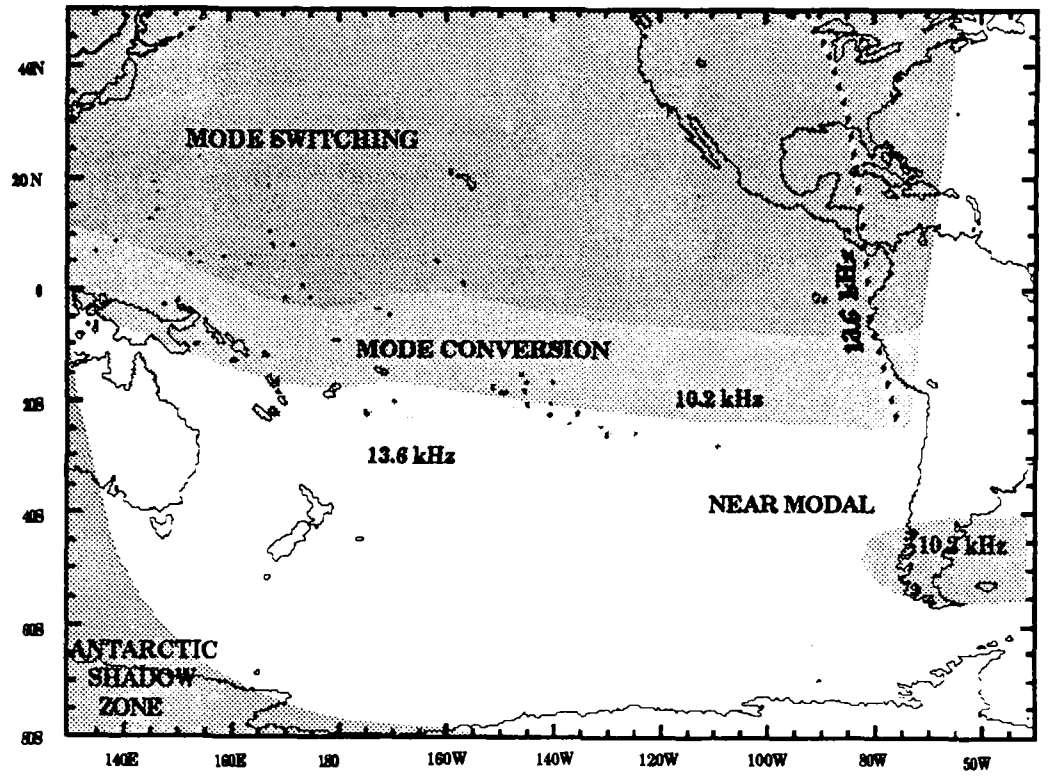

Figure A-13 Modal Competition Zones for the Argentina Signal

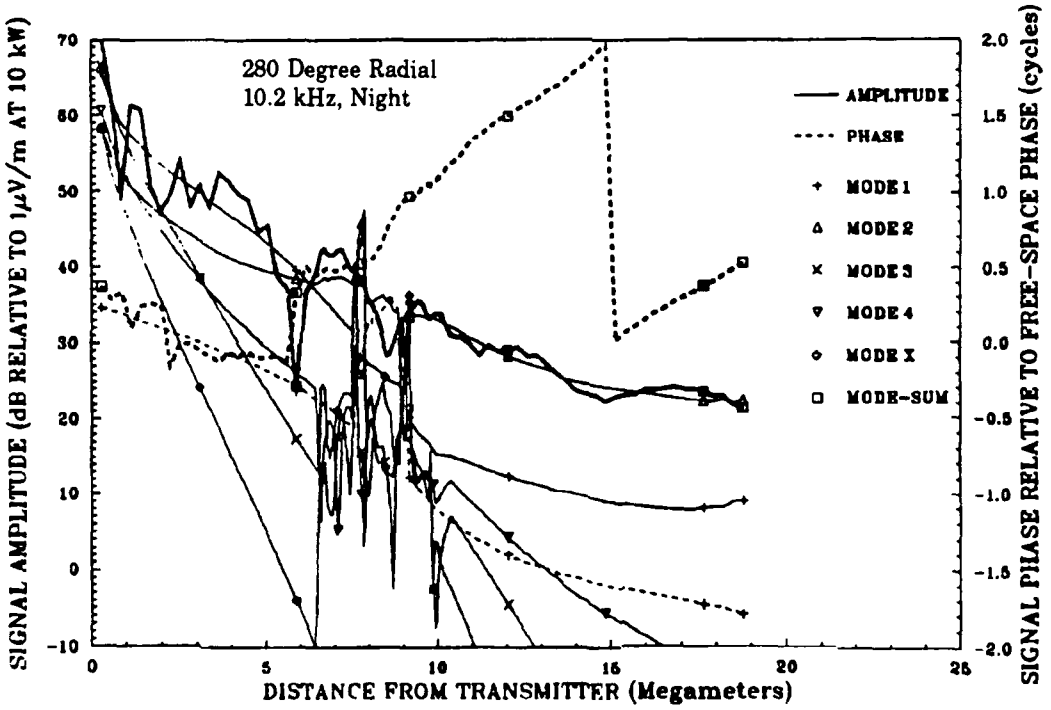

Figure A-14. Argentina Signal Propagation to the South Pacific.

south the boundary is respectively 0. 9 and 1.3 Mm, and to the northeast (60°) the border extends to 6 Mm.

The total area at nighttime (1000 to 2330 GMT at the transmitter, east edge, and 0900 to 1000 GMT on the western edge) over which unusable phase may be possible is as much as 50 percent of the South Pacific validation region.

(G) AUSTRALIA:

For Australia, the only zone of possible unusable phase is the *Near Modal* around the transmitter. This zone for nighttime is shown in expanded scale in Figure A-15. For 10.2 kHz this extends to 0.6 north, 0.9 Mm east, 0.7 Mm south and 0.7 Mm west. For 13.6 kHz the zone extends 1.1 Mm north, 2.4 Mm east (100° & 110°), 1.4 Mm south and 1.9 Mm west. The boundary shape for both frequencies is a smooth near oval.

The total area at nighttime over which unusable phase may be possible is a very small portion of the South Pacific validation region. No long-path self-interference is expected in the South Pacific validation zone.

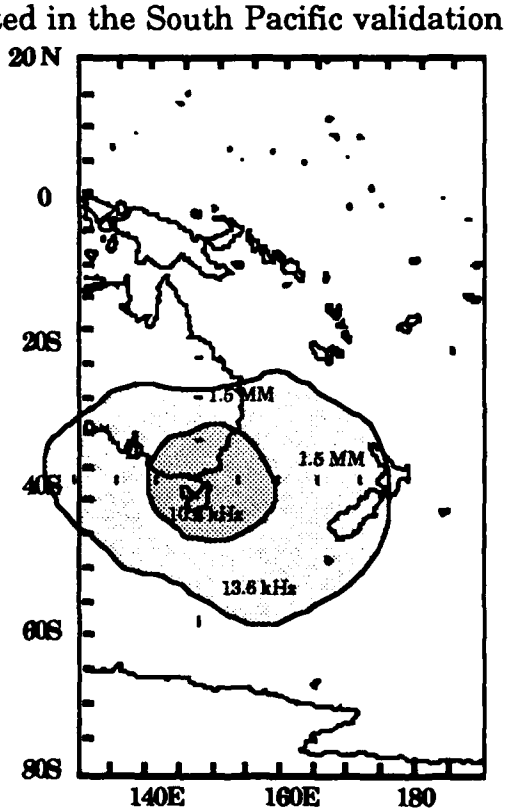

Figure A-15. Modal Near Zone for the Australia Signal.

(H) JAPAN:

The zone of possible poor phase on Japan signals in the South Pacific is shown in Figure A-16. The predictions show possible extended mode competition, *Near Modal*, extending into the northwest corner of the validation region. The phenomenon is the same as described for eastward propagation from Hawaii. A sample calculation showing the mode competition effects is shown in Figure A-17. For 10.2 kHz, the predicted boundary for maximum possible extent of mode 2 dominance does not quite reach the northern edge of the validation region. For 13.6 kHz, two boundaries are shown. The shaded area, labeled "Maximum" is the maximum possible extent of modal competition. The line labeled "Crossover" signifies the transition of dominance from mode 3 to 1. Near the crossover line the slope of mode 3 compared to mode 1 is only about 1 dB per Mm greater. Thus, this boundary line could vary quite a bit with expected variations in propagation conditions.

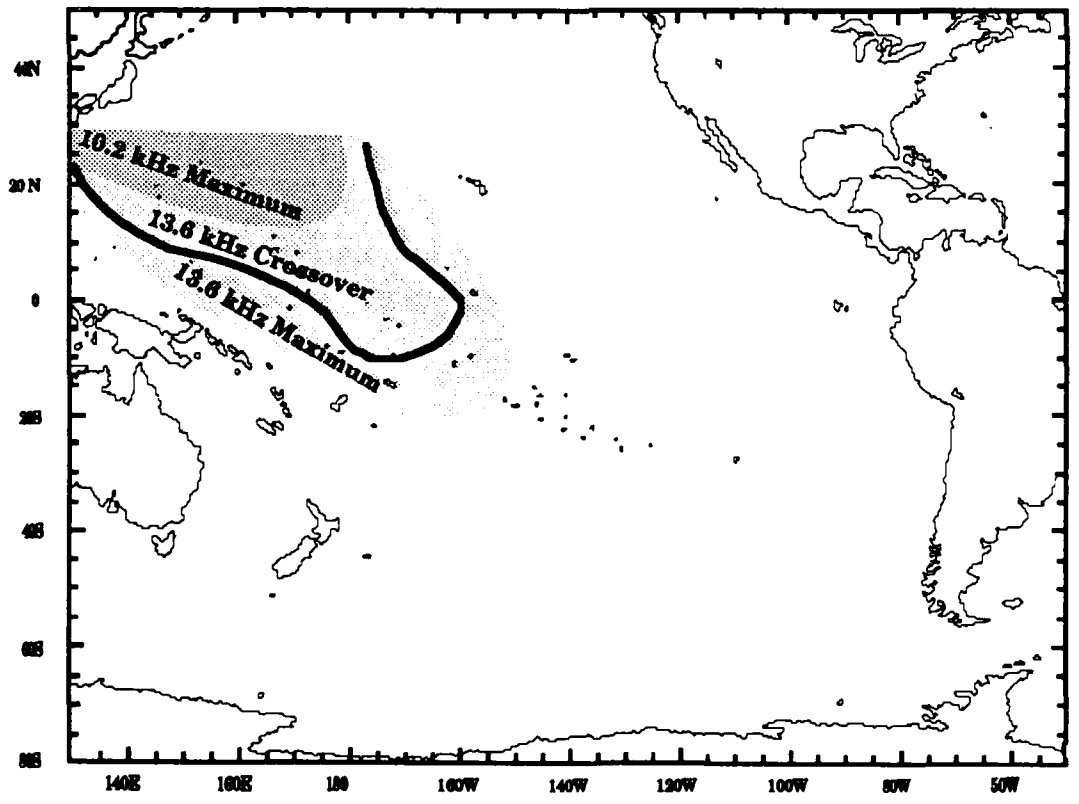

Figure A-16. Modal Near Zone for the Japan Signal.

The total area at nighttime over which unusable phase may be possible is probably less than 10 percent and could be less than 5 percent of the South Pacific validation region. All-night propagation to locations within the shaded area of Figure A-16 occurs between 0900, sunset at Japan, and 1600, sunrise at the eastern edge.

No long-path self-interference is expected from the Australian signal in the south Pacific validation region.

The propagation predictions from calculations are used in this section to serve as guidance for data analysis assessment and as a model for extending measurements to the total South Pacific Validation region. It should be emphasized that these charts are for nighttime propagation on each signal path and thus are time static. This means they do not take into account the diurnal variability of the zones of unusable phase. They are also seasonally static. Variations in solar illumination at the poles are not integrated into the analysis. While these charts are considered a good model for validation data assessment, further interpretation is needed to derive navigation guidance.

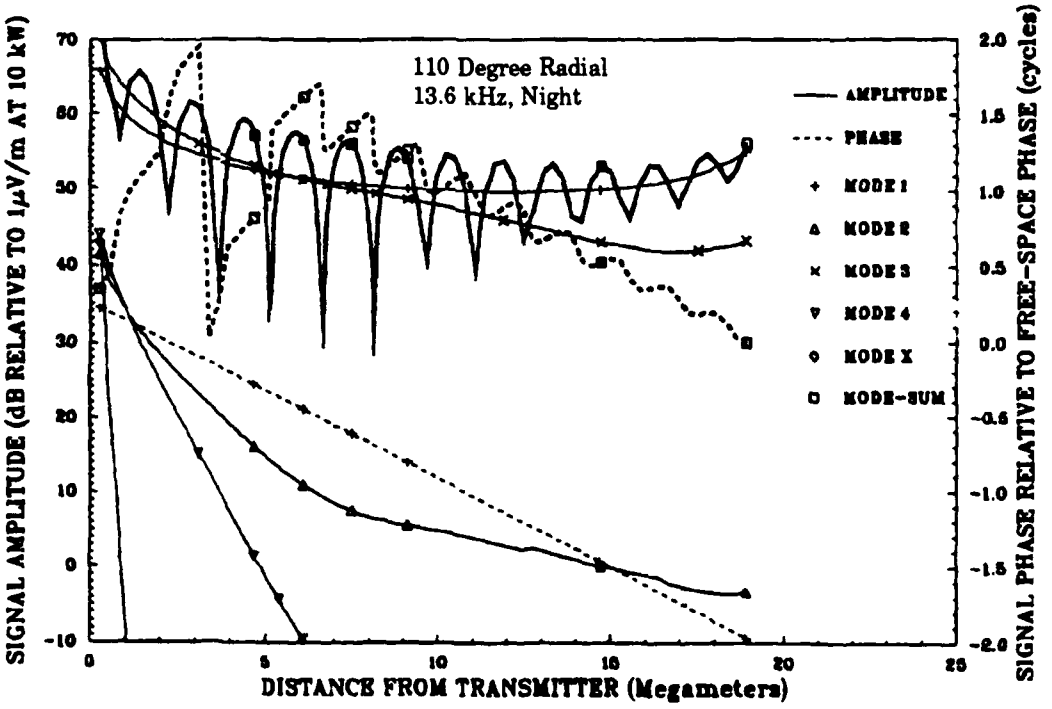

Figure A-17. Japan Signal Propagation Showing Modal Structure.

Appendix B

Modal Interference Data Analysis

OVERVIEW

The procedure used for data interpretation was to work across the validation region following the sequence of flights. The process used for each flight was (1) for each station, to determine what the calculations predicted in terms of dominant mode and signal amplitude structure along the flight and at each flight terminal, (2) to compare flight amplitude data with calculations, and (3) where available, to examine fixed-site phase data for possible modal effects.

Since the flight paths usually varied in both distance and azimuth with flight time, it was generally necessary to construct a predicted signal from a cross section of calculated radials. An example of deriving cross section calculations is shown in Figure B-1. When the distance from the transmitter was large, the available radials, generally calculated at ten degree intervals, produced rather sparse prediction values along the flight path. This sparseness was a problem when the computed signals changed markedly between radials as shown in Figure B-2. Cross sections similar to the example of Figure B-1 were prepared for each station for each flight. The cross section data were then compared with received flight amplitude data.

The fixed-site phase and phase-difference data were used for two purposes. First, a check was made to determine, as much as possible, the propagation conditions at the time of flights. Second, a check was made to determine how the data at flight time related to the total data set available at that site.

The fixed-site data were processed in several different ways. First, at those sites where the received phase was referenced to an atomic frequency standard, the diurnal phase for each received frequency (10.2, 11.33, and 13.6 kHz) was examined for evidence of modal influence.

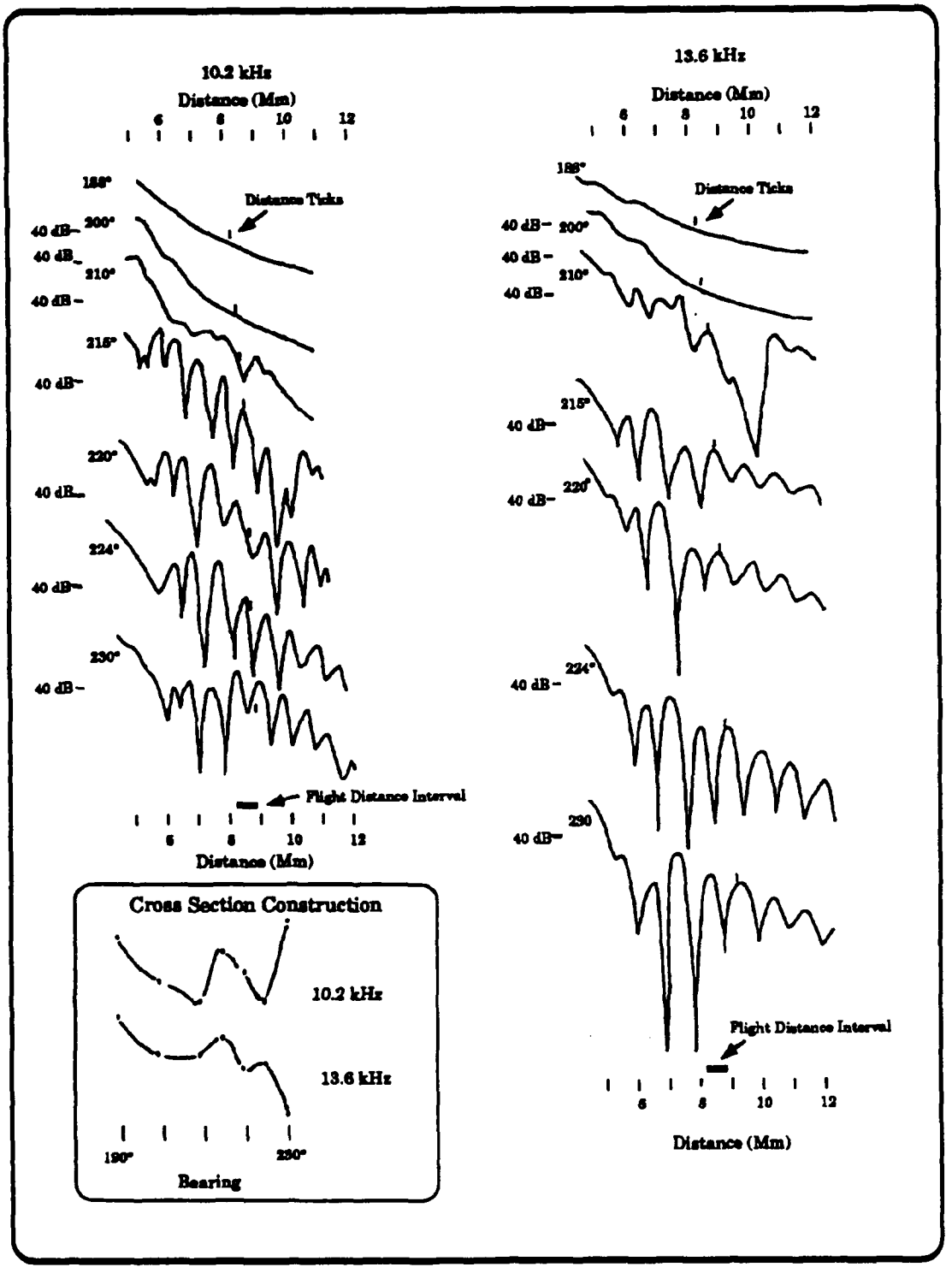

Figure B-1. Example Showing an Amplitude Cross Section Derived from Data on Several Radials

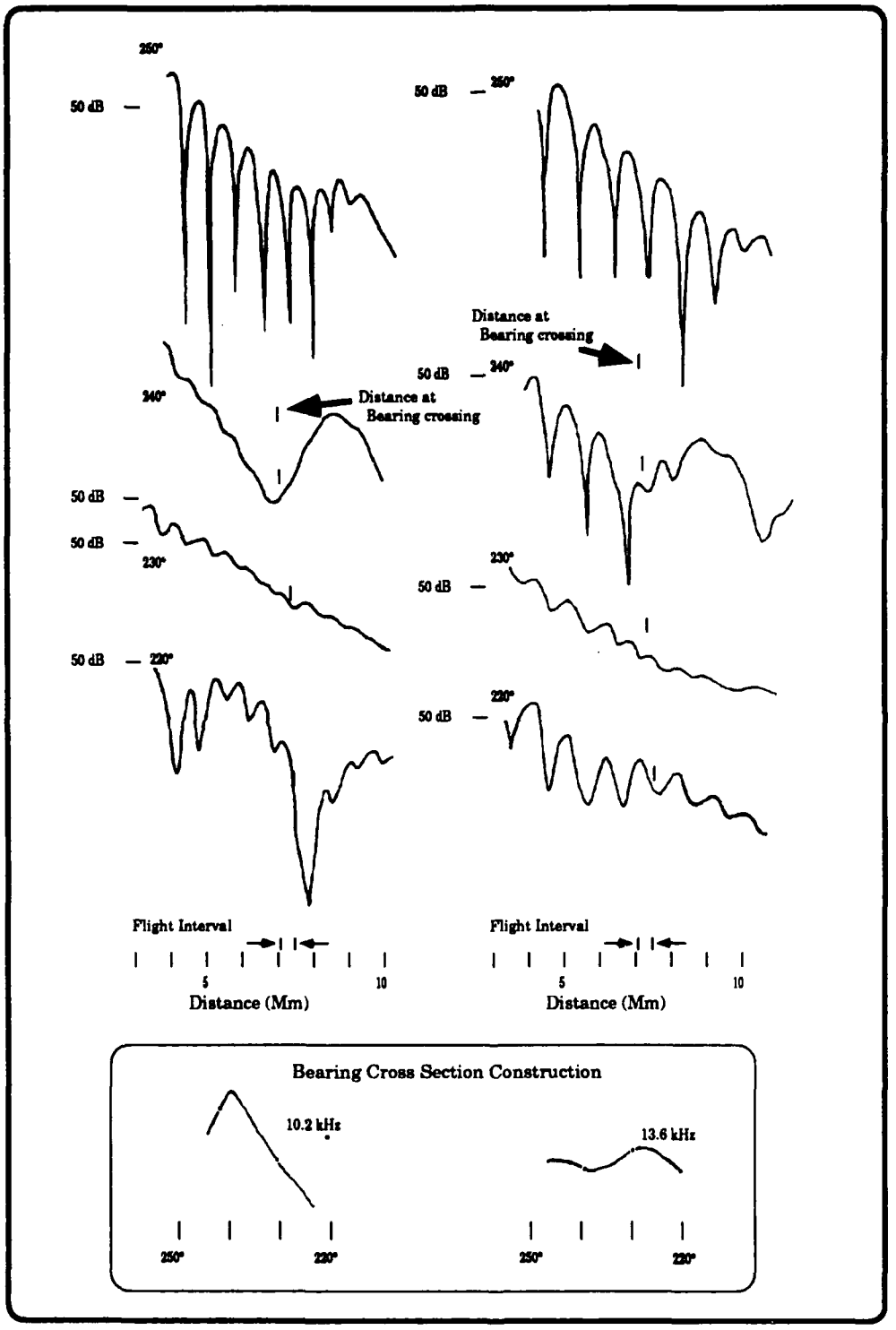

Figure B-2. Example Showing an Amplitude Cross Section from Widely Seperated Radials

Second, where an atomic frequency reference was not available, two processing methods were used. In the first method, an estimate was made of the linear reference oscillator drift from the measured phase offset between successive midpath noon times on the best quality signal. The drift rate was then incrementally subtracted from all measurements. The ideal result was a nearly stable phase reference diurnal phase curve for each measured signal. In most cases, the reference oscillator frequency offset was sufficiently constant over a 24-hour period, that the correction process made possible phase plots from which signal self-interference could easily be evaluated. In a few cases the reference frequency change was too rapid to instill high confidence in the interpretation. In the second method, phase-difference data between two received stations were examined. In using phase-difference data, an attempt was made to use a strong signal containing only a first mode as a reference for evaluating those signals suspected of having modal interference.

Several examples of diurnal phase data are presented to illustrate the information content in the data. In Figure B-3a, an example is given of received signals where mode 1 is strongly dominant. Two characteristics are very evident. First, the diurnal phase pattern follows a very characteristic shape with the following properties: (1) different day and night reflection heights with smooth transitions between, (2) the expected solar zenith angle effect during daylight, and (3) some continuing relaxation of the ionosphere throughout the night. Second, when fluctuations due to naturally varying propagation conditions do occur, the phase response at all frequencies is very similar as shown in Figure B-3b. The data for the two dates show evidence for different propagation conditions as seen in the different phase patterns for each group. Even though the groups differ, the phase records for each frequency within a group show nearly the same trend. Many variations within hours and between days are observed in the data, yet these variations across a set of frequencies are very similar.

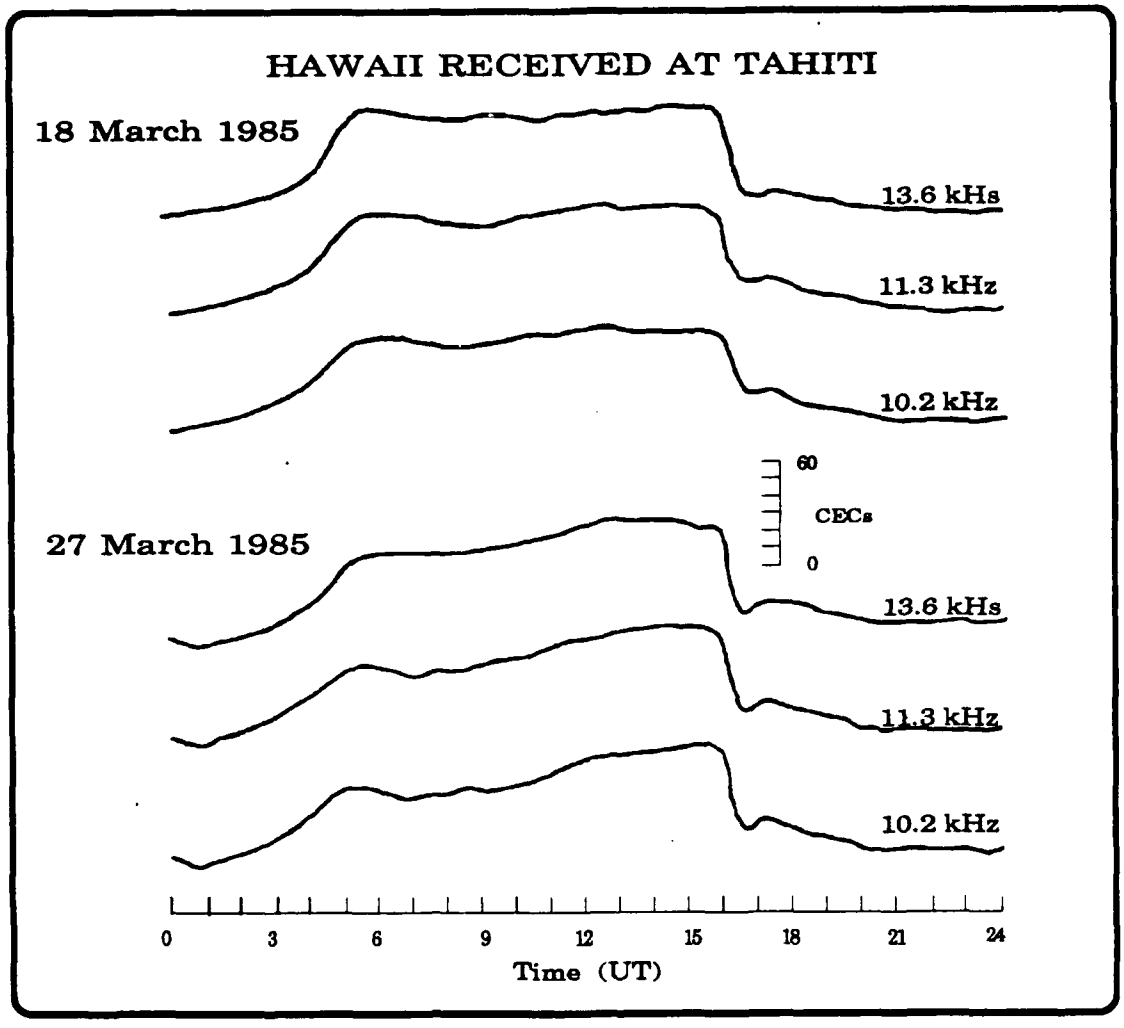

Figure B-3. Example of Measured Phase when Mode 1 is Dominant.

When modal competition is present, there is much less similarity between phase records across frequency. Modal competition exists on many transmissions, one being North Dakota propagating to the South Pacific. Many data samples from Tahiti show the presence of multiple modes. An example of the type of phase data obtained is shown in Figure B-4. This figure shows phase records of three frequencies for 24-hour periods for two separate days. The objective is to show that the phase records between sets and within a set are quite different at night and at transition times (0300 to 1600) between frequencies and between days. This is in marked contrast to the single-mode phase behavior shown in Figure B-3. Each trace for each frequency is quite different.

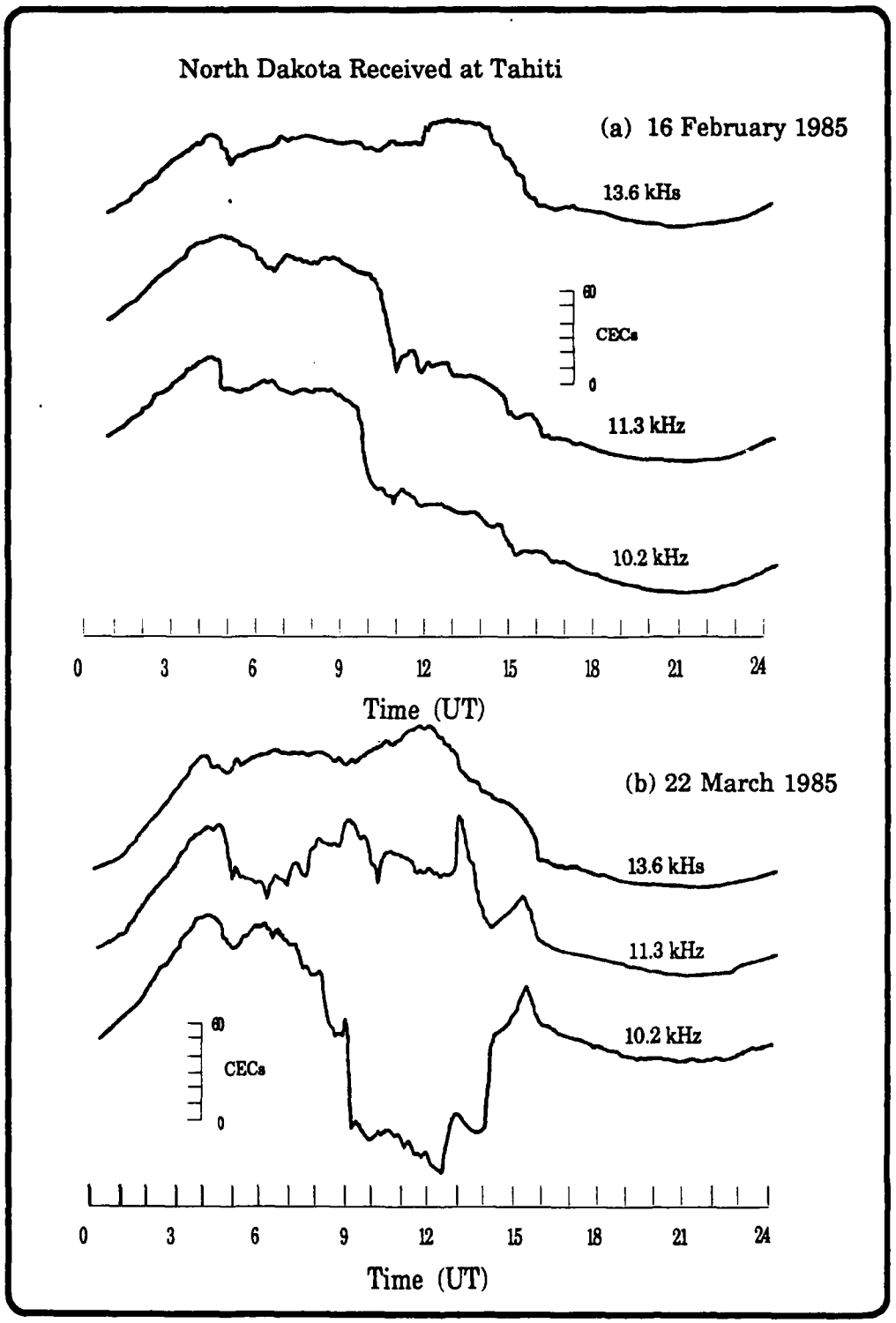

Figure B-4. Example of Measured Phase when Strong Modal Competition is Present.

In Figure B-4a, recorded on 16 Feb. 1985, the two lowest frequencies undergo a cycle advance in the middle of the nighttime period. This is not the case for the 13.6 kHz signal where the phase is either steady or moving in the opposite direction until sunrise. The composite signals that caused these rapid phase transitions at 10.2 and 11.3 kHz had to be nearly the same amplitude and phase. In fact, throughout the whole night and into sunrise, the phase of the two signals follows very much the same pattern. The dominant mode during daytime remains dominant until 0300. At this time a new mode appears that is probably in near phase opposition at 10.2 and 13.6 kHz and initially at about 90° at 11.3 kHz. This new mode rotates relative to the original mode to be near 90° phase at 13.6 kHz while rotating into more phase opposition at 11.3 kHz. At 10.2 kHz the new mode rotates away from phase opposition, but not as far as at 13.6 kHz. This new mode continues to grow, causing the composite phase to advance further throughout the night. The very rapid phase swing around 0930 indicates that the original and the new mode are transitioning through phase opposition. Even the small phase deviations, such as between 0300 and 0700, are quite different between frequencies. Yet an experienced observer can interpret the vector relationships between the dominant mode and the small rotating component from the relationships between the three frequencies.

Figure B-4b shows a very different pattern; here the 10.2 kHz signal undergoes an abrupt change of more than one cycle and then returns during the transition period. The 11.3 kHz signal does not follow. Yet the 11.3 kHz signal originally incurred a larger phase shift when the new mode appeared. Its gradual rotation shows that its initial position was beyond the point of phase opposition for the direction of rotation at 11.3 kHz and before at 10.2 kHz. The counter-rotation resulting from the ionosphere being lowered during sunrise caused the 10.2 kHz signal to go back through phase opposition while the 11.3 kHz signal makes a complex phase change. The phase pattern of the 13.6 kHz signal in relation to the lower frequencies shows that the new mode's amplitude is smaller compared to the originally dominant mode. Calculations predict that mode 1 remains dominant at 13.6 kHz but not at the lower frequencies. This is consistent with this record.

We note that it is generally easier to recognize the existence of modal competition in the presence of normal propagation variability by comparing the diurnal phase data between multiple frequencies. The occurrence of a cycle jump, as seen in some of the above examples, does make identification of multimode easy even without additional frequency data.

The recorded phase data of a single signal is much easier to interpret for phase quality than the phase-difference data which includes propagation effects of two signals. The signal phase data facilitates comparison of modal effects between frequencies, a condition particularly difficult to interpret using phase-difference data. For this reason, extra effort is devoted to obtaining the phase records from those sites not having atomic frequency references. The challenge results from the reference oscillators being generally significantly offset in frequency from the Omega signals and from a gradual variation of the reference frequency with time. In most cases enough of the frequency offset could be removed from the data so that the diurnal phase patterns could be easily recognized. The quality of the processed data varied quite a bit from site to site and at a site over time.

The procedure used to reduce reference frequency drift effects is as follows: first, an Omega signal is selected for reference based upon expected signal quality and propagation stability. The received phase offset of this reference signal over a 24-hour period is determined by counting the cycles of phase change between times of mid-path noon. Assuming that the received phase at mid-path noon is the same value for successive days, the phase offset versus time (drift rate) is subtracted from the phase data by distributing the offset over the 24-hour period. The error caused by variation of phase from day to day, while large for navigation purposes is generally not significant when checking for modal effect patterns. The drift rate is then subtracted from all other signals. Proportional adjustments are made for the other frequencies. The drift rate is adjusted as needed when progressing through a sequence of days.

The reference oscillators at some monitor sites were found to be quite stable. Other oscillators were much less stable. An example of processed phase data for the Easter Island site, using the Hawaii signal as a reference, is shown in figure B-5. This site had a stable reference oscillator, thereby

allowing the same drift rate to be used for several successive days. The frequency offset typically resulted in about nine cycles of phase offset during a 24-hour period. The Samoa monitor had a much less stable reference oscillator, as shown in Figure B-6. This figure shows the Australia signal used to derive the reference phase drift. The average drift over a 72-hour period has been removed. This average drift was several times larger than the drift at Easter Island. This figure illustrates the change in drift rate that occurred over the three days shown. The solid curved line fitted to the 13.6 kHz phase record indicates the likely drift rate over time during the period shown. It was not necessary to remove this varying drift to check for modal effects.

The phase records of Figures B-5 and B-6 both show minimal evidence of modal effects. The nighttime portion of the phase curves (1600 to 0200 GMT for Hawaii at Easter Island and 0800 to 1800 GMT for Australia at Samoa) shows a characteristic diurnal shape that tracks very closely across the three frequencies with changing time. Strong modal interference effects are incurred on the Hawaii signal measured at Samoa, as shown in Figure B-7. In these data none of the nighttime curves (0600 to 1600 GMT) has the characteristic shape, nor is the track between frequencies very close. We note that the modal effects are quite evident, even though the phase baseline is not straight over time.

DATA ANALYSIS SUMMARY; AIRCRAFT AND FIXED SITE

We found that the analysis was more definitive when it was possible to examine a grouping of data consisting of several aircraft flights and a fixed site, with the fixed site being a hub for the flights. Not all flights fit into a convenient group.

We have chosen to summarize the analysis by following the flights in approximate sequence, starting with the northeast corner of the validation region and progressing generally westward. Some exceptions are made in following the sequence of flights when it is considered beneficial to group the flights around a hub. An example is the Hawaii hub group which includes flights 11, 23, 12 & 13, and 19 & 22.

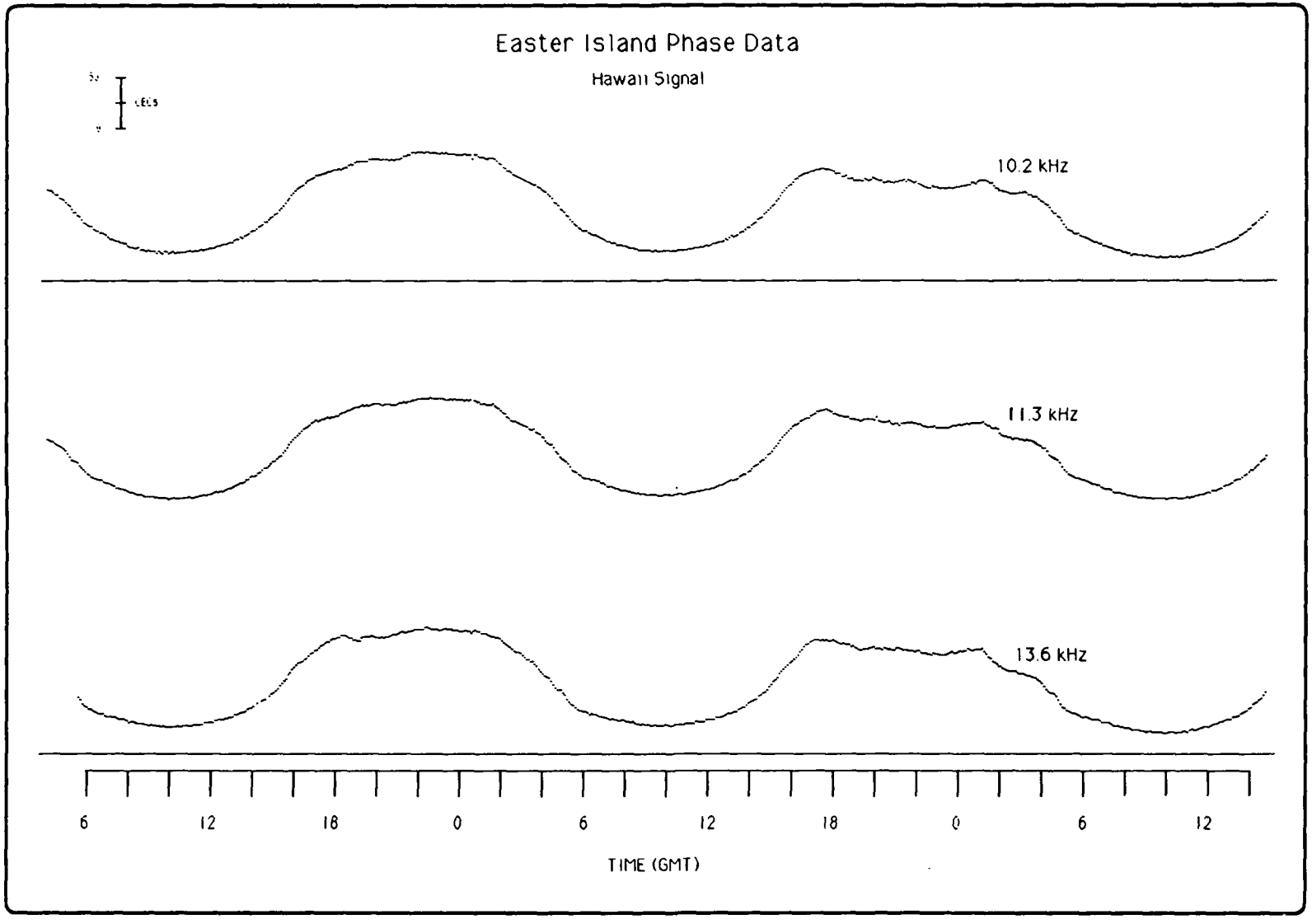

Figure B-5. Example of Phase Record with Reference Drift Removed

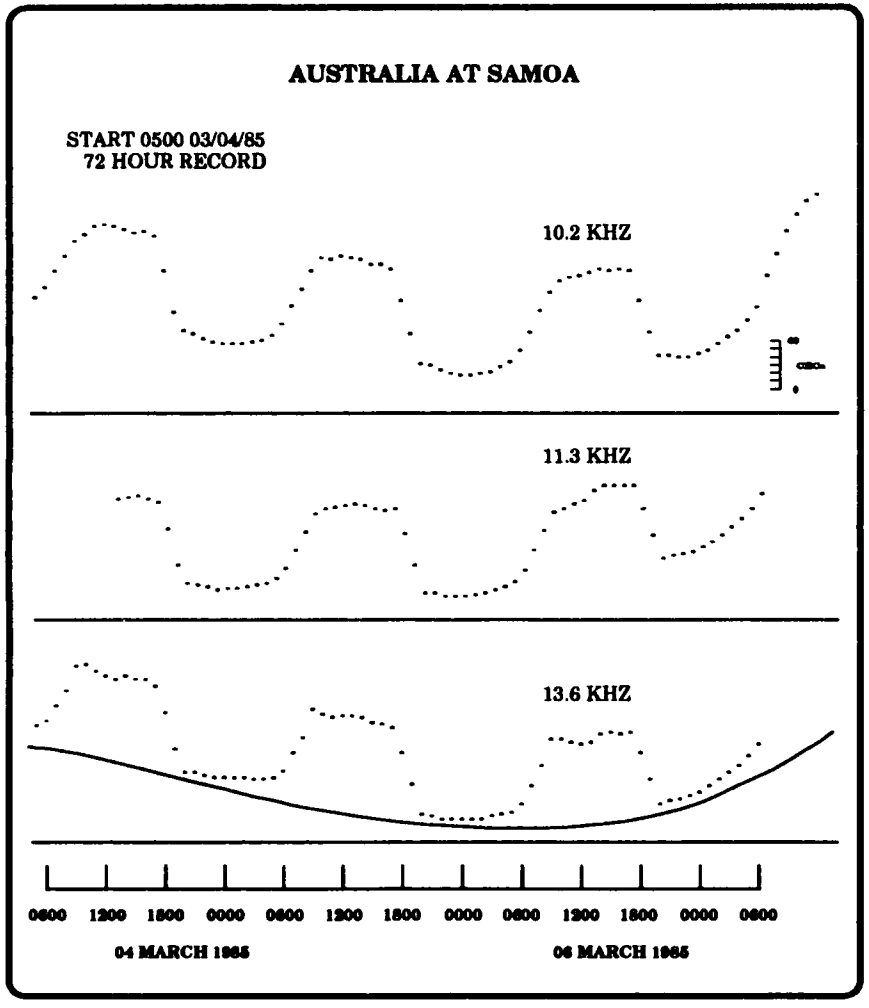

Figure B-6. Example of Phase Record with Reference Drift Partially Removed

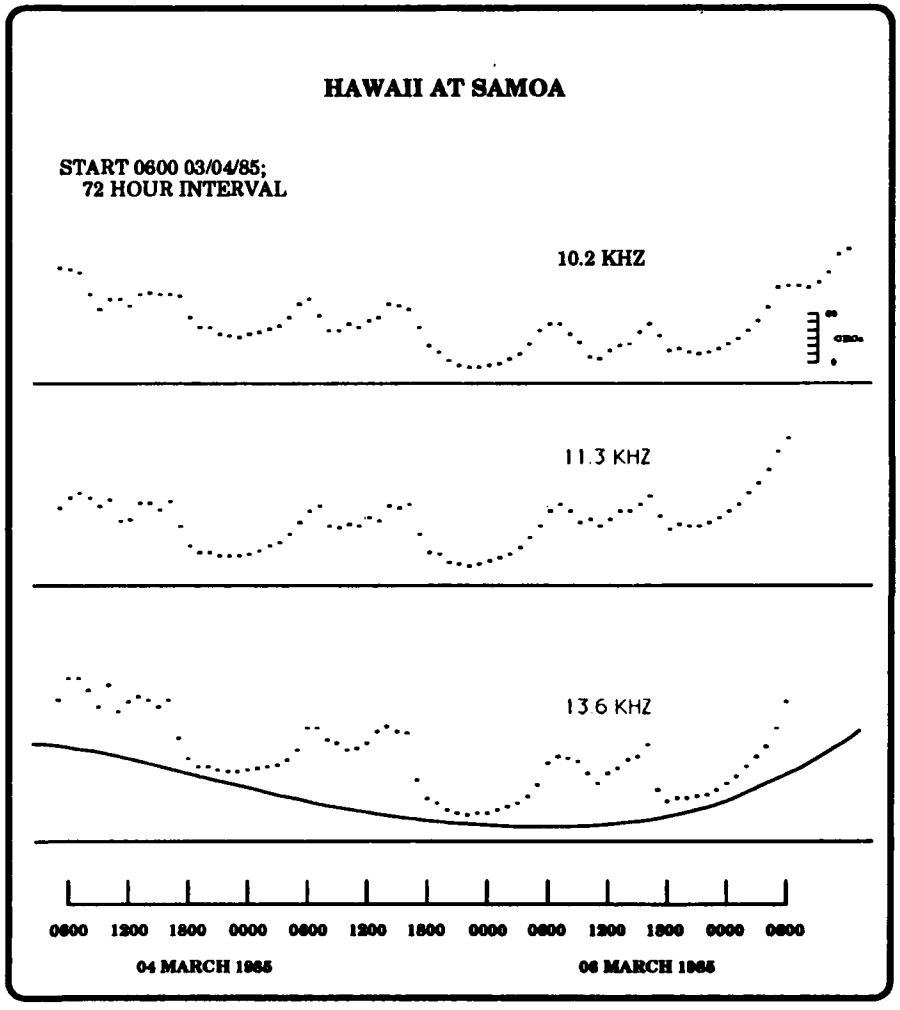

Figure B-7. Example of Phase Records Showing Modal Effects

Flight 1: (28 Jan 1985; 2240-0700) This flight data collection started near San Diego and ended just before Panama, Figure 3-6. While this flight was north of the validation region, many signal radials either entering or exiting the validation region cross this flight path. The summary by stations is as follows:

(A) Norway: The radials are predicted to be mostly mode 1. One radial at 10.2 kHz (310°) and 3 radials at 13.6 kHz (310° - 290°) show mode 2 dominant at the receiver location, all essentially due to traversing low conductivity terrain. No flight data were collected.

(B) Liberia: The radials are predicted to be mode 2, all essentially due to initial traverse of the equatorial zone. The flight path was north of the equatorial zone. From calculations, structure in the received signal is expected. Some structure was evident in the data but was not closely correlated with calculations. We expect that the calculations' products are very sensitive to the ionosphere model in the vicinity of Liberia. Conclusion: Comparison between calculations and flight data produced no definitive results.

(C) Hawaii: The day/night transition existed on the path for most of the flight (6 of 9 hours). For the next two hours no data were available. Calculations show greater than 10 dB fades in the vicinity of Panama. From cross section construction, one signal fade was expected during the last 1.5 hours. Flight data showed no fades. If modal constructive peak occurred in the middle of this time interval (requiring a slight ionosphere adjustment from predicted), no fade would have been recorded.

Conclusion: Insufficient data were obtained to test calculations or to measure depth of fades.

(D) N. Dakota: Calculations show mode 1 for both frequencies. For 10.2 kHz, the signal is shown to be fairly flat, having a slight amplitude decrease with distance. For 13.6 kHz, a 4.7 dB dip and recovery is predicted during the first half of the flight, which occurred during sunset transition, approximately 3 hours. Data at 10.2 kHz followed the prediction after the transition interval; at 13.6 kHz, a 6.5 dB dip occurred later than predicted.

Conclusion: Mode 1 is \predicted with little modal structure. Data are consistent with predictions.

(E) La Reunion: Calculation cross sections show switching between modes 1 and 2 at 10.2 kHz several times and at 13.6 kHz from mode 1 to mode 2 and back once during flight. At 13.6 kHz mode 2 is predicted for most of the flight. The cross sections show significant structure, 20 dB peak to peak variation. After full night on the propagation path, the flight data show minimal evidence of structure, about 5 dB variation. Since distance to the transmitter is decreasing (approximately 17 to 14.9 Mm), signal increase with time is expected and is shown on the calculations. All three frequencies of the flight data show an amplitude decrease over the last 4 hours (8, 5 and 4 dB at, respectively, 10.2, 11.33, 13.6 kHz).

Conclusion: The fit between measurements and calculations is not particularly good. As with Liberia, less structure was observed than predicted. The situation is expected to be more complex than calculations show because of possible long-path effects. We do not expect the flight data to provide much information regarding possible modal problems.

(F) Argentina: Calculations show flight path to be north of the equatorial mode conversion zone. Both 10.2 and 13.6 kHz are predicted as mode 2 on the flight path. The cross sections of calculations show about 3.5 cycles of interference fade with a fade depth of about 4 dB. Flight data show fades about 5 dB but there are too many gaps in the data to count the number of fades. There seems to be less range effect in the data than expected.

Conclusion: These data are the best match for flight 1 with calculations The agreement is close enough to support the calculations (See later comments, flight 5, on evaluation of a more complete radial for Argentina).

(G) Australia: The path was in day-to-night transition throughout the flight. No modal effects were observed or expected.

Conclusion: Mode 1 dominance occurs as predicted.

(H) Japan: The path was in day-to-night transition throughout the flight. No modal effects were observed or expected.

Conclusion: Mode 1 dominance occurs as predicted.

Flight 1 Overall Summary: The data were neither consistent or inconsistent with calculations. Overall the data did not show the magnitude of structure or distance effects expected from the calculations. Collectively this supports an interpretation that the propagation parameters were changing throughout the flight. Some of the observed lack of predicted mode structure was on signals from northern latitudes. This may be partly seasonal. Seasonal changes in propagation are observed but have not been incorporated into VLF propagation models. Lacking more definitive information, we assume that the modal conditions shown in the calculations prevail.

Flight 2 and Arequipa: (28 Jan 1985; 0150-0800 GMT) This flight originated in Costa Rica and terminated west of Arequipa, Figure 3-6. This flight originated north of the equatorial zone and crossed most of the zone during the second half of the flight. Phase data were obtained for the Arequipa site. The analysis summary by stations is as follows:

(A) Norway: All radials, 10.2 kHz and 13.6 kHz, are predicted mode 1, changing to mode 2 dominance for the last 1/4 of the flight. The calculations show a 20 dB signal decrease at 10.2 kHz and a 15 dB decrease at 13.6 kHz during the flight, partly due to a fade at the end. The flight data respectively show a 20 and 15 dB decrease for 10.2 and 13.6 kHz but no fade associated with the switch to mode 2. Sunrise occurred on the Norway end of the signal paths about the time the fade was expected, thus making the existence of the proper night conditions suspect.

No data were recorded at Arequipa.

Conclusion: The data are consistent with the calculations.

(B) Liberia: Calculations show the short-path radials to be all mode 2, essentially due to initial traverse of the equatorial zone. In the vicinity of Arequipa the

signals become very complex with distance. Very little distance change occurred, 0.47 Mm, but about 30° azimuth change. From cross sections of calculations, structure in signals were expected, but with both 10.2 and 13.6 kHz moving mostly along a mode sum peak. The long-path/short-path boundary should have been west of the flight path during the flight time interval. The long-path/short-path boundary is expected to be close to Arequipa at its western most position but it is not known if it reaches or crosses over Arequipa.

The 10.2 kHz data go through a gradual small dip at 0.5 hours into the flight, then gradually increases over a two hour period by about 12 dB, then gradually decreases by about 20 dB. The 10.2 data follow the cross section curve very closely until sunrise at Liberia 1.5 hours before flight end. The 13.6 kHz data follow the 10.2 kHz data with time more closely than the cross section calculations. The 11.33 data also closely follow the other two frequencies. Some small modal effect, less than 5 dB, can be detected across the three frequencies.

The Arequipa phase records start on 30 Jan., two days after the flight. These records show phase jumps on all frequencies (10.2, 11.33, 13.6 kHz) and all 24-hour days for the duration of the measuring interval, less one case of a jump at two frequencies. The existence of mode competition as well as mode switching is obvious in the fixed-site data. The case for long-path interference is rather weak. The data could be interpreted many ways, none definitive.

Conclusion: The flight data are reasonably consistent with calculations. A very small distance interval and a relatively wide angle was traversed. The calculated signal structure changed mark-edly with angle, yet the cross sections closely followed near a mode sum peak. Only slight differences in propagation parameters would produce markedly different calculation results. The flight was basically a poor test for determining modal problems. However, the Arequipa phase data produce an overwhelming case for modal effects.

(C) Hawaii: The day/night transition existed on the path for much of the flight (4 of 7 hours). Approximately three hours of full night data were recorded. Calculations show that 12 to 14 dB fades at 10.2 kHz and 18 to 20 dB

fades at 13.6 kHz are possible along the flight path. One fade in the signal was expected during the last three hours of measurement. The flight data showed none at any of the three frequencies.

The Arequipa data produce strong evidence for essentially one mode received at all times. No mode switching occurred. Occasionally, about five percent of the time, a small amount of modal was evident.

Conclusion: The flight data did not support the mode structure shown in calculations. The Arequipa phase data confirmed that the mode structure had to be much less than the calculations showed. The expectation is that the eastward modal boundary for Hawaii lies westward of that predicted by calculations.

(D) N. Dakota: Calculations show mode 1 for both frequencies. For 10.2 kHz, signal is shown to be fairly flat, having a slight amplitude decrease with distance, 3 dB over the flight. For 13.6 kHz, a 6 dB dip and recovery is predicted during the first 2 hours of flight, followed by a small dip half way through the flight. Data at 10.2 kHz followed predictions; at 13.6 kHz a 6.5 dB dip didn't occur, but some slight modal might have existed later in the flight.

The Arequipa data show very minimal evidence of modal effects. No mode switching occurred. Occasionally, less than five percent of the time, a small amount of modal was evident.

Conclusion: Mode 1 predicted with little modal structure. Flight data are consistent with little modal structure. The Arequipa site data strongly confirm mode 1 for all signals and all periods.

(E) La Reunion: Calculations show mode 1 for the short-path at 10.2 kHz on the radial just south of Panama and mode 2 or higher for all other radials. At 13.6 kHz mode 2 or higher is predicted for all of the flight. The cross sections are difficult to interpret because the signal structure changes greatly between radials. A simple extrapolation of the long-path/short-path boundary position model from the 90°/270° radials to Arequipa indicates that the boundary moved eastward over Arequipa at about 0600 and moved westward past Arequipa at about 1900. The width of the boundary has not been estimated. No flight data were obtained.

The Arequipa data show very strong evidence of modal effects on all frequencies. Cycle switching occurred on every diurnal period of the data. The 10.2 kHz did not undergo nearly as much mode switching as the other two frequencies, but the diurnal cycle had almost no day/night change when cycle switching did not occur.

Conclusion: The Arequipa data confirm strong modal problems, showing exceptional variability with time and between frequencies. The 100% cycle switching on at least one frequency confirms that the self-interference is a major factor during each diurnal period.

(F) Argentina: Calculations show the flight path to traverse the equatorial mode conversion zone. Both 10.2 and 13.6 kHz are predicted as mode 2 over most of the flight path with 13.6 kHz just extending into a mode 1 dominant condition for the last tenth of the flight. The 10.2 kHz flight data show three fades about 8 to 10 dB. The 13.6 kHz data also have three fades but at different locations. The calculations predict a large signal increase over the path, 25 and 18.7 dB for 10.2 and 13.6 kHz, respectively. The data show much less increase, 10 and 4 dB for 10.2 and 13.6 kHz. The general shape of the flight data are also quite different. Calculations from NOSC show a significantly different amplitude versus distance pattern for a radial calculation differing by only two degrees. (See later comments, flight 5, on evaluation of a more complete radial for Argentina).

Arequipa diurnal phase data show a clear indication of a single mode being continuously dominant throughout the diurnal period and for all days with good data. Any modal effect must be very minimal as the phase records track very closely between frequencies.

Conclusion: The calculations place Arequipa right at the very edge of the modal competition zone for 10.2 kHz and just outside the zone for 13.6 kHz. The flight data show slight modal effects along the path which is consistent with the mode 2 predicted dominance as shown in Figure 3-16. The Arequipa data demonstrate clearly that this site is outside the mode competition region. A slight adjustment of boundary is suggested.

(G) Australia: The path was in day-to-night transition throughout the flight. No modal effects were detected.

Most of the the Arequipa phase records strongly support the prediction that mode 1 is dominant at all times. On occasion 10.2 kHz undergoes some unexpected excursions that probably cannot be explained away by weak signals. Sunrise at the transmitter in early February coincides with a frequently occurring sharp phase offset at 10.2 kHz. This phase offset is also evident at 11.3 and 13.6 kHz but is not generally near so marked.

Conclusion: The flight data are consistent with predictions of mode 1 strongly dominant at all times. The Arequipa data with a few exceptions also strongly support the predictions.

(H) Japan: The path was in day-to-night transition throughout the flight. No modal effects were detected.

The Arequipa phase records show a very different diurnal pattern for 10.2 kHz relative to the other frequencies. Both 11.3 and 13.6 kHz evidence quite clean mode 1 reception at all times. The 10.2 kHz phase is quite variable from day to day. Many days have a strongly depressed diurnal change, some show a single mode curve, and others show marked changes from one condition to another.

Conclusion: The flight data were acquired when no modal was expected and is consistent with predictions of mode 1 being strongly dominant at all times. An improved model of the diurnal location of the interference boundary is needed to establish a more definitive interpretation of this data.

Flight 2 Overall Summary: We conclude that the flight data provided a weak case for determining mode dominance or self-interference conditions. The trends identified provided some support for the calculations. Overall, the calculations showed more structure than was observed in the flight data. On the other hand, the Arequipa diurnal phase data produced clear evidence for the existence or non-existence of either mode competition or mode switching. The findings from Arequipa are in general agreement with boundaries established for that location from calculations shown in

the composite charts of Figures 3-4 and 3-5. The Argentina 10.2 kHz boundary should be moved slightly north or west. The onset of mode switching from Argentina is expected to be very abrupt in moving northward; thus it probably is not safe to move this boundary very far. The Hawaii boundary probably does not extend as far east as shown. Based upon the lack of modal structure in the flight data and the clear single mode dominance at Arequipa, the worst case condition shown on the Hawaii chart, Figure A-7, is not probable. We estimate that the boundary, at least for this time of year, is slightly west of the mode crossover line shown in Figure A-7. Caution should be exercised in moving boundaries, especially for other seasons, as propagation conditions may change with time and season.

Flight 3: (28 Jan 1985; 1100 to 1300 GMT) Flight 3 was a short flight from Lima to Arequipa. Since Arequipa was in early daylight, the flight did not produce data useful for modal analysis.

Flight 4: (30 Jan 1985; 2200 to 0600 GMT) This flight originated west of Arequipa and flew over the Argentina transmitter. All of the flight was well south of the equatorial mode conversion zone. Phase data obtained at the Arequipa site was described as part of flight 2. The analysis summary by stations is as follows:

(A) Norway: The calculations show the 10.2 kHz signal is dominantly mode 2 leaving Arequipa, but it soon becomes dominantly mode 1 for the rest of the flight. Amplitude fluctuations exceeding 10 dB are shown for the first half of the flight. The 13.6 kHz is predicted dominantly mode 2, throughout the flight. The calculations show periodic modal fades. Sunset was occurring on the path for the first three hours of the flight. Modal structure is present, exceeding 10 dB on both 10.2 and 13.6 kHz but not with the pattern shown on the calculations. Again no data were recorded at Arequipa.

Conclusion: The data are reasonably consistent with the calculated prediction of some modal competition. The mode 1 dominance for 10.2 kHz or the mode 2 dominance for 13.6 kHz cannot be resolved from the flight data.

(B) Liberia: Calculations show the radials to be all mode 2, again due to initial traverse of the equatorial zone. Very little distance change occurred, about 0.3 Mm, over an azimuth change of 26°. From calculations, mode structure in signal is possible, but the distance between radial crossings is large and all the calculated change is due to azimuth change.

The channel was in calibration mode (the channel was being used to inject a calibration signal) for the first three hours. Three signal fades are noted on the flight data. All three are relatively weak at 10.2 kHz, 10 dB or less. The first and third fade are quite strong at 11.3 kHz, respectively, 24 and 16 dB. At 13.6 kHz the second fade is quite deep, 18 dB. The modal effect across the three frequencies is more evident than on flight 2.

The Arequipa phase records start on 30 Jan, so data cover this flight but not flight 2. The data covering 0100 to 0530 on 31 Jan, the flight time of interest, are quite different than for 30 Jan. The phase was changing on both days during this period but with a significantly different pattern. The next four days have no data.

Conclusion: The flight data provide agreement that signal structure is present. The fades observed are more likely due to propagation changes rather than distance or bearing effects. The Arequipa data show that the records are quite variable from diurnal day to day. Most likely the mode switching strongly evidenced at Arequipa extends to the Argentina transmitter.

(C) Hawaii: Calculations show that ail frequencies should be in a safe mode 1 dominant zone. The flight data did not conflict with this prediction.

The Arequipa data showed that the phase pattern for the flight record time was quite different than on the previous night, confirming the above comments for Liberia.

Conclusion: The flight path is probably in a mode 1 dominant zone. The path is too far from the expected zone boundary to aid in determining the boundary position.

(D) N. Dakota: Calculations show mode 1 for both frequencies. After full sunset on the path, the flight data are consistent with the calculations.

The Arequipa data show the phase record for this and the previous night to be more alike than the records of Hawaii and Liberia.

Conclusion: Mode 1 predicted with little modal structure. Flight data are consistent with little modal structure. Since the Arequipa site data strongly confirm mode 1 for all signals and all periods, no change is expected to the south.

(E) La Reunion: Calculations for 10.2 kHz show mode 2 for the first part of the flight south of Arequipa changing to mode 1 at about 1/3 along the flight. At 13.6 kHz mode 2 or higher is predicted leaving Arequipa, changing to mode 1 dominant about half way through the flight. Flight data were obtained for the first 3 hours. A steady decrease in the 10.2 kHz amplitude is consistent with the calculations that show moving into a fade. The calculated fade is associated with the mode dominance switch. The 13.6 flight may be traversing a relative peak in the structure.

The Arequipa data show large phase changes during the flight time. The 13.6 kHz signal undergoes a cycle slip at 0300, shortly after the flight record ends. The phase records are quite different from the same time on the previous night when the 13.6 kHz phase went through a cycle change near 2230 GMT.

Conclusion: The strong modal problems confirmed at Arequipa are supported by this flight data.

(F) Argentina: The calculations show mode 1 to be dominant throughout the flight. The flight data, after completion of the sunset transition, show no modal until near the end of the flight where the near zone modal is beginning to build up.

Conclusion: No significant modal occurs in this geographic area. The predicted mode 1 dominance is probably valid.

(G) Australia: The path was in day-to-night transition throughout the flight. The data show no significant evidence of signal self-interference.

Conclusion: No self-interference was predicted for the time interval of the flight and none was observed. The signals are likely mode 1 dominant at these times.

(H) Japan: The path was in day-to-night transition throughout the flight. The data show no evidence of modal or self-interference effects.

Conclusion: Predictions show that the boundary should have moved to the east of the flight path. Aircraft phase data need to be examined for evidence of phase sense.

Flight 4 Overall Summary: The combined flight and monitor site data support the phase dominance conditions established by predictions. A zone boundary for Norway at 10.2 kHz was predicted near the middle of the flight path. The flight data show modal, but the particular mode dominance cannot be tested. The zone boundary for La Reunion at 10.2 kHz is predicted from calculations to be approximately 1/3 of the way along the path. The flight data show evidence of modal. Considering the strong modal effects evident at Arequipa, the zone could extend farther south than predicted.

Flights 5, 6, and 7 Argentina Near Zone Radials: (01, 02 and 04 Feb. 1985; respectively 0600 to 1130, 1630 to 2200, and 1930 to 0100) These flights were most useful for assessing the near-zone modal effects for the Argentina transmitter.

Flight number 5 was inbound on the Argentina 340° radial. Ground sunrise occurred about 50 minutes before station flyover. The calculations predict a null at 10.2 and 13.6 kHz that could produce mode switching for a short interval about 800 km. The flight data support this prediction as a possibility.

Flight number 6 was outbound on the 190° radial from Argentina. The calculations predict a progressively deepening null moving from 10.2 to 13.6 kHz and moving out in range from about 400 to 600 km. At 10.2 kHz this null could produce mode switching for a short interval about the maximum fade. At 13.6 kHz the dominant mode is changing from mode 3 to mode 1. The flight data support the predictions. The deepest null moves out in range from about 450 to 600 km and deepens from about 8 to 22 dB in going from 10.2 to 13.6 kHz.

Flight number 7 was flown across the transmitter at a heading of 265°. The flight was either during daylight or within the sunset transition. The data support the day predictions.

Flights 5, 6 and 7 Overall Summary: The predictions place the greatest extent of near zone modal to the east of the Argentina transmitter. No flights covered this sector of the near zone. The predictions along flights 5 and 6 show the zone to extend slightly farther than the data indicates. When considering ionosphere variability and need for safe predictions, the near zone boundary is considered appropriately located at night for the two radials checked.

Flight 8: (06 Feb. 1985) This flight originated west of the Argentina transmitter and followed approximately a 280° radial from the transmitter to Easter Island. The flight path does not cross any boundaries between the modal zones shown in Figures 3-4 and 3-5. The analysis summary by stations is as follows:

(A) Norway: The calculations show the 10.2 kHz signal is dominantly mode 2 at both frequencies throughout the flight. The 10.2 kHz signal possibly starts out as mode 1 dominant but is right on the border of switching to mode 2 dominant. The distance increases from 14 to 14.4 Mm and the bearing changes from the 247° to the 288° radial from Norway. The calculations show that amplitude fluctuations greater than 10 dB are likely. The flight data show amplitude fluctuations exceeding 10 dB on all frequencies and throughout the flight.

Conclusion: The data are reasonably consistent with the prediction from calculations of some modal competition. The mode 2 dominance for both 10.2 and 13.6 kHz predicted by calculations cannot be resolved from the flight data, but is considered likely.

(B) Liberia: Calculations show the radials to be all mode 2, again due to initial traverse of the equatorial zone. The distance change incurred was 3 Mm, the azimuth change about 19°. Based on the calculations, we conclude that mode structure in the signal is possible, but the structure is very sensitive to bearing from the transmitter.

Conclusion: Since no flight data were obtained, guidance must be obtained from the calculations. Other experience with the Liberia signal lends credence to the prediction that mode 2 dominance is likely.

(C) Hawaii: Calculations show that all frequencies should be in a mode 1 dominant zone. The modal structure should be strong, approximately 10 dB at 10.2 kHz and 20 dB at 13.6 kHz. The flight data include a sunset transition for the first 4.5 hours. Following the transition, the data contain samples recorded at approximately 45-minute intervals. The data at all four frequencies show little evidence of modal. About 1.5 cyclic periods of fade structure should have been traversed after the sunset transition.

Conclusion: The flight path probably is in a mode 1 dominant zone as predicted by the calculations. The signal modal structure is much less than predicted. There is a good possibility that the safe modal zone boundary can be placed north of Easter Island for February.

(D) N. Dakota: Calculations show mode 1 for both frequencies with no modal structure. The flight data are consistent with the calculations.

Conclusion: Mode 1 is predicted with no modal structure. Flight data are consistent with negligible modal structure. Since the transition boundary is predicted about one megameter to the west, this zone should be safe mode 1.

(E) La Reunion: Calculations for 10.2 kHz show mode 1 throughout the flight. A strong fade, greater than 15 dB exists at 13.7 Mm on the calculations. At 13.6 kHz mode 2 is predicted throughout the flight. An even greater fade, 20 dB, is shown on the 13.6 kHz calculations. The flight occurred during the sunrise transition on the path. Modal effects are observed, particularly at 11.3 kHz where three fades greater than 10 dB occur.

Conclusion: Because of sunrise on the path the calculations cannot be validated with the flight data. The evidence for modal competition during sunrise does support the prediction that modal competition is strong along this flight path.

(F) Argentina: The calculations show mode 1 to be dominant for 10.2 kHz and mode 3 to be to be dominant for 13.6 kHz to 3.4 Mm and then mode 2 to be dominant for the rest of the flight. The flight data show modal decrease with distance at 10.2 kHz, with the modal negligible beyond 2 Mm. The 10.2 kHz data show less modal than the calculations. The modal increases with frequency, becoming quite strong at 13.6 kHz for the entire flight. Three major fades are recorded that are similar to the fades predicted in the calculations.

Conclusion: The flight data fit the calculations quite well. The data are consistent with 10.2 kHz being mode 1 dominant and 13.6 kHz being higher-ordered mode dominant.

(G) Australia: The path was in day-to-night transition throughout the flight. Thus no analysis was conducted.

(H) Japan: The path was in day-to-night transition throughout the flight. Thus no analysis was conducted.

Flight 8 Overall Summary: With the exception of the Hawaii signal, the modal zones predicted from calculations are largely confirmed. All signals appear to have somewhat less modal than the calculations show. The Hawaii signal has much less modal structure than the calculations predict. Adjustment of the Hawaii modal zone boundary to smaller distances than the calculations predict is the only change that appears appropriate. As yet, how much adjustment to recommend and whether by seasons is uncertain.

Flight 9: (09 Feb. 1985) This flight originated at Easter Island and terminated at Tahiti. Several modal zone boundaries are crossed along the flight path, the most significant being for North Dakota (see Figures 3-4 and 3-5). Phase data obtained at Tahiti are described as part of the next flight group. The analysis summary by stations is as follows:

(A) Norway: The calculations show the signal is dominantly mode 2 at both frequencies throughout the flight. The distance increases from 14.2 to 14.8 Mm and the bearing changes from the 288° to the 340° radial from Norway. The calculations show that the effect on signal amplitude due to bearing change is quite large. The 10.2 kHz calculations show an amplitude

range of 40 dB which is considered suspect. The flight data are affected by sunrise at Norway after about 3 hours. Prior to that time the 10.2 kHz signal is relatively noisy. A predicted signal amplitude increase occurs at all frequencies by about 10 dB, but is less than half of the predicted. Some hint of modal competition exists in the data.

Conclusion: The data are reasonably consistent with the prediction from calculations of some modal competition. The mode 2 dominance for both 10.2 and 13.6 kHz predicted by calculations cannot be resolved from the flight data, but is considered likely.

(B) Liberia: Calculations show the radials to be all mode 2, again due to initial traverse of the equatorial zone. The distance change incurred was 4.2 Mm, the azimuth change about 8°. From calculations, mode structure of about 10 dB is predicted. Less than three hours of the flight data are for propagation in total darkness. Negligible modal structure was recorded during the all-night part of the record.

Conclusion: The flight data did not provide any clues of modal structure. Other experience with the Liberia signal adds support to the predictions that mode 2 dominance is likely.

(C) Hawaii: Calculations show that all frequencies should be in a mode 1 dominant zone. The modal structure predicted to be strong in the vicinity of Easter Island, approximately 10 dB at 10.2 kHz and 20 dB at 13.6 kHz, gradually decreases with increasing bearing. At Tahiti the modal structure is predicted to be about 1 dB at 10.2 kHz and about 6 dB at 13.6 kHz. The flight data include a sunset transition for the first hour. Following the transition, the data contain samples recorded at approximately 40 minute intervals. The data at all four frequencies show some evidence of modal, about 1.5 fades. The calculations predict 1.5 fades for the path interval. The 10.2 kHz structure is stronger than the calculations predict, but weaker than the 13.6 kHz data.

Conclusion: The flight path is probably in a mode 1 dominant zone as predicted by the calculations. The signal modal structure is more in evidence at 10.2 kHz and less so at 13.6 kHz than predicted. There is a good possibility that the safe modal zone boundary

placed well north of Tahiti should be moved to the south.

(D) N. Dakota: Calculations show mode 1 for both frequencies with no modal structure at the start of the flight. Both 10.2 and 13.6 kHz transition into mode 2 dominant about 1/3 along the flight. No flight data were acquired.

Conclusion: Since no flight data were acquired and, as shown later, the Tahiti fixed-site data show mode switching, it is assumed that the zone of mode 2 dominance was crossed during this flight.

(E) La Reunion: The La Reunion signal propagates to this flight path under mixed conditions of day and night. During most of the flight, the signal traverses the Antarctic icecap which is in 24-hour daylight. The flight recorded the Calibration mode, or the path was well into the sunrise transition. The last two hours of the data record show evidence of the signal coming out from traversing the Antarctic icecap.

Conclusion: No conclusions are drawn because calculations were not available for the actual propagation conditions and because no useful flight data were available.

(F) Argentina: The calculations show mode 1 to be dominant for 10.2 kHz and mode 3 dominant for 13.6 kHz for all of the flight. The distance traversed is from 4.3 to 8.2 Mm and the bearing decreases from 279° to 261°. The calculations show that 10.2 kHz should undergo one fade of about 12 dB and that 13.6 kHz should largely follow the crest of a maximum. The flight data show no noticeable modal on either 10.2 or 11.3 kHz. The 12.9 kHz record shows some modal structure, less than 5 dB. The 13.6 kHz record shows significant modal with two prominent fades before the sunrise transition appears, the first fade being almost 12 dB.

Conclusion: The flight data tend to support the predictions of 10.2 kHz being in the mode 1 zone and the 13.6 kHz signal being within the mode 2 zone.

(G) Australia: The path was in day-to-night transition throughout the flight. Thus no analysis was conducted.

(H) Japan: The path was in day-to-night transition throughout the flight. Thus no analysis was conducted.

Flight 9 Overall Summary: The data recorded on flight 9 follow the overall pattern of the flights indicating that boundaries where modal dominance switches are not easy to define. This is particularly true where the switch in dominance is due to bearing from the transmitter rather than distance, and where the dominance is the result of either terrain conductivity effects or traversing the equatorial mode conversion zone. We conclude that so far as the data are interpretable, the data support the zone boundaries established from calculations. Some adjustments may be possible, but an overall decision should be based upon all of the analysis and is better addressed in the analysis summary in Section 4.2.

Tahiti Phase Data and Flights 10, 11, 20, and 21: (11 & 13 Feb., 1 & 3 Mar. 1985) Tahiti is the hub for all of the flights grouped for this sub-analysis. The Tahiti phase data provide a definitive interpretation of modal conditions, especially mode diurnal switching, and is thus strong support for interpretation of the adjacent flight data. Tahiti and all of these flights are to the east of the most critical subregions for unusable phase (see Figures 3-4 and 3-5). The analysis summary by stations is as follows:

(A) Norway: For Tahiti the calculations show the mode 2 signal is dominant at both frequencies at night, by about 10 dB for 10.2 kHz and 8 dB for 13.6 kHz. The Tahiti phase data show diurnal mode switching to occur 87% of the time on at least one frequency. Mode switching at 10.2 kHz also occurs 87% of the diurnal days; at 13.6 kHz the occurrence is 37% of the days. The sunrise transition is very abrupt. Towards the end of the month the terminator lies almost on the entire path from Norway to Tahiti. The Tahiti phase data show that the night propagation conditions extend from sunset to sunrise at Tahiti and that mode 2 dominance can occur at any time during this time interval. The polar part of the path does not have much influence on the diurnal phase curve for this time of the year. Figure B-8 illustrates the diurnal phase curves and shows that a higher-ordered mode is evident by 0500 GMT.

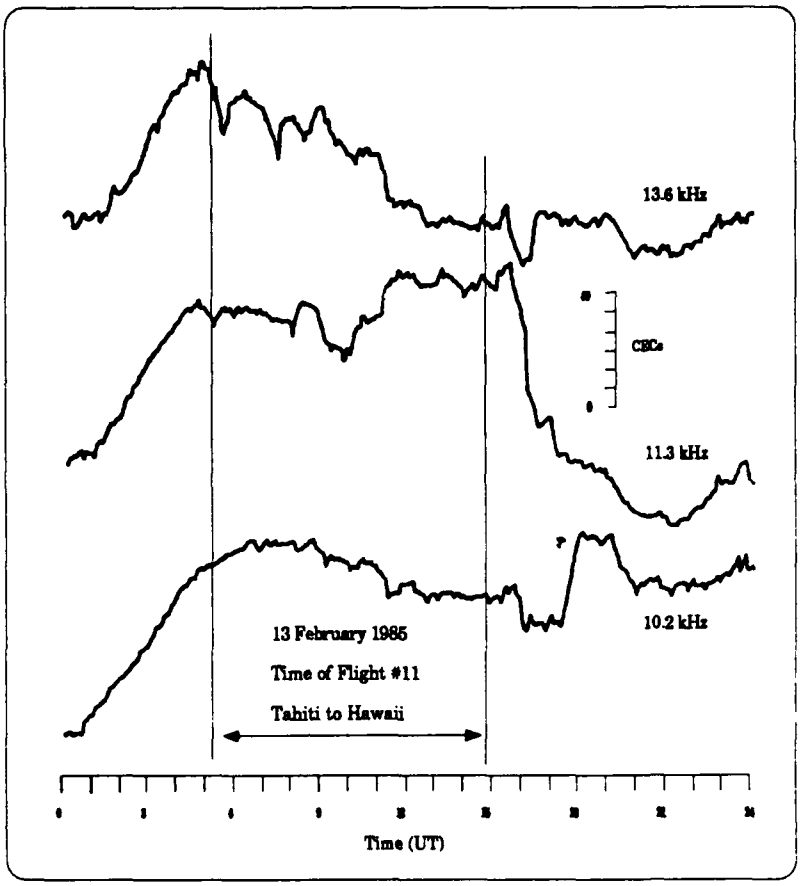

Figure B-8. Measured Phase Norway Signals at Tahiti

Flight 10, 0700 to 1500 GMT, occurred during low resolution recording at Tahiti with the 10.2 kHz possibly on calibration. The flight record shows 10.2 kHz dipping into a null 1.5 hours into the flight and returning through a shallower null about 1330. The 13.6 kHz signal shows a null occurring about flight turnaround. The 11.3 kHz signal shows weak nulls shifted in time. The signal for all frequencies is weak and noisy, making identification of signal fades difficult.

Flight 11, 0500 to 1500 towards Hawaii, shows evidence of modal competition, mostly at 11.3 kHz and within the first two hours of flight. The Tahiti records show strong phase fluctuations between 0430 and 0930 GMT, reaching 30 CECs on 13.6 kHz about 0530. The flight left the Greenland shadow slightly over halfway along the flight. The 13.6 kHz signal

shows a slight decrease before this time. Any other possible effects are masked in the signal fluctuations.

Flight 20, 0600 to 1200 GMT from Tonga, should be in a mode 1 dominant zone until entering the Greenland shadow at about 0.7 of the flight distance. The first part of the flight data show the effects of the last of the sunset transition. The signal amplitudes gradually decrease over time, with the 13.6 kHz signal decreasing (by 25 dB) more quickly during the last hour of flight. The other frequencies do not show this added decrease. The Tahiti phase records are relatively stable near the flight arrival time.

Flight 21, 0500 to 0930 GMT towards Samoa, shows the reverse of flight 20. The 13.6 kHz signal rapidly increases by 19 dB in the first hour of the record, and then reaches a plateau for the rest of the flight. The 10.2 and 11.3 kHz frequencies gradually increase throughout the flight with the 11.3 kHz signal having a slight bow, with a shape in between the 13.6 and 10.2 kHz shapes.

Conclusion: The data are consistent with the prediction of a transition west of Tahiti from a zone of mode 2 dominance to mode 1 dominance. The mode 2 dominance at Tahiti is strongly evident in the Tahiti phase records for all frequencies and weakly evident in the flight data. The zone boundary does not produce a marked perturbation in amplitude data.

(B) Liberia: Calculations show the area around Tahiti to be dominant mode 2. The distance to Tahiti is 15.5 Mm. At the antipode the eastward propagating path is predicted to be 28 dB stronger than the westward path for both 10.2 and 13.6 kHz. No flight data were obtained for any of the flights in this group.

Conclusion: Since no useful flight data or Tahiti site data were obtained, the predictions cannot be confirmed.

(C) Hawaii: Calculations show that all frequencies should be in a mode 1 dominant zone. Flight 10 might get close to the 13.6 kHz boundary for strong mode competition. Flight 11, 167° bearing from Hawaii, is predicted to cross the boundary for both 10.2 and 13.6 kHz at respectively 0.8 and 0.7 of the flight path.

Flight 10, round trip to the northeast, showed the effects of the ionosphere continuing to rise after sunset on the entire flight. A very slight indication of modal interference is evident in the data. Since the data were sampled on 50-minute intervals for most of the flight, determination of evidence is more difficult.

Flight 11, to Hawaii, shows the modal interference structure building up as distance to Hawaii decreases on all four frequencies, 10.2, 11.3, 11.8 and 13.6 kHz. Both 10.2 and 13.6 kHz show the potential for fade up to 20 dB out to 2 Mm from the transmitter. This places the modal boundary slightly south of the predicted one, about 300 km.

Flight 20, from Tonga, may show a very slight modal structure departing Tonga. Otherwise all frequencies undergo a very constant amplitude increase with flight time.

Flight 21, to Samoa, is the inverse of flight 20; its data show a constant amplitude decrease with flight time. No evidence of modal is observed at the end of the flight.

Conclusion: The area around Tahiti is definitely safely mode 1 dominant. This area extends westward to, or almost to, Samoa and Tonga. To the northeast the location of the predicted boundary was not confirmed. Along the path to Hawaii the boundary needs to be moved south by about 300 km.

(D) N. Dakota: Calculations show Tahiti to be well within the mode 2 zone for both frequencies. The 230° radial from North Dakota through Tahiti shows mode structure with 6 dB fades at 10.2 kHz and 14 dB fades at 13.6 kHz. The distance interval between fade is 0.7 and 1 Mm for respectively 10.2 and 13.6 kHz. Modal structure is expected to extend eastward to beyond the end of flight 10 and westward beyond flights 20 and 21.

The Tahiti phase data show mode switching on 60% of the diurnal periods, most at 11.3 kHz. The 10.2 kHz signal shows mode switching 37%, the 11.3 kHz 60% and the 13.6 kHz none. Both 10.2 and 11.3 kHz switching occurs on 15% of the periods. The evidence for modal competition is stronger than the mode switch statistics indicate. The 13.6 kHz phase records have much less fluctuation than the other

two frequencies. We suspect that conditions are more modal than implied. Occasionally phase excursions on 13.6 kHz are incurred, some exceeding 20 CECs and a few exceeding 30 CECs.

Flight 10, round trip to the northeast, shows little symmetry but significant modal interference, mostly nearer Tahiti.

Flight 11, to Hawaii, exits the modal zone at about 0.7 of the flight distance. The last modal effects are at about .6 of the flight distance. The modal fades are about 10 dB on the flight data and occur at different times on the three measured frequencies, 10.2, 11.3 and 13.6 kHz.

Flight 20, from Tonga, amplitude data show a different pattern for each frequency. The modal structure is more pronounced with increasing frequency, being less than 5 dB at 10.2 kHz and as much as 12 dB at 13.6 kHz. The Tahiti 13.6 kHz phase record undergoes a 50 CEC phase advance and retardation shortly after the null on the 13.6 kHz flight data. The 10.2 kHz Tahiti phase record has less phase fluctuation than the 13.6 kHz during the flight period.

Flight 21, to Samoa, shows more modal structure than flight 20, ranging from 9 dB at 10.2 kHz to 15 dB at 13.6 kHz. The Tahiti phase data show a 45 CEC phase retardation on 13.6 kHz bracketing 0700 that may coincide with 3 fades at 13.6 kHz on the flight data at about the same time interval. As expected, due to relative phasing, the 10.2 and 13.6 kHz signal excursions are small during this time, around 10 CECs.

Conclusion: The prediction from the calculations of mode 2 being dominant is confirmed by the Tahiti phase data and supported by all of the flights. Neither the calculations or the flight data show evidence of deep fades due to modal. This is consistent with mode 2 being dominant in the area about Tahiti. Flight 11 exiting the zone of mode 2 dominance produced only weak evidence of the boundary. This evidence, however, is consistent with the placement of the boundary.

(E) La Reunion: The La Reunion signal propagates to the Tahiti area under mostly mixed conditions of day and night. In early February total path night exists for only about 30 minutes and total daylight for about 2 hours. Earlier in the month the propagation path is directly on the terminator. Tahiti lies just west of the Antarctic shadow zone. The signal is predicted mode 1 during all-night propagation. All of the flights in this group are predicted within the mode 1 safe zone.

Flight 10, round trip to the northeast, shows a very steady increase in amplitude throughout the flight, indicating that solar control is the dominant factor.

Flight 11, to Hawaii, has the same pattern as flight 10, as does much of the fixed site data for the flight time period.

Flight 20, from Tonga, again shows the same trend with time.

Flight 21, to Samoa, is a repeat of the above.

Conclusion: Mode 1 is dominant at all times at Tahiti and in the areas covered by this set of flights. The transition times, which dominate the diurnal period, follow a mode 1 phase pattern in the Tahiti data.

(F) Argentina: The calculations show mode 1 to be dominant for 10.2 kHz and mode 3 dominant for 13.6 kHz at Tahiti. Flights 10 and 11 should traverse the boundary to where 10.2 kHz becomes second mode. Flights 20 and 21 should stay within the same conditions predicted at Tahiti.

The Tahiti phase data show phase jumps for 28% of the diurnal days. Of this total, 13% occurred on only 13.6 kHz, 7% were both 13.6 and 11.3 kHz and 9% were only 11.3 kHz. The data show evidence of modal interaction on most nights even though a cycle jump may not have occurred. The modal effects on 10.2 kHz are significantly less than on 11.3 and 13.6 kHz, yet there is enough modal observed to lend credence to the predicted boundary lying north of Tahiti.

Flight 10, round trip to the northeast, shows modal effects at 11.3 and 13.6 kHz. Sunrise at Argentina occurred 2.5 hours into an 8-hour flight. The transition masked any evidence of entering into the 10.2 kHz mode 2 zone.

Flight 11, to Hawaii, is predicted to have entered the mode 2 zone for 10.2 kHz after one tenth of the flight. No indication is seen on the flight records. The last 60% of the flight was during a sunrise transition on the propagation path.

Flight 20, from Tonga, shows no modal effects prior to onset of sunrise about half way through the flight.

Flight 21, to Samoa, shows slight modal effects that have a distance dependence on frequency. Sunrise starts at Argentina just before arrival at Samoa.

Conclusion: The Tahiti data add strong support to the predictions of 10.2 kHz being in the mode 1 zone and the 13.6 kHz signal being within the mode 2 zone. The flight data weakly support the calculation predictions.

(G) Australia: The calculations predict small modal structure in the vicinity of Tahiti of about 5 dB at 10.2 kHz and 8 dB at 13.6 kHz. Mode 1 dominates over mode 3 by 15 and 8 dB at respectively 10.2 and 13.6 kHz.

The Tahiti phase records are clearly mode 1 dominant at all frequencies and times. The 13.6 kHz signal occasionally shows some modal effects at night that are not evident on the other two frequencies; typical fluctuations are 10 to 15 CECs.

Flight 10, round trip to the northeast, although sampled at 40-minute intervals, shows no evidence of modal

Flight 11, to Hawaii, although sampled at 40-minute intervals, likewise shows no evidence of modal while the propagation path is all night.

Flight 20, from Tonga, although sampled at 40-minute intervals, also shows no evidence of modal. Most of the flight is during sunset transition on the propagation path.

Flight 21, Samoa, also sampled at 40-minute intervals, shows no evidence of modal. All of the flight is during sunset transition on the propagation path.

Conclusion: The Australia signal is safely mode 1 dominant in this area.

(H) Japan: The area around Tahiti is predicted as phase 1 dominant. The flight path to Hawaii could cross over the southeast tip of possible strong modal on 13.6 kHz. The crossover to mode 3 dominance is to the east of the flight path by about 0.5 Mm, about 40% of the path distance from Tahiti.

The Tahiti phase data show the Japan signal to be strongly mode 1 dominant at all times on all frequencies. Minimal evidence of modal effects at night can be infrequently detected. The deviations are small, usually about 10 CECs.

For all flights of this group, no modal effects were detected.

Conclusion: The Japan signal is safely considered mode 1 dominant in this area.

Tahiti Area Overall Summary: The phase data for Tahiti confirm the prediction from calculations of modal zones at Tahiti. The flight data tend to support both the predictions and the Tahiti data. As observed before, the flight data are a weak indicator of the transition between modal zones. The Hawaii signal has modal structure that extends 300 km further south than predicted. Other positions of zone boundaries could not be determined with sufficient accuracy to test predictions.

Hawaii Area and Flights 23, 22 and 12: (6 & 4 Mar & 15 Feb. 1985) Two objectives are emphasized for analysis in the Hawaii area. The first objective is to explore the extent of the near zone for Hawaii, and the second is to test those predictions for Hawaii and the associated flight paths that can confirm predictions for the South Pacific Validation region. Flights from or to Hawaii, number 23 to San Diego, number 11 from Tahiti, number 22 from Samoa, and number 12 & 13 to north east Australia, produce a good test of the Hawaii signal near-zone predictions. The analysis summary by stations is as follows:

(A) Norway: The calculations show the signal is dominantly mode 1 at Hawaii and to the South for both frequencies. Flight 23 to the East is predicted to enter the Greenland shadow one hour into the flight.

Flight 23, to San Diego, data show some small evidence of an amplitude perturbation on all frequencies at the time of entering the Greenland shadow. However, the perturbation is of the same order as other fluctuations. About three hours into the flight, ionosphere sunrise begins to traverse Greenland, and the signal levels on all frequencies decrease over a period of one hour by 25 dB.

Flight 22, from Samoa, began during all-night on the propagation path; sunrise at Norway begins 30 minutes into the flight. Sunrise is confined to the Arctic end of the propagation path for the duration of the flight. Only that part of the path from Norway to North of Greenland is in daylight by the end of the flight. No evidence of modal structure was detected in the flight data.

Flight 12, to the west, occurs after Norway sunrise but before much expected effect on the path. The data show no significant fluctuations in amplitude.

Conclusion: The transition into a zone of mode 2 dominance for both 10.2 and 13.6 kHz predicted for flight 23 by the calculations cannot be resolved from the flight data but is considered likely. For flight 23, the effect of daylight onset is closely related to sunrise over Greenland. The area west of Hawaii is probably mode 1 dominant, though some small sectors of mode 2 dominance are predicted from the calculations.

(B) Liberia: Calculations show the area around and south of Hawaii to be all mode 2, due to initial traverse of the equatorial zone.

Flight 23, to San Diego, was during the sunrise transition on the propagation path. Some modal effects are evident during the first three hours of the flight.

Flight 22, from Samoa, data recorded was the calibration signal. No Liberia phase data was acquired.

Flight 12, to the southwest, data was obtained for 80 minutes 1.5 hours into the flight. Small evidence of modal occurs on the 10.2 and 13.6 kHz records.

Conclusion: The flight data provide minimal clues of modal structure. Other experience with the Liberia signal and the cumulative experience with flight data add support that mode 2 dominance is likely.

(C) Hawaii: Comparisons of predictions from calculations and flight data for propagation radials of 64°, 202° and 244° are shown respectively in Figures B-9, B-10, and B-11. Calculations by TASC show that on the 64° radial to San Diego, Figure B-9, mode 1 is dominant at 10.2 kHz beyond 0.9 Mm, but that modal fades exceeding 10 dB may exist to 7 Mm. At 13.6 kHz mode 1 is dominant beyond 3.4 Mm, but modal fades exceeding 10 dB may exist to 9.5 Mm. The 202° radial, flight 22 compared with NOSC calculations in Figure B-10, is predicted to enter the equatorial modal conversion zone at 2.5 Mm along the path. On exiting the equatorial zone, the signals are predicted to be on the border of modal zone. The 244° radial, flight 7 compared with NOSC calculations in Figure B-11, is predicted to enter the equatorial modal conversion zone at 2.2 Mm along the path. At that time a complex structure is generated and mode 2 becomes dominant upon exiting this zone, about 3 Mm along the path.

Flight 23, to San Diego, is 4.2 Mm in length, Figure B-10. The modal fades at 10.2 kHz are initially about 8 dB and decrease to 4.5 dB at 3.3 Mm. The fade depth for the last fade of the flight increases with frequency, progressively becoming 7, 10 and 20 dB respectively for 11.33, 11.8 and 13.6 kHz. The 20 dB fade at 13.6 kHz is the position of the deepest predicted fade from the calculations.

Flight 22 plus Flight 19, [illegible]moa and Wellington respectively, data show the near zone modal zone to lie within 1 Mm on this 202° radial, Figure B-10. The Equatorial zone modal structure begins at 2.5 Mm and continues until 4 Mm. The NOSC calculations show the modal structure to be reduced beyond 4 Mm, but the data show

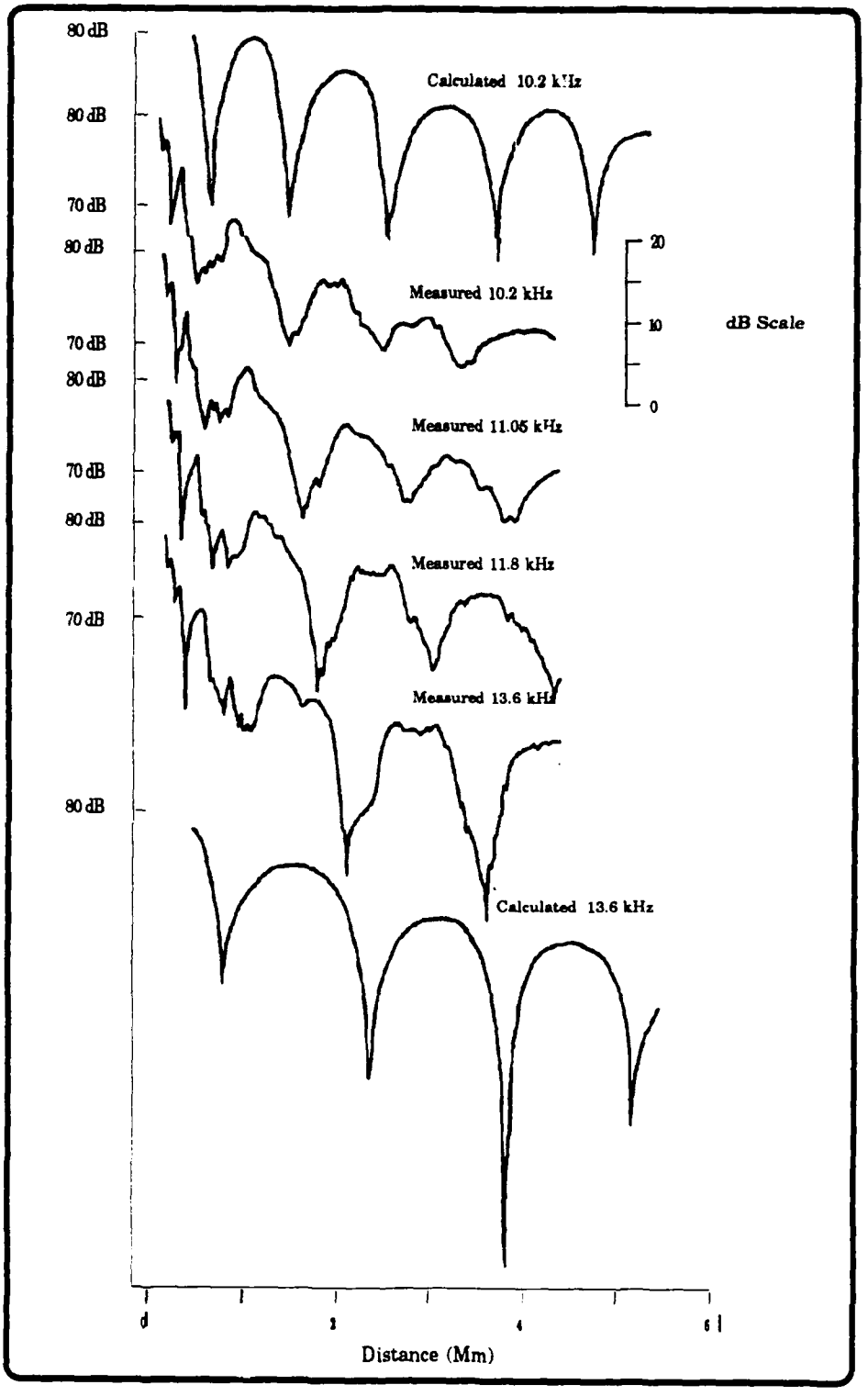

Figure B-9. Calculated and Measured Hawaii Signals, 64° Radial

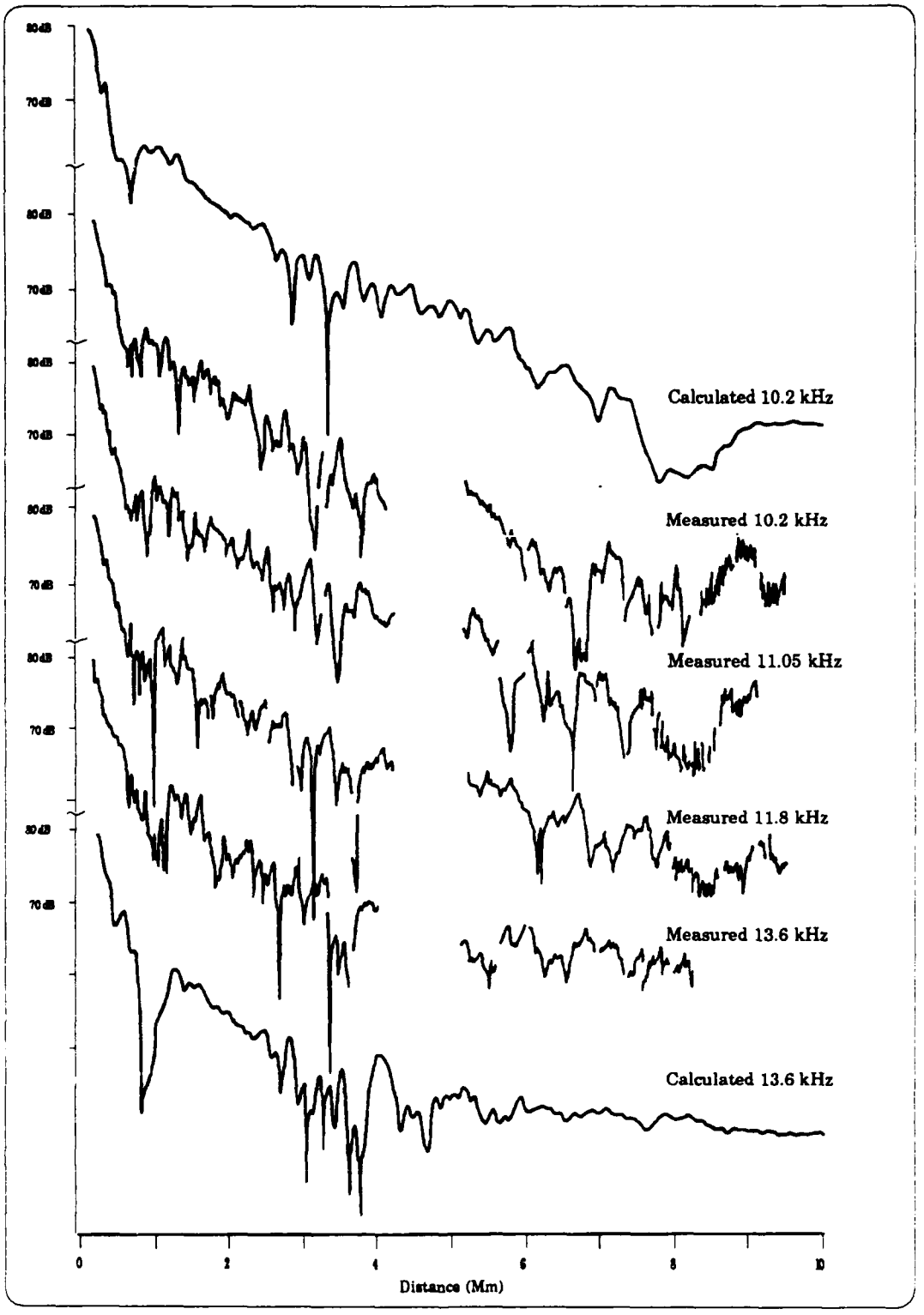

Figure B-19. Calculated and Measured Hawaii Signals, 202° Radial.

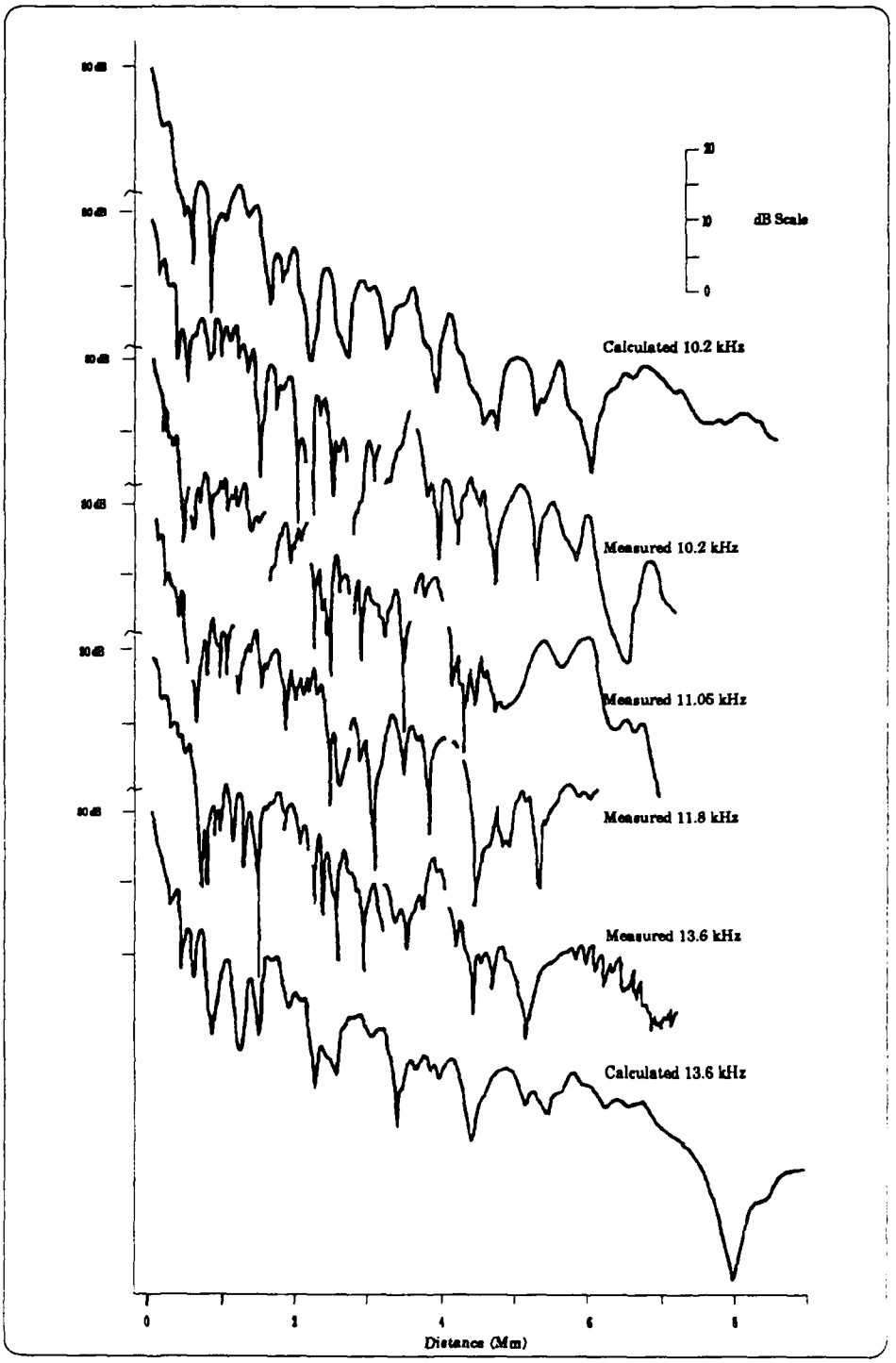

Figure B-11. Calculated and Measured Hawaii Signals, 244°Radial.

strong modal at 10.2 and 11.05 kHz to 8 Mm. The calculated modal structure at 11.8 kHz is significantly less than measured, and at 13.6 kHz the calculated structure is 6 dB or less in amplitude. The TASC calculation predicts even less modal structure than the NOSC calculations. Of the two, the NOSC calculations produce the better fit of structure across the equatorial zone.

Flights 12, 13 and 14, to the southwest, data show exceptional structure at all frequencies, starting at 1.5 Mm and continuing beyond 6 Mm. Fades greater than 15 dB occur throughout the range and frequency interval. Calculations provided by NOSC (202° bearing) show much more detail than the TASC calculations (205° bearing), and in general are more similar to the data. The amplitude data plots of field strength versus distance are shown in Figure B-10. The NOSC field strength calculations are also shown in Figure B-10.

Conclusions: The modal structure to the east, 64° radial, dampens more quickly with distance than the calculations predict. This observation is consistent with other measurements. The flight path, however, is too short to determine the extent of the 13.6 kHz safe modal boundary. The 10.2 kHz boundary probably is within 1 Mm. Data of flights from other validations, particularly other seasons, should be checked for confirmation. The propagation along the 202° and 244° radials are very strongly affected by higher-ordered modes to the maximum distance of the data, 7 and 9 Mm. The pronounced mode structure extends well beyond the equatorial zone, as predicted by the NOSC calculations, but is not as evident in the TASC calculations. The boundary for mode 2 dominance predicted to lie approximately along the 205° bearing needs to be placed along a bearing less than 202°.

(D) N. Dakota: Calculations show mode 1 for both frequencies with minimal modal structure in the vicinity of Hawaii or on either the first or last flight of this group. Flight 22 is predicted to cross the modal zone at about 0.6 of the flight duration. During the last 1/4 of flight 12 the flight enters the equatorial zone. Mode switching occurs for both 10.2 and 13.6 kHz but not much modal structure exists.

Flight 23, to San Diego, has data samples at 40-minute intervals. These data show amplitude fluctuations more consistent with propagation changes than with modal effects.

Flight 22, from Samoa, has data recorded essentially from sunset at Samoa to sunrise at North Dakota. Modal structure is evident on the data through the first half of the flight, mostly 10.2 and 11.3 kHz. The flight position at the time of last evidence of modal structure is about 10° north of the magnetic equator. This is about what is expected from predictions.

Flight 12, to the southwest, shows some small amplitude variability probably due to propagation variations. Sunrise at North Dakota occurs at the time the flight should be entering the equatorial zone. A 15 dB drop in the 10.2 kHz signal level looks similar to a dip at that location on the calculations but is more probably part of the sunrise effect.

Conclusion: The area of these flights is predicted to be mostly mode 1 dominant, except for Flight 22. The flight data is consistent with this prediction. For Flight 22 the modal structure locations coincide roughly with the predicted crossing from the mode 2 dominant zone. The modal effects exist to the maximum measured distance, thus suggesting that the modal zone boundary should be placed east of this radial. For flight 12, the possible entry into the equatorial zone could not be confirmed because of the simultaneous occurrence of sunrise at the North Dakota end of the path.

(E) La Reunion: The La Reunion signal propagates to Hawaii via Indonesia and to San Diego via Greenland. Thus, on flight 23 the propagation path goes through a bearing change of 112°. The modal fades at Hawaii are predicted to be 6 dB at 10.2 kHz and 8 dB at 13.6 kHz. The all-night condition occurs at Hawaii from about 1500 to 1630. As the transmission bearing increases, the modal structure decreases. By the termination of flight 12 the predicted modal, all-night path, is less than at Hawaii, even though the distance has decreased from 16.6 to 10.7 Mm.

Flight 23, to San Diego, on all frequencies shows a gradual increase with flight time, even though the distance from La Reunion is increasing. As the propagation path was always over 50 % daylight, no evidence of the predicted slight modal structure is observed, as expected. A signal amplitude decrease of about 25 dB occurs on all frequencies as the propagation path enters the Greenland shadow. The shape of this curve is almost identical to the Norway signal on the same flight. The La Reunion signal decrease occurs about two hours later. The times are consistent with first contact of Greenland by the two signal propagation paths to the aircraft. For both signals the onset of daylight may occur about the same time. The timing depends upon the model of screening height used to predict first ionosphere illumination.

Flight 22, from Samoa, occurred during sunset on the propagation path. No evidence of modal effects was detected.

Flight 12, to the southwest, occurs with sunset on the propagation path; sunset at La Reunion occurs just as the flight ends. At the start of the flight over 2/3 of the propagation path is in daylight. No modal effects were detected.

Conclusion: The flight data were not a good test of the available prediction model or of the expected worst case conditions. The prediction of mode 1 dominance except where the propagation path crosses the Greenland icecap, is probably valid.

(F) Argentina: The calculations show mode 2 to be dominant for both 10.2 and 13.6 kHz north of the equator in the sectors covered by flights 23 and 12. Negligible modal structure is predicted in the vicinity of Hawaii. Some modal structure is predicted for both flights, near midpath for flight 23 and on the last half for flight 12. For flight 22, the modal zone boundary is predicted to be just north of Samoa for 10.2 kHz and well south of Samoa for 13.6 kHz.

Flight 23, to San Diego, recorded data for the first hour. The signal is weak and very noisy. Modal structure of about 10 dB on all frequencies is possible.

Flight 22, from Samoa, occurred with all-night on the propagation path for the first four hours. The sunrise transition was on the propagation path for the rest of the flight. Very deep modal fades occurred on first 13.6 kHz, 26 dB, and then at 11.3 kHz, 22 dB. Evidence of modal competition continued until two hours after onset of sunrise on the propagation path. Modal effects were evident on 10.2 kHz within one hour of the flight start.

Flight 12, to the southwest, recorded data in short one hour segments during four intervals. During the first two segments, leaving Hawaii and after three hours into the flight, no modal structure is evident. For the last two hours of the flight, two adjacent segments show modal structure on all three frequencies.

Conclusion: Except for Flight 22, the flight data are not of sufficient duration to support any determination of modal effects. Flight 22 data give strong confirmation of mode competition between Samoa and Hawaii. The observed modal effects on 10.2 kHz near Samoa suggests that the zone boundary is as predicted or further south. It is assumed that the prediction from calculations of mode dominance is correct.

(G) Australia: The calculations predict mode 1 dominant for both frequencies and no mode structure for any of the flights of this group.

Flight 23, to San Diego, shows no mode structure during that portion of the flight with all-night on the propagation path.

Flight 22, from Samoa, data show no evidence of modal effects after sunset on the propagation path.

Flight 12, to the southwest, shows no mode structure during that portion of the flight with all-night on the propagation path.

Conclusion: The Australia signal is safely mode 1 dominant within the measured area.

(H) Japan: The calculations show that some modal structure can extend to San Diego, 8 dB at 13.6 kHz. The 13.6

kHz modal structure at Hawaii is predicted to be 15 dB. As the bearing from Japan moves clockwise and the distance decreases, the modal increases, peaking at 120° and 5.2 Mm at 33 dB. The modal then gradually decreases and distance remains about constant to a bearing of 150° where the 13.6 kHz modal becomes about 10 dB. Flight 22, from Samoa, is predicted to cross the 13.6 kHz zone of mode 2 dominance.

Flight 23, to San Diego, occurs with sunset on the propagation path for the first half of the flight. After Japan sunset, near the end of the flight, modal structure is evident, reaching at least 8 dB at 13.6 kHz. The 10.2 kHz modal is negligible.

Flight 22, from Samoa, occurred mostly during the sunset transition on the propagation path. No evidence of modal structure was detected.

Flight 12, to the southwest, occurs with sunset at Japan one hour after data sampling starts. Data are sampled at approximately one hour intervals. Minimal modal structure was observed. A cross section of the prediction from calculations shows that less than 1/2 a phase cycle should have been crossed. The traverse for 13.6 kHz is across a peak of the structure. For the data to have matched the prediction that closely would be fortuitous, yet structure was not detected.

Conclusions: Strong modal structure was predicted to the southwest of Hawaii. None was evident in the data. Either the flight geometry or solar illumination conditions were poor to test for modal effects. Given the total flight experience with Japan and Hawaii signals, we consider it likely that the modal structure to the southeast of Japan is not as large as predicted.

Hawaii Area Overall Summary: The region around Hawaii largely fits predictions. For both the Hawaii and Japan signals on bearings to the southeast, the modal structure could be, on the average, somewhat less than predicted. Where a higher-ordered mode dominance was predicted, the flight data supported (or at least did not conflict with) the predictions. The 202° radial from Hawaii shows significant modal structure on the Hawaii signal. The modal zone boundary for Hawaii

should be moved counterclockwise a few degrees, at least for February. Until further confirmation is obtained, the other predictions from calculations should be considered valid.

Flight 13: (16 Feb. 1986) Flight 13 was located in the northwest end of the validation region on an extended radial from Hawaii to northern Australia. In that part of the validation region covered by flight 13, the signals of primary concern for possible self-interference are; stations (B), Liberia antipode, (C) Hawaii, (D) North Dakota and (F) Argentina. The analysis summary by stations is as follows:

(A) Norway: The calculations show the signal is dominantly mode 1 in the vicinity of flight 13 for both frequencies.

The flight data has a small perturbation on all frequencies probably associated with sunset at Norway. The rest of the record is consistent with mode 1 dominant and no modal structure. The perturbation could also result from predicted traversal of a low conductivity area in Siberia.

Conclusion: The mode 1 dominance over most of the path is supported with the flight data. The possible existence of a modal conversion zone in northern Siberia could not be confirmed.

(B) Liberia: This flight comes very close to the antipode. Calculations show that the path to the east of the antipode has a very complex field structure. The path to the west of the antipode is predicted mode 1.

The flight data show very marked structure in traversing close to the antipode. On the east side, westward propagation, the signal peaks about 5 dB weaker at 10.2 kHz and 12 dB weaker at 13.6 kHz than on the west side. Near the time of closest approach to the antipode a deep signal fade occurs on 10.2 and 11.3 kHz. The fade is 18 and 30 dB for respectively 10.2 and 11.3 kHz. At the time of closest approach the eastward propagation path was about 3/4 night.

Conclusion: The flight data provide a good demonstration of the long and short-path interfer-

ence. The nature of the interference is expected to change throughout the diurnal period. For the time of measurement the region of significant interference appeared to extend less than a megameter on either side of the antipode.

(C) Hawaii: The data for flight 13 were included in the above description of measured radials from Hawaii.

Conclusions: The propagation along the 244° radial is very strongly affected by higher-ordered modes to the maximum distance of the data, 7 Mm.

(D) N. Dakota: Calculations show this flight to be crossing the equatorial mode conversion zone and extending slightly south of the zone.

The flight occurred in or after sunrise at North Dakota. About two hours of flight time were recorded. Modal structure is evident during this time.

Conclusion: The data cannot be used to test the predictions from calculations.

(E) La Reunion: The La Reunion signal is predicted mode 1 dominant, with minimal modal structure, 6 dB at 13.6 kHz.

After sunset at La Reunion the flight data, consisting of hourly samples, show minimal effects of modal structure.

Conclusion: The flight data are consistent with predictions.

(F) Argentina: The calculations show mode 2 to be dominant for both 10.2 and 13.6 kHz for the area covered by flight 13. Some modal structure is predicted within the equatorial zone.

Over half of the propagation path was in daylight throughout the flight. By the end of the flight the short-path was essentially all daylight and the long-path 3/4 dark. There is some indication of possible long and short-path interference during the last two hours of the flight. At this time mode 1 should be safely dominant on the short-path.

Conclusion: The flight data did not provide a valid test of the calculation predictions

(G) Australia : The calculations predict mode 1 dominant for both frequencies and minimal mode structure for the flight.

The flight data, sampled hourly until just before sunrise at the transmitter, show minimal modal at 13.6 kHz and none on other frequencies.

Conclusion: The prediction of safe mode 1 dominance is considered valid.

(H) Japan: The calculations show that the radials traversed on this flight are strongly mode 1 dominant. No modal structure is predicted.

The flight data, taken in hourly samples, show no evidence of modal structure.

Conclusions: This region is safely considered mode 1 dominant at all times.

Flight 13 Overall Summary: No disagreements with the predictions from calculations were found. The tests for modal where predicted were weak. The predictions from calculations should be used to define regions of modal problems until additional testing is undertaken.

Flights 14, 15, 16: (18, 21 & 22 Feb 1985) These flights were in the vicinity of Australia. In that part of the validation region covered by these flights, the signals of primary concern for possible self-interference are stations (C) Hawaii, (D) North Dakota and (G) Australia. Hawaii and North Dakota are predicted to have mode 2 dominant from traversal of the equatorial zone. The predicted near-zone modal of Australia was measured in this flight set. The analysis summary by stations is as follows:

(A) Norway: The calculations show the signal is dominantly mode 1 throughout the area for both frequencies.

Flight 14 data were obtained during the sunset transition on the propagation path.

Flight 15 data were obtained with the propagation path almost all in daylight.

Flight 16 data were obtained with the sunset transition on the propagation path during the first half of the flight and all-night for the rest of the flight. The last half contained two legs in almost opposite directions. The two segments produced very similar data. More amplitude fluctuation was noted on the 13.6 kHz signal than the other two. The fluctuation appears position dependent.

Conclusion: The prediction of mode 1 dominance over the area is supported with the flight 16 data. The possible existence of some modal conversion in the signal traversing northern Siberia could not be confirmed.

(B) Liberia: The Liberia signal is predicted mode 1 dominant for flights 14 and 15. Flight 16 is expected to penetrate the Antarctic shadow zone on the north east leg and exit on the south west leg. The shadow zone is predicted as mode 2 dominant for an all-night path.

Flight 14 starts with the propagation path all daylight and ends with the path about half daylight. No modal structure is evident.

Flight 15 data starts just before sunrise at Liberia and ends just after sunset at the flight location. No modal effects were observed.

Flight 16 starts just after sunset at Melbourne where the flight originated. Entry into the Antarctic shadow zone begins about two hours into the flight. At that time a portion at Antarctica is in daylight. The signal gradually fades, becoming submerged in the noise at 10.2 and 11.3 kHz and decreasing by 15 dB at 13.6 kHz. On the outbound leg of the flight the signal returns to much higher values, 16, 15 and 9 dB above the early flight values for respectively 10.2, 11.3 and 13.6 kHz. By full exit from the Antarctic shadow the propagation path is in total darkness.

Conclusion: The flight data, because of propagation path illumination conditions, do not provide a good test of predictions. We expect that the Liberia

signal in this region is safely mode 1 dominant, except within the Antarctic shadow zone under night propagation across Antarctica, (a local winter condition).

(C) Hawaii: The calculations predict both the 10.2 and 13.6 kHz signals to be mode 2 dominant in the area of these flights. Both signals, 10.2 and 13.6 kHz, are predicted to have some modal structure, generally less than 10 dB.

Flight 14 data show that after sunset in Australia modal structure exists on all frequencies, exceeding 10 dB on 11.3 kHz. The fade pattern is sufficiently different between frequencies to support a modal interpretation.

Flight 15 data, recorded just before sunset on the flight path, show the typical amplitude increase associated with pre-sunset.

Flight 16 data show pronounced modal structure at 10.2 kHz, approaching 20 dB excursions. Less structure is shown at 11.3 and 13.6 kHz, being less than 5 dB at 11.3 kHz and about 10 dB at 13.6 kHz. The onset of sunrise at Hawaii creates a very deep fade at 11.3 kHz, almost 30 dB. Such deep fades are usually associated with a mode switch.

Conclusions: The Hawaii signal over eastern Australia and to the east shows strong evidence of modal structure. The predicted mode 2 dominance for both 10.2 and 13.6 kHz is supported by the flight data. The predictions from calculations are considered valid for the area of these flights.

(D) N. Dakota: Calculations show the area of these flights to be mode 2 dominant at all frequencies. Some modal is expected at all frequencies and distances.

Flight 14 data were not obtained.

Flight 15 data are of too short a time interval to analyze.

Flight 16 data are only for an hour before North Dakota sunrise. The 10.2 kHz signal is mostly in the noise. The 11.3 and 13.6 kHz signals show modal structure of about 10 dB.

Conclusion: The flight 16 data, although of very short length, provide support for the predictions from calculations. The predicted mode 2 dominant zone for nighttime propagation is expected to extend over Australia.

(E) La Reunion: The La Reunion signal is predicted mode 1 dominant on all flights, with negligible modal structure, 4 dB at 13.6 kHz.

Flight 14 data were obtained during sunset transition on the propagation path. No modal structure was observed.

Flight 15 data were obtained during all daylight on the path and just at sunset on the flight path.

Flight 16 data were obtained during sunset on the propagation path for the first half of the flight; the propagation path was in total night for the second half. No modal structure was detected in the data.

Conclusion: The flight 16 data are consistent with predictions of safe mode 1 dominance in the vicinity of eastern Australia.

(F) Argentina: The calculations show mode 1 to be dominant for both 10.2 and 13.6 kHz for the area covered by these flights. Negligible modal structure is predicted in the vicinity of Australia.

Flight 14 data show no modal effects. The propagation path for this flight is in total darkness for only about 50 minutes, 0850 to 0940 GMT.

Flight 15 data were collected during all daylight on the path and just at sunset on the flight path. No modal effects were detected.

Flight 16 starts just after sunrise at Argentina. The flight data show a gradual decrease in signal amplitude as the sunrise transition moves toward the receiver. About 1310 GMT the negative slope increases on 11.3 and 13.6 kHz. The 11.3 kHz signal drops into the noise at about 1620. By 1900 the 11.3 kHz signal begins to recover. The 13.6 kHz signal goes through a fade at 1610 and then another small fade at 1710, after which it begins to increase in amplitude.

Conclusion: While the flight data could not be used to confirm the predictions from calculations of mode 1 dominance in the vicinity of Australia, flight 16 showed no evidence of modal effects as the sunrise terminator began to move across the propagation path.

(G) Australia: The calculations have been used to predict the near zone of modal effects for both frequencies as presented in Figure A-15.

Flight 14, at night, showed that the 10.2 kHz near zone boundary on the 30° radial should be placed at 1.4 Mm. The calculations had predicted 0.7 Mm. The 13.6 kHz boundary on a 27° radial should be placed at 2.2 Mm. The calculations had predicted 1.2 Mm.

Flight 15, at day, on the 27° radial, placed the near zone boundary for 10.2 kHz at 0.4 Mm and for 13.6 kHz at 0.6 Mm.

Flight 16, at night, on the 51° radial showed that the near zone boundary for 10.2 kHz should be placed at 1.8 Mm and for 13.6 kHz at 2.5 Mm. The calculations had predicted respectively 0.8 and 1.8 Mm.

Conclusion: For the two samples measured, the nighttime propagation near zone modal boundary extended further than the calculations predict. Other measurements should be correlated with the predictions to determine the proper boundary at a sufficient number of angles to create a reliable boundary envelope.

(H) Japan: The calculations show that propagation to the vicinity of eastern Australia is strongly mode 1 dominant. No modal structure is predicted.

Flight 14 data show no evidence of modal structure. The sunset terminator is almost parallel to the propagation path and crosses the flight path near 0900, about one hour into the flight

Flight 15 data were collected during all daylight on the path and just at sunset on the flight path. No modal effects were detected.

Flight 16, an all-night flight, show no modal effects in the data.

Conclusions: This region is safely considered mode 1 dominant at all times.

Flights 14, 15 & 16, Overall Summary: The near-zone modal boundary for Australia was checked at night on two radials. Both sets of measurements showed that at least for those nights and on the measured radials the boundary distance should be increased. The distance increase should be about 100% for both frequencies.

The predicted mode 2 dominant conditions for both the Hawaii and North Dakota signals was confirmed.

Long-path effects were noted on the the Argentina signal. We estimate that the long-path interaction could be significant for as much as 14 hours along the eastern edge of Australia.

Wellington, NZ site and Flights 17, 18 & 19: (24, 26 & 28 Feb. 1985) The area around New Zealand is predicted to have five signals available to the west and six to the east. New Zealand is predicted to be on the border of the modal zone for the Hawaii signal, within the modal zone for the North Dakota signal, and on the border for near zone modal for the Argentina signal. The analysis summary by stations is as follows:

(A) Norway: The calculations show the signal is dominantly mode 1 in the vicinity of Wellington and this group of flights for both frequencies. The Norway antipode is at Lat. 66.42 S, Long 166.85 W.

Flight 17, to Wellington, has two hours of data recorded, 0830 to 1030 GMT. The flight data start when the flight end is in the dark, about 50% of the path being dark. The record ends with the path about 4/5 in the dark. No modal structure was detected.

Flight 18, round trip to the south of Wellington, starts with the short-path in all daylight. The data are very dissimilar on the two flight legs. At flight start the 10.2 kHz signal is essentially in the noise; the 11.3 and 13.6 kHz signals decrease with

time for the first 2.5 hours. The 11.3 kHz signal reaches a minimum about 0750, 40 minutes before the 13.6 kHz signal at about 0830. The 13.6 kHz signal increases the fastest, gaining 25 dB in 90 minutes. The 10.2 kHz signal increases above the noise by 0930. The signal level increase continues for the rest of the flight. The signal buildup begins just before flight turn around.

Flight 19, to Tonga, starts when the sunset transition is over 50% along the propagation path and ends with the path in total darkness. No modal structure was detected.

Wellington phase data showed considerable variability in the diurnal phase records. Cycle jumps were recorded for 37% of the diurnal days at 10.2 kHz. No cycle jumps occurred at 11.3 kHz and 1 jump occurred at 13.6 kHz. Most 10.2 cycle jumps occurred near the start of sunset on the propagation path, i.e. at Wellington. A few less than 30% occurred during sunrise on the path, usually during late sunrise. A phase jump occurred on 10.2 kHz just before the start of flight 18.

Conclusion: The Norway signal at and to the south of Wellington is subject to long-path interference in the February time frame. The time interval of likeliest interference at Wellington is from 2100 through midnight to 0600 GMT. None of the flights occurred in this time interval, so the geographic extent of the interference could not be assessed.

(B) Liberia: The Wellington site and all flights of this group were within the Antarctic shadow zone. The calculations show all frequencies to be extremely weak when the propagation path over Antarctica is in daylight or to be mode 2 dominant when this path is in the dark.

Flight 17, to Wellington, was recorded from 0500 to 0830. The propagation path conditions went from 1.5 hours before sunrise at Liberia to two hours after. Sunset occurred at Wellington about 1 hour before the end of recording. The 10.2 and 11.3 kHz signals are in the noise. The 13.6 kHz signal decreases by about 8 dB, reaching the noise level after 80 minutes of flight recording.

No other flights recorded data.

The Wellington phase data were used for the calibration channel, so no Liberia phase information is available.

Conclusion: No information was derived from the flight data, except that the signals are very weak. Weak signals are predicted for propagation over the Antarctic icecap.

(C) Hawaii: New Zealand is just to the east of the predicted modal zone boundary. TASC calculations show that at a 200° bearing from Hawaii the equatorial mode conversion zone converted modes are greater than 15 dB below mode 1 at 5 Mm distance from the transmitter for both 10.2 and 13.6 kHz. At 205° bearing and 5 Mm distance mode 2 exceeds mode 1 by 16 dB at 10.2 kHz and at 13.6 kHz mode 2 is about 1 dB below mode 1. The bearing to New Zealand is about 202°. If either mode 1 or mode 2 is dominant, negligible mode structure is predicted in the vicinity of New Zealand, 7.5 Mm distance.

Flight 17 occurred during the sunset transition on the propagation path. Total night for the path occurred approximately 0800 GMT. A large amplitude increase, over 15 dB at 10.2 and 11.3 kHz, occurred just before sunset at the aircraft. A much more gradual increase occurred on 13.6 kHz. The sharpness of the increase at 10.2 and 11.3 kHz strongly suggests modal switching. Other small evidence of modal effects was observed on the 10.2 kHz signal both before and after the major amplitude increase.

Flight 18, round trip south of Wellington, data show reasonable symmetry for the two flight segments. No data were recorded at 11.8 kHz for the outbound segment. The modal structure decreases with frequency, being about 12 dB at 10.2 kHz and 8 dB at 13.6 kHz.

Flight 19, to Tonga, data show very different modal structure on each of the four frequencies measured. The deepest fades, 13 dB, occur at 10.2 and 11.3 kHz.

The Wellington phase data showed that phase jumps occurred 44% of 24-hour intervals, primarily at 10.2 kHz. A few jumps occurred at 11.3 kHz and none at 13.6 kHz. When days of large phase perturbations occurred, the disturbed periods cover 70% of the days. Jumps occurred over a wide time range and were in both directions, advanced and retarded. The 13.6 kHz phase records were consistently representative of a clean mode 1 signal at all times.

Conclusions: The Wellington phase data make the case for Wellington being inside the mode 2 dominant boundary at 10.2 and 11.3 kHz. These data also clearly show that Wellington is outside the 13.6 kHz boundary. The flight data tend to support these findings. The modal zone boundary for Hawaii at 10.2 and 11.3 kHz needs to be placed further east in the vicinity of New Zealand.

(D) N. Dakota: Calculations show the region about Wellington to be mode 2 dominant at all frequencies. The boundary for 10.2 kHz is predicted to lie about 0.5 Mm south of Wellington. The 13.6 kHz boundary is predicted about 2 Mm south.

Flight 17 data are very noisy prior to local sunset; after sunset modal structure of 10 dB or more on all frequencies is evident.

Flight 18, round trip south of Wellington, data show the 10.2 kHz signal in the noise. The 11.3 kHz signal is in the noise for the first leg of the flight. Modal structure is evident on the second leg for 11.3 kHz and on both legs for 13.6 kHz. Greater than 10 dB fades were measured.

Flight 19, to Tonga, initially occurred during all-night (for the first 1 hour) on the propagation path. The last three hours were during daylight transition on the propagation path. The 10.2 kHz signal is in the noise except for the last 80 minutes, when it has a slight amplitude increase. Some evidence of modal is suggested by the different shape between the 11.3 and 13.6 kHz amplitudes.

The Wellington data show mode switching (evidenced by cycle jumps), 100% of the 24-hour

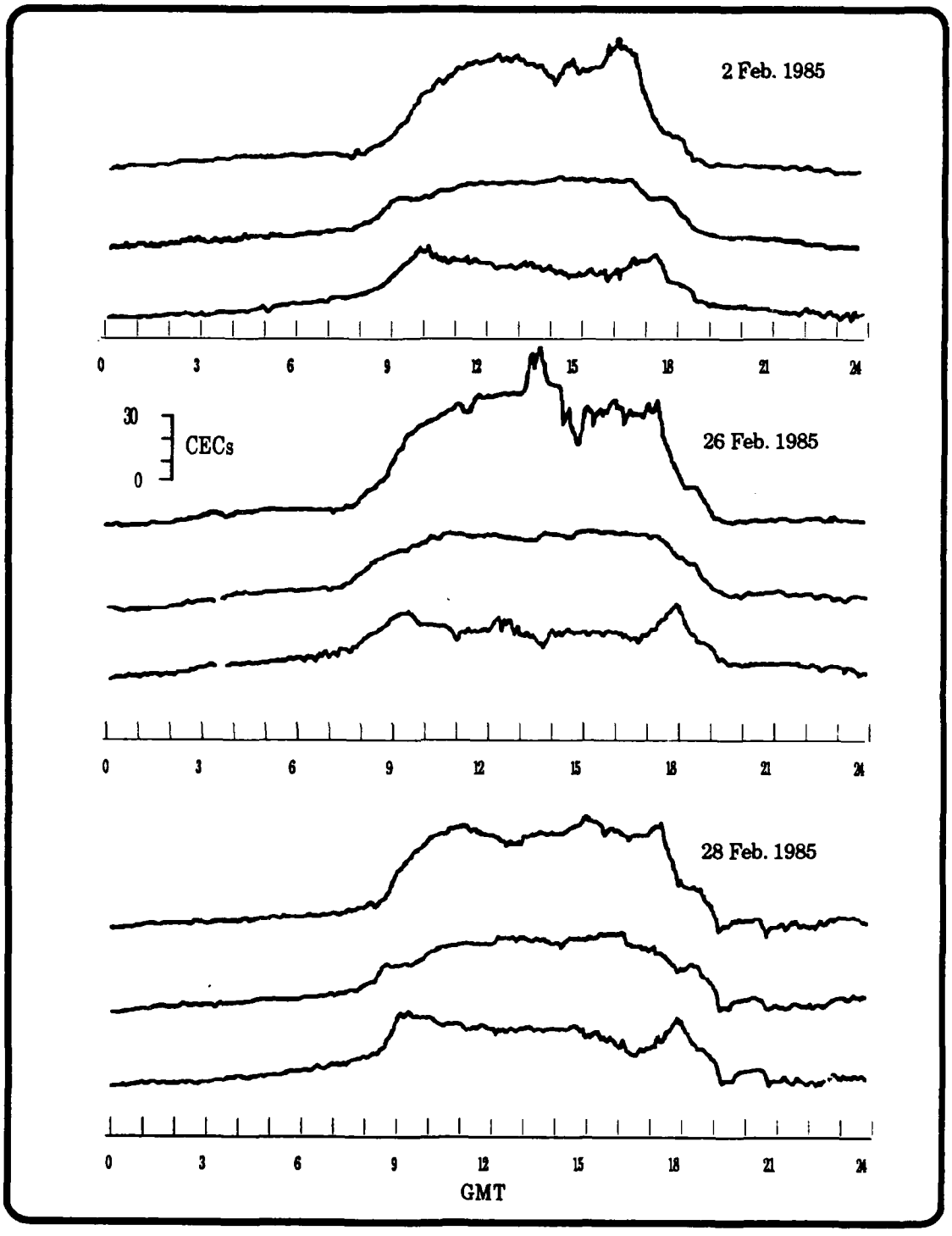

Figure B-12. Wellington Phase Data, Australia Signal

days at 10.2 kHz, 86% at 11.3 kHz and 29% at 13.6 kHz. Further, if days with no mode jumps but with phase swings sufficient to predict a mode jump at another location are included, the 13.6 kHz percentage increases to 55%.

Conclusion: The Wellington phase data produce conclusive evidence of mode switching at all

frequencies. Wellington clearly is within the mode 2 dominant zone for all frequencies as predicted. Flight 18 to the south apparently did not traverse the zone boundary. It is possible that the 13.6 kHz boundary should be placed farther south.

(E) La Reunion: The La Reunion signal is predicted mode 1 dominant, with negligible modal structure.

Flight 17, to Wellington, data are for an all daylight propagation path until about 0750 GMT. The rest of the flight is during early sunset on the propagation path. No evidence of modal structure was detected.

Flight 18, round trip to the south of Wellington, occurred either when the propagation path was in daylight or during sunset transition. No evidence of modal structure was detected.

Flight 19, to Tonga, occurs during sunset transition and one hour of all-night on the propagation path. No modal structure was found.

Wellington phase data consistently showed a clean mode 1 diurnal record for all frequencies and days.

Conclusion: The good flight data are consistent with the Wellington phase data, all confirming predictions of safe mode 1 dominance in the vicinity of New Zealand.

(F) Argentina: The calculations show mode 1 to be dominant for both 10.2 and 13.6 kHz for the area covered by Wellington and this group of flights. Negligible modal structure is predicted within this area.

Flight 17, to Wellington, data show an amplitude increase across frequency with local sunset. No modal structure was detected.

Flight 18, round trip south of Wellington, data show good symmetry for both legs of the flight. A systematic ampelitude decrease is noted at sunrise over Argentina. No modal effects were noted.

Flight 19, to Tonga, data were recorded during sunrise on the propagation path. No modal structure was detected.

Wellington phase data are very clean phase 1 at all frequencies and all diurnal days.

Conclusion: The flight data support the Wellington phase data in confirming that the Argentina signal is safe mode 1 in this area.

(G) Australia: The calculations predict that the near zone modal interference could extend as far east as Wellington.

Flight 17, to Wellington, occurred while the propagation path was in daylight. No modal effects were detected.

Flight 18, round trip south of Wellington, occurred with the propagation path in daylight for the outbound leg and in darkness for the inbound leg. No modal effects were detected during the outbound leg. Hourly samples were taken during the inbound leg. Modal structure about 10 dB in magnitude was detected.

Flight 19, to Tonga, occurred during all-night conditions on the propagation path. Hourly samples were recorded. Modal structure, noted on all frequencies over the path, was strongest at 11.05 kHz. Fades of about 12 dB were noted at both 11.05 and 13.1 kHz, but at different locations.

Wellington phase data show the effects of modal competition, but no mode switching was recorded. Figure B-12 shows phase recordings of the Australia signal for three representative days near the flight schedule. The top set of recordings is a

typical day of moderate modal competition. Note that the nighttime phase pattern for 10.2 kHz begins with mode 1 being dominant. At about 1000 GMT evidence of a second mode appears, at which time the 10.2 kHz phase reverses the direction of change. At the same time the 11.3 kHz phase momentarily stops its shift to larger values, and the 13.6 kHz phase increases its rate of change. Thus the diurnal phase change for 10.2 kHz is reduced over what is produced with a single mode, and 13.6 kHz phase change is increased. After 1700 the effect of the second mode is no longer present. If amplitude data, instead of SNR data, were recorded, vectors of modal components could be constructed between the three frequencies to obtain a good measure of each component magnitude. The second mode on the average subtracts roughly 15 CECs from the 10.2 kHz signal and adds about 20 CECs to the 13.6 kHz signal. The next two phase record groups are recorded phase data for two of the flight dates, 26 and 28 February. The 13.6 kHz record for 26 Feb. shows a marked phase excursion between 1330 and 1530. Disturbances similar to this example, where the phase deviation exceeds 30 CECs, occur about 22% of the time. Several disturbances were noted where the 13.6 kHz signal deviation exceeded 50 CECs. Disturbance deviations are much smaller on 11.3 and 10.2 kHz.

Conclusion: The prediction that the near zone boundary lies close to Wellington for the 13.6 kHz signal are confirmed by the Wellington phase data. The nighttime flight data support the prediction that modal structure is strong in the vicinity of New Zealand. It is estimated that the near zone boundary is almost correct to the east of the Australia transmitter.

(H) Japan: The calculations show that the radials traversed on these flights are strongly mode 1 dominant. Minimal modal structure is predicted, 1 dB at 10.2 kHz and 4 dB at 13.6 kHz.

Flight 17, to Wellington, occurred mostly during daylight and sunset on the propagation path. No modal effects were detected.

Flight 18, round trip south of Wellington, occurred with sunset on the propagation path during the

outbound leg and all-night on the propagation path during the inbound leg. The amplitude records show sunset effects but contain no evidence of modal structure.

F'.ght 19, to Tonga, occurs during all-night on the propagation path. No evidence of modal structure was detected in the data.

Wellington phase data are a very clean record of mode 1 propagation at all times and frequencies. No hint of modal structure was detected.

Conclusions: The predictions from calculations for safe mode 1 phase in the vicinity of New Zealand are strongly confirmed by the Wellington phase data and supported by the Flight data of this group. This region is considered safe mode 1 dominant at all times.

Wellington site and Flights 17, 18 & 19, Overall Summary: The major uncertainties in prediction of signal quality were for the Hawaii, North Dakota and Australian signals. Both the Hawaii and North Dakota signals are within a modal zone in the vicinity of Australia.

The modal zone border for Hawaii, derived from calculations, needs to be moved further to the east, at least for February. Since the calculations predict a very abrupt transition from mode 1 dominance to mode 2 dominance with bearing change, it is difficult to estimate how far east the boundary should be moved.

For North Dakota the calculations predicted that the New Zealand area is well within the mode 2 dominance zone. The confirmation from measurements adds credence to the calculation model. Some evidence was produced to suggest that the 13.6 kHz boundary may actually extend further south in the area of flight 18 than predicted. The prediction that the 13.6 kHz modal near zone would extend close to New Zealand was confirmed. A conservative approach is to place this boundary slightly to the east of Wellington.

This completes the development of a guidance-model of modal-interference effects for each of the Omega stations. The material of this

appendix is summarized and interpreted in sections 3 *EXECUTION AND FINDINGS* and 4 *INTERPRETATION OF VALIDATION ANALYSIS* of the report.

Appendix C

Generation of Geographic Plots Showing Predicted Long Path Interference Boundaries

OVERVIEW:

The set of plots described in this appendix show the signal self-interference resulting from the dominant signal propagating more than halfway around the world, 20 megameters (Mm). The mechanism for long-path interference was described in Section 3.4.1. We note that the Omega signals from distances greater than 20 Mm are not in general used for navigation, although such use has been considered (Ref. 23, P. B. Morris). We show in this appendix, that under certain conditions the dominant signals propagate well beyond 20 Mm; i.e. the received signal is a long-path signal. These long-path signals are not considered suitable for navigation. A geographic plot of the long-path/short-path boundary is constructed in this appendix for each station in which long-path interference is a potential problem in the South Pacific validation region.

The analysis of long-path interference conditions was derived from a series of Omega field strength calculations produced by TASC for ONSCEN (GUPTA 1988, Ref. 20). This set of calculations is described in Appendix A. The calculations are for two frequencies, 10.2 and 13.6 kHz, and two propagation conditions, either all day or all night on the path. These calculations were made for each station generally on 10° radial intervals and to a radial distance of 19 Mm. The antipode, being halfway around the world, is 20 megameters from each station. The prediction of field strengths beyond 19 Mm were made using an extension to the calculations which is derived for this analysis and which is described in this appendix.

The procedure used for each station was (1) first to determine if long-path was likely to exist in the validation region; (2) if it is likely, to select the radials that would best represent the long-path effects in the region; (3) to determine the greatest extension of the long-path on each selected radial;

and (4) to estimate the time history of the long-path/short-path boundary location along the radial. Important factors for locating the boundary between long- and short-path propagation include: location of each station antipode, relative field strength of signals at the antipode incident from opposite radials, propagation beyond the antipode, and the effect on propagation of relative solar illumination of the long and short propagation paths.

The antipodes of the eight Omega stations are listed in Table 1. The locations of the six station antipodes that are in close proximity to the validation region are shown in Figure C-1. The two station antipodes not shown, Hawaii (C) and North Dakota (D), were well outside the display area. Signals from these two stations also had to be evaluated for long-path effects.

Station	Location		Antipode	
	Lat	Long	Lat	Long
A Norway	66.42 N	13.15 E	66.42 S	166.85 W
B Liberia	6.31 N	10.66 W	6.31 S	169.34 E
C Hawaii	21.41 N	157.83 W	21.41 S	22.17 E
D North Dakota	46.37 N	98.34 W	46.37 S	81.66 E
E La Reunon	20.97 S	55.29 E	20.97 N	124.71 W
F Argentina	43.05 S	65.19 W	43.05 N	114.81 E
G Australia	38.48 S	146.93 E	38.48 N	33.07 W
H Japan	34.61 N	129.45 E	34.61 S	50.55 W

Table C - 1. Omega Station Antipodes

The incident signal levels at a distance of 19 Mm from each transmitter, the maximum distance calculated, are shown in Figures C-2 though C-9 for both day and night propagation and for both 10.2 kHz (part A) and 13.6 kHz (part B). For these plots, the horizontal ordinates which are bearing scales for day and night propagation, are the bearings of the radials from the transmitter. These scales are offset 180° from each other. This was done to allow direct comparison between the relative strengths of signals incident

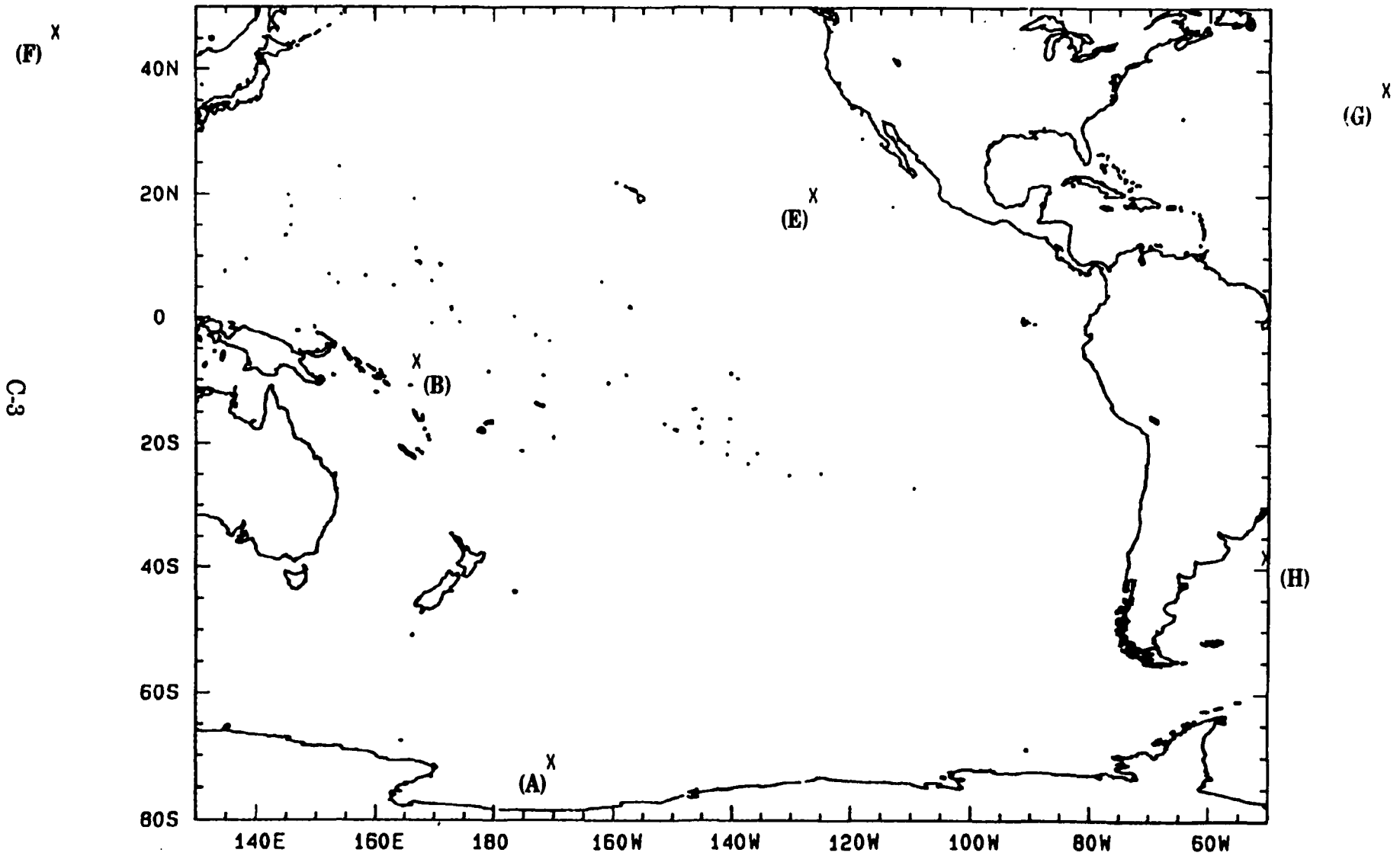

Figure C-1. Station Antipodes

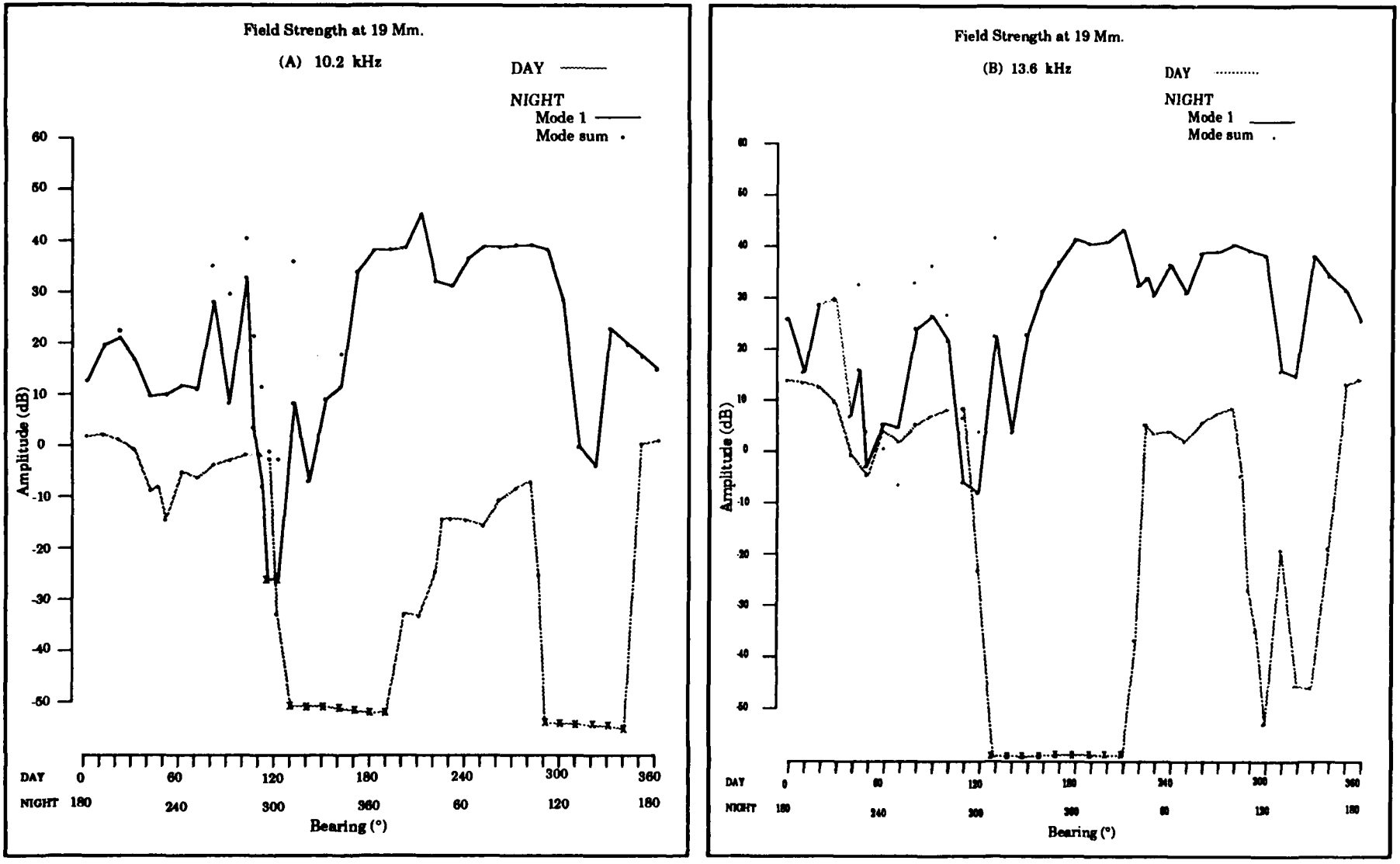

Figure C-2. Predicted Norway signal levels.

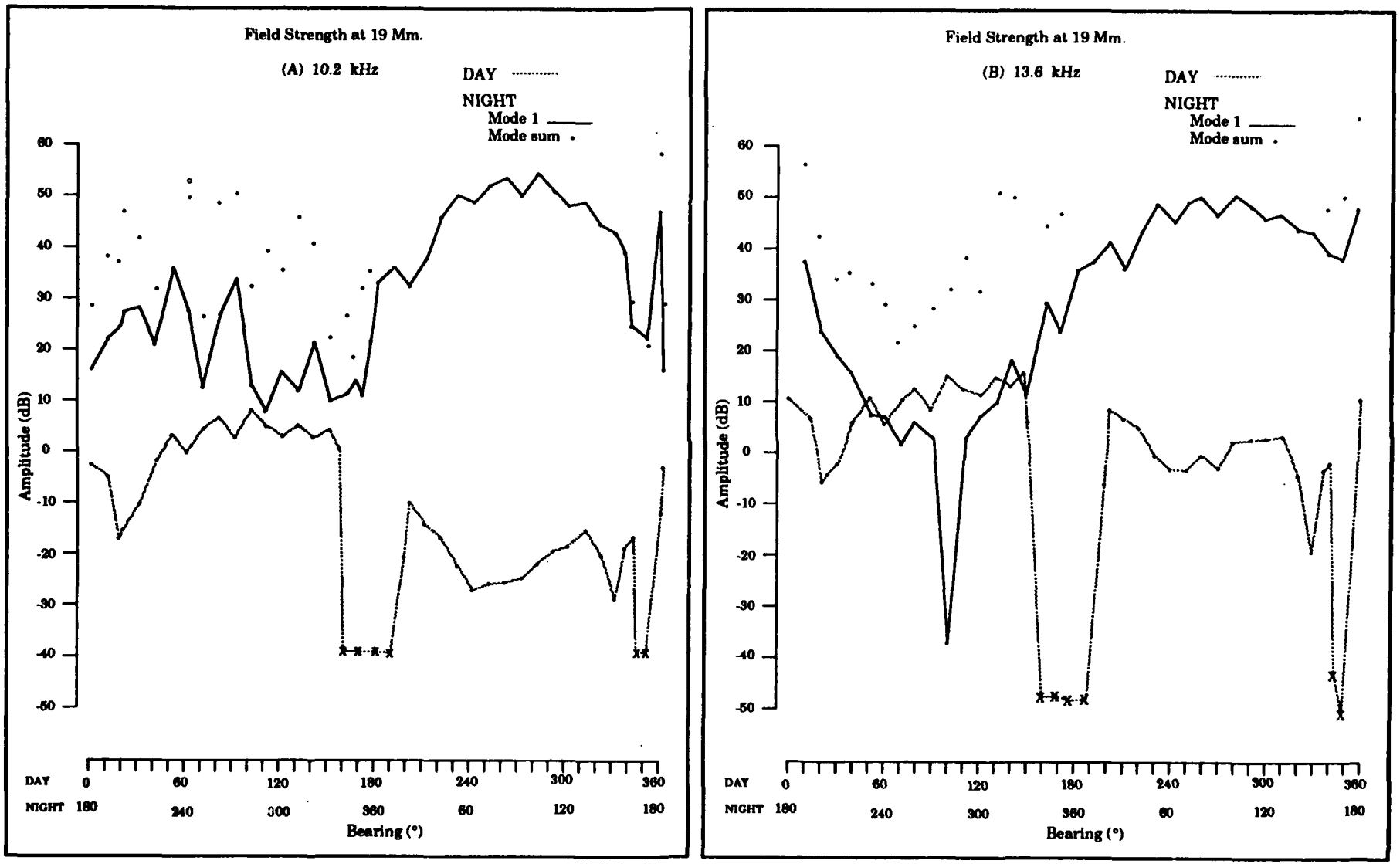

Figure C-3. Predicted Liberia Signal Levels

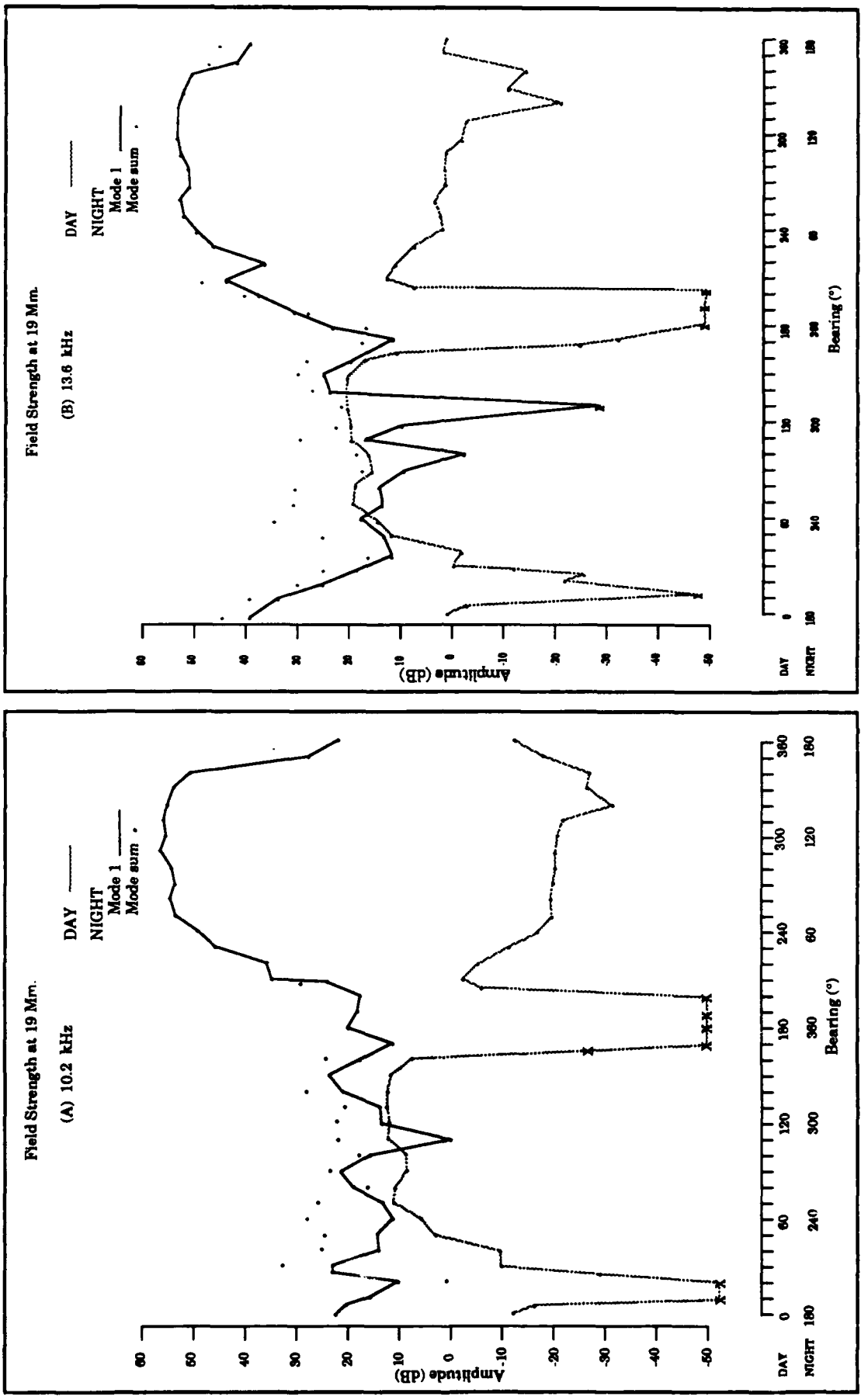

Figure C-4. Predicted Hawaii Signal Levels.

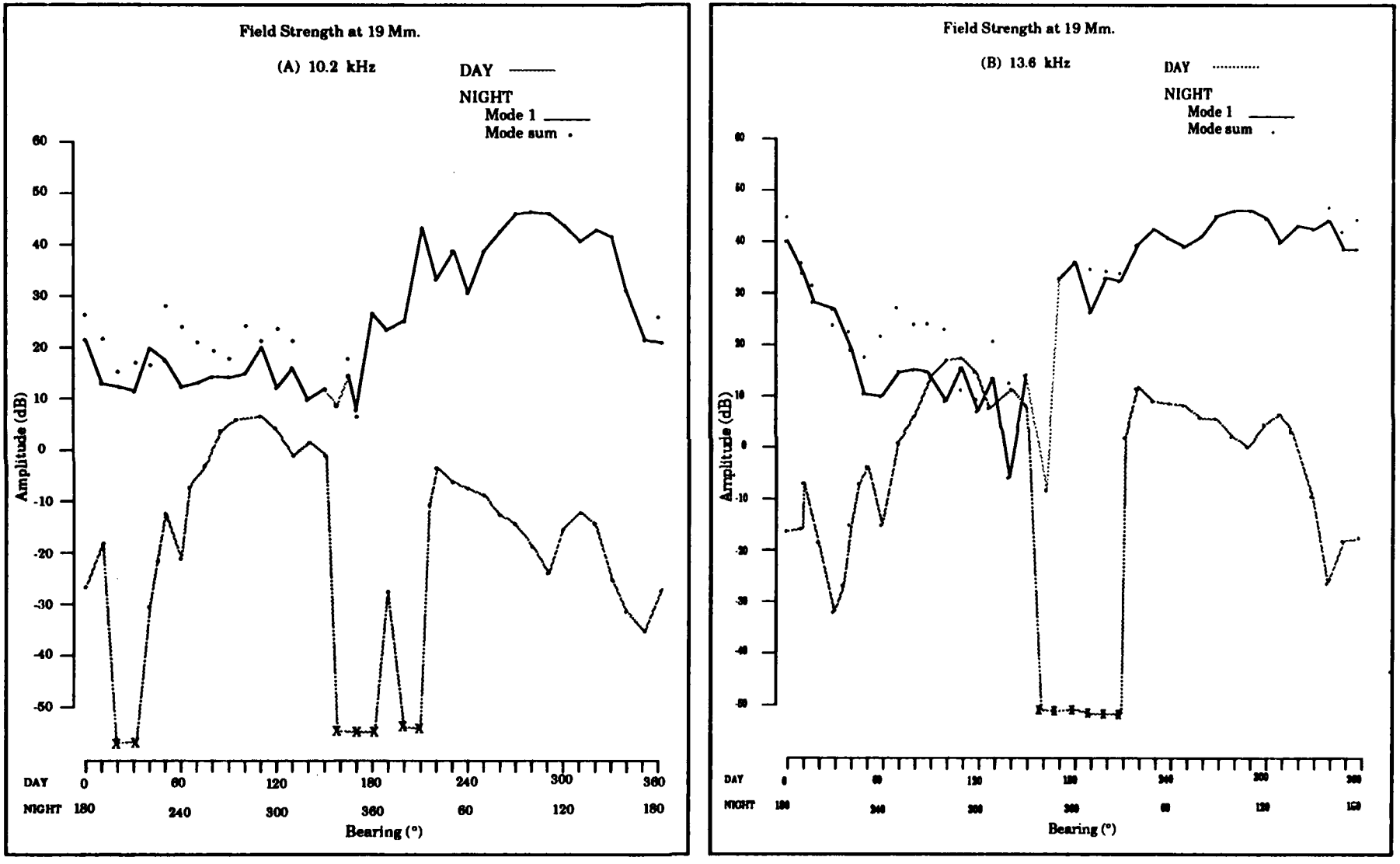

Figure C-5. Predicted North Dakota Signal Levels.

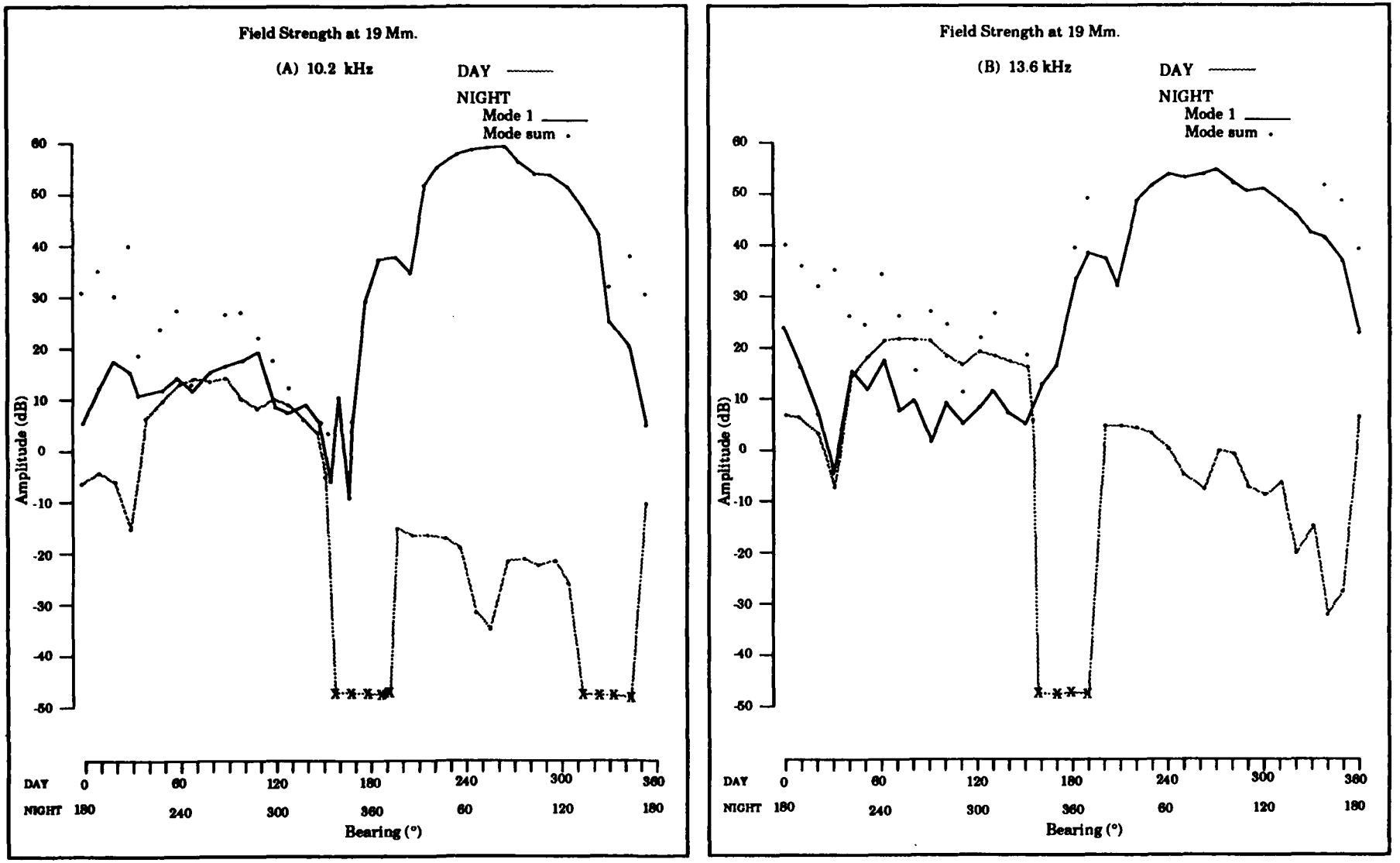

Figure C-6. Predicted La Reunion Signal Levels.

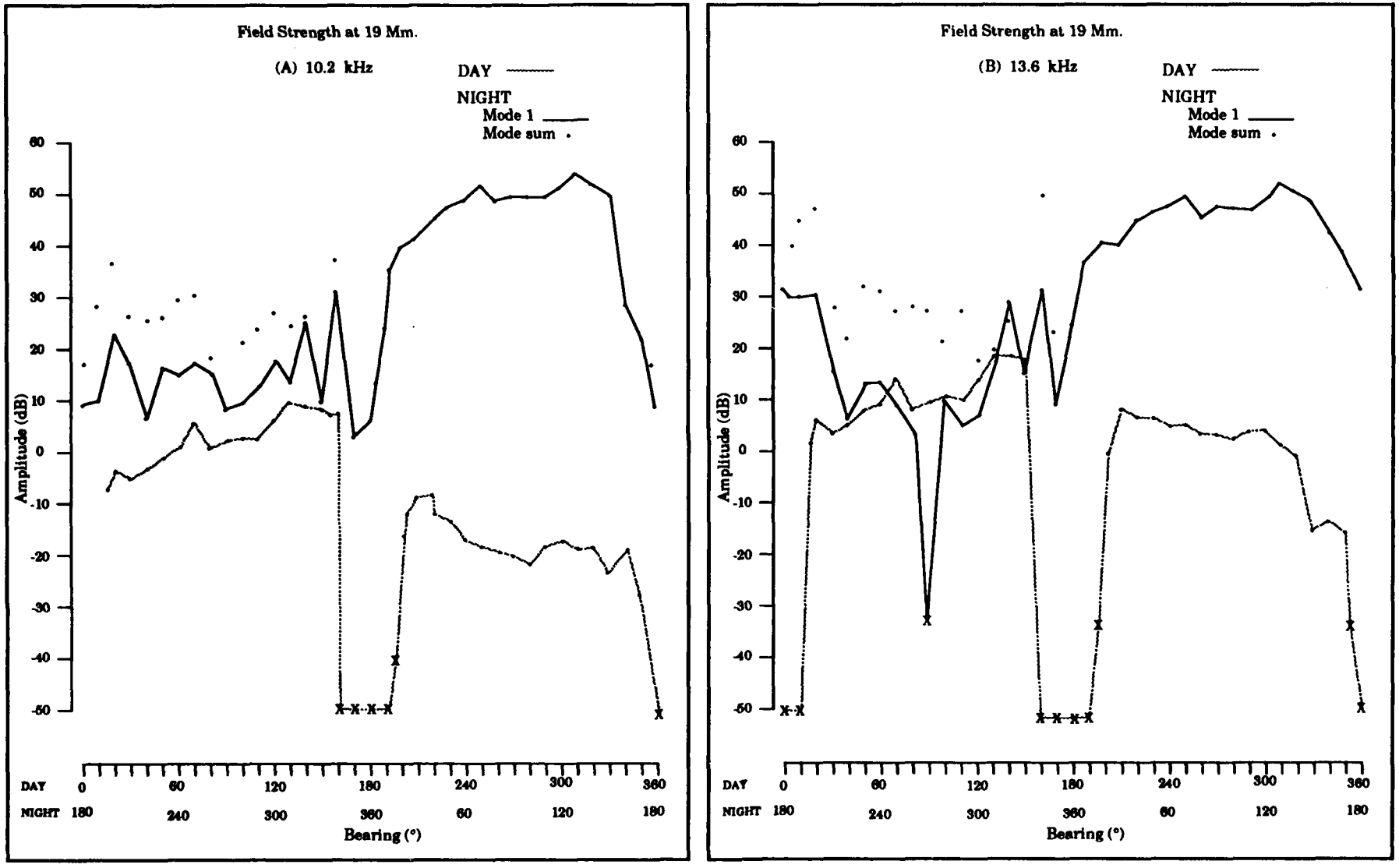

Figure C-7. Predicted Argentina Signal Level.

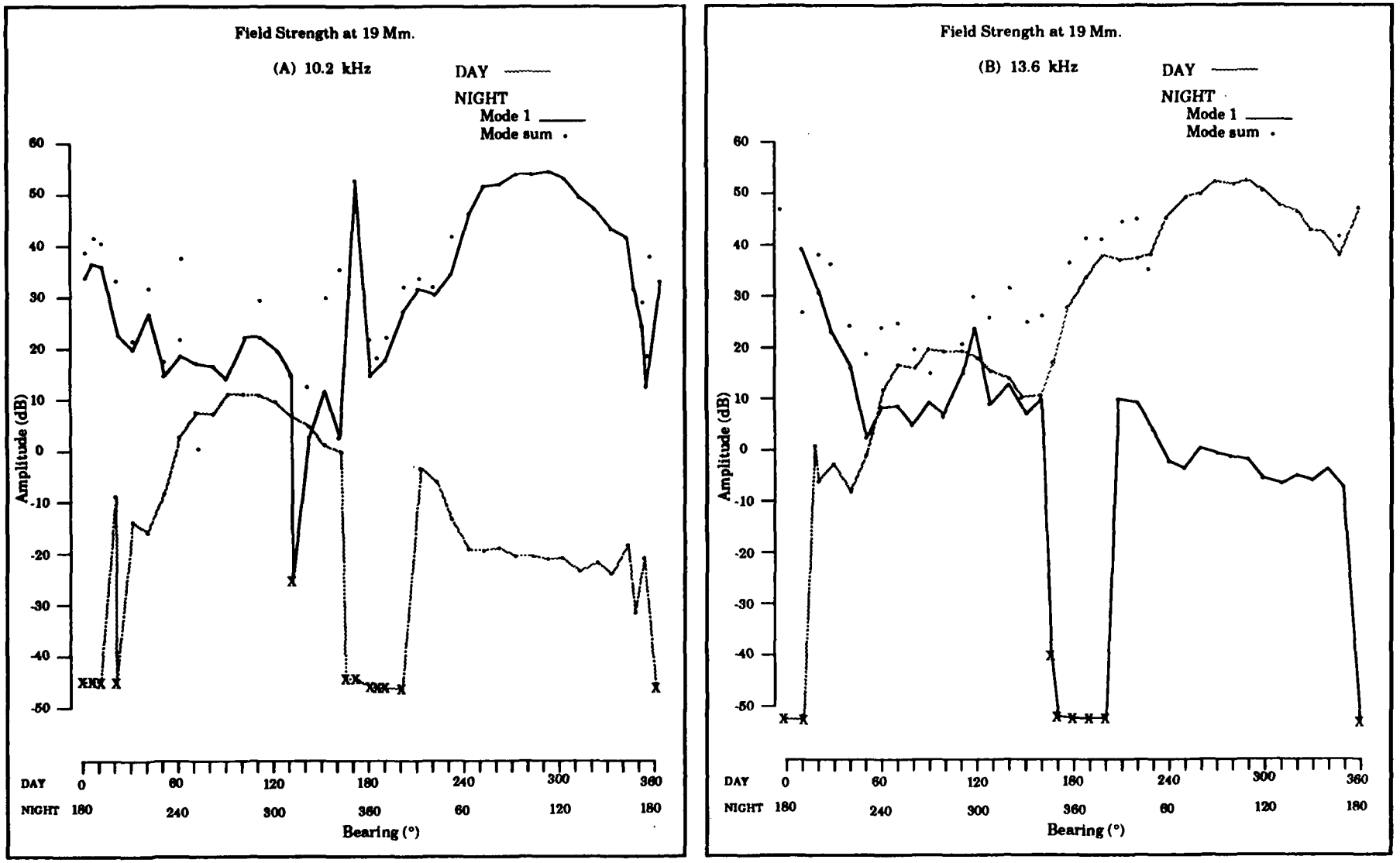

Figure C-8. Predicted Australia Signal Levels.

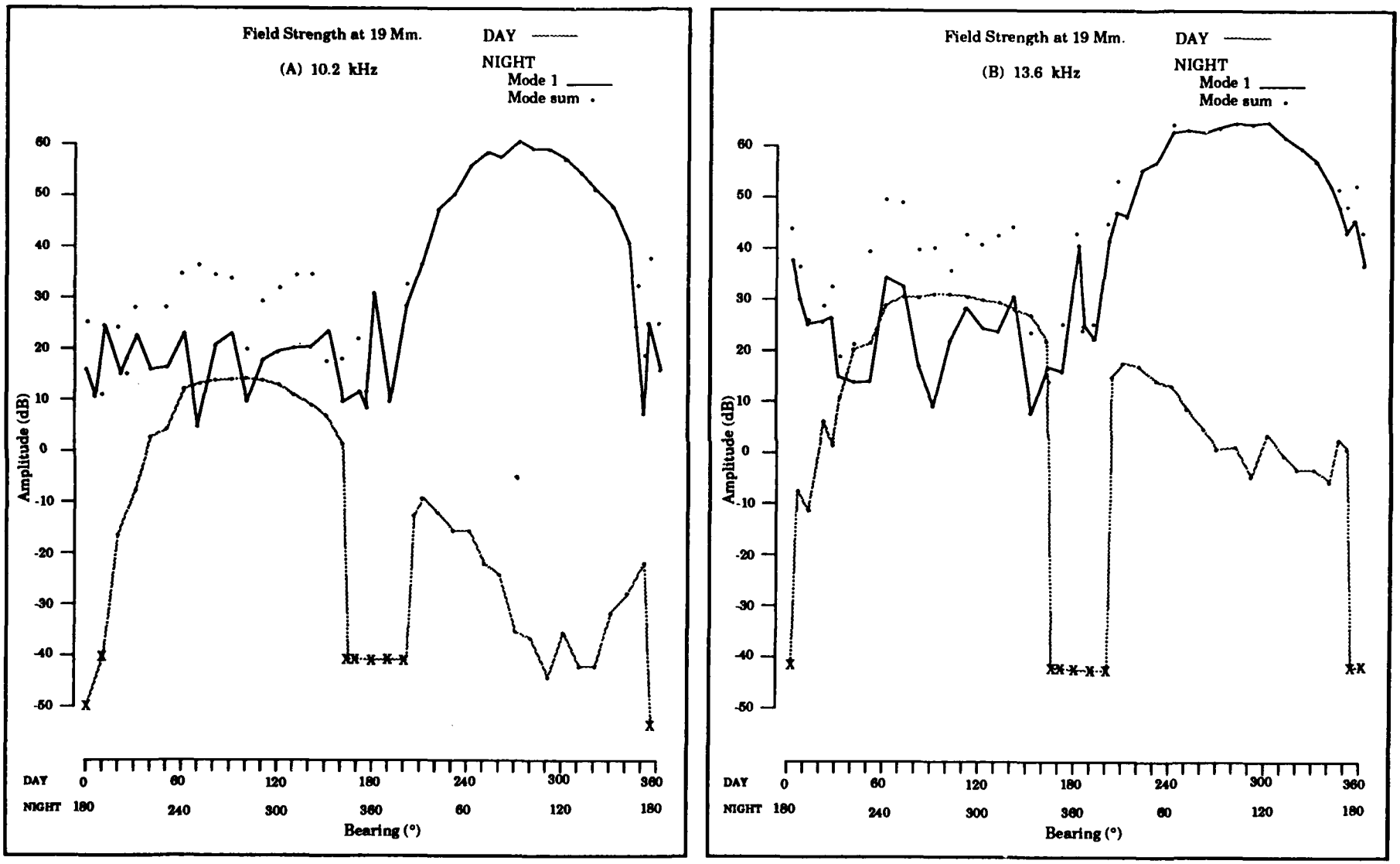

Figure C-9. Predicted Japan Signal Levels.

from opposite directions. The arrival angle at the antipode for each radial is 360° minus the plotted angle. For night propagation both total fields and mode 1 fields are plotted where their levels are significantly different. These plots show that:

(1) the field strength for all daytime propagation at 19 Mm is almost always less than or equal to the field strength for all nighttime propagation in the opposite direction,

(2) the signal propagating at nighttime in a broad sector, to the east of the transmitter (30° to 150° for Hawaii in Figure C-4a) arrives at the antipode with a much higher signal level than when propagating to the west,

(3) when a signal propagates over a low conductivity region during daytime (150° to 210° for Hawaii in Figure C-4a) the signal arriving at the antipode is much weaker than otherwise,

(4) the combined effects on propagation result in complex variations of field strength with bearing change, and

(5) the mode 1 level in propagation to the west at nighttime is often much lower than the total field, i.e. mode sum (For an example see Liberia Figure C-3 180° to 330°). The low level of mode 1 relative to the total field is often strongly associated with signals having incurred mode conversion in propagation through the equatorial zone.

The conditions depicted in Figures C-2 through C-9 are useful for determining if long-path interference is likely to occur and along what radials. These plots also show how the maximum extent of the long-path/short-path boundary will change with radial bearing and frequency. The actual determination of the boundary position was done by extending the propagation calculations produced by TASC using the following technique.

Since creation of a computational model was not considered practical within the time and resource constraints of this validation, a first order model for determining long-path/short-path boundaries was devised from the TASC field strength calculations previously described. The technique involves extending the field strength predictions beyond the 19 Mm by attaching "mirrored" segments of calculations that represent the predicted propagation conditions. An example is shown in Figure C-10. The process consists of three operations:

First, the signal levels versus distance for propagation in opposite directions and for both day and night are plotted. The plot is created by figuratively breaking the great circle path at the transmitter and transforming the circle to a straight line so that the transmitter is located at both ends of the plot. The antipode, 20 Mm from the transmitter is placed in the middle of the graph an equal distance from each representation of the source. This first or reference plot places the day/night terminator at the transmitter and the antipode. Each of the paths is either in all daylight or all night.

Second, the paths are extended in either direction beyond the antipode by joining appropriate segments of the propagation curves. For example, (as shown in Figure C-10), the nighttime propagation curve on the 80° radial is extended beyond 20 Mm using the slope and shape of the nighttime curve inside 20 Mm.

Third, "real" propagation situations are represented by joining appropriate segments of day or night propagation curves at the distance where the terminator intersects the propagation paths. An example of the terminator crossing about 12 Mm from the transmitter is shown in Figure C-10. Another example shows the day propagation curve attached to the end, 20 Mm, of the nighttime eastward propagation curve. The intersection of this daytime extension with the curve of daytime propagation along the 260° radial establishes the long-path/short-path boundary for the time when the terminator crosses the transmitter and the antipode. The positions of crossover for the dominant fields that are propagating in opposite

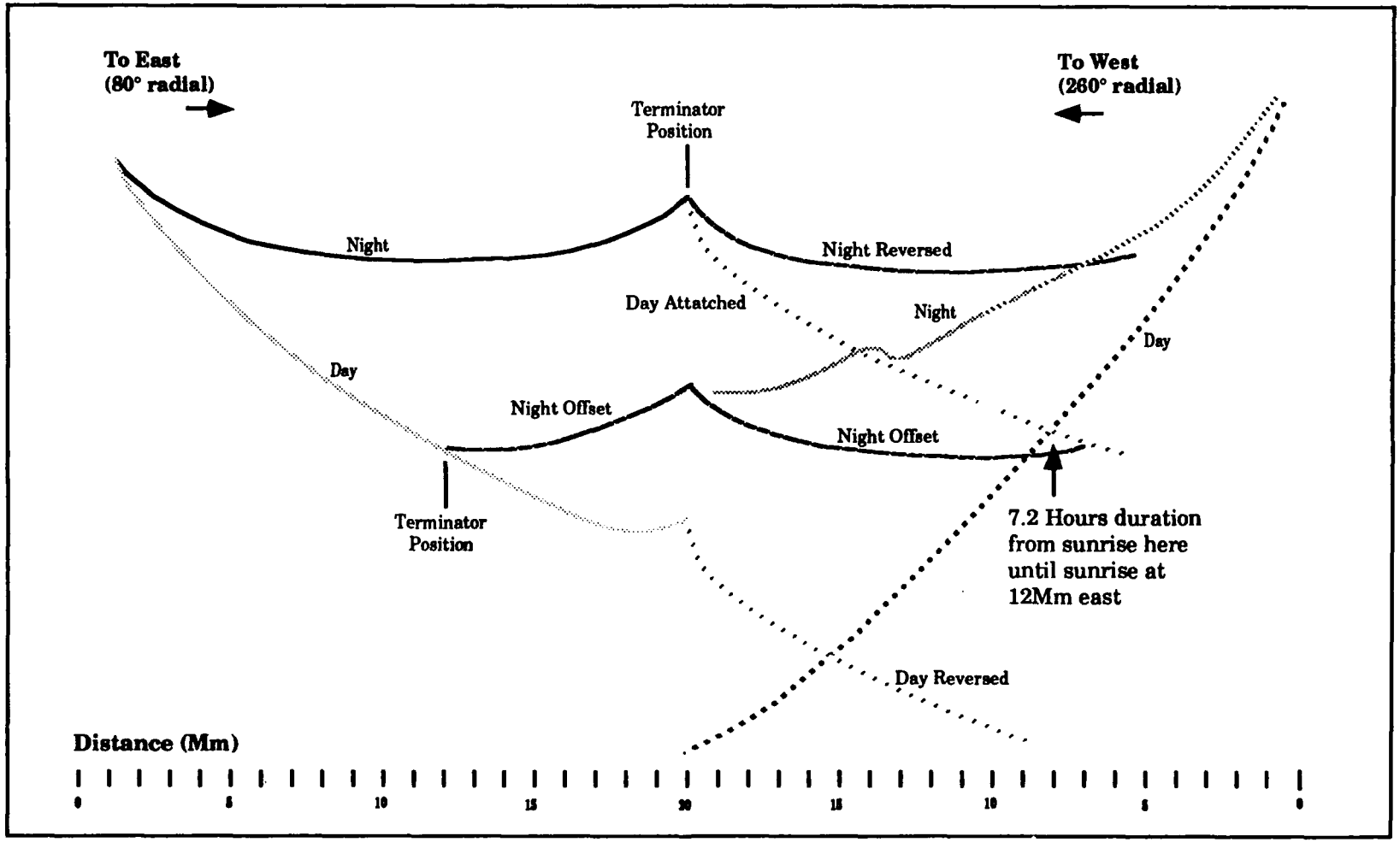

Figure C-10. Sample Long-path Propagation Construction

directions (i.e. long-path/short-path boundaries) are obtained for representative solar positions. The variation in position along a radial establishes the time history of the boundary location. A set of these positions for different radials establishes the geographic boundaries.

When a daytime segment is attached to a nighttime segment, the attachment is made to the mode 1 component of the nighttime signal when this field differs significantly from the mode sum. The mode 1 component is joined because this component is expected to be the primary source for the daylight path. The higher ordered modes are rapidly attenuated in the daylight side of the terminator. The procedure used does not account for mode conversion across the terminator. We do not know the errors that can be incurred by not accounting for mode conversion. The best way to assess errors will be to compare the derived predictions with measurements of both modal boundaries and of times when boundaries cross measurement sites.

Geographic plots showing the maximum extent of the long-path/short-path boundaries at 10.2 kHz on 22 February are presented in Figures C-11 through C-15 for each of the stations having a boundary in or near the South Pacific validation region. The general shape shown in these boundaries is more significant than the shape detail because the construction was generated using data from relatively few radials. More insights regarding the boundary shape between the radials used can be derived from examination of the relevant figure of Figures C-2 through C-9. The following comments apply in a general way to all Omega frequencies. As the Omega frequency increases, some effects will be more pronounced and others less so. For example, the long-path/short-path boundaries at 13.6 kHz will lie inside the 10.2 kHz boundaries, ie. towards the antipode.

A general feature of the prediction is that the greatest extent of a boundary from the antipode occurs when the short path to the boundary is in total daylight. The boundary reaches this greatest extent on any given radial approximately when the sunrise terminator reaches the same location and remains there until approximately sunset over the transmitter. Thus, the

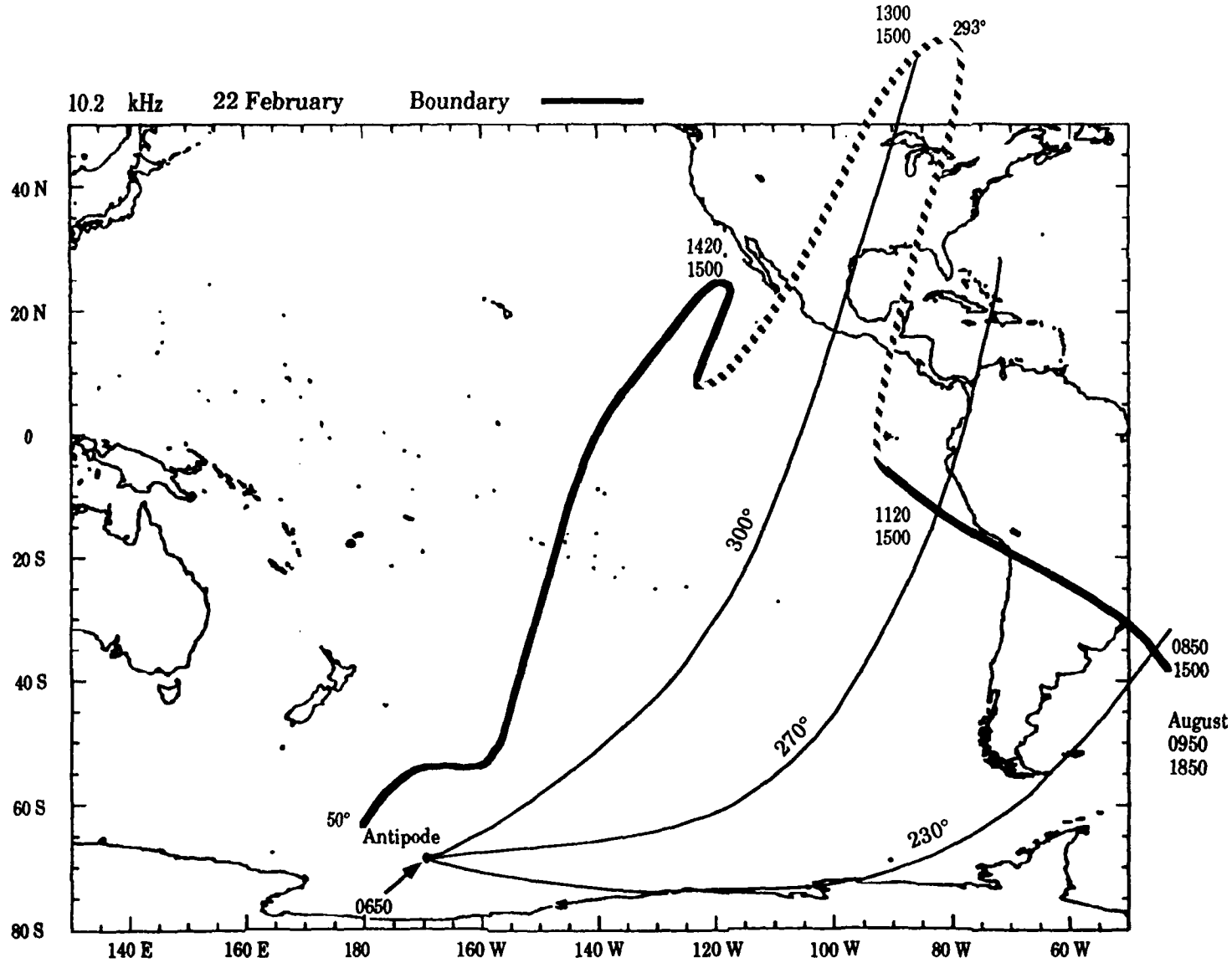

Figure C-11. Norway Signal Long-path Maximum Extent

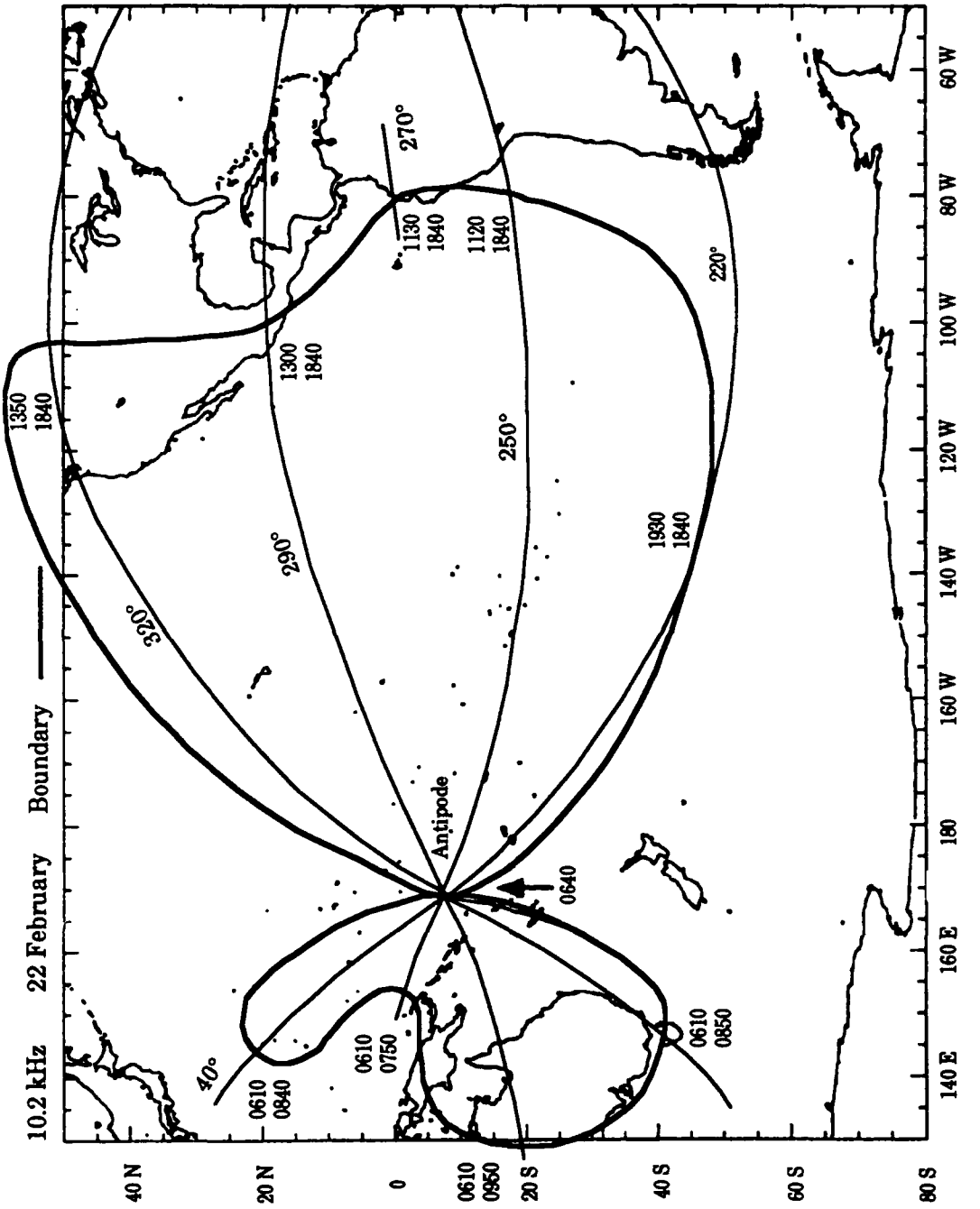

Figure C-12. Liberia Signal Long-path Maximum Extent

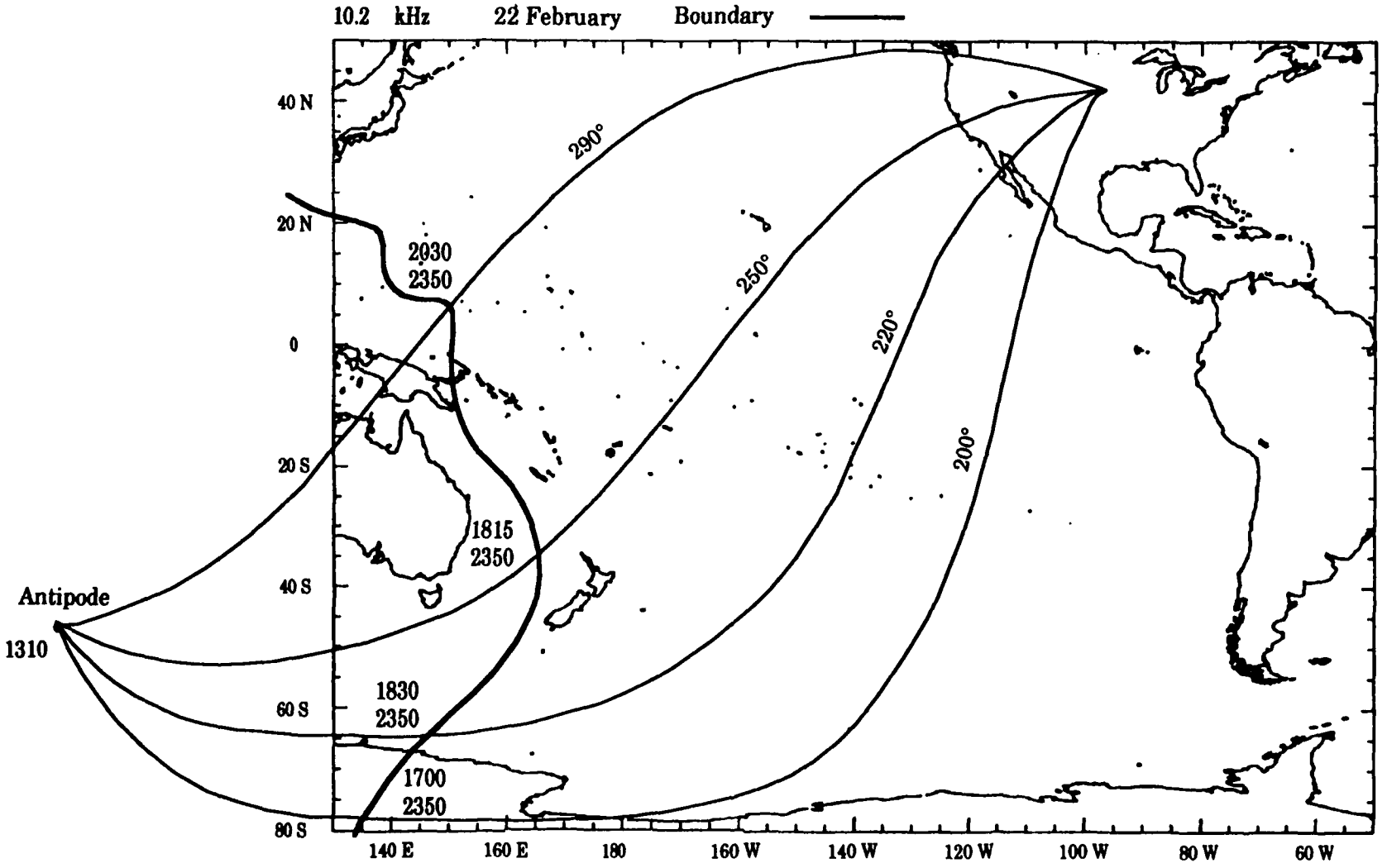

Figure C-13. North Dakota Signal Long-path Maximum Extent

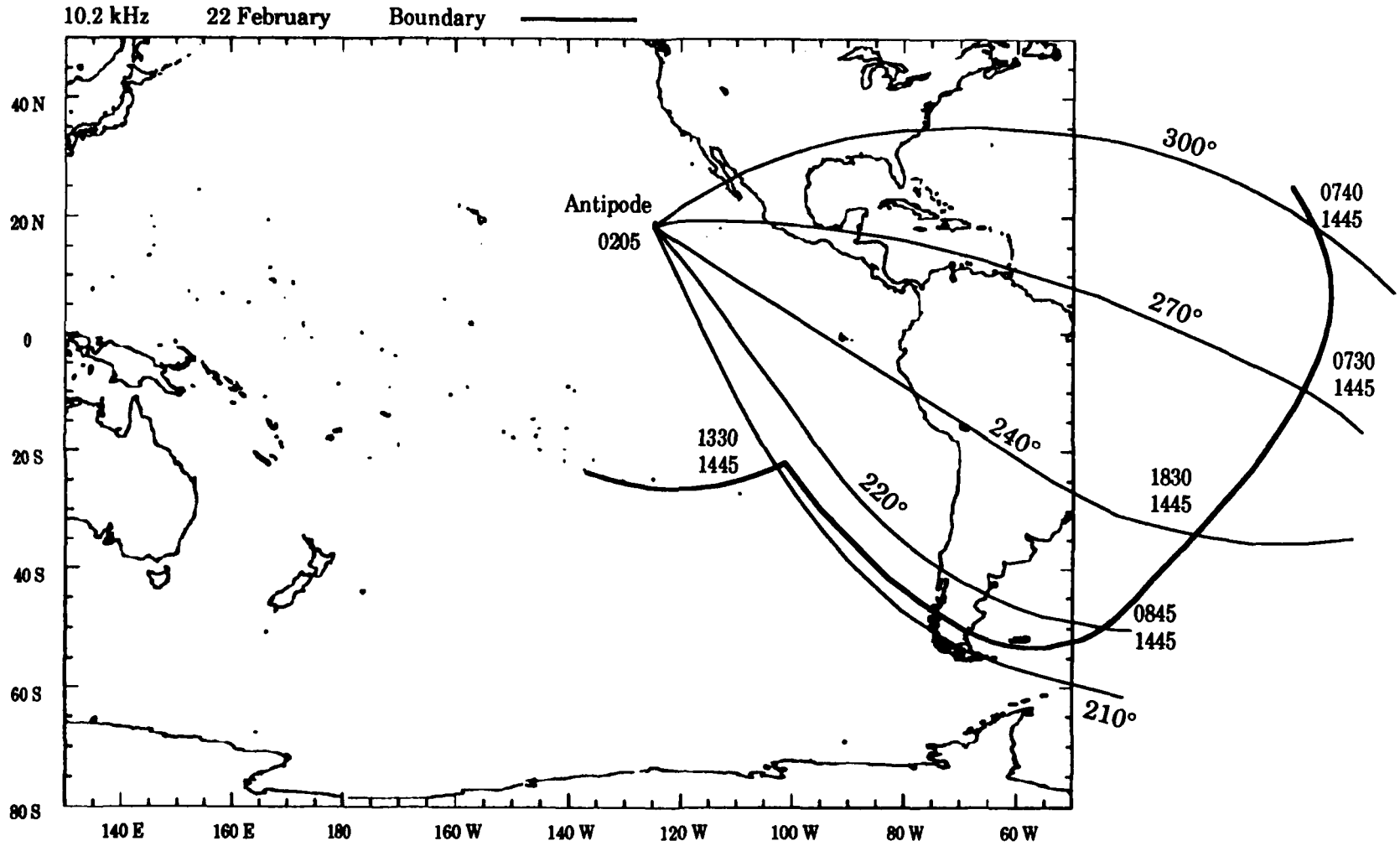

Figure C-14. La Reunion Signal Long-path Maximum Extent

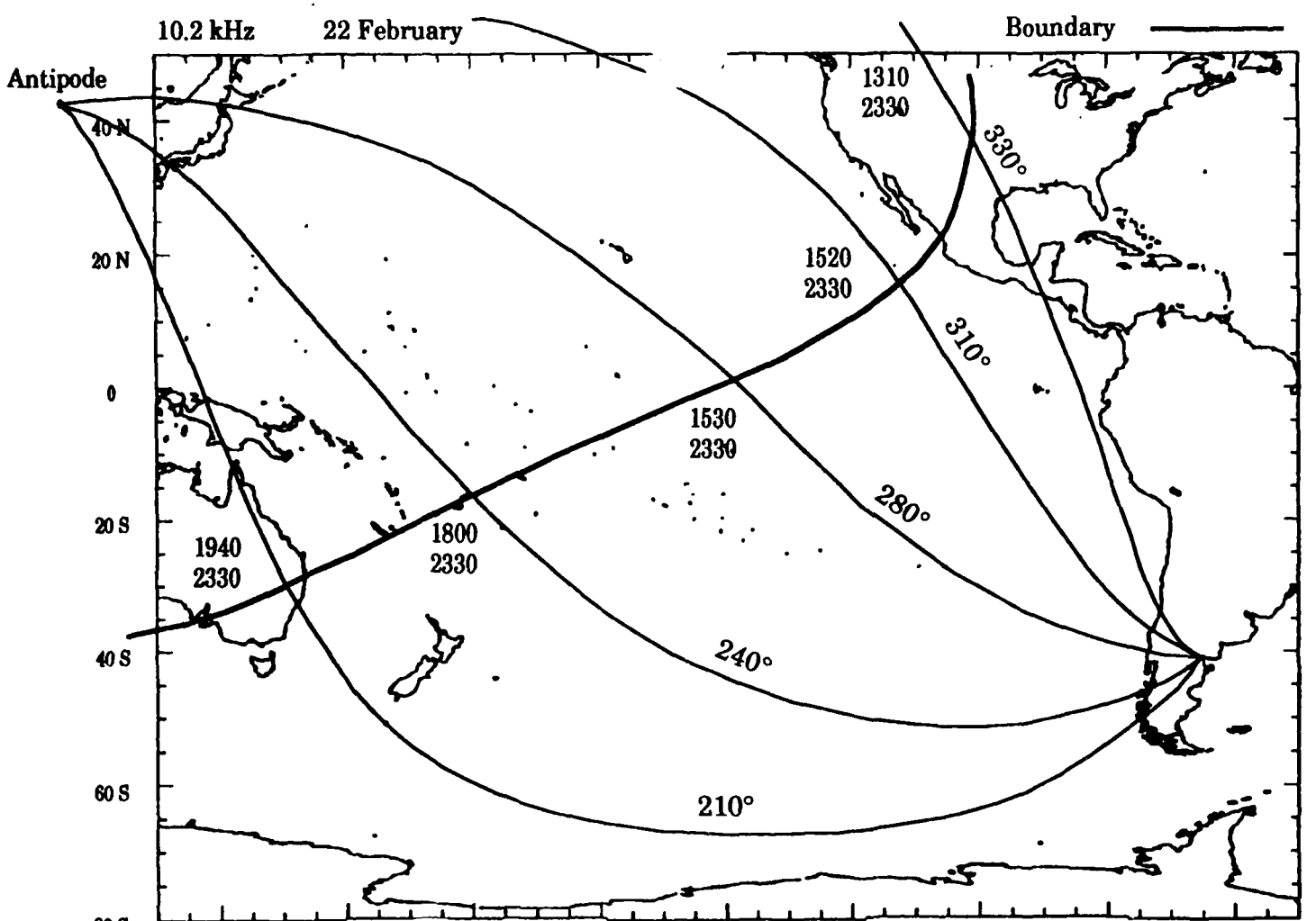

Figure C-15. Argentina Signal Long-path Maximum Extent

further away from the antipode that the boundary moves the longer it remains at its farthest extent. The time difference with longitude is illustrated in Figure C-11 for the Norway 10.2 kHz signal where the dwell time on the 230° radial is from 0850 to 1500 GMT, 6+ hours, and on the 330° radial, is from 1420 to 1500 GMT, 40 minutes. These times will change with season. The westernmost extent of the boundary seldom goes much beyond the broad area typically defined as the antipode zone. The boundary dwell time at this western end is usually quite short, from a few minutes to an hour or so. The rate at which the boundary moves along a radial increases as the angle the terminator forms with a radial decreases. The rate is slowest when the terminator is nearly parallel to the equator and can be very high (almost instantaneous in time) over many megameters in those rare situations when the terminator is nearly parallel to the radial for some distance. As a rarely occurring example, Figure C-16 shows a terminator situation where the entire length of the propagation paths from the transmitter to the antipode on the 255°/75° radials from Norway undergo a switch from night to day and vice versa in a matter of minutes. The 255° radial extends just south of Arequipa, which lies on a 258.4° radial from Norway.

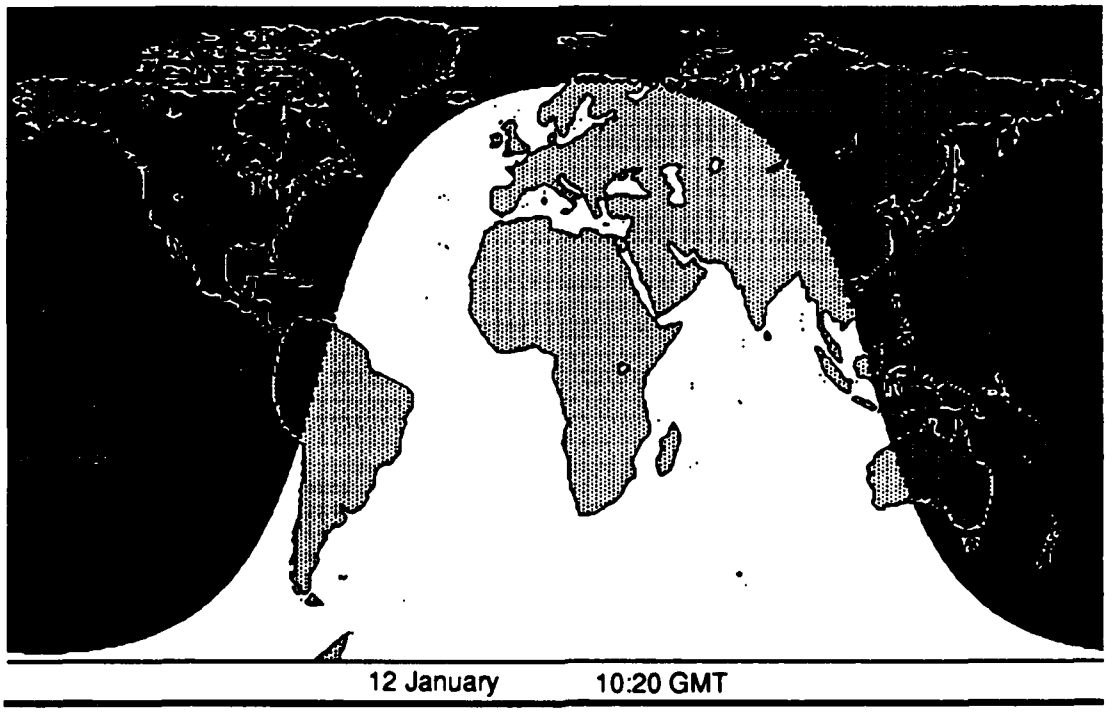

Figure C-16. Propagation Path Along Terminator

A great deal of uncertainty is associated with predicting the boundary location when the terminator intersects the radial within a mode conversion zone, as occurs on many westward paths. This is because the data analysis shows the mode conversion effects, and therefore the level of mode 1, to be highly ionosphere parameter dependent. An example of a very rapid change in mode 1 amplitude with distance is shown in Figure C-17. In this figure the mode 1 component is predicted to decrease by 23 dB in a propagation distance of 2.2 Mm. While ionosphere conditions are expected to be different at sunrise or sunset, a similar situation but quite different in detail is probable. The resultant signal level, obtained by mating the day and night segments over this distance interval (10.8 to 13 Mm), is expected to have a high prediction uncertainty. Such uncertainty makes placement of the boundaries to the west of the antipodes suspect.

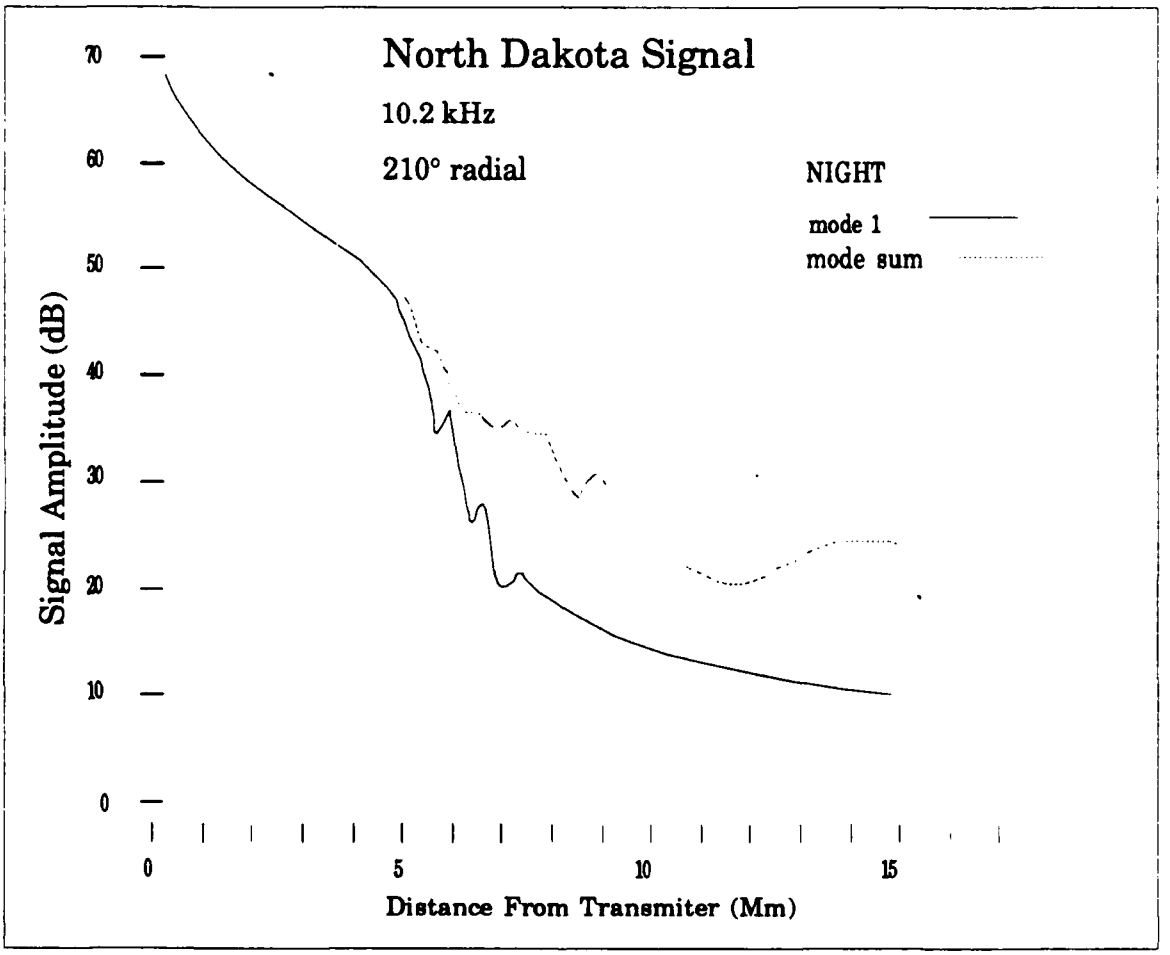

Figure C-17. Sample of Modal Propagation

Specific comments regarding analysis results for each figure are as follows:

Norway: As shown in Figure C-11, the TASC model of propagation across the arctic in daylight creates a complex boundary that at its greatest extension from the antipode is predicted to extend well north of the Great Lakes. The boundary shown is for the special conditions of arctic daylight and antarctic night and includes ground conductivity parameters that are not fully validated. The segment of boundary shown as a dashed line is considered questionable and needs evaluation. The transition time of boundary movement along the radials is very different between the two terminator transits. For example, on the 230° radial in February, this time interval is two hours for the sunrise transition and 15 hours 20 minutes for the sunset transition. In August, for the 230° radial, the time interval when the boundary is the farthest east is from 0950 to 1850 GMT. The westernmost boundary occurs at about 0250 GMT. The transition times between these two locations are seven and eight hours respectively for the sunrise and sunset transitions.

Liberia: The propagation at low latitudes incurs a strong nonreciprocal west/east and day/night effect. The Liberia signal long-path/short-path boundary, Figure C-12, extends as much as 12.8 Mm to the east of the Antipode. The boundary on the 250° radial is at its easternmost position between 1120 and 1840 GMT on February 22, a period over seven hours. This boundary location results, as shown in Figure C-3a, from a combination of the maximum eastward propagating signal strength and a relatively weak westward propagating signal. The 13.6 kHz signal does not incur as much attenuation difference, 54 versus 78 dB, as is noted by comparing the curves of Figures C-3a and C-3b. Thus the 13.6 kHz boundary will be to the west of the 10.2 kHz boundary. Of all the signals, the Liberia signal showed the farthest boundary movement to the west of the antipode. The position of this boundary is expected to be quite sensitive to the relative composition of day and night components. If

the portion of the long path to the west of the antipode is in nighttime, the boundary should lie farther west than depicted in Figure C-12.

Hawaii: A figure for Hawaii is not presented since the long-path effects do not extend into the south Pacific validation region. The easternmost extent of the boundary is near 110° East. The 290° radial intersects this meridian at about 20°N Latitude.

North Dakota: As shown in Figure C-13, the predicted eastern extension of the long-path/short-path boundary just enters the validation region in the southwest corner. The easternmost part of this boundary is just west of New Zealand. The boundary is at this location for almost six hours, from about 1800 to near 2400 GMT. The boundary for the 13.6 kHz signal may just reach the western edge of the map at its easternmost excursion. The field strength curves, Figure C-5 A & B, show that the shape of the boundary would be quite complex.

La Reunion: The La Reunion boundary, Figure C-14, can extend as far east as the west coast of Africa. On the 270° radial, the easternmost position occurs from about 0730 to 1445 GMT, an interval of about seven hours. The boundary would reach its westernmost extent around 0200 GMT. On the 260° radial the boundary is predicted to move across Panama going east at about 0400 GMT, and going west at about 2130 GMT. On the 240° radial the boundary is predicted to move across Arequipa going east at about 0600 GMT and going west at about 1900 GMT. The long-path boundary is predicted to remain just north of Easter Island.

Argentina: As shown in Figure C-15, the 10.2 kHz long-path/short-path boundary at its easternmost extent makes a broad diagonal sweep across the validation zone from just south of Brisbane, through Samoa, to the west coast of Mexico at about 20°N. The dwell time at the easternmost extent is predicted to vary with radial from four hours near Brisbane to about ten hours in the central United States.

Australia: A figure is not presented for Australia since the long-path/short-path boundary is predicted always to be east of the validation region. Any long-path effect in the validation region would be produced from the signals in the 110° to 160° day bearing sector shown in Figure C-8 (A & B). In this sector, the night long-path signal is generally within 10 dB of the day short-path signal.

Japan: A figure is not presented for Japan. The long-path/short-path boundary for Japan is predicted to always be east of the validation region. Any long-path effect in the validation region would be produced from the signals in the 60° to 120° day bearing sector shown in Figure C-9 (a&b). Within this sector the opposing signal amplitudes are close together.

Model Assessment: We feel that this analysis technique provides a good start for assessing/validating long-path effects. This is a model that needs calibration with additional measurements and could benefit from calculations beyond 20 Mm propagation distance. The models validity will be largely determined through experience gained in its use.

During discussions of this long-path analysis Eric Swanson of NOSC brought our attention to a similar analysis he had conducted (Swanson, E. 1976, Ref. 24) which was a case study of Omega coverage in India. For this study he used full-wave calculations out to radial distances of 40 Mm on paths from each Omega transmitter through the India receiving site. These calculations were for (1) both directions on each great circle path, (2) all day and all night on each path, and (3) the mode sum, i.e. total field. We contend that his calculations lend strong support to our method, noting some important differences. The two most important differences, other than location, are accounting for earth conductivity and for the day/night mix on the propagation paths.

Swanson's calculations used the predicted earth conductivity along the path. We applied the attenuation rate of the calculations which was before the antipode to the path extension beyond the antipode. Where the extended

path covered terrain differing from the calculated path we estimated an adjustment to the attenuation rate. Since most paths were similar in terrain, often sea water, we feel that the resulting error is not great and is certainly adjustable through calibration from measurements. Further, in Swanson's calculations where terrain on both sides of the antipode have similar conductivities, the resulting plots are very similar to ours.

The composite plots of nighttime field strength used be Swanson show that modal interaction often is very strong well beyond the antipode. Thus his plots include several modes contributing significantly to the total field. Swanson, having a different goal, did not specifically construct mixed day/night paths similar to our analysis. Thus, direct comparison is not appropriate. Since our prediction was for the location of the boundary at the end of the long-path as contrasted to signal details along the path, we used the assumption that any significant daylight on the total long path would make the contribution of any higher-ordered modes negligible. For this reason our nighttime plots are of the first mode. This assumption needs to be tested.

Appendix D

Long-Path/Short-Path Effects Data Analysis

OVERVIEW:

In this appendix fixed site data is evaluated for evidence of long-path/short-path interference effects and is compared with the predictions derived in Appendix C. The primary evidence on fixed site data for existence of long-path signals within the short-path region, is a reversal from normal of the diurnal pattern of phase. For example, the phase changes as if transitioning from a day to night propagation during a time interval when normally either no phase change or a night to day transition would occur. Also, the long-path signal can have a very different phase than the short-path signal. If it does, the emerging long path can cause the received phase to change in an unpredictable manner. The observed phase change should not occur if only the short-path signal is received.

DATA INTERPRETATION:

The following material describes the analysis conducted on fixed site data to test for long-path effects:

Norway: The Norway signals are expected to exhibit long-path effects in the southeastern portion of the validation zone. As noted in Figure C-11 the Arequipa and Tahiti monitoring sites are located right at the edge of the predicted boundary that indicates the farthest extension from the antipode. The analysis results of the Norway signals are as follows:

> **Arequipa:** The Norway channel was used for monitor calibration. No signal data was acquired.
>
> **Easter Island:** No data was processed. It is assumed that the "A" channel was used for monitor calibration.
>
> **Tahiti:** The propagation path to Tahiti is very complex. The first portion of the propagation path is polar, which for the February period is almost

always in darkness. The furthest extension of the long-path signal depicted in the model probably does not occur because of the nighttime propagation conditions prevailing on this arctic portion of the path. The data shows a very rapid sunrise transition that coincides with the terminator rapidly crossing the propagation path on the segment traversing from the Canadian northern coastline to Tahiti. Any possible long-path effects are masked in this rapid transition. We conclude that, at least for February, the long-path boundary did not reach Tahiti.

Norway Discussion: The prediction of the Norway boundary for maximum long-path extent could not be confirmed with the limited analysis conducted. This analysis is not considered an adequate test of the boundary prediction. The complex phase transition at sunrise, which is peculiar to the season, is a good example of the need to include season effects in predictions.

Liberia: The maximum extent of the eastern long-path boundary is predicted to cover the validation region north of a line that runs from the antipode approximately to the southeast corner of the region and out to the western coastline of South America. The prediction shows that both the Panama and Arequipa monitoring sites are just outside of this boundary. The Easter Island and Tahiti monitoring sites are predicted well inside of this maximum extent boundary. The analysis results of the Liberia signals are as follows:

Arequipa: The Liberia signals at Arequipa exhibit very strong evidence of long-path effects. The phase records, which are complicated by nighttime propagation modal effects, vary greatly from day to day. A sample data set is shown in Figure D-1 for 12 February 1985, along with a scale showing propagation conditions on the short-path. The short path is an all dark path from 0000 GMT to 0630 GMT. This time period often shows short-path multi-mode effects. The night portion of the long-path is being reduced at the station end and increased at the receiver end. Sunrise on the short-path begins near 0630 GMT at which time the phase should begin to decease (move down on the chart). In Figure D-1 the phase change is flat at 10.2 kHz and moving upward at 11.3 and 13.6 kHz. This phase change characteristic could be due to modal effects, but if so the daytime phase characteristic would be evident after 1000 GMT. Rather, all frequencies

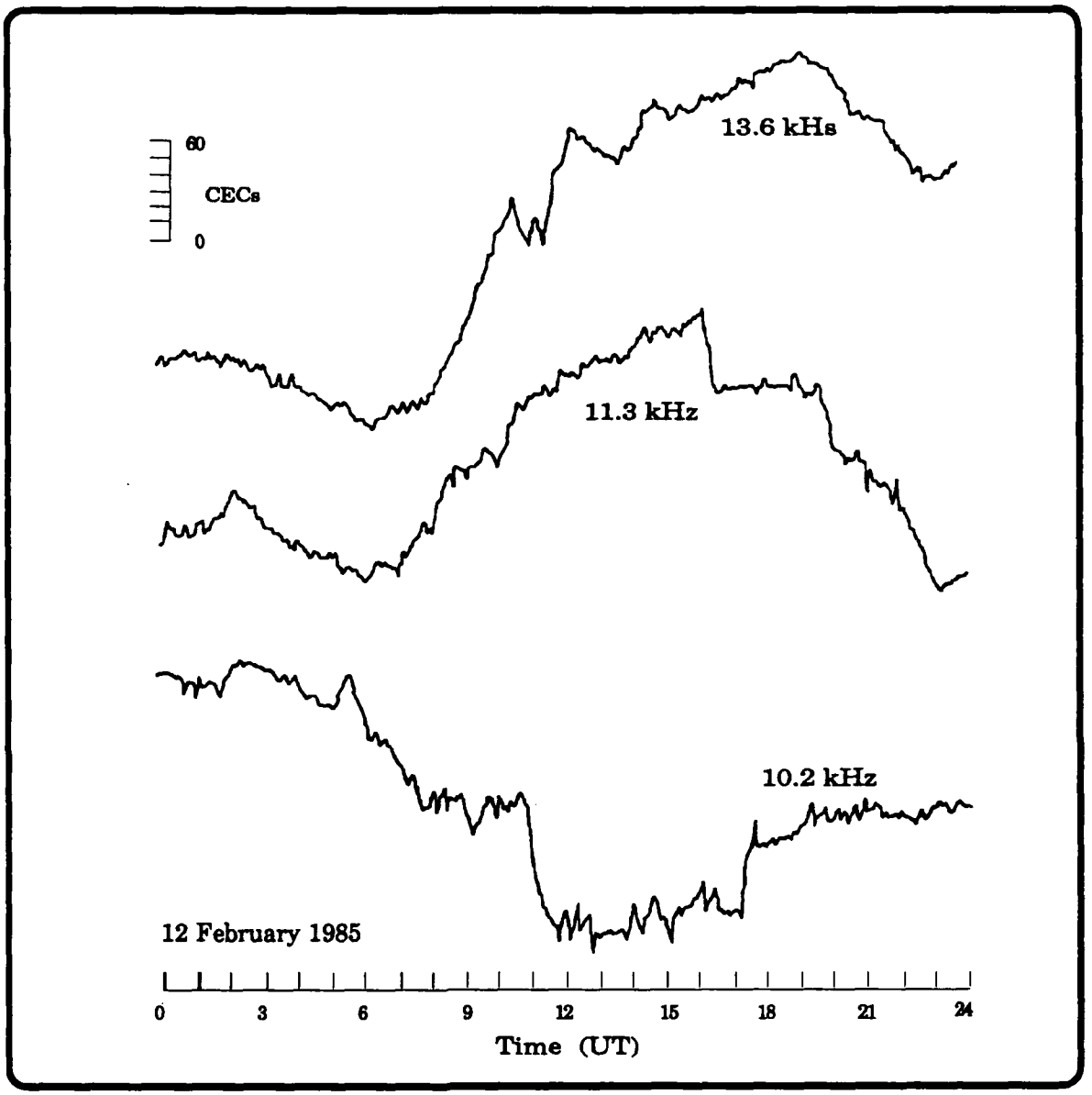

Figure D-1. Liberia Signal Phase at Arequipa

exhibit phase characteristics that are not normal for a dominant daytime short-path. This sample is representative of many data records for this site. The short-path sunset should begin about 1840. This is the time of phase change reversal at 11.3 and 13.6 kHz, but the direction of change is wrong. The phase moves in the direction of a sunrise transition. The 10.2 kHz phase does not follow. The relationship of the long-path and short-path phase at a fixed site would be very sensitive to propagation conditions and site position. Thus the different pattern between 10.2 kHz and the other frequencies may be expected. The large diurnal phase change occuring at 11.3 and 13.6 kHz is consistent with that expected for the long-path. At 2315 the short-path again seems to dominate at 11.3 and 13.6 kHz as evidenced by the phase pattern moving in the direction of the sunset transition in the short path. With few exceptions the 11.3 and 13.6 kHz signals have a similar diurnal pattern over the three-month interval analyzed. The onset of recognizable long-path dominance varies randomly over about an hour interval. The 10.2 kHz signal phase pattern is very inconsistent from day to day and seldom shows any trends associated with the terminator movement.

Easter Island: The Liberia phase records have a pattern that is consistent with long-path reception occurring most of the 24-hour period. Clear evidence of path switching was not detected. The diurnal phase pattern for day and night conditions was generally strong on all three frequencies. Cycle jumps frequently occurred at sunrise over Easter Island, often at all three frequencies.

Liberia Discussion: Our interpretation of the data is that the long-path boundary definitely passes through Arequipa. The transition to long-path occurs near 0630 and 2300. These times are 4.5 hours before and 4 hours after the predicted times, and coincide with the beginning and end of any sunlight in the short-path. These times of boundary crossing suggest that the boundary maximum extent lies considerably east of Arequipa at least for the 11.3 and 13.6 kHz frequencies. The calculations predict the largest propagation attenuation difference, east vs. west, at 10.2 kHz. For this reason we would conclude that the 10.2 kHz maximum extent boundary is also east of Arequipa. As an added note, the time interval between

boundary crossings is very close to that observed for the La Reunion signal. The La Reunion signal long-path boundary is predicted to move almost to the western coast of Africa.

Hawaii: No evidence of long-path effects as expected or detected in the data.

North Dakota: The long-path boundary at maximum eastward extent for North Dakota is predicted to penetrate into the western edge of the validation region almost to New Zealand. Only the Wellington data was examined.

Wellington: The North Dakota signals at Wellington are weak and they contain multi-mode effects from propagation on the short-path through the equatorial zone. The poor signal quality masks any possible evidence of long-path effects. In particular, the 10.2 kHz signal is usually very weak.

North Dakota Discussion: The exploration of long-path effects is more appropriately left to the forthcoming Western Pacific regional validation. The monitoring sites are better located to assess the boundary locations.

La Reunion: The long-path boundary at maximum eastward extent for La Reunion is predicted to penetrate well beyond the eastern edge of the validation region, extending almost to the most western edge of Africa.

Arequipa: The movement of the long-path boundary past Arequipa is very evident in the phase data. The time of boundary transition varies significantly from day to day. A typical time for first evidence of long-path is 0330 GMT, but onset can vary from 0300 to 0430. Transition of the boundary moving towards the antipode typically occurs near 1930, but can occur between 1800 and 2300. As with the Liberia signal, the long-path effects are much easier to detect in the 11.3 and 13.6 kHz signals as compared to the 10.2 kHz signal. The 10.2 kHz phase has a very inconsistent pattern, although the long-path boundary transition is occasionally quite marked. All frequencies have a complex phase pattern due to modal effects occuring during night and into transition times on the short-path.

La Reunion Discussion: The long-path boundary movement across Arequipa is consistent with the expected transition times from the

predicted location of the maximum boundary extent. The time interval between crossings of about 16 hours versus a predicted dwell time at the eastern extent of about six hours provides good evidence that the boundary moves quite far east from Arequipa.

Argentina: The maximum penetration of the long-path boundary into the validation region is predicted to extend from just south of Brisbane through Samoa and across to central Mexico. A quick look was taken at the Samoa phase data. The records included cycle jumps that occurred on quite a few days whose times were associated with possible long-path occurrence. However, the data requires additional processing to obtain a more definitive analysis.

Australia: The predictions place the western extent of the long-path boundary east of any of the monitoring sites used in this validation. The Arequipa data was examined to check for any possible long-path effects. No effects were detected. The Panama monitoring site should provide a better data set for testing the possible Japan long-path boundary.

Japan: The predictions place the western extent of the long-path boundary east of any of the monitoring sites used in this validation. The Arequipa data was examined to check for any possible long-path effects. No effects were detected.

General Discussion: Identifying long-path effects in the presence of other effects is very difficult using the monitoring site data. The prediction model seems reasonably consistent with observations of boundary transitions across sites. Some adjustments are definitely needed, the most obvious being to move the Liberia boundary significantly farther east. Much more analysis than was possible is needed to produce a useful test of long-path effects. Useful products of this model presentation and the associated data analysis are (1) to place a time history on the movement of the boundary between the extreme locations, (2) to illustrate the complexity of the boundary curve that results from variations in propagation attenuation with azimuth, and (3) to show the large changes in rate of boundary movement as the terminator orientation changes with season.

Appendix E

Navigation Fix Accuracy Assessment

OVERVIEW:

This navigation fix accuracy assessment is presented in three parts. The first part describes comparisons made between PPC calculations and measured phase at fixed sites. Illustrations are given of representative observed conditions. The first part assumes the reader is familiar with phase measurements and phase propagation corrections. The second part presents selected graphical examples comparing PPCs and measured phase. The examples are selected to illustrate observed trends in the data that we considered important to highlight. This second part serves to emphasize the findings of part one. The graphical presentation of this second part should be easier to follow by those not versed in the technical aspects of phase measurement. The third part extends the observations to the use of shipboard navigation data. The shipboard data proved particularly valuable in confirming many of the observations of part two at additional locations. The analysis of shipboard data served to illustrate that real-world navigation accuracy is consistent with that expected from fixed site phase accuracy determination.

PART I: ACCURACY ASSESSMENT DESCRIPTION

The objective for this phase of the validation analysis is to check the basic ability to derive a position fix from provided predictions. Our perspective is that of the navigator, who has to use the signals, associated correction aids, and auxiliary support as they exist at a time of a fix. We concentrate on the information content in the measured phase of each signal available for navigation. The signal processing aspects of the navigation fix process are more appropriately assessed on a laboratory bench. By concentrating on assessment of phase prediction, the complexity of interpretation is minimized and navigation model capabilities are more directly evident. In this analysis, we generally only check signals that do not have known self-interference problems during the time interval of assessment. To amplify,

if our assessment is for daytime propagation and the night on a path is known to incur modal effects, the day signal is considered good for our assessment purpose.

Obtainable OMEGA navigation fix accuracy is dependent upon two components of received phase, the predictable and unpredictable. The predictable component must be large enough to ensure the needed accuracy. By improving prediction methods the predictable component is made a larger portion of the total signal. By comparing numerous measurements with predictions, some estimate can be derived of the relative magnitude of the predicted, and not predicted, signal phase components. Propagation prediction calculations are produced for semi-monthly intervals and include seasonal, yearly and long term parameters. We chose this semi-monthly interval as the basic interval to check predictions. Several types of checks are described which include estimates for predicting phase at midpath noon, the day to night phase change and the accuracy of predicting the phase change during sunrise and sunset transitions. Checks are also made on the variation about the predicted and observed medians.

The examples illustrating these types of checks are taken from sites in the western half of the validation region for two reasons. First, the 10.2 kHz signals at Arequipa incurred considerable interference. Thus, we could not be sure what was due to propagation and what was due to interference. (The signal quality required for accuracy assessment is significantly greater than that needed for identifying modal and long-path effects.) Second, the closer proximity of the three western sites, Tahiti, New Zealand and Brisbane, facilitates comparison of observations.

The data, presented in Tables E-1 through E-8, shows the received phase for selected hours for each day of a semi-monthly interval. The hours selected were chosen to match conditions of propagation, i.e., day, night or day/night transition. Other values shown for each hour include: the median value for the semi-monthly interval, the range of phase values, the predicted phase (PP) and the Median minus PP. Our term predicted phase includes all of the parameters that must be included to compare predictions

with measurements. Parameters included are, calculations of Predicted Propagation Corrections (PPC's), adjustments for site location (centicycles from the PPC calculation) and adjustments for the site reference oscillator time offset. Our method for deriving predicted phase is described below. Most Tables for 10.2 kHz show the change in phase from day to night for both the median measured phase and the PP. Many of the same comparisons are described in graphical form in Part II of this Appendix. Data items considered of most interest in these tables are the range about each hourly median, the variation in the values of (M-PP) and the comparison between M and PPC of the day to night phase change.

The comparison between median phase and predicted phase cannot be absolute because the clock at each site has a small but unknown time drift. This drift is not important for LOP determination as the phase difference measurements remove the unknown time offset. For phase comparison purposes we have estimated the time offset for each assessment interval and correspondingly adjusted the phase predictions. Our choice of a method for estimating time offset is based on many considerations, two important ones being utility and accuracy. The most stable and predictable propagation period is near mid-path noon for each station signal path. We found that the range of phase values for mid-path noon varied considerably between station signals. For the three sites we will describe this range was generally smallest for the closest station which was either Hawaii at Tahiti or Australia at New Zealand and Brisbane. The range was only slightly larger for the other two stations at these receiving sites. All other signals incurred much larger ranges of mid-path noon phase values. We derived a method for estimating time offset from the recorded phase. This method, illustrated in Table E-1, uses the measured and predicted phase difference between the 10.2 and 13.6 kHz signals. This method requires the signals to be clean mode 1 at midday on each path and assumes that the prediction of 13.6 kHz phase relative to 10.2 kHz is accurate. This condition is most likely on signals from the three closest stations. Referring to Table E-1, the measured phase at 10.2 and 13.6 kHz is recorded for three stations during the June 1985 first bi-monthly period. Also recorded, are (1) the phase differences between 13.6 and 10.2 kHz for each day, (2) the median (M) phases and phase differences, (3) the predicted phases (PP) and predicted

Received Phase At Tahiti June 1985

	HAWAII 2300 GMT			AUSTRALIA 2300 GMT			JAPAN 0000 GMT		
Date	10.2 kHz	13.6 kHz	(13.6 - 10.2)	10.2 kHz	13.6 kHz	(13.6 - 10.2)	10.2 kHz	13.6 kHz	(13.6 - 10.2)
03	10	39	29	54	23	69	71	67	96
04	7	37	30	54	23	69	64	60	96
05	7	37	30	54	22	68	57	53	96
06	12	41	29	56	24	68	72	69	97
07	11	41	30	57	25	70	71	68	97
08	11	41	30	55	22	67	71	66	95
09	11	41	30	55	23	68	71	67	96
10	12	41	29	58	25	67	71	67	96
11	11	40	29	55	23	68	68	64	96
12	11	41	29	54	23	67	71	67	96
13	12	41	29	58	27	69	72	67	95
14	10	39	30	54	23	69	69	66	97
15	04	39	30	50	17	67	62	58	96
M	11	41	30	55	23	68	71	67	96
NLOP	40	19		76	68		07	76	
PPC	03	-53		02	-81		13	-120	
NLOP -PPC	37	72	35	74	49	-25	-6	96	102
M-PPC'	-26	-31	-5	-19	-26	-7	77	-29	-6
Phase Difference Due To Time Offset			-5			-7			-6
Corr*	-8	-7		-1	-2		-5	-5	

* OFFSET PHASE = $\frac{\text{Phase Difference}}{\text{Frequency Ratio} - 1} = \frac{6}{1.33333-1} = 18$ CECs $_{10.2\,\text{KHz}}$ & 24 CECs $_{13.6\,\text{kHz}}$

Table E-1. Example of Method For Estimating Time Correction at Receiver

phase differences, and (4) the differences between the measured median and predicted phases (M-PP) and phase differences. In the phase difference column (13.6 - 10.2 kHz), the difference between the measured and predicted phase is attributed to the clock offset. This clock offset value averages 6 CECs. The actual time offset is determined from the fact that the phase offset between frequencies is a function of the frequency ratio (13.6/10.2) times the time offset. Using the equation at the bottom of the table, the phase correction for the time offset for 10.2 kHz is determined to be 18 CECs. We note from the data of Table E-1, that the phase difference (13.6 - 10.2 kHz) and thus the time offset was constant over the shown bi-monthly interval. The pattern strongly suggests that any observed variations in phase difference are due to propagation effects. The time corrected values of M – PP are shown in the row labeled Corr. While these

time corrected offsets are small in both this Table and the example shown in Table E-2, we found that the derived time offset could always be adjusted to achieve a better overall fit of the measured phase to the predicted. The further improvement can be attibuted to compensating for differences in propagation versus prediction and for phase shifts between frequencies within the equipment.

A summary of the receiver time offset calculations for Tahiti during the first semi-monthly interval of February 1985 is shown in Table E-2. The required time correction was significantly less, 6 CECs versus 18 CECs.

Recieved Phase At Tahiti February 1985

	HAWAII 2200 GMT			AUSTRALIA 0000 GMT			JAPAN 0100 GMT		
Freq	10.2 kHz	13.6 kHz	(13.6 - 10.2)	10.2 kHz	13.6 kHz	(13.6 - 10.2)	10.2 kHz	13.6 kHz	(13.6 - 10.2)
M	28	61	33	62	37	75	91	92	-101
PPC	3	-53	-56	10	-75	-85	11	-121	-132
PP	37	72	35	66	143	77	-4	197	201
M-PP	-9	-11	-2	-4	-106	-2	95	-105	-301
Phase DifferenceDue To TimeOffset			6			6			5
Corr.*	-3	-3		2	2		1	3	

*OFFSET PHASE = $\frac{\text{Phase Difference}}{\text{Frequency Ratio} - 1} = \frac{2}{1.33333-1}$ = 6 CECs $_{10.2\ kHz}$ & 8 CECs $_{13.6\ kHz}$

Table E-2. Estimation of Time Correction at Receiver

After applying the time correction all of the differences between the mean and predicted phase for midday at 10.2 kHz were small. We note that the Australia prediction, both in the examples and in general, is the best. Possibly this is due to the trans-equatorial propagation from the other two stations. At the New Zealand and Brisbane sites the data was not nearly so well behaved. We attribute this condition to two possible factors. First, it is possible that the predictions are not as accurate. Second, the estimated time offsets are quite large and we suspect there is some contamination from other Omega signals due to sub-optimum synchronization. Because the results in estimating time offset were usually not optimum, we also made an additional adjustment in time offset based on a "best fit" of the combined 10.2 and 13.6 kHz signals from the three selected reference

stations. For the values shown in Tables E-3 through E-8, the values of PP listed have already been adjusted, per the above procedure, to account for clock offset.

The significance of each data category selected for presentation can be illustrated by example. Referring to Table E-3, the Hawaii data at Tahiti for (1-15 June 1985), the following is noted: (1) the range of measured phase values varies from a minimum of 4 to a maximum of 16 CECs, (2) the values of (M-PP) range from –15 to +10 CECs and, (3) the median measured diurnal phase change is 42 CECS and the predicted is 49. A more detailed examination of the (M–PP) values can be accomplished along the following lines. Note that midday occurs at about 2200. Subtract the value of (M-PP) at 2200 from the (M-PP) row to obtain:

Modified (M–PP) 1, –6, –7, –7, 18, 13, –1, –0

Because of the subtraction, each value above is a direct reading, for the associated time, of how the (M-PP) varies from its midday value. Thus the third and fourth values, corresponding to nighttime conditions, indicate that the median diurnal change is predicted to be seven CECs higher than what was observed. The fifth and sixth values show that larger differences between the observations and predictions are seen at 1600 and 1700, i.e., during the sunrise transition. We note in passing that with decent fix geometry, these errors (e.g., 7 CECs, 13 CECs and even 18 CECs) are not large enough to cause navigation concern. However, Hawaii is relatively close to Tahiti so this example might be viewed as a relatively benign one.

The above example was simply presented to show further ways to use the data of the Tables. We do not present the "modified M-PP" row as was done above in all the Tables. However, we do think it is worthwhile to point out the hours, of those listed, which are closest to midday and midnight. Accordingly on the 10.2 kHz Tables we include the notation m(12-22), for example, and then list the median observed values for 1200 and 2200. We subtract the values for these times to obtain the observed diurnal phase variation. The same procedure is carried out for the predicted values.

TIME

DAY	2	5	7	12	16	17	19	22
4	15	44	51	54	27	19	8	7
5	12	35	49	43	32	21	14	5
6	15	41	43	47	33	23	17	12
7	19	44	48	53	35	22	14	11
8	19	41	51	56	30	20	16	11
9	17	42	51	50	29	19	17	11
10	17	44	51	57	31	21	16	11
11	18	45	52	57	31	22	16	11
12	17	43	51	52	30	18	15	11
13	16	44	54	50	33	23	16	12
14	16	40	50	49		19	14	9
15	12	39	36	54	33	23	15	4
M	16	42	51	53	31	21	15	11
Range	7	10	16	14	8	4	9	8
PP	23	-44	-34	-32	21	16	24	19
M - PP	-7	-14	-15	-15	10	5	-9	-8

M (12 - 22) 53 - 11 = 42
PPC (12 -22) -46 + 3 = -49

Hawaii at Tahiti June 1985

TIME

DAY	2	3	7	12	15	18	22
4	78	76	137	172	202	167	144
5	85	69	124	162	194	176	144
6	99	83	127	177	207	169	138
7	90	55	111	153	189	158	124
8	67	61	104	147	194	171	141
9	96	72	125	159	193	166	112
10	83	73	112	141	172	159	119
11	63	54	94	146	186	164	126
12	62	44	102	157	183	159	123
13	93	75	110	179	194	167	126
14	69	48	113	153		174	153
15	88	79	109	167	199	164	113
M	84	70	111	158	194	167	126
Range	37	35	43	26	35	18	41
PP	2	-7	48	-15	7	-26	46
M - PP	-18	-23	-37	-27	-13	-7	-20

M (15 - 2) 194 - 84 = 110
PPC (15 -2) -97 +8 = -105

La Reunion at Tahiti June 1985

TIME

DAY	1	5	10	14	18	21	23
4	56	93	119	111	96	51	54
5	53	92	120	119	100	60	54
6	53	93	123	126	107	59	56
7	55	99	126	126	104	60	57
8	55	91	126	116	106	55	55
9	55	91	125	112	103	57	55
10	54	90	109	126	101	58	58
11	56	97	123	116	102	57	55
12	53	95	119	109	100	55	54
13	55	91	121	126	104	67	58
14	56	98	113		103	58	54
15	56	93	116	119	103	52	50
M	55	93	120	119	103	57	55
Range	3	6	17	17	11	16	8
PP	-45	-11	19	19	-13	-46	-44
M - PP	0	4	1	0	16	3	-1

M (14 - 23) 119 - 55 = 64
PPC (14 - 23) -61 - 2 = -63

Australia at Tahiti June 1985

TIME

DAY	1	4	7	11	14	17	20
4	73	91	138	172	184	158	86
5	66	86	135	169	185	171	93
6	68	89	131	166	192	166	96
7	72	95	133	165	191	166	95
8	71	90	139	174	188	165	94
9	71		139	159	180	159	94
10	71	89	138	170	188	171	95
11	71	90	141	180	186	164	92
12	69	90	131	173	186	160	94
13	69	87	140	163	178	157	92
14	72	89	133	175		166	94
15	69	89	134	175	183	168	91
M	71	89	137	171	186	166	94
Range	7	5	10	21	14	14	10
PP	-25	-10	32	-23	-18	44	-19
M - PP	-4	-1	5	-6	4	22	13

M (14 - 1) 186 - 71 = 115
PPC (14 - 1) -93 - 14 = -107

Japan at Tahiti June 1985

Table E–3. Received Phase at Tahiti, 10.2 kHz, June 1985

TIME

DAY	2	5	7	12	16	17	19	22
1								
2								
3					57	46	40	41
4	43	75	85	86	53	44	37	36
5	40	68	85	78	57	46	43	35
6	43	73	80	81	58	48	46	41
7	47	75	84	85	59	48	43	40
8	46	70	88	89	56	45	44	41
9	45	73	87	80	55	44	44	40
10	45	73	85	89	56	46	44	41
11	46	75	86	87	57	47	44	40
12	44	74	82	83	56	43	44	40
13	44	75	85	87	58	47	44	40
14				82		43	42	39
15	41	71	83	82	60	47	42	33
M	44	73	85	84	57	46	44	40
Range	7	7	8	9	7	5	9	8
PP	–43	–10	2	5	–49	47	–42	–46
M–PP	–13	–17	–17	–21	6	–1	–14	–14

Hawaii at Tahiti June 85, 13.6 kHz

TIME

DAY	2	3	7	12	15	18	22
1							
2							
3						63	51
4	987	80	43	80	109	74	53
5	998	80	32	73	101	81	53
6	010	88	34	83	113	76	51
7	003	66	26	57	100	64	35
8	985	68	21	57	104	75	51
9	005	78	36	71	102	73	31
10	996	79	24	50	082	67	29
11	981	66	13	59	098	66	36
12	979	57	16	70	087	64	37
13	000	81	21	83	103	73	35
14				64		78	27
15	993	80	25	76	104	69	24
M	996	979	25	71	103	73	36
Range	31	31	30	33	31	18	29
PP	–27	–12	4	–7	37	15	25
M–PP	23	–9	21	–22	–34	–42	11

La Reunion at Tahiti June 85, 13.6 kHz

TIME

DAY	1	4	7	11	14	17	20
1							
2							
3						956	884
4	869	882	930	972	979	952	877
5	863	878	932	971	979	962	882
6	864	881	923	968	982	958	886
7	867	886	927	969	984	960	883
8	866	882	933	974	978	955	884
9	866		933	963	982	950	885
10	867	882	930	972	979	962	886
11	867	882	933	983	982	957	882
12	864	881	923	976	981	954	883
13	866	879	934	964	978	949	881
14	866			977		955	881
15	865	881	930	976	978	957	879
M	66	82	30	72	79	56	83
Range	6	8	11	20	6	13	9
PP	–22	–10	30	–23	–17	40	–23
M–PP	–12	–8	0	–5	–4	16	6

Japan at Tahiti June 85, 13.6 kHz

TIME

DAY	1	5	10	14	18	21	23
1							
2							
3					64	23	23
4	26	58	94	84	66	19	23
5	22	58	90	90	66	25	22
6	21	59	91	99	73	25	24
7	24	64	101	100	71	26	25
8	23	57	99	89	73	21	22
9	23	55	98	87	71	23	23
10	23	55	83	96	68	23	25
11	25	62	96	91	70	23	23
12	22	60	92	80	66	23	23
13	24	57	94	99	71	33	27
14	25		91		70	25	23
15	24	57	89	91	70	19	17
M	23	58	93	91	70	23	23
Range	5	9	18	20	9	14	10
PP	31	–40	–4	–4	–41	26	31
M–PP	–8	–2	–3	–5	11	–3	–8

Australia at Tahiti June 85, 13.6 kHz

Table E-4. Received Phase at Tahiti, 13.6 kHz, June 1985

TIME

DAY	1	4	10	12	16	17	18	22
1		55	70	77	67	52	45	30
2	32	57	73	78	66	52	44	29
3	28	57	62	68	74	51	44	28
4	32	56	74	77	66	50	44	28
5	32	55	67	80	69	49	43	28
6	32	54	84	85	67	50	42	28
7	31	54	69	78	67	48	42	27
8	30	53	69	75	65	48	42	28
9		54	74	82	70	48		28
10	32	53	66	71	64	47	41	
11			72	74	65	47	41	27
12	30	51	75	76	64	46		27
13	30	52	64	63	63	44	39	26
14	29	51	71	71			38	26
15	28	48	75	76	66	45	40	26
M	31	54	71	76	66	48	42	28
Range	4	9	22	22	11	8	7	4
PP	35	49	–18	–18	–41	26	38	33
M – PP	–4	5	–11	–6	7	22	4	–5

M (12 – 22) 76 – 28 = 49
PPC (12 – 22) -46 - 3 = -49

Hawaii at Tahiti February 1985

TIME

DAY	0	4	7	12	15	16	17	20
1		75	103	132		193	163	129
2	98	80	97	149	207	192	170	129
3	95	75	105	159	200	193	171	133
4	101	76	111	163	225	212	185	142
5	96	73	97	152	200	196	166	133
6	93	72	101	148	200	191	163	126
7	88	72	112	135	198	183	157	135
8	86	59	99	142	202	187	162	122
9		68	105	146	198	185	166	133
10	93	64	97	149	194	194	168	114
11	94		101	148	205	189	162	127
12	83	75	91	152	202	196	171	134
13	101	76	111	160	214	197	177	125
14	87	68	98	150				141
15	83		94	153	221	214	183	136
M	93	74	101	149	201	193	167	133
Range	18	21	21	31	31	31	28	28
PP	–23	–40	–11	31	-27	46	23	9
M – PP	16	14	12	18	28	47	44	24

M (12 – 0) 149 – 93 = 56
PPC (12 – 0) -42 – 12 = -54

La Reunion at Tahiti February 1985

TIME

DAY	2	4	7	12	15	16	17	18	22
1		–25	13	44		37	17	–1	–36
2	–35	–23	16	49	47	36	17	–2	–35
3	–35	–23	19	45	46	39	19	1	–34
4	–35	–23	17	46	46	37	16	–1	–34
5	–35	–22	20	46	46	40	20	1	–34
6	–35	–25	17	44	47	35	16	–3	–36
7	–36	–24	15	47	46	35	18	1	–35
8	–35	–26	16	47	49	32	13	–4	–36
9	–36	–27	16	44	45	37	17		–34
10	–35	–25	13	37	44	35	14	–4	
11			12	48	46	39	17	–3	–37
12	–36	–26	14	41	46	36	17		–37
13	–36	–26	16	42	46	40	19	1	–36
14	–49	–25	16	44				0	–36
15	–41		10	42	44	37	15	–4	–37
M	–35	–25	16	44	46	37	17	–1	–36
Range	14	5	10	12	5	8	7	5	3
PP	–38	–33	1	31	31	15	–9	–22	–37
M – PP	3	8	15	13	15	22	26	21	1

M (15 – 22) 46 + 36 = 82
PPC (15 – 22) –61 – 7 = –68

Australia at Tahiti February 1985

TIME

DAY	1	5	7	11	14	17	18	19	22
1		39	73	112		97	91	80	20
2	–3	40	78	105	99	105	96	78	16
3	–8	35	76	98	109	114	101	81	18
4	–7	34	80	100	108	103	94	77	19
5	–9	34	73	106	114	101	92	77	20
6	–8	36	83	107	119	109	95	78	17
7	–9	33	76	100	119	101	92	75	14
8	–10	31	71	111	113	97	83	69	13
9		34	80	94	110	103			14
10	–8	33	68	98	110	87	75	63	
11		32	66	101	112	100	82	62	12
12	–8	31	69	102	94	80			12
13	–9	30	61	100	98	85	79	64	12
14	–9	29	74	100	107	91	78	63	12
15	–9	30	79	96	116	94	83	66	12
M	–9	33	74	100	110	100	87	75	14
Range	7	11	22	18	25	34	26	19	8
PP	–10	12	–48	–8	–6	–38	41	31	–10
M – PP	1	21	22	8	16	38	46	44	24

M (14 – 22) 110 – 14 = 96
PPC (14 – 22) –93 – 11 = –104

Japan at Tahiti February 1985

Table E-5. Received Phase at Tahiti, 10.2 kHz, February 1985

TIME

DAY	1	4	10	12	16	17	18	22
1					102	80	76	59
2	69	88	112	114	100	80	75	61
3	64	87	104	110	105	80	76	62
4	64	87	107	114	099	80	75	62
5	65	86	111	113	103	76	74	62
6	64	85	121	117	100	78	74	61
7	63	84	111	111	100	76	73	60
8	63	84	109	110	101	76	73	61
9		84	108	117	103	76		62
10	64	83	103	107	098	75	72	
11			112	108	100	75	73	60
12	63	82	109	108	100	73		60
13	62	82	105	104	097	73	71	60
14	62	80	107	106			70	59
15	61		108	112	101	72	71	59
M	64	84	108	110	100	76	73	60
Range	8	5	47	41	8	8	7	3
PP	–32	–25	16	17	–10	–47	–31	–34
M – PP	–4	9	–8	–7	10	23	4	–6

Hawaii at Tahiti February 1985 13.6 kHz

TIME

DAY	0	4	7	12	15	16	17	20
1								
2	12	995	13	62	112	102	81	44
3	11	991	23	67	108	101	79	47
4	15	992	24	73	127	116	93	59
5	10	989	14	65	107	100	75	49
6	10	988	18	60	111	100	75	40
7	05	986	24	51	108	96	66	50
8	01	978	16	56	112	97	73	37
9		984	19	60	110	96	75	52
10	10	982	14	60	106	104	78	36
11	11		16	60	114	97	72	44
12	01	990	08	62	109	106	80	51
13	14	992	25	74	122	105	80	43
14	04	984	19	60				53
15	03		11	69	130	122	87	51
M	10	88	17	61	111	101	78	48
Range	14	17	17	23	24	26	21	23
PP	3	–13	14	–44	–2	–31	44	35
M – PP	7	1	3	5	13	32	34	13

La Reunion at Tahiti February 1985 13.6 kHz

TIME

DAY	2	4	7	12	15	16	17	18	22
1							85	68	37
2	40	50	88	131	117	111	85	67	39
3	43	50	89	118	122	111	88	70	41
4	40	50	89	121	125	110	85	68	41
5	40	50	92	128	130	113	88	69	40
6	40	48	87	123	130	107	85	65	41
7	39	48	87	126	124	107	88	68	39
8	39	47	85	123	128	104	82	64	39
9	38	46	87	126	125	111	86		39
10	40	46	83	114	124	107	84	64	40
11			83	124	128	112	85	64	
12	38	46	84	120	128	109	85		38
13	38	46	87	119	121	113	88	66	39
14	35	46	86	121				67	38
15	35	37	80	125	125	112	85	64	38
M	39	47	87	123	123	111	85	67	39
Range	8	13	12	17	17	9	6	6	4
PP	39	43	–27	7	8	–10	–38	50	40
M – PP	0	4	14	16	15	21	23	17	–1

Australia at Tahiti February 1985 13.6 kHz

TIME

DAY	1	5	7	11	14	17	18	19	22
1							988	974	908
2	896	936	976	003	007	001	991	975	909
3	892	932	976	003	013	012	997	977	912
4	893	930	977	000	007	003	991	973	915
5	892	930	975	003	013	000	989	974	917
6	894	932	982	004	028	005	992	973	912
7	891	929	975	001	023	998	990	971	908
8	890	928	974	001	014	992	978	978	907
9		928	975	999	008	998			909
10	893	928	971	002	009	985	972	957	
11		928	968	003	012	997	976	957	908
12	892	926	969	001	998	980			
13	891	925	963	002	000	990	973	959	908
14	890	924	972	005	001		975	957	910
15	890	925	975	000	013	991	978	960	908
M	892	928	975	003	011	997	88	73	9
Range	6	12	19	6	30	18	25	21	10
PP	–9	9	47	–7	–5	–41	43	28	–13
M – PP	1	19	28	10	16	38	45	45	22

Japan at Tahiti February 1985 13.6 kHz

Table E-6. Received Phase at Tahiti, 13.6 kHz, February 1985

TIME

DAY	1	2	3	4	8	16	19	21
1	108		48	69	85	179	185	177
2	130	108	87	94	107	194	183	
3	125	105	80	80	98	192	200	187
4	105	90	85	78	108	164	167	149
5	121	109	85	82	95	178	178	165
6	92	82	53	50	80	175	173	150
7	92	80	53	54	98	170	183	164
8	116	101	79	97	77	171	153	155
9	114	82	36	23	58	171	177	146
10	109	84	51	60	86	164	167	132
11	123	112	73	64	94	164	166	166
12	110	84	66	40	91	161	160	146
13	119	91	71	77	111	158	162	139
14	105	95	57	68	75	169	168	161
15	123	94	60	69	83	178	185	168
M	114	92	66	69	91	171	173	163
Range	38	22	51	74	53	36	47	55
PP	-22	0	18	6	-20	20	18	39
M–PP	36	-8	48	-37	11	-49	-45	24

M (16 – 3) 171 – 66 = 105
PPC (16 – 3) -80 – 17 = -97

La Reunion at New Zealand July 1985

TIME

DAY	0	3	8	12	14	16	19	22
1	26	39	66	61	47	36	24	13
2	17	25	53	51	37	28	12	8
3	19	40	62	54	35	27	19	21
4	28	44	57	50	32	21	9	16
5	11	28	46	55	39	30	12	18
6	19	36	60	55	39	33	16	14
7	24	38	60	56	41	29	11	26
8	25	42	59	56	44	33	7	19
9	14	41	59	57	50	34	19	21
10	24	40	67	60	52	41	19	17
11	23	42	62	58	47	25	3	7
12	15	34	57	47	28	14	-3	5
13	12	17	43	46	37	21	-7	1
14	9	16	54	49	35	26	-2	6
15	9	25	56	54	42	22	7	7
M	19	38	59	55	39	28	11	14
Range	19	28	24	15	24	27	31	25
PP	19	39	-42	50	33	21	-11	9
M–PP	0	-1	1	5	6	7	22	5

M (12 – 0) 55 – 19 = 36
PPC (12 – 0) -71 + 40 = -31

Argentina at New Zealand July 1985

TIME

DAY	0	6	9	12	19	20	21	22
1	26	40	55	53	52	45	33	30
2	26	42	58	48	49	44		21
3	25	40	65	49	58	42	34	29
4	25	38	57	53	52	41	35	30
5	24	38	63	46	60	46	34	31
6	27	38	55	55	60	42	29	30
7	28	39	55	51	48	47	32	33
8	29	45	51	48	46	44	35	31
9	27	39	60	50	51	42	23	23
10	24	38	52	46	48	42	21	25
11	26	35	59	51	46	40	26	25
12	23	33	53	50	58	40	27	26
13	26	35	62	52	60	38	23	24
14	25	34	58	49	55	40	23	23
15	24	34	62	54	57	38	25	28
M	26	38	58	50	52	42	28	28
Range	6	12	14	9	14	9	12	12
PP	31	44	-46	-45	-45	44	29	31
M–PP	-5	-6	4	-5	-3	-2	-1	-3

M (12 – 0) 50 – 26 = 24
PPC (12 – 0) -30 + 7 = -23

Australia at New Zealand July 1985

TIME

DAY	0	7	9	14	19	20	21	22
1	34	78	110	126	130	66	62	50
2	32	78	114	122	125	68		
3	30	80	113	130	137	70	67	51
4	32	79	113	140	132	71	61	49
5	33	79	116	126	121	65	62	51
6	34	75	111	131	137	60	62	48
7	33	79	116	136	135	64	59	49
8	30	77	109	123	133	66	60	54
9	31	77	112	122	125	69	56	47
10	29	74	113	122	130	60	61	51
11	31	76	114	124	116	58	55	46
12	29	73	111	122	132	72	64	51
13	33	76	109	131	128	67	60	51
14	31	77	113	128	130	68	58	47
15	30	75	113	129	117	63	59	48
M	31	77	113	126	130	66	61	50
Range	5	7	7	18	21	14	12	8
PP	34	66	1	30	30	18	26	46
M–PP	-3	11	12	-4	0	48	35	4

M (14 – 0) 126 – 31 = 95
PPC (14 – 0) -85 – 11 = -96

Japan at New Zealand July 1985

Table E-7. Received Phase at New Zealand, 10.2 kHz, July 1985

TIME

DAY	2	5	9	15	17	18	19	21	23
1									
2									
3	44	50	61	141	143	138	136	104	80
4	42	44	58	144	153	141	133	113	83
5	55	50	58	143	147	135	132	114	81
6	47	49	59	155	153	142	137	120	100
7	58	51	60	147	150	141	131	116	95
8	63	54	60	148	143	123	130	97	89
9	58	50	56	135	133	125	119		85
10	55	44	45	135	143	127	124	110	93
11	53	48	47	133	150	135	121	107	91
12	57	46	59	137	149	130	125	110	89
13	53	41	59	146	143	137	131	116	95
14	57	56	51	142	147	139	135	120	99
15	61	59	67	151	157	142	132		–51
M	56	50	59	143	147	137	131	113	89
Range	21	18	22	22	24	19	18	23	151
PP	42	41	56	30	27	16	6	–13	–26
M–PP	14	9	3	13	20	21	25	26	12

M (15 – 21) 143 – 113 = 30
PPC (15 – 21) –65 + 28 = –37

La Reunion at New Zealand January 1985

TIME

DAY	0	2	4	11	14	15	16	21
1								
2								
3		59	73	89	68	62	49	48
4	57	53	95	91	69	62	57	40
5	47	64	78	91	70	62	47	41
6	46	58	73	92	71	61	51	48
7	46	66	78	94	72	62	51	26
8	48	59	79	97	70	66	56	27
9	46	58	74	89	58	71	63	
10	36	58	79	90	73	62	49	50
11	42	60	73	93	70	61	53	39
12	48	61	77	95	71	61	52	39
13	44	60	77	93	73	60	51	44
14	43	62	80	98	69	64	56	41
15	48	57	78	97	72	66	53	
M	46	59	78	93	70	62	52	41
Range	21	13	22	9	15	11	16	24
PP	38	54	70	92	61	50	39	31
M–PP	8	5	8	1	9	12	13	10

Argentina at New Zealand January 1985

TIME

DAY	0	5	7	14	16	17	18	22
1								
2								
3		93	96	120	114	115	101	90
4	89	91	94	116	118	115	101	89
5	88	92	96	115	114	116	101	90
6	89	90	95	119	116	119	101	
7	88	91	95	119	118	118	101	91
8	89	91	96	118	114	116	97	91
9	89	92	94	112	114	117	99	
10	86	90	94	111	113	119	101	90
11	87	91	94	112	116	116	101	90
12	87	91	96	110	109	119	102	89
13	87	83	91	114	112	116	100	88
14	86	90	95	109	106	119	101	88
15	85	89	94	116	114	118	103	
M	87	91	95	115	114	117	101	90
Range	4	10	5	11	12	4	6	3
PP	93	94	97	120	120	113	100	94
M–PP	–7	–3	–2	–5	–6	4	1	–4

M (16 – 22) 114 – 90 = 24
PPC (16 – 22) –30 + 4 = –26

Australia at New Zealand January 1985

TIME

DAY	0	7	11	14	16	17	18	22
1								
2								
3		36	98	94	103	95	87	26
4	3	35	96	90	97	93	80	23
5	1	39	104	102	111	101	84	27
6	3	40	96	98	100	102	91	
7	5	41	103	108	111	103	89	35
8	3	36	91	93	101	96	85	33
9	2	40	101	107	106	102	89	
10	0	39	105	111	108	103	90	33
11	5	39	97	91	104	96	82	28
12	2	41	96	105	106	101	87	29
13	2	35	92	100	103	99	83	30
14	0	39	96	105	105	103	85	28
15	1	36	102	101	103	100	87	
M	2	39	97	101	105	101	87	28
Range	5	6	14	21	14	10	11	12
PP	98	12	91	95	95	88	72	98
M–PP	4	27	6	6	10	13	15	30

M (14 – 0) 101 – 2 = 99
PPC (14 – 0) –85 – 12 = –97

Japan at New Zealand January 1985

Table E-8. Recieved Phase at New Zealand, 10.2 kHz, January 1985

Some general comments for all three sites are as follows. The agreement between diurnal phase change, i.e. day to night, is generally good. For the data shown, the largest deviation from predicted is Australia at Tahiti for February as illustrated in Table E-5. In this case the observed diurnal phase change exceeds the predicted by 14 CECs. After time correction for local reference time offsets, the median and PP values consistently show the largest differences during the sunrise transitions. The range of measured phase values varies quite a bit between stations and receiving sites. For the data presented, the La Reunion signal has the largest range at each site. Its range is particularly large at Tahiti in June and New Zealand in July. Interesting differences are observed between the 10.2 and 13.6 kHz data tables. These differences are suttle and will require additional analysis before comments are in order. Some of the observations described in this section will be explored further in Part II.

PART II: EXAMPLES OF OBSERVED TRENDS

While the tabulated data of Part I contains valuable information, communication of this information to the casual reader is considered easier using graphical form. In this part we illustrate some of the more significant general findings of the accuracy analysis. The principle topics to be discussed include, prediction matches during transition times, observations of large phase ranges about the median, poor fits to the predicted shape of the diurnal phase curve and some systematic deviations from the median over many hours.

Transition Time Phase Predictions: We stated in Part I that the most consistent deviation of measured from predicted phase occurred during signal day/night transition intervals. This situation will be illustrated with two examples. Figure E-1 shows the phase of the Hawaii signal received at Tahiti for seven consecutive days in June 1985. Also shown with the top set of curves is the predicted phase, PP. Of prime interest is the sunrise transition occurring between 1500 and 1800 GMT. The PP hourly values are connected with a dashed line interval. It is emphasized that only hourly values are predicted and should be compared with the data. We choose to

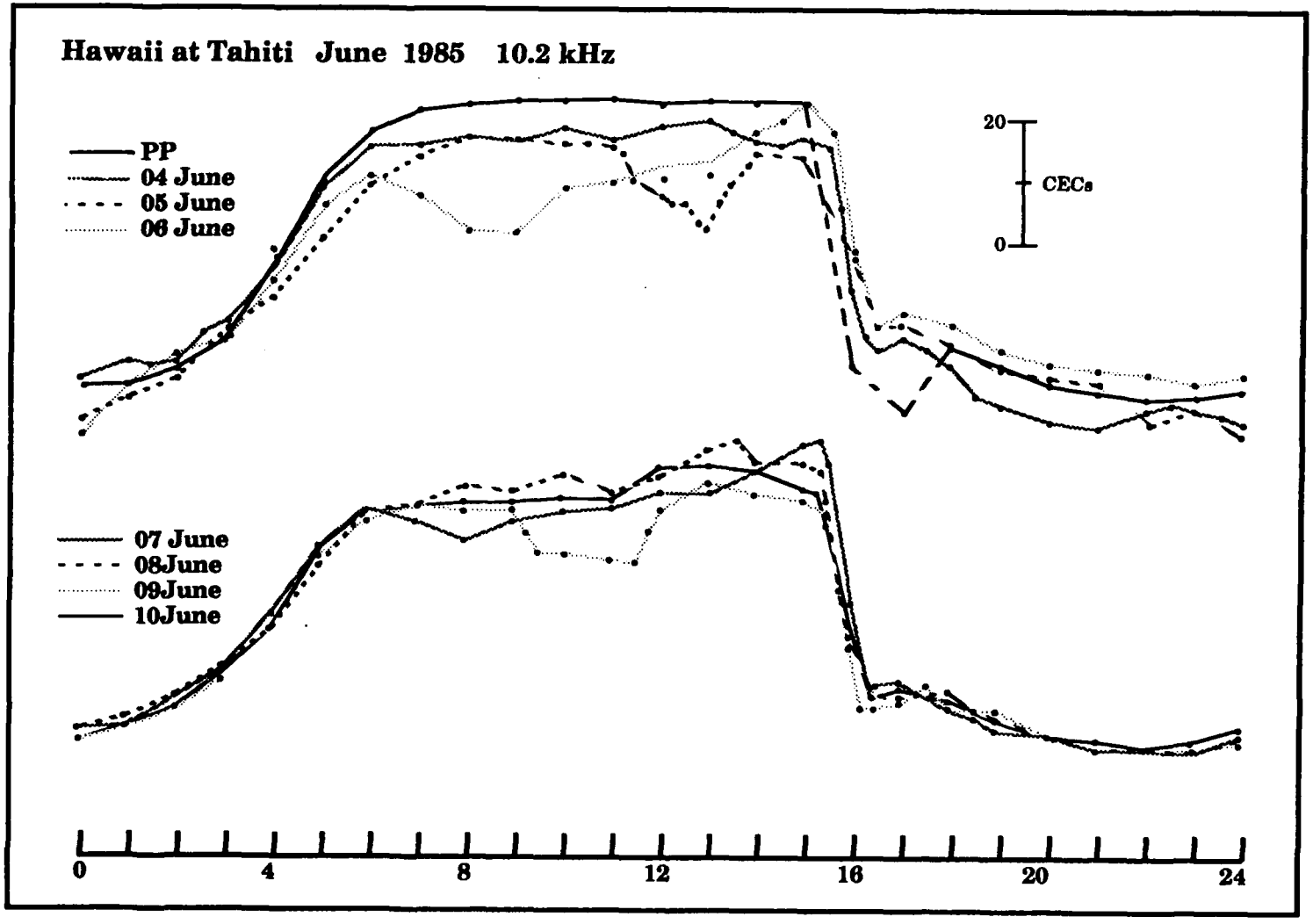

Figure E-1. Comparing PPC to Measured Phase; Hawaii Signal

use higher time resolution for the measured data. The PP shows a marked phase dip occurring between 1600 and 1800 which either does not occur or is minor on all of the data. We have examined many days of data recorded at 6 minute intervals to establish that the dip is much less than predicted.

A more striking example of these phase differences is shown in Figure E-2. This Figure shows the Japan measured phase at New Zealand. The vertical bars show the range of measured phase for each hour during the 15 day interval. At 2000 the median phase is over 60 CECs above the predicted phase. During the sunset transition the PP is low, by 20 CECs at 0900. Our analysis of selected samples were taken over limited time periods, and for only a few years. It is known that the PPC model does not predict the transitions particularly well. These observations of sunrise phase showing biases in PP predictions serve to illustrate todays prediction accuracies. The overall model improvement problem is complex. Not all paths and times show this sunrise difference.

Observations of High Latitude Propagation: We first noted in assessing shipboard data, that the La Reunion signal on occasion seemed to produce rather large offsets for long periods of time. This observation led to a closer examination of the La Reunion signals at New Zealand and Brisbane. We note that in Table E-7 the Range values for La Reunion get as high as 74 CECs for July. The January signals, Table E-8, incur smaller ranges, about 20 CECs. Figure E-3 shows the ranges (vertical bars) of the measured July signals superimposed on the PP curve. The curve is offset in the center to allow using a larger scale. We note that the PP has a smaller diurnal change than the measured median, by about 40 CECs. The measured values have a range of over 60 CECs in and near the all-day portion, and 30 to 40 CECs during the all-night portion. A more detailed examination of the data reveals interesting features. Figure E-4 shows the phase records for 4 selected days in July, each having a different minimum phase. We note a tendency for the phase to select a specific path for this part of the diurnal period. Not all days are as clean as these, some records "switch paths" during this period. The sense is as if the phase attempts to set a path but the ionosphere won't quite support it and it has to settle for another path. In quite a few cases though, the early phase record heralds

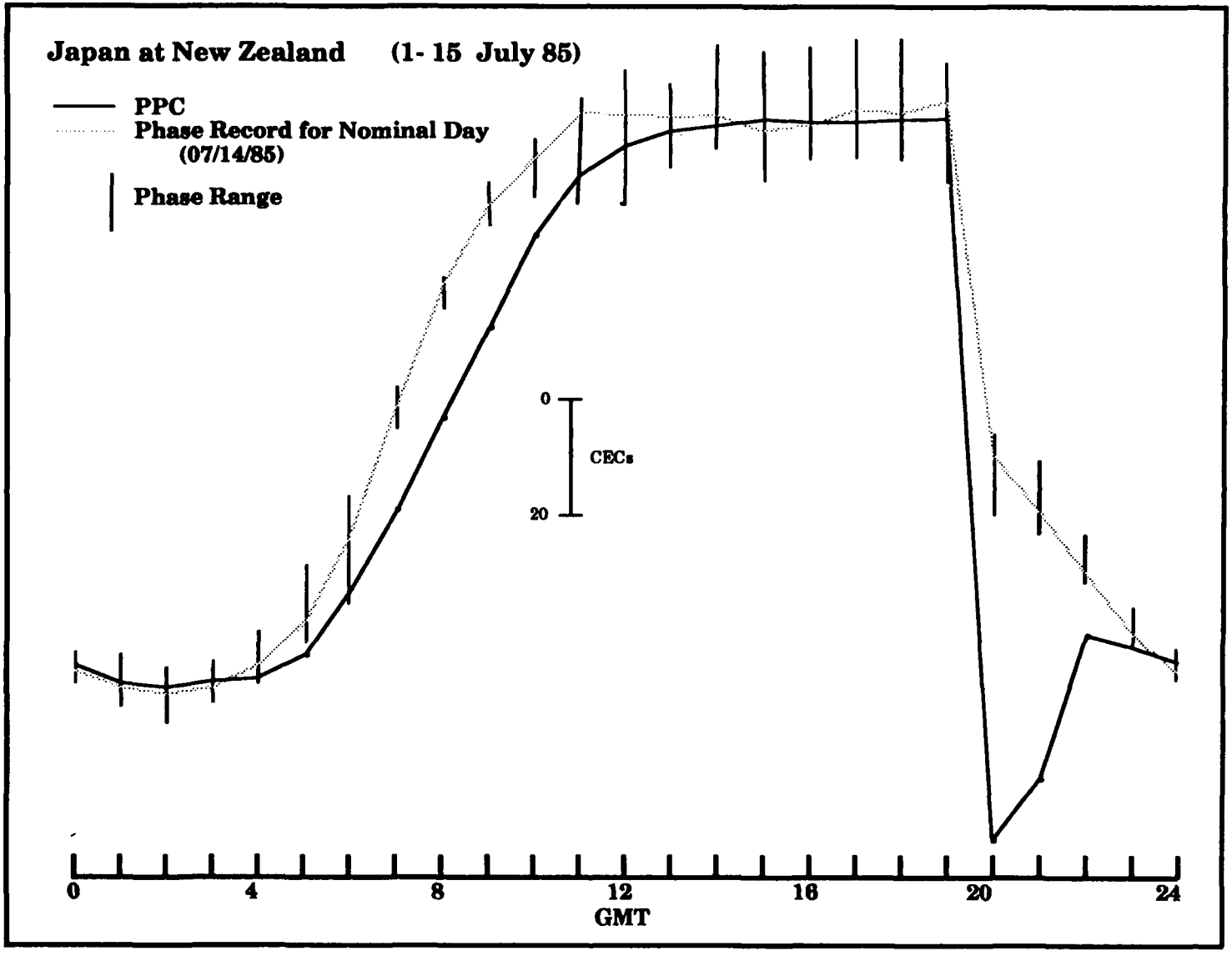

Figure E-2. Comparing PPC to Measured Phase; Japan Signal, 10.2 kHz

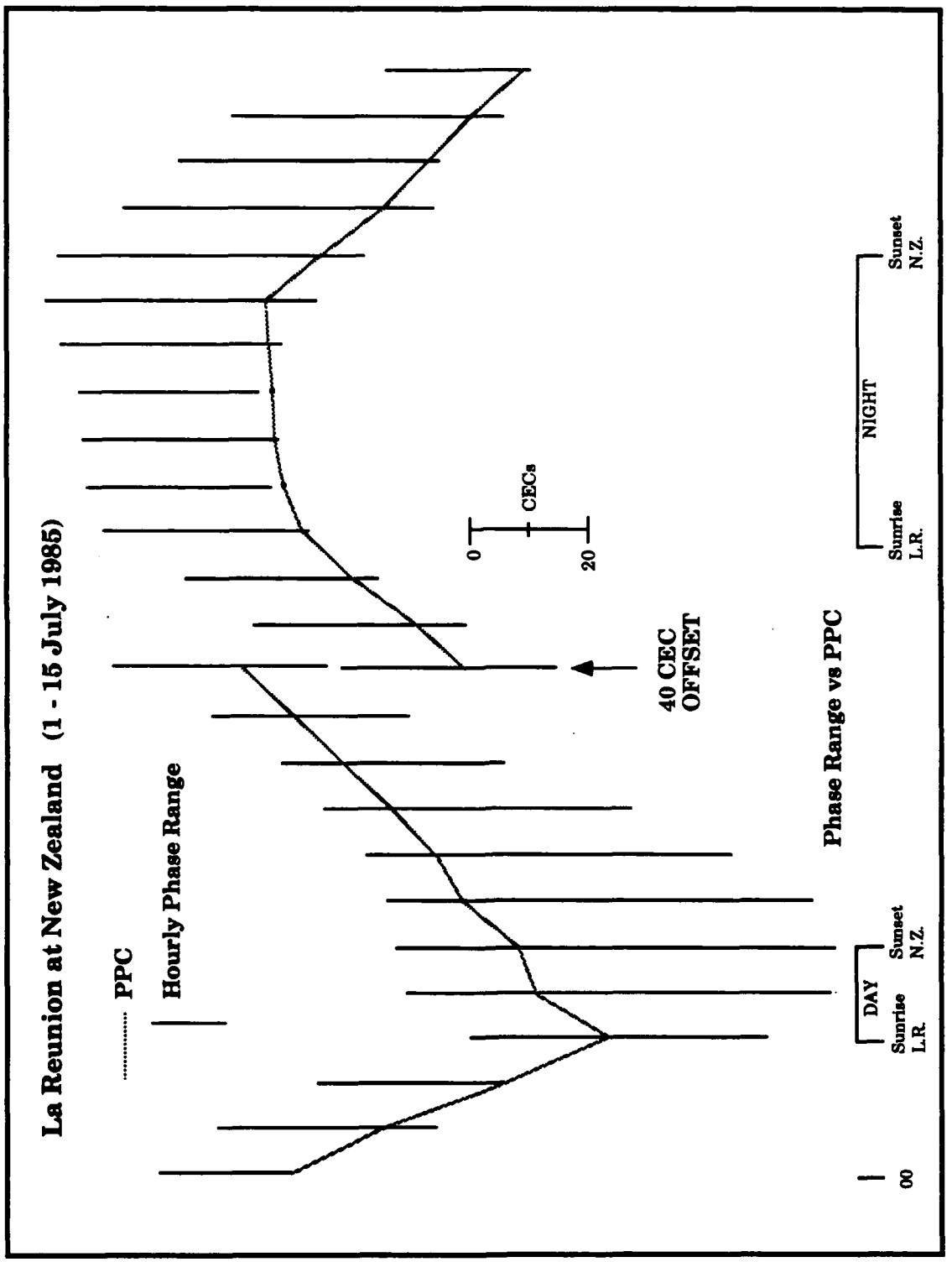

Figure E-3. La Reunion Signal Phase Variability at 10.2 kHz

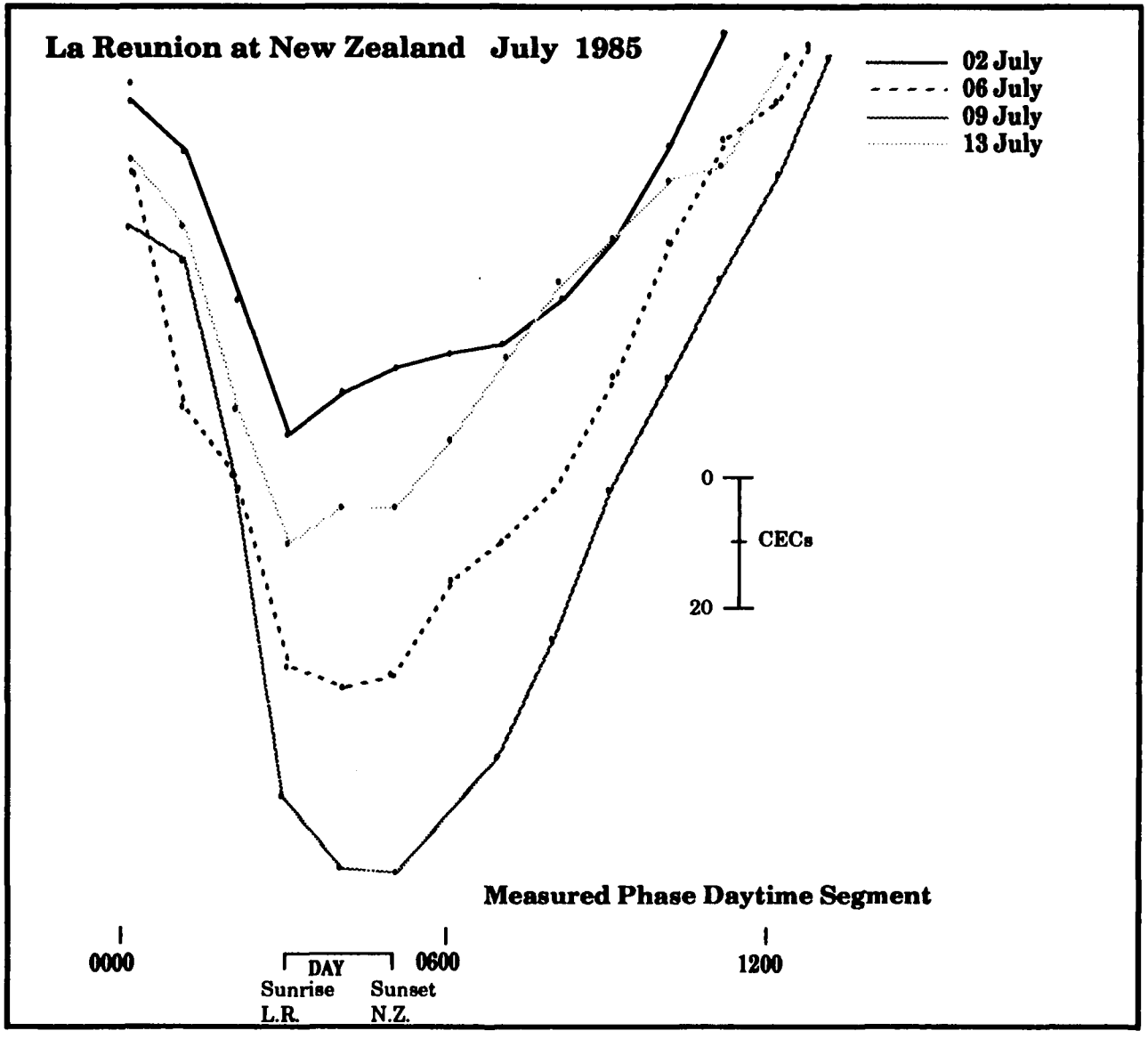

Figure E-4. Measured Daytime Phase; 10.2 kHz

the phase behavior for the entire interval. The conditions described in Figures E-3 and E-4 will likely have to be treated as unpredictable for some time in the future. We feel that there is potential for at least characterizing their occurrence. The clues gleaned to date indicate that large variability is associated with the highest latitude portion of the path and with local winter. By knowing when and where the large fluctuations occur, a choice for deselection can be made.

The case for the high latitude interpretation of large phase variability is supported by data for the same time interval recorded at Brisbane. As shown in Figure E-5, the La Reunion signal incurs much less variability. This Figure shows the PP in relation to two phase curves, one representing the minimum and the other the maximum diurnal phase change. Included in this Figure for 7 selected times are columns of dots showing individual phase values. It is noted that the scatter is reduced from Figure E-3. The values in parentheses note the offset of the Median from the PP.

Another example of high signal phase variability is shown in Figure E-6, the Argentina signal at Brisbane. For this 1 to 15 July period, the range is typically 30 CECs as shown by the vertical columns of dots. Phase records for two dates are shown to illustrate that the phases can maintain a near constant offset for long periods of time. We further note that these records are for consecutive days. The propagation path from Argentina to Brisbane is below the zone predicted to have modal self-interference. The deep dips in the phase records occurring near 0400 and 2100 seem to be a consistent feature of this path for this year. The same date interval for 1986 shows different results as presented in Figure E-7. This figure shows the Argentina signal persistent offset of phase from the median on selected days. The insert table in Figure E-7 compares the median values for the two years at select hours. We note that while the average of all hourly medians is close, the individual hours can have quite different values. The bottom row of the table relates the average of medians to the average of the PP. We interpret the data for Argentina at Brisbane to signify that considerable phase variation from the PP is likely. We believe the observed variaion is related to the day/night terminator being closely

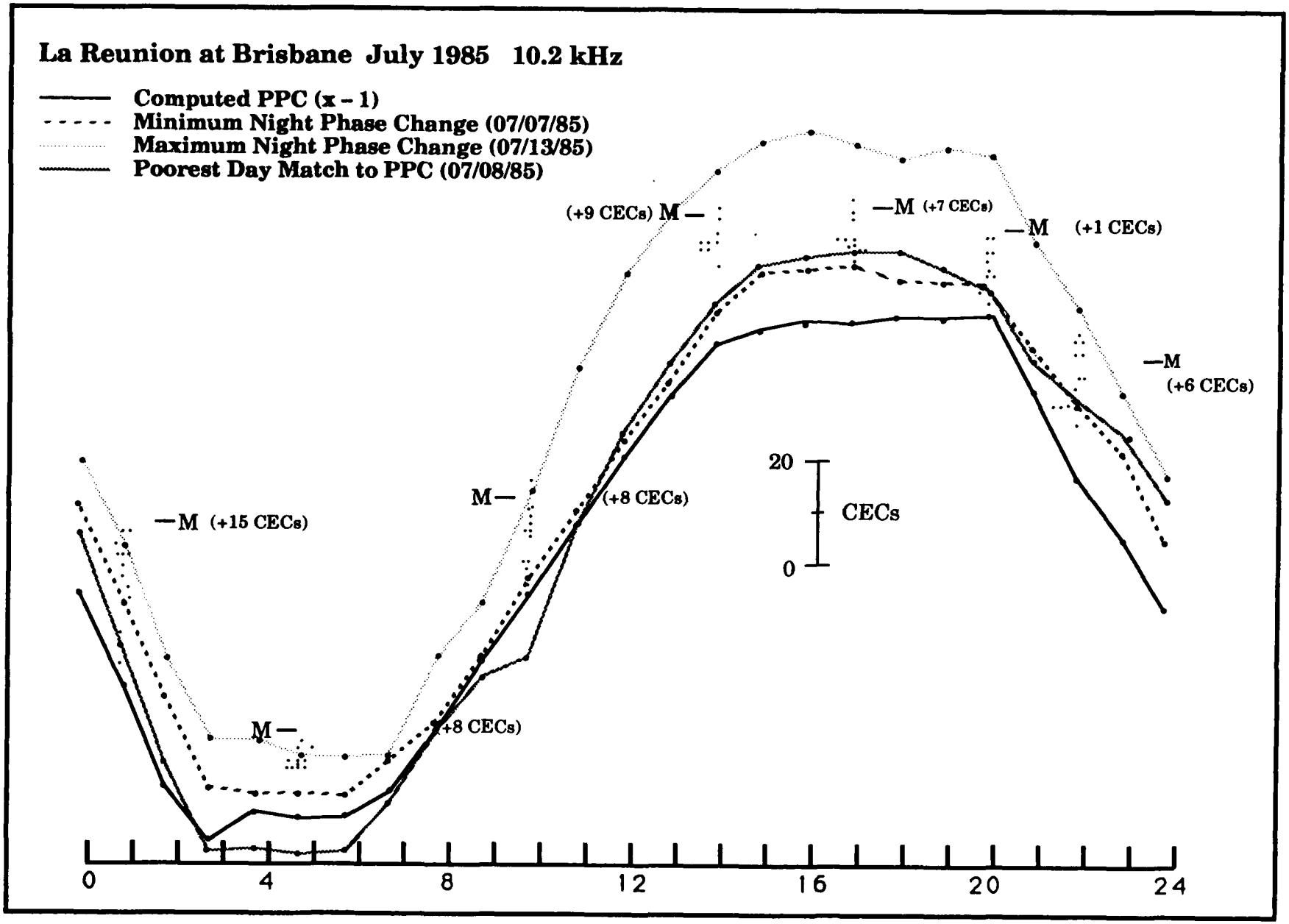

Figure E-5. Comparison of Predicted with Measured Phase for Selected Days

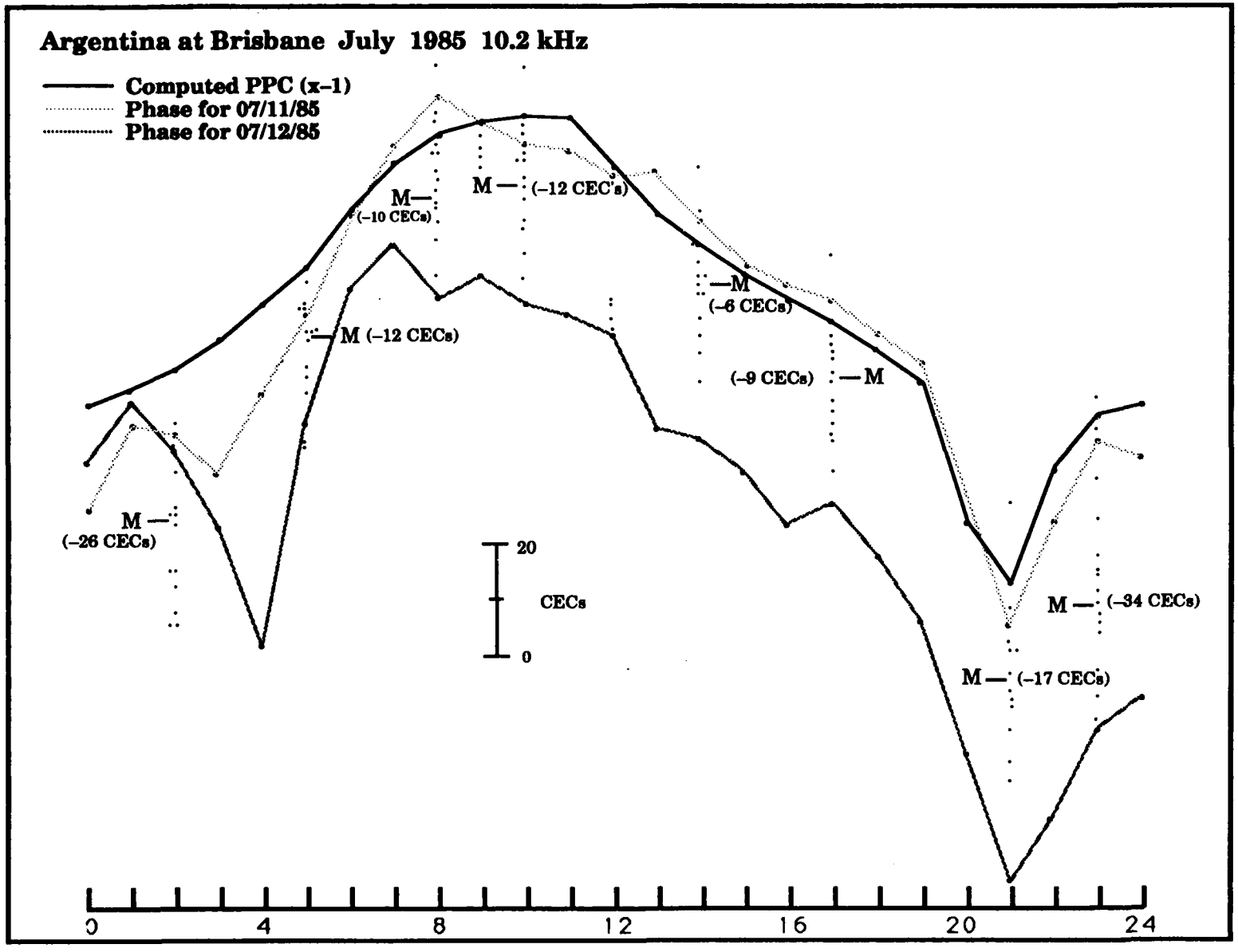

Figure E-6. Argentina Signal Phase Variability

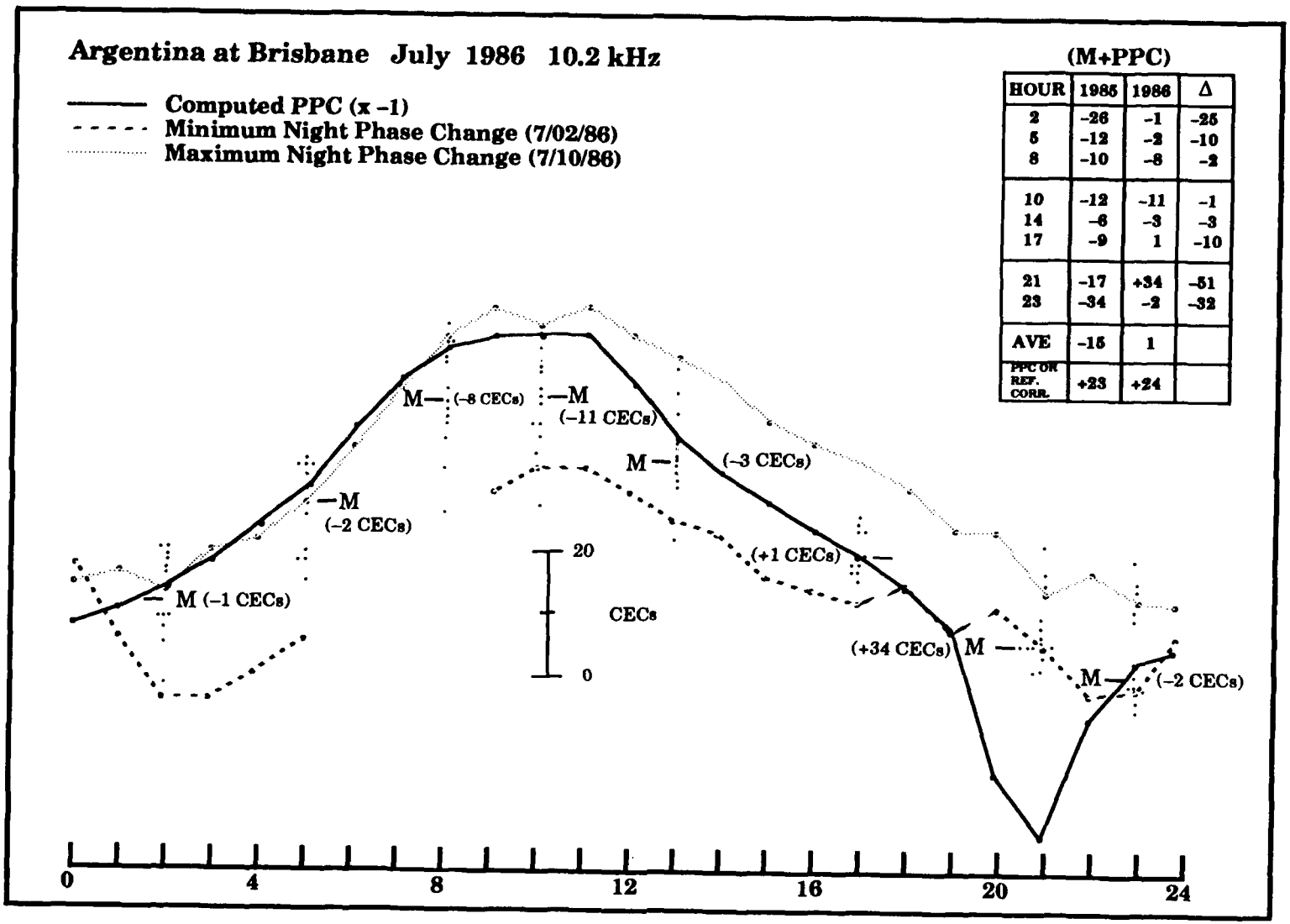

Figure E-7. Argentina Signal Phase at Brisbane

parallel to the propagation path in July. Brisbane is also predicted to be on the south-eastern edge of the long-path interference zone (See appendix C).

Miscellaneous Examples of Phase Deviations: We note that the Japan signal phase at Brisbane for July 1985 and 1986 was more variable than at New Zealand. In Figure E-8, we show phase curves for three days during July 1985. The ranges at selected times are depicted by columns of dots. The spread of points about the median is generally small. The example curves clearly are exceptions. When exceptions do occur, the large deviation usually persists for most of the 24 hour period. We note, in comparing this data with Figure E-2, that for Brisbane the Range is a larger portion of the day night phase change. An interesting observation is that the night of maximum phase change, 13 July, is also the maximum for La Reunion at Brisbane, Figure E-5, and the very low Daytime Phase of La Reunion at New Zealand, Figure E-4.

Figure E-9 shows the data for July 1986. The ranges of phase values are quite similar. For both years the day/night median phase change is respectively 17 and 12 CECs less than predicted. The phase record shown, shows large transitions in phase during the night interval. While these records are exceptions, they also suggest that this path may be experiencing some modal effects. For both years the sunrise dip is less than predicted by at least 20 CECs.

General Comments: The PPCs reflect the average, which to be tested requires many years of data. The observations of this analysis can only be considered a flag to indicate that further investigation is warranted. The values of phase for individual hours determine a position fix, so the differences from predicted result in real navigation errors. We believe that the findings show both real variability that should be accounted for in navigation use and possibilities for prediction refinements. Knowledge of both can lead to improved navigation.

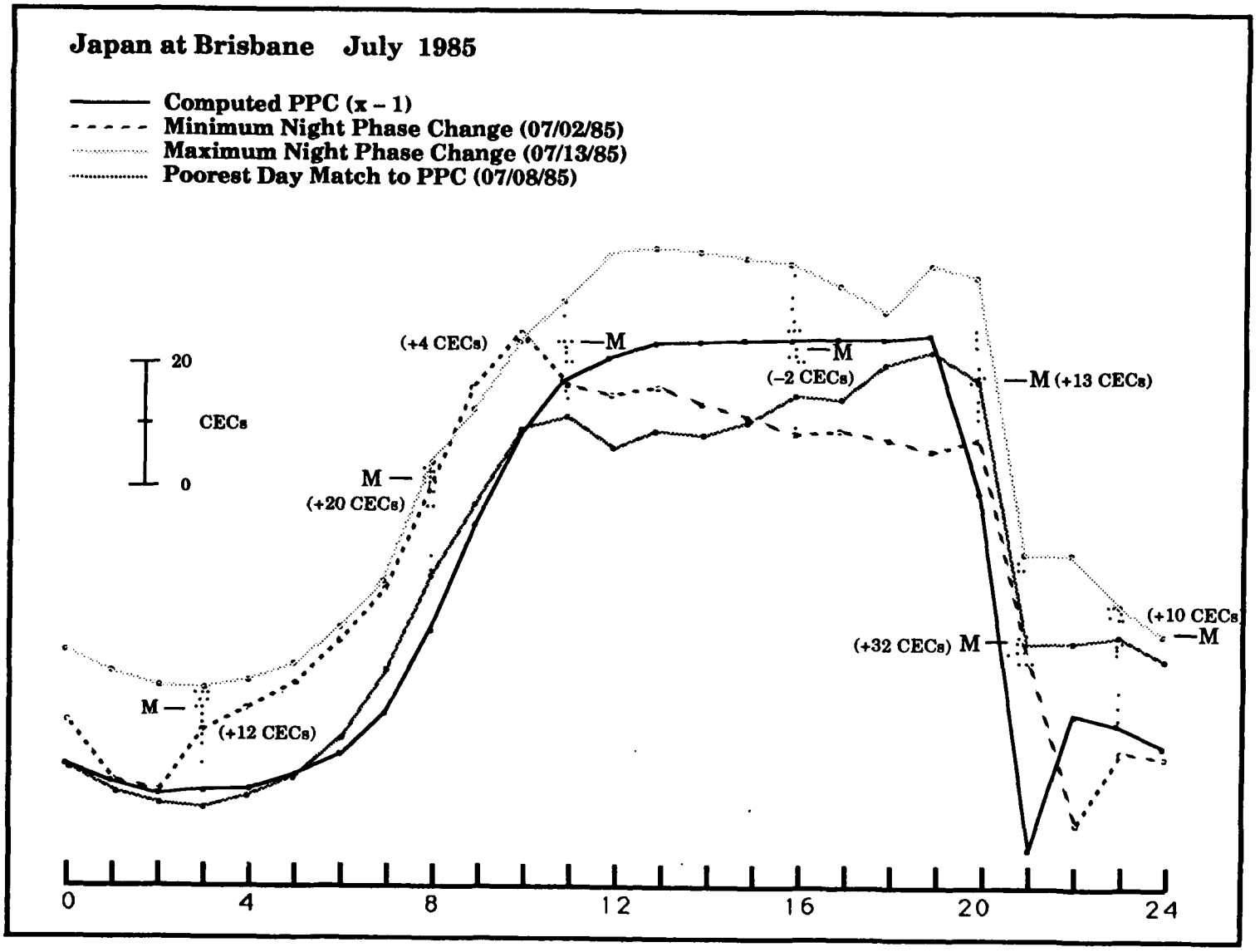

Figure E-8. Japan Phase at Brisbane; 10.2 kHz

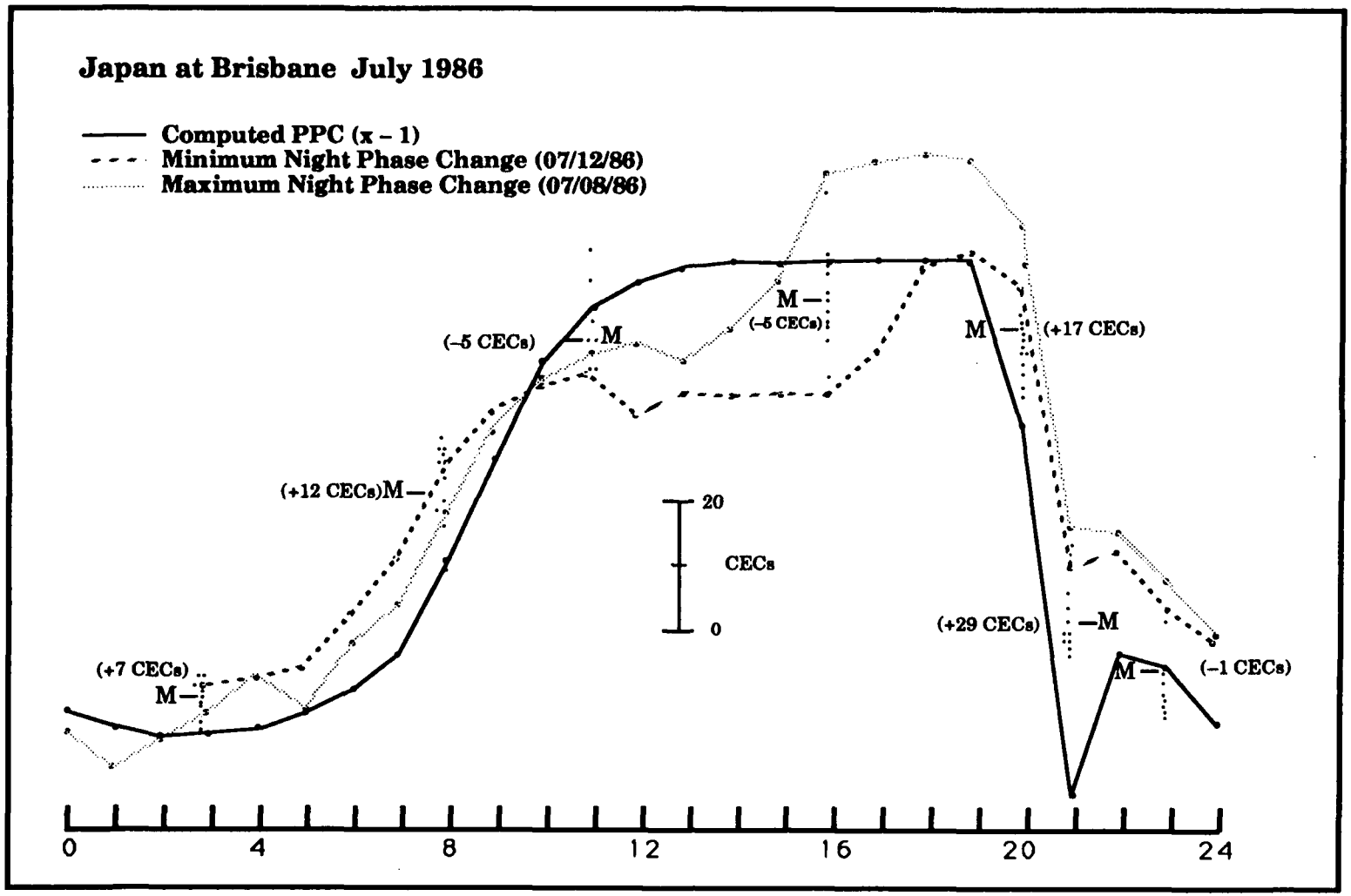

Figure E-9. Japan Signal Phase at Brisbane; 10.2 kHz

PART III: ANALYSIS OF SHIPBOARD LOP MEASUREMENTS

Shipboard recorded phase data is used to selectively validate navigation accuracy and to check findings from other analysis phases. In general we find that the shipboard data confirms that OMEGA position fixes when compared to satellite fixes produce position differences consistent with observed variations in signal propagation. Our checks of accuracy are primarily for median values of the LOP difference between the Omega and Transit Satellite measured positions. The medians are determined for periods of all day or all night propagation. Samples of tabular listings are presented in Tables E-9 and E-10. Each table includes data for a ship transit. Each table entry is the median calculated LOP difference for a station pair for a specific transit interval of day or night. The data is grouped into day and night and into columns allowing comparison of pairs having a related station. As an example, the top left subtable of Table E- 9, the data for transit K, contains a panel for daytime medians for station pairs having C as the common station. The columns of data under each station pair heading are the median LOP errors for each successive daytime intervals of the transit period. The panel in the lower left shows the nighttime medians. Other station combinations are shown to the right of these two examples. This data was not as informative to us as were plots showing LOP errors in relation to the calculated PPCs. We will describe sample plots along with some interpretations and offer the Tables for those interested in statistics.

The ACT6 Ship tracks for both sets of data to be described follow a sequential track starting near 30° S, 56° W moving in a near great circle path to 21° S, 118° W for segment K and from 19° S, 119° W to 03° S, 93° W for segment L. The transits which occured during the first half of January 1986 are separated by two and one quarter days.

Figure E-10 is representative of the data to be shown. Three traces are drawn for the duration of the transit. The top trace is the calculated PPC for the first station, the second trace the PPC for the second station, and the third trace is the computed LOP difference. The PPCs are plotted in degrees and the LOP difference is plotted in CECs. The PPC plots serve to identify the diurnal phase change for each station, thereby allowing easy

determination of day, night,and day/night transition times. The time intervals when both propagation paths are either all day or all night are identified just above the horizontal time ordinate. Under each of these bars is a number which is the median LOP difference for the marked time interval. The median difference is the difference between the location of the median and the satellite determined LOP, the horizontal line through the LOP data. To us the important information is the time history of the LOP difference data as related to the propagation conditions.

Refering to Figure E-10 which is for station pair CD each period of time has a unique characteristic. The first period marked night has a median LOP difference of 30 CECs. The LOP difference continously increases throughout the night ranging from 21 to 42 CECs. The following day period is fairly constant throughout the full interval. The following short duration transition period reaches an error of 80 CECs. The next night recovers from an initial error near 35 CECs. Similar characteristics are observed for following intervals. The large transition errors that show on many of the segments are consistent with the propagation of the North Dakota signal predicted to be modal.

The plot for each station pair of a transit reveals characteristic trends. Figure E-11 shows the transit records of K for station pair CG. We expected this station pair group to produce the most accurate LOPs. The plot shows that the daytime median values are consistent and small, varying ±1 CEC about –4 CECs. The entire day has low errors. Night difference values are generally larger, averaging –11 CECs, and are more variable both from night to night and during a night. We find the sunrise transition period interesting due to the repeatable pattern similar to a dampened oscillation.

The station pair combination GH shown in Figure E-12 shows a number of interesting features. The day LOP errors are both larger than in Figure E-11 and show a systematic trend starting with the largest difference and progressing to small errors just before sunset. The night LOP errors frequently are smaller than the day errors. Both transition times have realitively large errors and both show consistent patterns. These patterns indicate the potential for improving the prediction of transition time intervals.

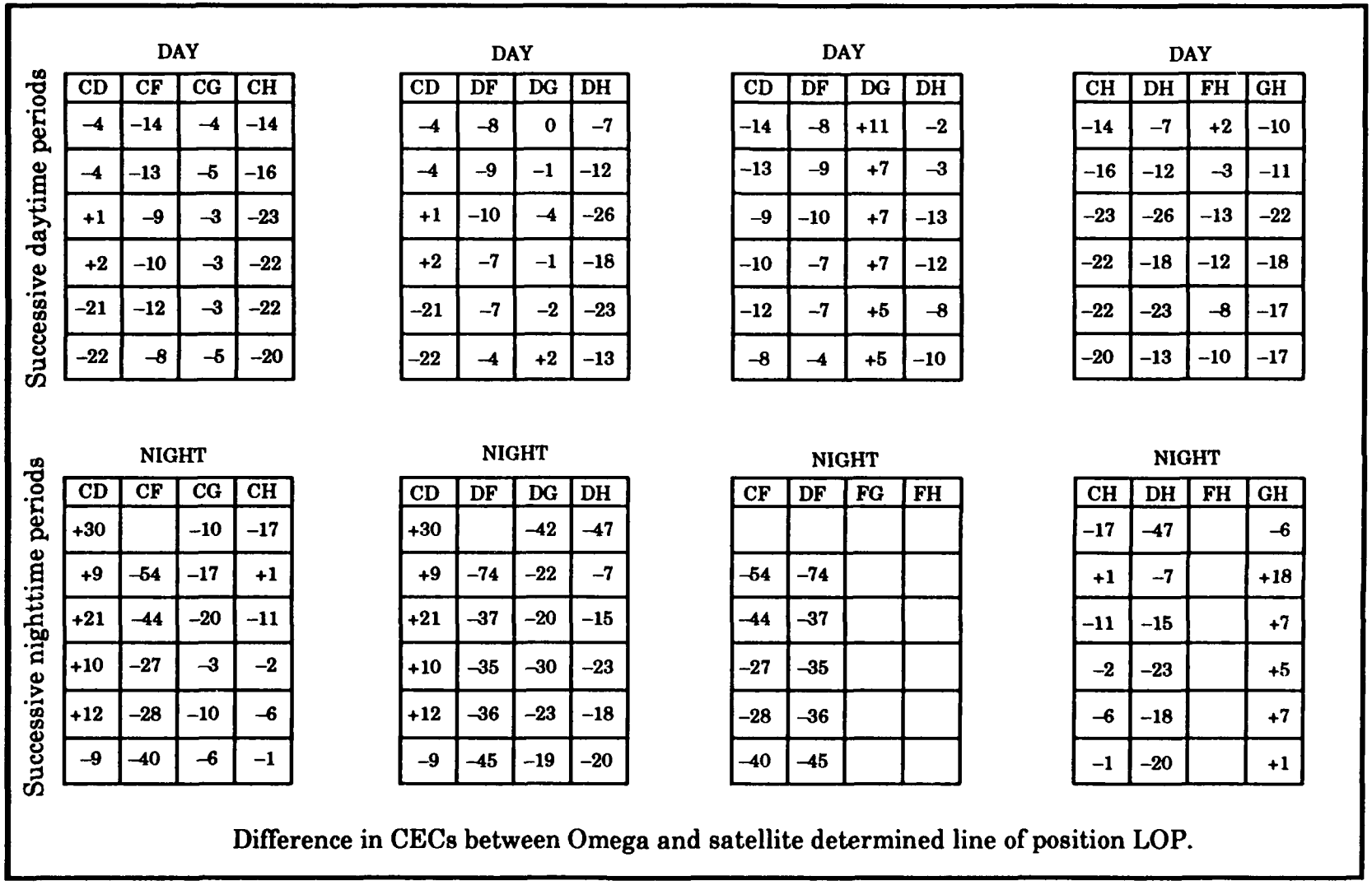

Table E-9. Comparing Station Pairs of Median LOP Errors for Ship Transit Act 6-K; 10.2 kHz

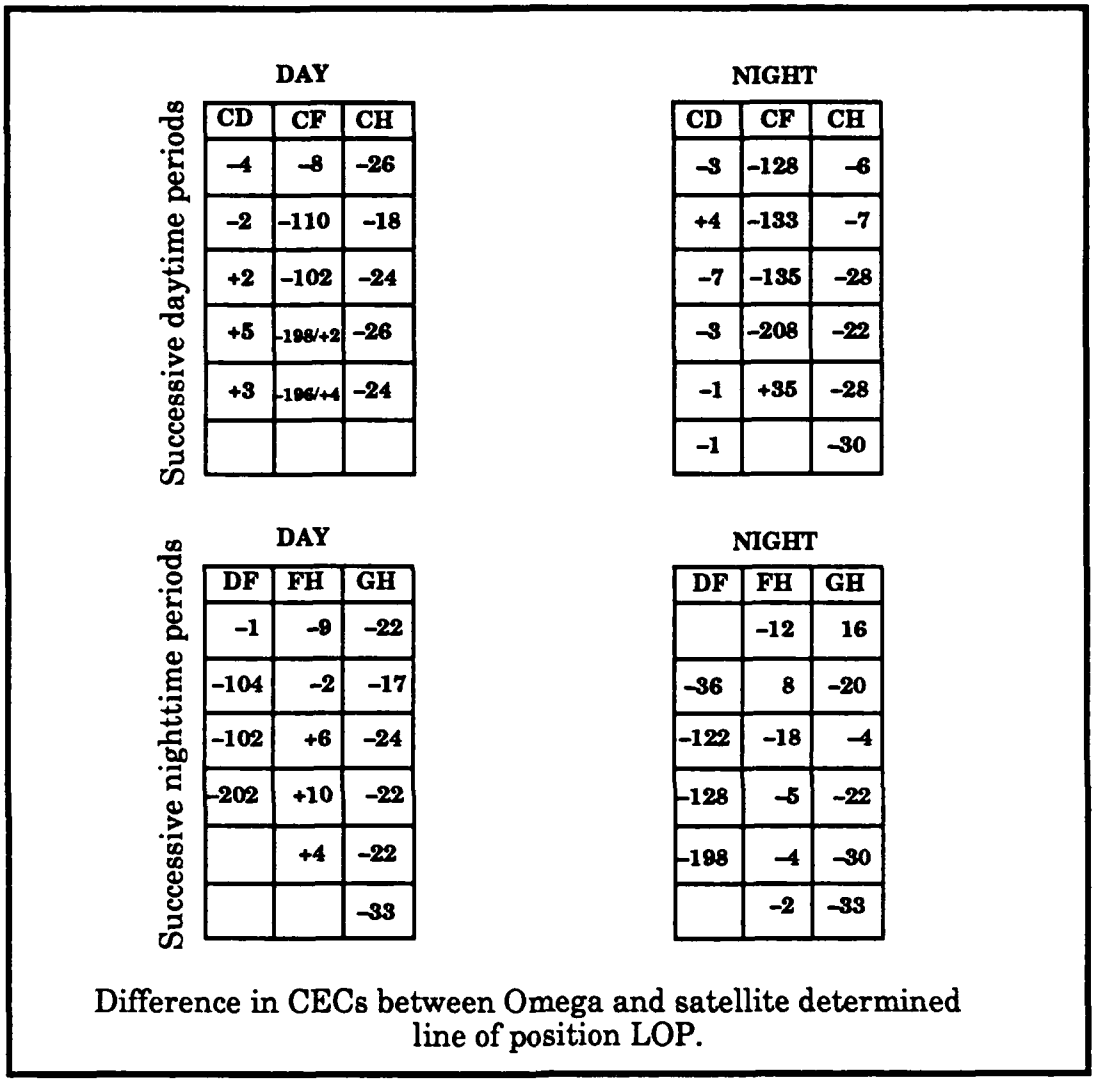

Difference in CECs between Omega and satellite determined line of position LOP.

Table E-10. Comparing Station Pairs of Median LOP Errors for Ship Transit Act 6-L; 10.2 kHz

Figure E-13 shows the CD station pair combination for the L segment of the ACT 6 transit. By this time the ship is moving across the predicted boundary for the station D modal zone. The data show generally small LOP errors for both day and night. The transition times have higher errors but also show systematic patterns. The transition intervals just prior to 0000 and after 1200 on 15 January show large offsets, 100 CECs. These offsets suggest that the modal effects could extend further east than our predictions indicate. The database is too limited to establish a conclusion.

The plot for station pair CF on segment C is shown in Figure E-14. Modal effects are strongly evident in this record. Many cycle offsets occur. This ship transit was within the zone predicted modal for station F. We conclude that the modal prediction is confirmed. The day periods, if reinitiated to remove cycle jumps produce acceptable LOP errors. Day periods of measured phase are always good if not offset by increments of a cycle.

General comments on Part III: We found the shipboard data a very useful addition to the validation database. The wealth of information contained in this database could easily warrant an independent analysis. We found the time plots particularly interesting because of the revealed patterns and trends. Because of uncertainties in determining true ship position, we are hesitant to draw conclusions from the measured median LOP errors. Nevertheless, it is evident that good quality navigation was taking place. We believe that some of the larger observed offsets are attributable to the PPC predictions. In particular, the Japan signal in the Western South Pacific showed consistent offsets on several ship transits. We found that the transition intervals on most station pair combinations consistently had relatively large LOP errors. These errors generally were systematic, indicating that better predictions are feasible. Finally, we note that several of the nearest stations are modal at night and during transition. The station pairs without modal effects can incur transition intervals that occupy one-hundred percent of the time. This makes accurate prediction of transition intervals all the more important.

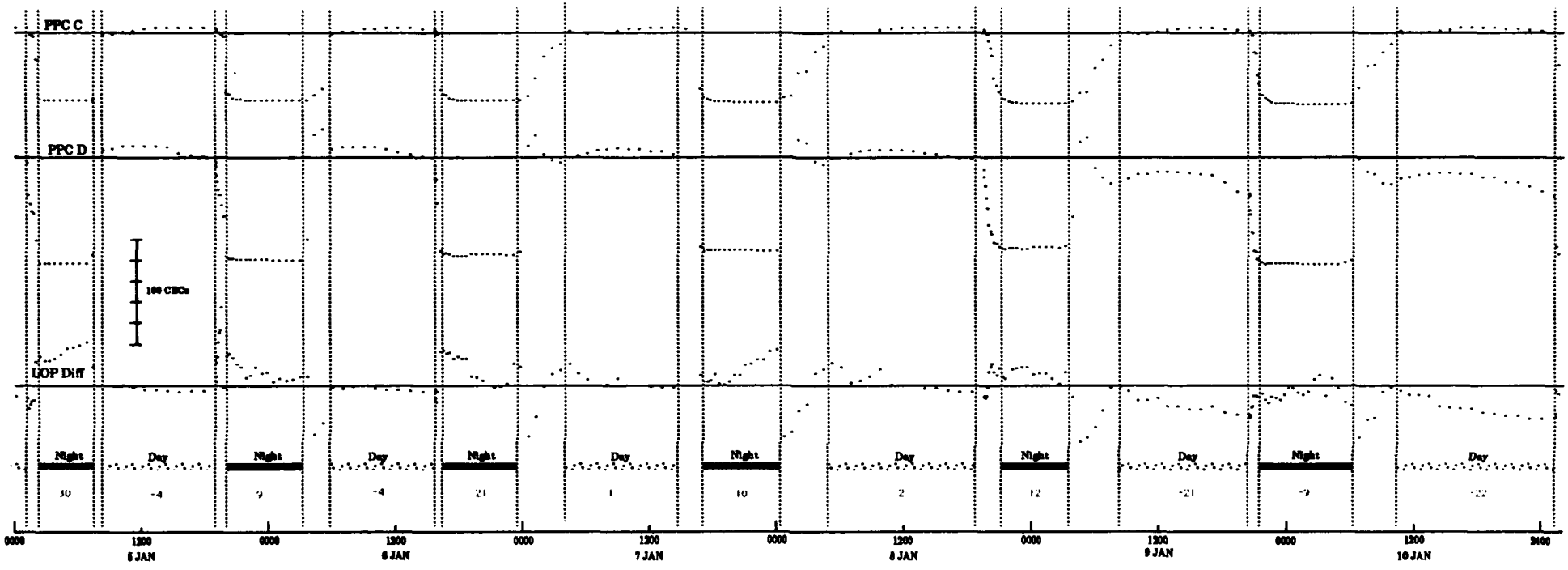

Figure E-10 ACT6 K 10.2 kHz CD PPC Plot

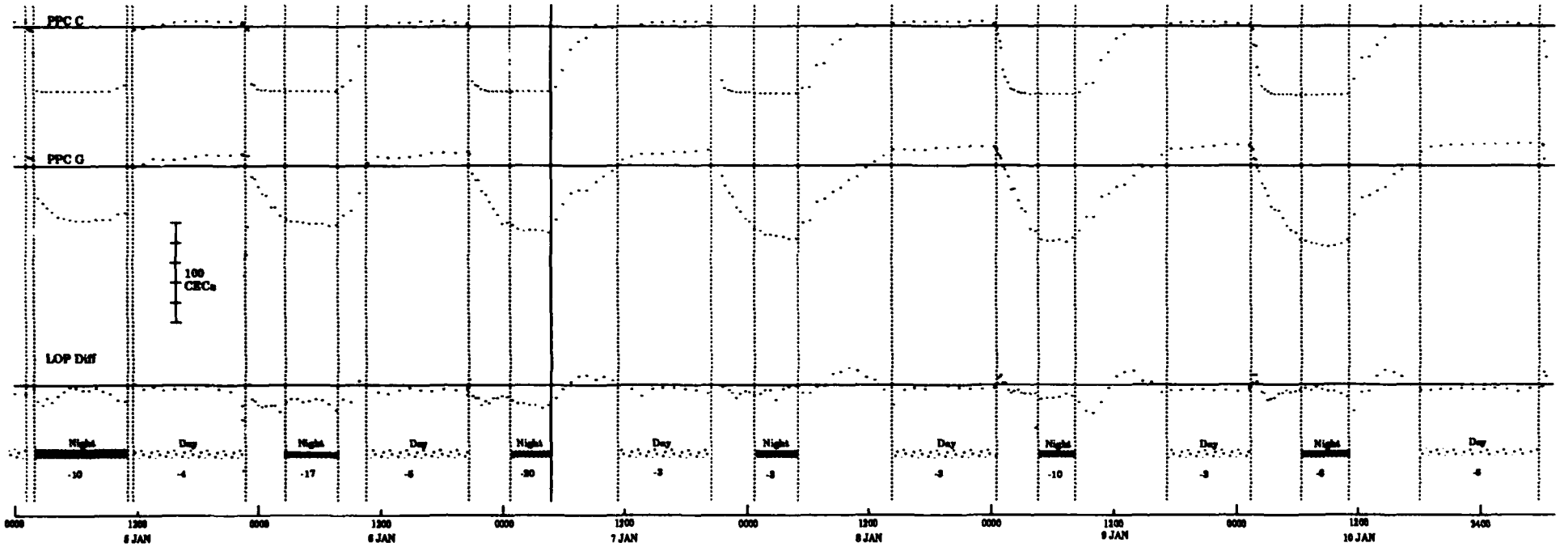

Figure E-11. Act6 K 10.2 kHz CG PPC Plot

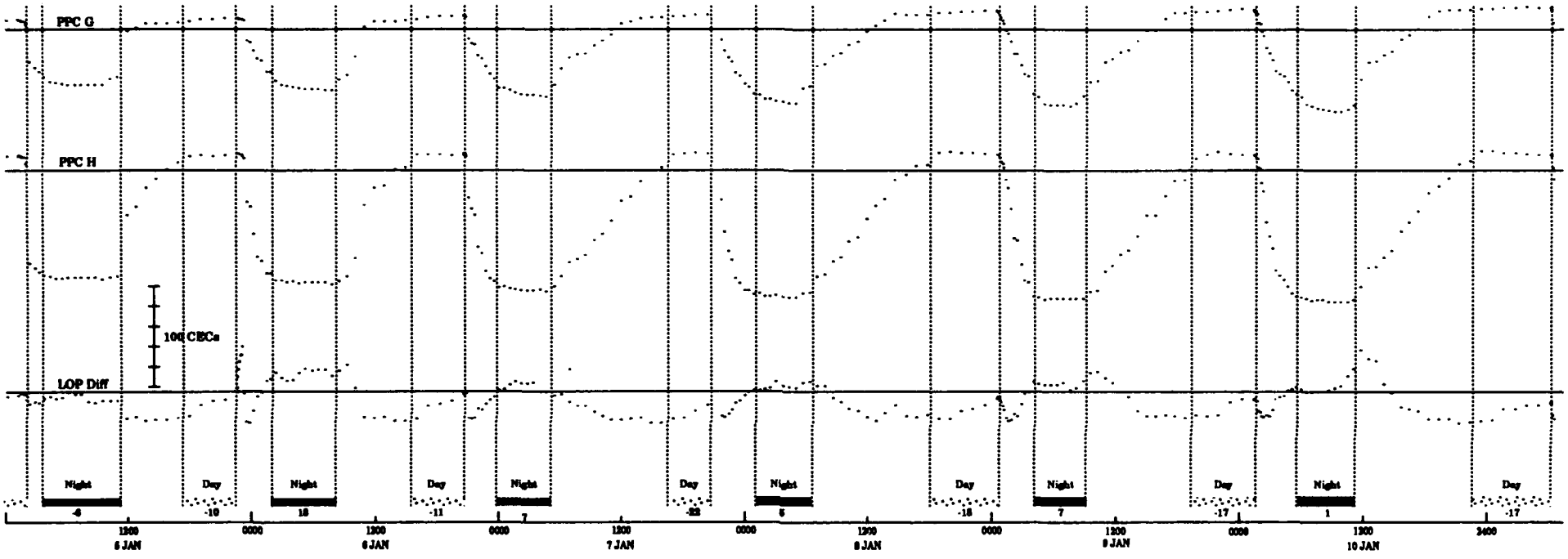

Figure E-12 Act6 K 10.2 kHz GH PPC Plot

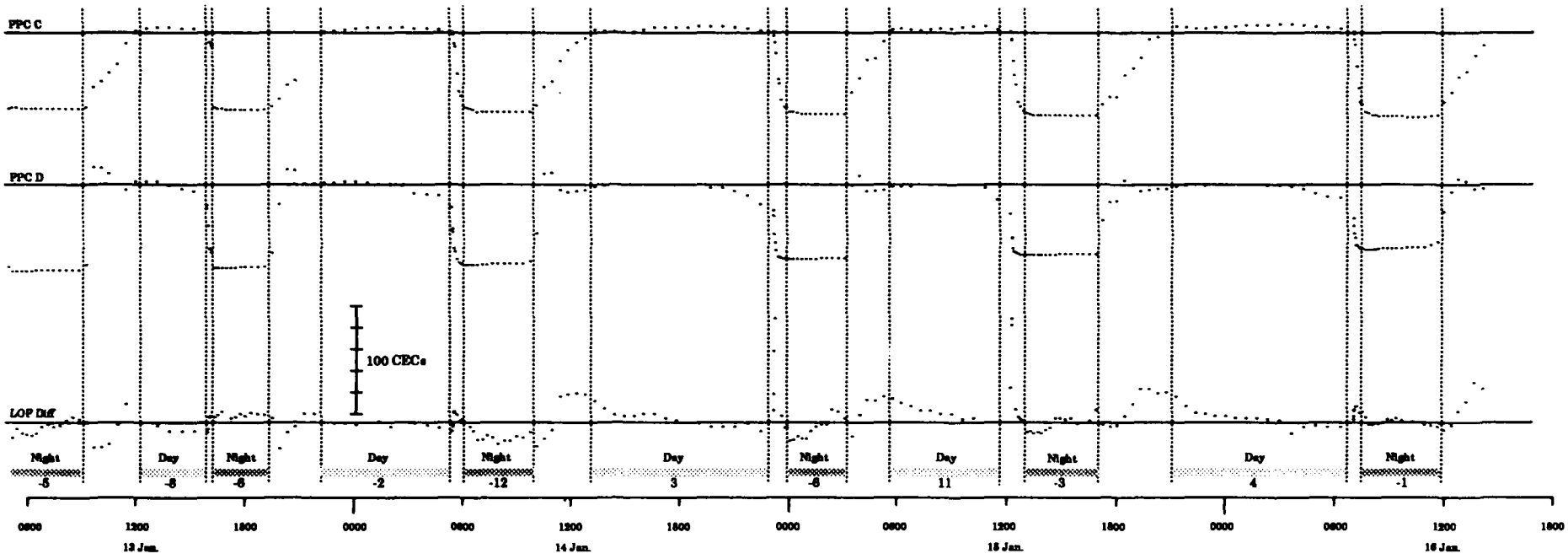

Figure E-13. ACT6 L 10.2 kHz CD LOP and PPC Plot

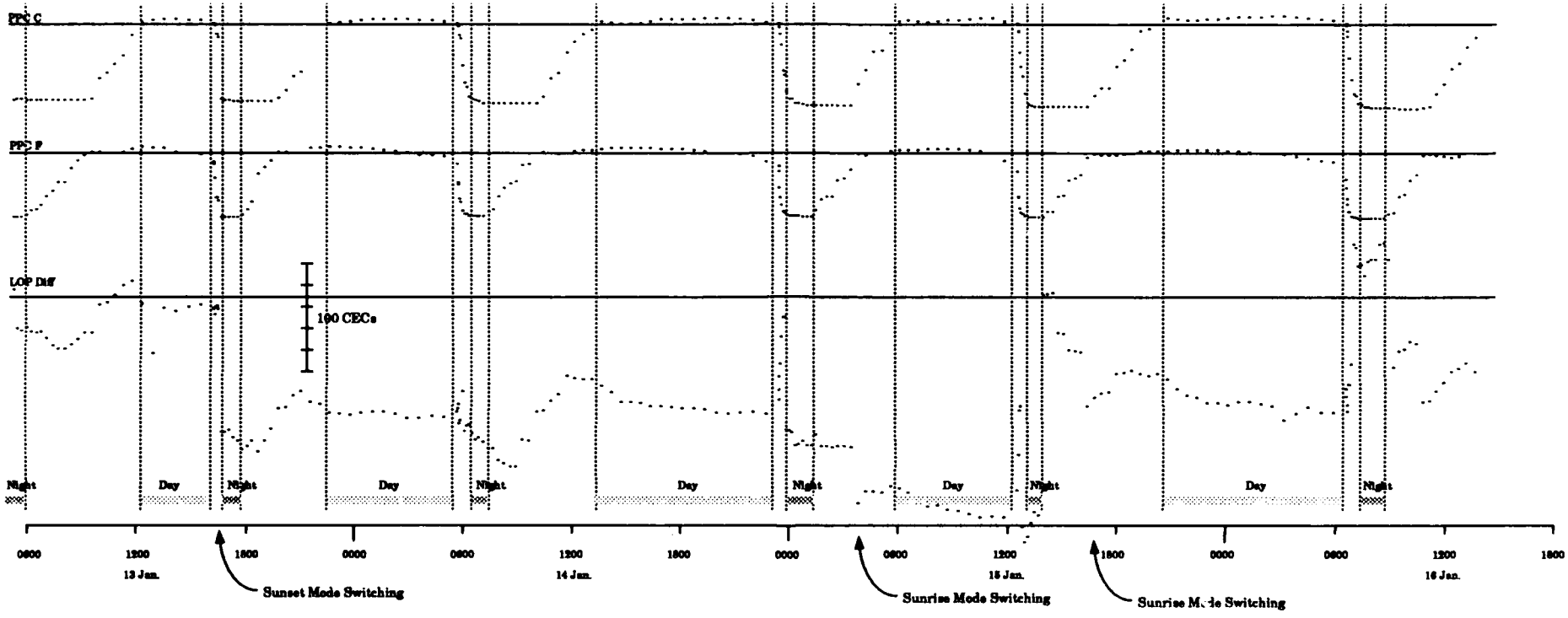

Figure E-14. ACT6 L 10.2 kHz CF LOP Plot